Homogeneous and Heterogeneous Oxidation of Gaseous Elemental Mercury

Graydon Snider
Department of Chemistry
McGill University, Montreal

November 2011

A thesis submitted to McGill University in partial fulfillment of the requirements for the degree of Doctor of Philosophy

Table of Contents

List of Figures

List of Tables

Abstract

Mercury is an atmospheric global pollutant with complex cycling behavior. Two-thirds of the mercury present in our atmosphere is anthropogenic in origin. Chemical oxidation of gaseous elemental mercury governs the deposition rate of mercury over most lakes, land, and oceans. A major uncertainty comes from the effect of atmospheric surfaces such as aerosols. Much research is devoted to mercury capture technologies to be used in coal fire power plants, which are the major source of anthropogenic emissions.

This thesis is a report on oxidation kinetics and mechanistic studies relevant to mercury-scavenging reactions. It provides an overview of the mechanisms of mercury oxidation by ozone, nitrogen dioxide, and titanium dioxide (exposed to ultra-violet light). The role of surfaces was quantified, as appropriate for each system. Crossover effects between gaseous co-pollutants (e.g. CO, SO_2) and surfaces (SiO_2, TiO_2) are discussed. Rate constants were measured for each process and product studies were performed and compared with the available literature.

The effects of different surfaces and gases on the oxidation of mercury by ozone were measured. This reaction was confirmed to be a surface-enhanced gas phase initiated reaction with a second-order rate constant for pure gas-phase (k_{gas} = (5.40 ± 0.56) × 10^{-19} cm^3 $molec^{-1}$ s^{-1}) and an enhanced surface component (k_{sur} = (2.91 ± 0.12) × 10^{-15} cm^7 $molec^{-1}$ s^{-1}), or k_{net} = (6.1 ± 1.1) × 10^{-19} cm^3 $molec^{-1}$ s^{-1}. Water vapor had no effect on the rate but liquid water and gaseous carbon monoxide both rapidly accelerated the reaction. Mechanisms were placed in context with atmospheric oxidative scavenging processes. Future work may combine aerosols (soot, acid, silica) in ozone oxidation reactions and/or addition of SO_2 gas.

The feasibility of removing mercury from a coal flue gas via titanium dioxide and ultra violet light was investigated. Discussed are some of the possible surface chemistry models of oxidation. The uptake rates of mercury over photosensitized titanium dioxide films was described by the Langmuir-Hinshelwood rate equation, where $K_{Hg} = (5.1 \pm 2.4) \times 10^{-14}$ cm^3 $molec^{-1}$ and $k = (7.4 \pm 2.5) \times 10^{14}$ molec cm^{-2} min^{-1}. Effects of sulfur dioxide and water were evaluated but neither was found to impede the reaction. By contrast low oxygen level strongly impeded oxidation rates. Deposits of HgO on titania surfaces were widely dispersed in concentrated clusters. Currently there is no explanation to this pattern. Future experiments may use light emitting diodes to capture $Hg^0(g)$ over TiO_2

The oxidation of mercury by nitrogen dioxide was found to be a pure gas phase reaction, second order with respect to NO_2, where $k = (3.5 \pm 0.5) \times 10^{-35}$ cm^6 $molec^{-2}$ s^{-1}. The mechanism was conjectured to be a two-step addition of NO_2 to Hg^0; at higher NO_2 concentrations the reaction may be first order with respect to NO_2 but further experiments would be required for validation. The rate constant was also found in agreement with a previous study. Rates were unaffected by changes in pressure, available surfaces, presence of SO_2, and water. It was discovered that TiO_2 surfaces saturated in HgO deposits, when exposed to NO_2 were 'revived' in Hg uptake activity. It is suspected the reaction between HgO and NO_2 re-disperses the deposits.

Résumé

Le mercure est un polluant atmosphérique globale avec le comportement les cyclismes complexes. Deux tiers du mercure présent dans notre atmosphère est d'origine anthropique. L'oxydation chimique de mercure élémentaire gazeux régit la vitesse des dépôts de mercure sur la plupart des lacs, des terres et des océans. Une incertitude majeure provient de l'effet des surfaces atmosphériques tels que les aérosols. Beaucoup de recherches sont consacrées aux technologies de captage du mercure pour être utilisés dans les centrales au charbon de puissance de feu, qui sont la principale source d'émissions anthropiques.

Cette thèse est un rapport sur la cinétique d'oxydation et d'études mécanistiques relatives au mercure-balayage réactions. Il donne un aperçu des mécanismes d'oxydation du mercure par l'ozone, le dioxyde d'azote et dioxyde de titane (exposé à la lumière ultraviolette). Le rôle des surfaces ont été quantifiés, comme il convient pour chaque système. Effets de coupure entre gazeux co-polluants (par exemple CO, SO_2) et les surfaces (SiO_2, TiO_2) sont discutées. Les constantes de vitesse ont été mesurées pour chaque processus et études de produits ont été effectués et comparés avec la littérature disponible.

Les effets de différentes surfaces et de gaz sur l'oxydation du mercure par l'ozone ont été mesurés. Cette réaction a été confirmé à une phase gazeuse augmenter a la surface réaction initiée avec un taux de second ordre constant de pures en phase gazeuse (k_{gaz} = (5,40 ± 0,56) × 10^{-19} cm^3 $molec^{-1}$ s^{-1}) et une surface améliorée composant (k_{sur} = (2,91 ± 0,12) × 10^{-15} cm^7 $molec^{-1}$ s^{-1}), ou k_{net} = (6,1 ± 1,1) × 10^{-19} cm^3 $molec^{-1}$ s^{-1}. La vapeur d'eau n'a eu aucun effet sur la vitesse, mais l'eau liquide et de monoxyde de carbone gazeux, à la fois rapidement accéléré la réaction. Des mécanismes ont été mis en contexte avec l'atmosphère oxydant processus de balayage. Les travaux futurs peuvent combiner les

aérosols (suie, de l'acide, de la silice) dans les réactions d'oxydation de l'ozone et / ou ajout de SO_2.

La faisabilité de l'élimination du mercure des gaz de combustion de charbon par du dioxyde de titane et de lumière ultra-violette a été étudiée. Discuté sont quelques-uns des modèles possibles chimie de surface de l'oxydation. La vitesse d'absorption de mercure au cours photosensibilisées films de dioxyde de titane a été décrit par l'équation du taux de Langmuir-Hinshelwood, où $K_{Hg} = (5,1 \pm 2,4) \times 10^{-14}$ cm^3 $molec^{-1}$ et $k = (7,4 \pm 2,5) \times 10^{14}$ cm^{-2} $molec^{-1}$ min^{-1}. Effets du dioxyde de soufre et de l'eau ont été évalués, mais ni a été trouvée pour empêcher la réaction. Par niveau d'oxygène à faible contraste fortement entravé les taux d'oxydation. Dépôts sur des surfaces de HgO oxyde de titane ont été largement dispersés dans les amas concentré. Actuellement, il n'existe pas d'explication à ce modèle. Les expériences futures peuvent utiliser des diodes électroluminescentes à saisir Hg^0 (g) sur TiO_2.

L'oxydation du mercure par le dioxyde d'azote a été trouvé à une réaction gaz pur phase du second ordre par rapport au NO_2, où $k = (3,5 \pm 0,5) \times 10^{-35}$ cm^6 $molec^{-2}$ s^{-1}. Le mécanisme a été conjecturé être un ajout en deux étapes de NO_2 à Hg^0(g); à des concentrations élevées de NO_2 la réaction peut être de premier ordre à l'égard de NO_2, mais d'autres expériences seraient nécessaires pour la validation. La constante de vitesse a également été trouvé en accord avec une étude précédente. Les vitesses ont été affectées par les changements de pression, les surfaces disponibles, la présence de SO_2, et l'eau. On a découvert que le TiO_2 surfaces saturées dans les dépôts HgO(s), lorsqu'ils sont exposés à de NO_2 ont été 'relancé' dans l'activité d'absorption de mercure. Il est soupçonné de la réaction entre HgO(s) et NO_2 disperse les dépôts.

Acknowledgements

I would like to thank everyone who has encouraged me over the years to continue with my interests. My parent's hobbies and pursuits were good guides. My fiancé Heather has been patient with me throughout all these years I spent completing my PhD. Dr. Parisa Ariya has of course been the most directly involved and was very supportive throughout my time at McGill. She encouraged new ideas and suggestions and an unlimited source of ideas of her own right. She was also understanding of my dual life as scientist and sports, in particular when their schedules were at odds with one another.

Lab mates and peers have come and gone over the years but shall not be forgotten. Farhad Raofie, Dan Deeds, Ed Hudson, Si Lin, Nermin Eltouny, M. Subir, Gregor Kos, Elise-André Guerette. Dan and Ed have often reminded me that your real education begins when you step out of the classroom. The technical staff at McGill has been very helpful, i.e. Georges Kopp in glassblowing, Rick Rossi in electrical, and Fred Kluck in machinery. Dr. Wilczek supervised my physical chemistry lab TAing duties and was very helpful in guiding me through the labs.

My friends in chemistry, in particular the trio Paul, Kraig and Lee made the time between experiments as enjoyable as it could be. In each their own way they opened my eyes to see a life beyond school.

To all the cross-country runners at McGill University, including Ken D, D Kramer, Iain M, Stephen D, and the rest of the men's team over my four all-too-short years on the team.

To the McGill Nordic ski club, who re-ignited my passion for sports and the outdoors. In particular Katie Horn, Ryan Stoa, Sandra Mortimer, Guillaume, Jared, and Prof. André.

The Department of chemistry at McGill has been quite helpful, including good advice from Dr. Lennox and Sandra, and Chantal for all her tireless work in organizing myself and the remainder of the graduate chemistry department.

Manuscripts contributing to thesis

Ariya, P.A., Peterson, K., Snider, G. and Amyot, M.: 2009, **'Mercury chemical transformations in the gas, aqueous and heterogeneous phases: state-of-the-art science and uncertainties'**, in N. Pirrone and R.P. Mason (eds.), Mercury Fate and Transport in the Global Atmosphere, Springer US, New York, pp. 459-501.

Snider, G. and Ariya, P.: 2010, **'Photo-catalytic oxidation reaction of gaseous mercury over titanium dioxide nanoparticle surfaces'**, Chem. Phys. Lett. 491, 23-28.

Snider, G., Raofie, F. and Ariya, P.A.: 2008, **Effects of relative humidity and CO(g) on the O_3-initiated oxidation reaction of Hg^0(g): kinetic & product studies**, Phys. Chem. Chem. Phys. 10, 5616-5623.

Submitted works:

Snider, G. and Ariya, P.: 2011 **Kinetic and product studies of the reactions of NO_2 with Hg^0 in the gas phase, and in the presence of titania micro-particle surfaces at different relative humidity**
To be submitted to J. Water, Air, & Soil Pollution

Chapter 1

Literature Review

1.1 Chapter summaries

Chapter 1 reviews the available kinetic literature of gaseous mercury oxidation. A brief history and origin of early kinetics is established. The most significant modern studies of gaseous kinetic oxidation schemes are discussed, including Hg + O_3; it is established that gaseous HgO is unlikely. Measurement discrepancies regarding the lifetime of mercury are outlined. Mercury capture in coal fire power plants is discussed. The mechanism of oxidation capture by titiania is outlined.

Chapter 2, published as Snider, G., F. Raofie, and P.A. Ariya, *Effects of relative humidity and CO(g) on the O_3-initiated oxidation reaction of Hg^0(g): kinetic & product studies.* Physical Chemistry Chemical Physics, 2008. 10(36): p. 5616-5623 details the oxidation of mercury by ozone in variable conditions, including changes to surface/volume ratios, humidity, presence of carbon monoxide and addition of the radical scavenger trimethylbenzene. Here it is described how carbon monoxide and addition of the radical scavenger trimethylbenzene. This chapter describes how the mercury ozone reaction has some surface dependency, which is quantified with a semi-empirical mechanism.

Chapter 3, published as Snider, G. and P. Ariya, *Photo-catalytic oxidation reaction of gaseous mercury over titanium dioxide nanoparticle surfaces.* Chemical Physics Letters, 2010. 491(1-3): p. 23-28. describes the oxidation of mercury by titania under UV mercury lamp. Here a simplified surface mechanism (Langmuir Hinshelwood

kinetics) fits the oxidation data. For the first time a scanning electron images capture the pattern of mercury uptake on surface.

Chapter 4 submitted to the *Journal of Physical Chemistry C* as Graydon Snider and Parisa Ariya *Kinetic and product studies of the reactions of NO_2 with Hg^0 in the gas phase, and in the presence of titania micro-particle surfaces at different relative humidity,* expands on the ideas of chapter 4 and includes further analysis of competing gas species on mercury uptake. We measure the oxidation of mercury and mercury oxide by nitrogen dioxide, which is found to be surface-independent. In contrast surface oxidation of mercury oxide by nitrogen dioxide is surface-based.

Chapter 5 is an outline for future work, which includes determining the rates and surface dependencies of mercury oxidation by HCl, and BrO. The future of using mercury as a tracer gas in atmospheric chemical kinetics is discussed. Some recommendations are made for equipment and measurement techniques (e.g. for Flow meters, Denuders and Knudsen cell).

Appendices: In addition to chapters 1-5, appendices have been included with supplementary data. Correspondences can be made between chapters 1-4 and appendices A-E.

Appendix A was published as a book chapter as P.A. Ariya, K. Peterson, G. Snider, M. Amyot, in N. Pirrone, R.P. Mason (Eds.), Mercury Fate and Transport in the Global Atmosphere. Springer US, New York, 2009, p. 459. My contribution included tabulating and summarizing known atmospheric mercury kinetics and suggesting some future directions for research. Kinetics data includes environmental deposition rates and aqueous, surface, and gaseous kinetics. This appendix provides review data on all thee types of mercury oxidation (gas, surface and heterogeneous).

Chapter **1**	Appendix **B**	Historical mercury, physical properties, gaseous kinetics
Chapter **2**	Appendix **C**	Supplementary kinetic data
Chapter **3**	Appendix **D**	supplementary kinetic data, including flow tube experiments
Chapter **4**	Appendix **E**	additional kinetic data and desorption experiments

1.2 *Motivation for the study of atmospheric mercury*

All mercury is geological in origin, however the majority of the mercury found in fish enters the ecosystem through atmospheric deposition. Mercury, when released into the air by a variety of combustion processes (coal, waste incineration, forest fires) will act as a global pollutant. Mercury's atmospheric residence time is sufficiently long to reach across oceans or reach remote lakes, where it incorporates into the aquatic food chain. Remote populations can be exposed to an influx of atmospheric mercury (from dietary fish) including Amazonian tribes, northern Inuit populations, and Seychelles or Faroe islanders. There is a considerable volume of debate surrounding the degree of danger one is exposed to when consuming 'typical' amounts of fish, i.e. 2-3 servings per week. Due to various factors including individual dietary habits and bioavailability of mercury species when consumed, clear guidelines are difficult to establish and can generate a certain degree of debate. Details of this controversy lie beyond the scope of this thesis but a discussion of the likely dangers of 'background-level' mercury is readily available [1, 2]. The majority

of fish (both farmed and wild) is ultimately considered healthy to eat in moderate quantities [3].

We now have a detailed understanding of atmospheric mercury cycling, better understood now compared with even ten years ago. However some aspects remain unknown about the global transport of gaseous mercury. Specifically the lifetime of gaseous mercury is far more complex than its one-year estimate [4] and mercury oxidants (e.g. O_3, Br, H_2O_2) collectively show mercury has a residence lifetime of well under a year [5]. In some instances mercury oxidation occurs in a matter of hours, as in during mercury depletion events [6]. Despite the rise in coal combustion in Asian countries the amount of mercury in the atmosphere has remained stable over the last two decades [7], with a recent trend in decreasing concentrations [8] and it is difficult to explain why. Conversely, concentrations of mercury found in fish located in Kejimkujik National Park have shown both increases and decreases from the 1990s with no simple trend [9]. There are internal equilibria acting within the cycling mechanism that are not wholly understood. The degree to which heterogeneous aerosol chemistry enhances reaction rates is not well understood and speciation of gaseous oxidized and particulate mercury species is generally unknown.

Contemporary incidents of acute mercury poisoning are thankfully rare. Modern concerns over the effects of low-level mercury now center over the exposure derived from fish consumption spread over a number of years. Physiological studies look for decreases in motor and mental functionality among those who consume fish contaminated with methylmercury. There is some disputed evidence regarding the adverse effects of eating large quantities of 'background' mercury among those with heavy fish diets [10-12].

Proposed US-EPA guidelines require retrofitting coal fire power plants with new devices for mercury capture [13]. The removal of mercury from coal combustion has

raised questions regarding the interactions of gaseous oxidized, particulate, and elemental gaseous mercury with walls and during initial atmospheric release [14].

There is a rich field of pure atmospheric physical chemistry in gaseous mercury kinetics, as well as heterogeneous chemistry found in coal fire power plant exhaust. It is the author's observation that the study of mercury oxidation remains a worthwhile pursuit that transcends concerns over details of its toxicity in persons. Mercury kinetics can be potentially justified worthy of study even for their own sake.

1.3 *A brief history of mercury*

The people of ancient China, Egypt, Greece, Central America (Mayans) and Europe (Roman Empire) have all demonstrated some awareness of elemental mercury. The historical and cultural usages of mercury, from medicinal to alchemical, can be found in Swiderski's history [15]. Some of the earliest usages were decorative dyes and some traditional medicines. From ancient history to modern times we have grown increasingly aware of the role of mercury as an environmental pollutant. The scientific basis for mercury pollution was not well established until the 1960-70s. At this time in Sweden new research on the transportation cycle of mercury pollution -and its effects on remote fish populations- began to emerge.

1.3.1 Swedish research on atmospheric mercury

In 1980 Sweden began the first systematic continuous monitoring of atmospheric mercury concentrations [16]. Such measurements were motivated by the continued presence of high mercury contamination (> 1 ppm) in remote fish and bird populations. Despite earlier legislation restricting the use of mercury in pesticides and chlor-alkali

plants [17], in the 1980s over 10,000 Swedish lakes contained at least some fish contaminated with a dry weight of over 1 ppm MeHg [18].

Back-trajectories show lakes were contaminated with high levels of soot-containing mercury anthropogenic in origin [16]. As early as the 1970s it was known that untreated coal combustion released significant quantities of gaseous mercury [19, 20]. It was soon understood that sources of mercury contamination were long range, principally due to anthropogenic activities.

Sweden's stricter controls of mercury emissions led to a dramatic fall in mercury fish levels, yet concentrations remained greater than pre-industrial times [21]. Fish in remote regions were sometimes found to contain above 1 ppm methylmercury (dry weight), and up to 4.8 ppm closer to industries [22]. Pre-industrial background values (below 0.5 ppm Hg) were becoming difficult to locate. Influenced by the economic and cultural fish interests in Sweden, research interest into the propagation of mercury was considerable.

It was known that certain bacteria (i.e. *Pseudomonas* or *Penicillium roqueforti*) would reduce organo-mercury species to elemental mercury [23, 24]. Reduction led to the idea that mercury-contaminated lakes could "expel" volatile mercury into air, then re-deposited into surrounding water systems [21]. Hence mercury could spread to isolated fish populations more readily than had been assumed. Early reviews on environmental mercury pollution encouraged a shift in attention towards the study of the *transportation* cycle of mercury [22].

Research led to the following conclusions linking atmospheric mercury emissions with levels found in fish:

i) Combustion processes (such as coal, waste incineration, cremation) released gaseous elemental mercury, which is slow to oxidize

ii) Wet and dry deposition of gaseous mercury caused an uptake of mercury in remote lakes and bodies of water

iii) Certain bacteria methylated aqueous inorganic mercury into the bio-available methylmercury or reduce mercury chloride into $Hg^0(aq)$.

iv) Methylmercury bio-accumulated over a million-fold in fish from the surrounding water.

Though general pathways were established relatively early it became apparent that mercury cycling was also more complex than previously thought. Specifically the lifetime of mercury could only be vaguely approximated but not well quantified or chemically described. As well when three bodies of measurement data are compared, each yielded a different estimate of mercury's lifetime.

1) Emission inventories (collectively obtained by industry emission records) predicted a lifetime of months to years.
2) Deposition/emission fluxes (i.e. from *in situ* measurements of gaseous surface mercury fluxes) predicted a lifetime of hours to days.
3) Laboratory rates of mercury oxidation (as determined by measurement of chosen rate constants) predicted a lifetime of days to years.

The atmospheric lifetime of mercury can be described by emission budgets, deposition flues, and oxidation kinetics. Lifetimes of mercury as expressed by ozone oxidation rates as obtained through laboratory kinetics will be described in more detail.

1.4 Global mercury emissions and concentrations

1.4.1 Studies of emission budgets

The specific anthropogenic contribution to mercury pollution was uncertain before 1980. Jernelöv [22] conjectured that it "accounted for only a small fraction [about 10%] of the total mercury flux". Nriagu completed the first inventory estimate in 1988 [25] though his values were of low precision (Table 1-1). Reliable anthropogenic mercury emission inventories were only available after 1996 as compiled by Pirrone *et al.* [26]. They had found the annual *direct* emissions of anthropogenic mercury lay between 2000 and 3000 tonnes per year (t/yr).

Table 1-1 Global estimates of anthropogenic mercury emission

Emission year(s)	*Direct* annual $Hg^0_{(g)}$ emissions (t/yr)	Reference
1983	910 - 6200	[25]
1984	1900	
1987	2100	[26]
1990	2220	
1995	1910	[27]
2000	2190	[28]
2002	2400	[29]
2002	2600	[30]
2004 - 2006	2320	[31]
2000 – 2008	2909	[32]
2020	1750 - 2630	[28]
2050	2480 - 4860	[33]

Boldface dates = predicted future trends. Note: Cumulatively over a million tonnes of mercury have been mined over the past millennia [34]. The contribution of mined mercury in the atmospheric remains a source of uncertainty.

Table 1-2 Global estimates of natural mercury emissions

Emission year(s)	Annual Hg emissions (tonnes/yr)	Reference
1989	2200 - 3200	[35]
1994	1000	[36]
2002	2100	[29]
2002	1000	[30]
2004	1067	[37]
2010	5207	[31]

Compared to anthropogenic emissions, natural emissions (table 1-2) appear more uncertain. This uncertainty is in part due to the semantics of whether the re-emission of anthropogenic sources should count towards natural emissions. Reports attribute between 1000 t/yr (land and ocean) [30, 37] to over 5200 t/yr [31]. Pirrone *et al.* estimate total annual mercury emissions (anthropogenic and natural combined) to be 7527 t/yr and rising [31]. Siegneur *et al.* [37] estimated 50% of globally deposited mercury is from re-emitted sources.

Assuming that annual mercury emissions are in fact Pirrone's value of 7527 tonnes per year [31], and given that the total atmospheric burden is 6000 tonnes [38], then the lifetime of mercury must be 0.8 years. As total emissions contain a large source of error, the result is that early lifetime estimates vary between 0.5 and 1.5 years.

1.5 *Measurements of atmospheric mercury deposition*

The measurement of deposition flux data is of interest both for recording pre-industrial atmospheric mercury levels and modern lifetimes. Historical mercury concentrations in ice and earth core samples have been established in a number of studies. Schuster *et al*. [39] found ice cores containing over 270 years of mercury deposition (1720-1993) in the Upper Fremont Glacier, Wyoming. Boutron *et al.* obtained 40 years of

ice cores (1949-1989) from Greenland [40]. Roos-Barraclough *et al.* [41] found 14500 years of mercury in peat from the Swiss Jura mountains. Mercury from peat core samples from the Faroe Islands was found to correlate well with lead emissions for the past 5000 years [42].

Measuring mercury deposition in winter, Lalonde *et al.* [43] found mercury losses on snow can reach up to 54% and that "Direct extrapolation from snow cores could underestimate past ambient Hg levels... snow could be rapidly re-emitted instead of being accumulated throughout the winter" [43]. Dommergue *et al.* found depth profiles of snow ruled out mercury losses through diffusion but that snow melt water can remove 90% of mercury from a snowpack [44]. The evidence suggests that mercury, after depositing over ice and snow, is then rapidly lost.

Hylander *et al.* found that modern mercury deposition is roughly double the pre-industrial rate [34], which lay between perhaps 2-3 $\mu g/m^2/yr$. Reported deposition trends are still broadly estimated, with uncertainties ranging from 30 to 50% [45]. Atmospheric mercury measurements over the Atlantic Ocean between 1977-2002 show mercury emissions have remained fairly constant, especially after 1996 [7]. Likewise concentrations found in Pacific wild tuna have not significantly changed between 1971 and 1998 [46]. This constancy apparently contradicts the rise in total anthropogenic emissions [28]. Deposition of atmospheric mercury shows a rapid climb in the second half of the 20^{th} century (figure 1-1).

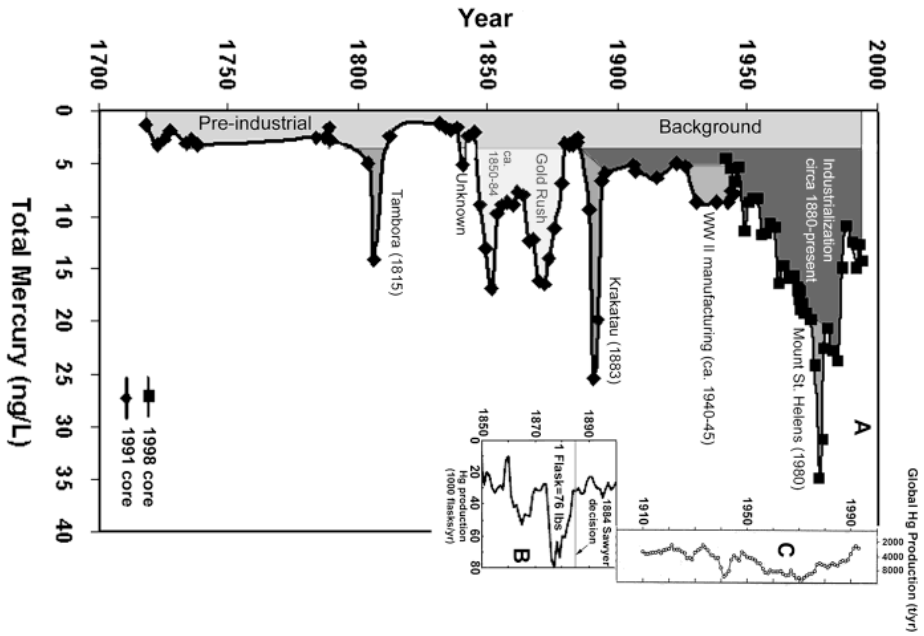

Figure 1-1 From Schuster *et al.* [39], an historic mercury deposition for the years 1700 – 1990 AD. Mercury deposition with time is obtained from core samples of a Wyoming glacier.

1.6 *Measurement of atmospheric mercury deposition via chemical kinetics*

The atmospheric lifetime of mercury *as measured by oxidation kinetics* yields shorter lifetimes, much shorter than six months. It is important to note that atmospheric mercury concentrations are very stable despite fluctuations from rising anthropogenic emissions and variable natural ones (figure 1-1). Either there exists a fast equilibrium between ground and air or mercury has a sufficiently long lifetime to "smear out" over the global atmosphere. For instance the stable vertical profile of mercury implies a long atmospheric lifetime [47] yet hourly concentrations of $Hg^0(g)$ over snowpacks [48] and $Hg^0(aq)$ in lakes [49] show diurnal behavior.

If the dynamics of atmospheric mercury are fast, then mercury cycling is governed by the kinetics of oxidation. We have already established that mercury does not passively

equilibrate between land and air; aqueous concentrations are far too high for this to be true. We now review the deposition flux estimates over land and snow.

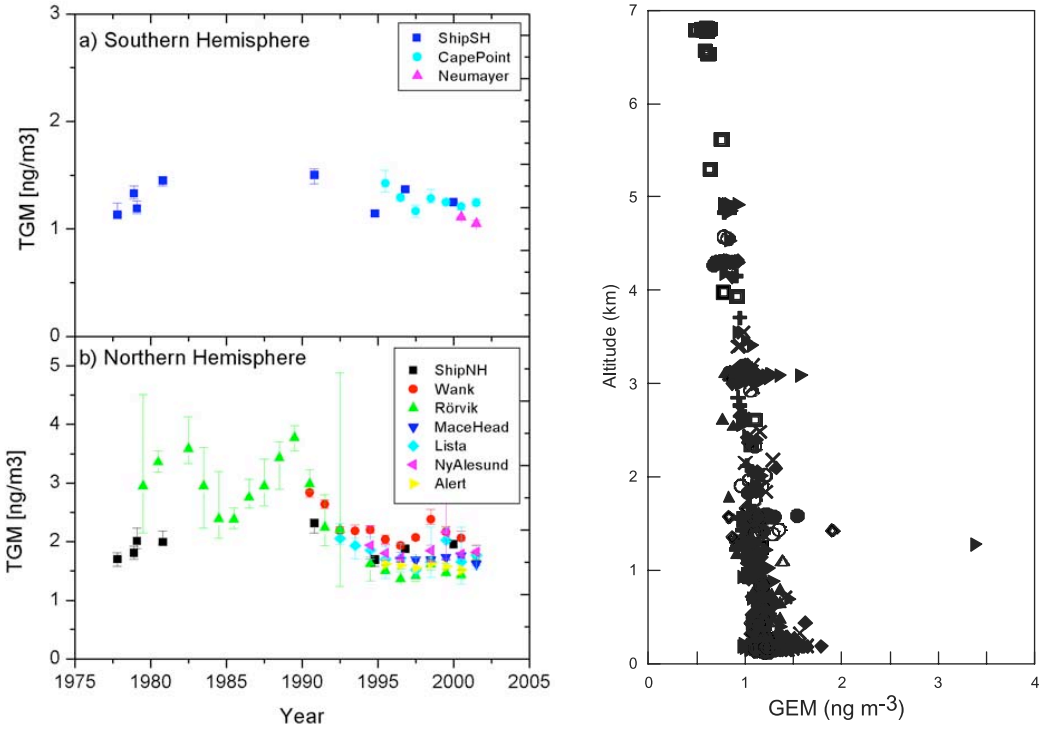

Figure 1-2 Globally consistent mercury levels. Historic total gaseous mercury (TGM) concentrations in the southern (top left) and northern (bottom left) hemispheres of the Atlantic ocean measured between 1977 and 2002 [7]. On right: Vertical profile (0.1 to 7 km) of gaseous elemental mercury (GEM) levels. Measurements were done over three weeks (Aug 24 – Sept. 16) of over Nova Scotia, Canada for the year 1995 [47].

In 1981, Slemr *et al.* recorded the remote background mercury levels over the north and south Atlantic Ocean to be 1.6 and 1.0 ng m^{-3}, respectively [50]. His measurements agree well with recent values [51]. He also estimated mercury's atmospheric lifetime was 0.9 years [38] as a function of the difference between the north and southern hemisphere gradients.

In 1985 Linqvist acquired aqueous mercury concentrations across the globe; concentrations of total aqueous mercury were found to be 0.5-3 ng/l in the open ocean, 2-15 ng/l in coastal seawater, and 1-3 ng/l in rivers and lakes [52]. Mercury speciation of soil samples confirmed that most long-term deposited mercury is typically sulfate- or organically-bound [53]. Aqueous mercury was subdivided into reactive (HgX_2, HgX_3^-, HgX_4^{2-}, X = Cl, OH, Br) and non-reactive (CH_3HgCl, CH_3HgOH) varieties. Mercury oxide (HgO) was listed as 'reactive' but specific to aerosols.

A significant discovery was that mercury levels in rainwater were far higher than predicted by Henry's law partition coefficients [50]. If gaseous mercury were in equilibrium with lake water, aqueous concentrations would have been close to 0.007 ng l^{-1} (assuming 2 ng m^{-3} Hg in air) an almost a 1000-fold difference! Uptake of gaseous mercury into lakes was therefore not though passive diffusion. Unexplained oxidation pathways were responsible for mercury scavenging in air.

Some possible routes of mercury oxidation were investigated. Ozone was of particular interest. Slemr had already corroborated his hemispheric-based lifetime estimate on the oxidation ozone but this value was low precision. A thorough investigation of oxidation pathways was needed as possible lifetimes ranged greatly [54].

More research was needed to determine which gaseous chemical reactions were involved in mercury scavenged and complicated by the little known about the speciation of anthropogenic emissions [52]. More studies were done to improve chemical kinetics. Schroeder's 1991 review found that mercury oxidation by $O(^1D$ and $^3P)$, O_3, NO_3, H_2O_2, or X_2 (X = Br, Cl) were all thermodynamically feasible but none had been studied in detail [55]. More emphasis was then placed on controlled laboratory kinetics such as for ozone, chlorine, and hydroxyl radicals. What laboratory kinetics revealed, especially for ozone,

was the lifetime of atmospheric mercury was surprisingly short, days or at most months. Schroeder's later 1998 review [56] acknowledged that mercury may be undergoing a global distillation, or a "grasshopper effect", with multiple cycles of deposition and re-emission. In 2005 a panel review regarding the state of atmospheric mercury knowledge concluded that "mercury redox chemistry varies dramatically in space and time, and uncertainties in those redox reactions and physical transformations significantly impact the ability to develop source/receptor relations" [4].

Emission inventories and the total atmospheric burden estimate the lifetime of mercury to be one year, but modern measurements of mercury show sudden losses in mercury concentrations [6]. Given the fluctuating deposition rates the lifetime of mercury is apparently more complex; mercury oxidizes and re-emits faster than the often-quoted one-year estimate would suggest. Laboratory kinetics provide a means of measurement for these regional fluctuations and permit atmospheric models to better explain mercury transportation cycling through chemical reactions [58, 59].

Mercury can form many oxides, including those with organics, halogens, sulfur and nitrogen oxides and shows an affinity to humic substances [60]. Concerning mercury (I) species, there is active discussion which surrounds the degree of stability received from binary pairs of Hg-X species in the gas phase [61] (i.e. Hg_2X_2 pairs with Hg-Hg bonds).

We will discuss more on ozone oxidation and the species HgO. This overview will be of primary importance to chapter 2 and provides support for the discussion that follows in chapters 3 and 4. Listed in table 1-3 and 1-4 are the collected physical properties of mercury oxide species that may have some role in the atmospheric cycling of mercury. The following section discusses the current state of knowledge of atmospheric oxidation pathways, in particular by ozone, nitrogen dioxide, and photolysis over titanium dioxide.

A

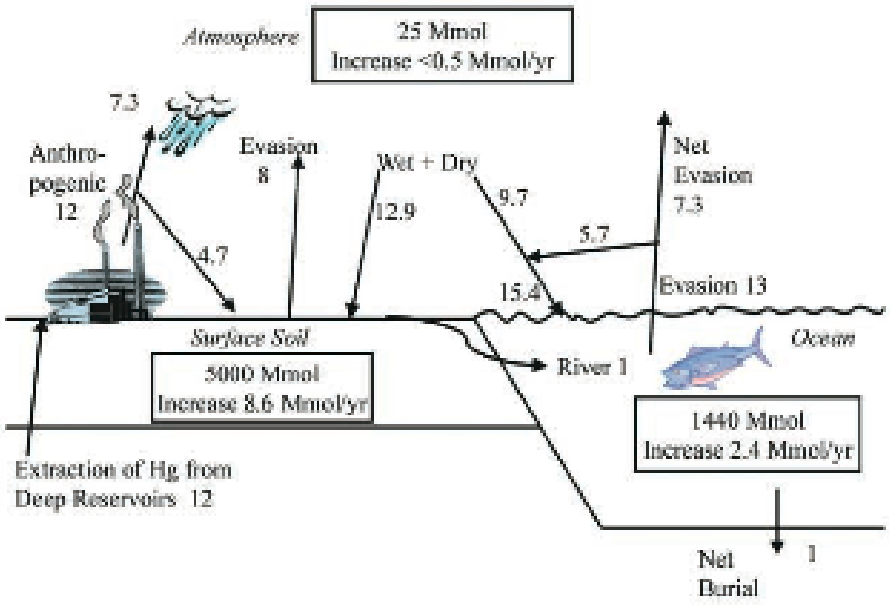

B

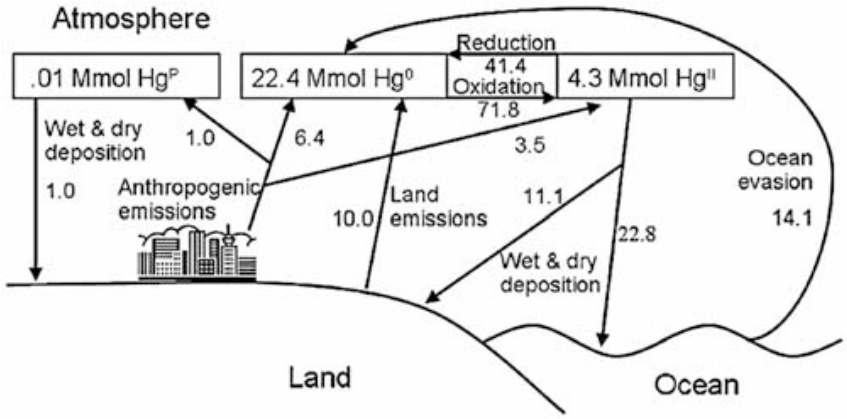

Figure 1-3 Current understanding of mercury pathways in the coupled atmosphere and ocean cycle: **A)** Mason and Sheu [29] **B)** Strode *et al.* [57]. Some confusion remains over the relative importance of wet/dry deposition, and atmospheric reduction and re-emission processes.

Table 1-3 Selected physical and chemical properties of mercury halides

	Hg_2F_2	HgF_2	Hg_2Cl_2	$HgCl_2$	Hg_2Br_2	$HgBr_2$	Hg_2I_2	HgI_2
Molecular Weight (g/mol)	439.18	238.59	472.09	271.50	560.99	360.40	654.99	454.40
Phys form	yel cub cry	Wh cub cry	Wh tetr cry	Wh orth cry	Wh tetr cry or powder	Wh romb cry or powder	Yel amorp powder	Red tetr cry or pow
Melting Point (°C)	-	-	-	276	-	236	-	259
Boiling Point (°C)	570 (dec)	645 (dec)	383 (sub)	304	340 (sub)	322	140 (sub)	354
Vapor pressure (Pa, 25°C)	?	?	-	0.16	-	$\sim 10^{-3}$	-	3.6×10^{-6} [62]
Solubility in water ($g_{HgX}/100g_{H2O}$, 25°C, pH 7) [63]	Sol, react w H_2O	Soluble, react w H_2O	4×10^{-4}	7.31	4.5×10^{-6}	0.61	2.4×10^{-8}	0.0055
K_{sp}	3.1×10^{-6}	-	1.3×10^{-18}	0.072	5.6×10^{-23}	6.2×10^{-20}	4.5×10^{-29}	2.9×10^{-29}
Henry's Law constant, K, (25°C, v/v)	-	-	?	2.9×10^{-8}	?	?	?	?
Density (g/cm^3)	8.73	8.95	7.16	5.60	7.31	6.03	7.70	6.28
-ΔH (kJ/mol, 25°C) [64]	485.4 ±10.5	422.6	263.2±0.8	sol: 230.1±2.3 gas: 149.0±2.7	204.2	169.5±1.3	119.0±0.8	105.4±1.7
ΔS (J/K*mol) [64]	80.3±8.4	116.3	95.8±0.8	sol: 144.5±0.4 gas: 288.7±1.7	109.4	170.3	120.6	170.7

Liq = liquid, sol = solid, gas = gaseous, dec = decomposition, sub = sublimates, "?" = data unavailable, "-" = not applicable

Wh = white, cry = crystals, cub = cubic, tetr = tetragonal, romb = rombic, amop = amporphous, pow = powder

Table 1-4 Selected physical and chemical properties of certain mercury compounds

	Hg(l)	**HgO**	**HgS**	**Hg_2SO_4**	**$HgSO_4$**	**$Hg(NO_3)_2$**	**$Hg(CH_3)_2$**	**$HgClCH_3$**
Molecular Weight (g/mol)	200.59	216.59	232.66	497.24	296.65	324.60	230.66	251.1
Phys Form	Heavy silv liq	Red or yel orth cry	Red hex cry, blk cub cry	Wh-yel cry pow	Wh monocl cry	Col hyg cry	Clear liq	Wh cry or pow
Melting Point (°C)	-38.72	-	red → blk at 344	-	-	79	-43	170
Boiling Point (°C)	256.73	500 dec	583 sub	335-500 (dec)	530-720 (dec)	160 (dec)	93	-
Vapor pressure (Pa, 25°C)	0.27	HgO ⇔ Hg: 9×10^{-12}	-	-	-	?	1.5	-
Solubility in water ($g_{HgX}/100g_{H2O}$, 25°C, pH 7) [63]	5.6×10^{-6}	5.1×10^{-3}	3×10^{-25}	0.051	Reac w water	Soluble, react w water	0.1	0.01
K_{sp}	2.8×10^{-7}	3.6×10^{-26}	blk: 2×10^{-53} red: 2×10^{-54}	7×10^{-7}	-	-	2×10^{-5}	2×10^{-7}
Henry's Law constant (v/v)	0.29	-	-	-	?	-	0.31	1.9×10^{-5}
Density (g/cm^3) [65]	13.579	11.14	Blk: 7.70 red: 8.17	7.56	6.47	4.3	3.19	4.06
-ΔH (kJ/mol, 25°C) [64]	Liq: 0 Gas: -61.4	90.8 ± 0.8	53.3±4.2	743.1±10.5	704.2±10.5	?	liq: -61.8±3.9 gas: -94.4±0.9	?
ΔS (J/K*mol) [64]	Liq: 75.9 Gas: 175.0	70.2±0.4	82.4±2.1	200.7±0.4	140.2	?	?	?

Liq = liquid, sol = solid, gas = gaseous, dec = decomposition, sub = sublimates, hyg = hygroscopic, "?" =data unavailable, "-" = not applicable

Wh = white, blk = black, yel = yellow, col = colored, silv = silver, cry = crystals, cub = cubic, pow = powder

1.7 Ozone and mercury $Hg_{(g)} + O_{3(g)} \rightarrow HgO_{(g)} + O_{2(g)}$

In 1949 the rate oxidation between gaseous mercury and ozone was approximately known [54]. Below is the net reaction and associated rate constant:

$$Hg_{(g)} + O_{3(g)} \rightarrow HgO_{(s)} + O_{2(g)} \qquad \text{Eq. 1-1}$$

$$-\frac{d[Hg]}{dt} = k[O_3][Hg] \qquad \text{Eq. 1-2}$$

Mercury can also react significantly faster with ozone (10 ~ 10^5 times faster) when in the presence of water [66, 67], which could be also interpreted as faster uptake by water with ozone. Compared with dry conditions, mercury uptake on water droplets is significantly enhanced, increasing atmospheric deposition rates and may explain the apparent high concentrations of mercury in rain.

The reaction between mercury and ozone was measured in earlier thermodynamic work [68], thought to yield $HgO_{(g)}$ as an intermediate:

$$Hg_{(g)} + O_{3(g)} \rightarrow HgO_{(g)} + O_{2(g)} \qquad \text{Eq. 1-3}$$

Schroeder states that "no unequivocal, recent data were available to us on the ultraviolet-visible absorption spectrum of $HgO_{(g)}$, hence its expected photochemical behavior in the troposphere remains unknown" [55]. $HgO_{(g)}$ was apparently reported to be quite stable in early experimental thermodynamic data, where the dissociation energy was measured to be D_0(HgO) = 221.1 ± 31 kJ/mol [68] and 268 ± 63 kJ/mol [69]. The bond strength was then found using computational thermodynamics to be much smaller, D_0(HgO) = 17 kJ/mol [70]. Calvert and Lindberg [71] point out the unlikelihood that such a low activation energy could be produced by a direct oxygen atom transfer. Hence gaseous mercury oxide is an unlikely species. Further

experiments failed to confirm the existence of gaseous HgO and doubt was cast on whether the original thermodynamics were in fact calculating a gas-phase species [55, 72].

P'yankov's study was the first to measure the oxidation rate constant between mercury and ozone [54]. Once ozone was proposed as potential major oxidative pathway for mercury, measuring this rate gained renewed focus. P'yankov's rate was reported as $k = 4.2 \times 10^{-19}$ cm^3 molecule^{-1} s^{-1} by Slemr [38], but then using the same data Schroeder interpreted the rate to be eleven times faster; $k = 4.9 \times 10^{-18}$ cm^3 molecule^{-1} s^{-1} [55]. Both rates predicted the atmospheric lifetime of mercury to be well below one year, at 44 days and 3.8 days, respectfully, assuming 25 ppb tropospheric ozone. Hall later re-measured the rate constant and obtained a value of $k = 3 \pm 2 \times 10^{-20}$ cm^3 molecule^{-1} s^{-1} [73]. For 25 ppb of ozone, the lifetime of mercury was then 1.7 years, apparently resolving the lifetime dilemma [20, 38]. This apparent resolution was short-lived as further laboratory experiments demonstrated the rate constant value was in fact closer to Slemr's original estimate. Pal and Ariya estimated the rate to be $k = (7.5 \pm 0.9) \times 10^{-19}$ cm^3 molecule^{-1} s^{-1} [74]. The rate constant was re-confirmed by Sumner *et al.* using a much larger chamber of (17 m^3), where $k = (6.4 \pm 2.3) \times 10^{-19}$ cm^3 molecule^{-1} s^{-1} [75].

Table 1-5 Lifetime estimate of gaseous atmospheric mercury assuming 25 ppb ozone (6.25×10^{11} molecules cm^{-3}) and the given rate constant

Rate $\times 10^{19}$ cm^3 molecule^{-1} s^{-1}	Hg lifetime (days)	Reference:
4.2	44	[38, 54]
49	3.7	[54, 55]
17	11	[66]
0.3 ± 0.2	617	[73]
$(7.6 \pm 3.5) \times 10^5$	2 seconds	[67]
7.5 ± 0.9	25	[74]
6.4 ± 2.3	29	[75]
Interhemispheric extrapolation	~330	[38]

Both Hall and Pal found the oxidation of mercury by ozone was a mixture of both homogeneous and heterogeneous behavior [73, 74]. The mechanism therefore included a gas-phase and surface (of the glass/flask) component:

$$Hg_{(g)} + O_{3(g)} \rightarrow HgO_{3(g)} \rightarrow HgO_{(g)} \qquad \text{Eq. 1-4}$$

$$Hg_{(g)} \rightarrow Hg_{(ads)} \qquad \text{Eq. 1-5}$$

$$O_{3(g)} \rightarrow O_{3(ads)} \qquad \text{Eq. 1-6}$$

$$Hg_{(ads)} + O_{3(ads)} \rightarrow HgO_{(s)} \qquad \text{Eq. 1-7}$$

Ozone reactions are now considered strongly associated to heterogeneous chemistry [76-78]. Hall anticipated this trend, suggesting "further research must be conducted on the order of reaction with respect to O_3; the effect of heterogeneous reactions on different surfaces such as glass, quartz, salt particles and soot" [79]. Pal and Ariya, however, found a linear correlation between the rate constant and ozone [74]. Hynes *et al*. noted that the oxidation by ozone, given the current understanding of its thermodynamics, could not possibly occur in the pure gas phase [80].

1.7.1 Mercury oxide (as a product)

Full decomposition of solid HgO into gaseous mercury occurs at 500ºC. As a solid, HgO crystals form as 'zig-zag' chains of $(\text{-Hg-O-})_n$, with near-linear O-Hg-O segments ($\angle$ = 179º), Hg-O-Hg angles of 109º and a Hg-O bond distance of 2.03 Å [81]. Yellow to red in colour, and sometimes brown when under high pressure conditions [82], the shade depends on mercury oxide cluster diameter. Red HgO can be formed by heating mercury and oxygen together on a surface at ~350ºC [79]. Yellow is formed by precipitation of Hg^{2+}(aq) [60].

Red and yellow mercury have similar solubility in water, 22.5 and 23.7 × 10^{-8} g/mol [83] and IR stretch frequencies shift slightly from 492, 575 cm^{-1} (yellow) to 480, 570 cm^{-1} (red) [82].

Raman stretch frequency of HgO is 325 cm^{-1} reported by [14], or 331 and 350cm^{-1} by [84]. Red HgO reacts at high temperatures (175-200ºC) with carbon monoxide to reduce back to Hg [85].

$$HgO_{(s)} + CO_{(g)} + \Delta \rightarrow Hg_{(g)} + CO_{2(g)} \qquad \text{Eq. 1-8}$$

This reaction will proceed at lower temperatures, at 95ºC for HgO(red) and 0ºC for HgO(yellow) [86].

Thermal decomposition of HgO is complex, and follows three distinct temperature regions: low 160-220ºC, intermediate 220-400ºC, and high 400-500ºC [72]. The vapour pressure of HgO at 20ºC is extremely low, and is debatable whether HgO itself rather than Hg is measured in the gas phase. High temperature decomposition is hypothesized to proceed via a two step gaseous process [72]:

$$HgO_{(s)} \rightarrow HgO_{(g)} \qquad \text{Eq. 1-9}$$

$$HgO_{(g)} \rightarrow Hg_{(g)} + O_{(g)} \qquad \text{Eq. 1-10}$$

Low temperature decomposition is a two step surface process:

$$2HgO_{(s)} \rightarrow Hg_2O_{(s)} + O_{(g)} \qquad \text{Eq. 1-11}$$

$$Hg_2O_{(s)} \rightarrow 2Hg_{(g)} + O_{(g)} \qquad \text{Eq. 1-12}$$

The mechanism of mercury oxide decomposition at atmospherically relevant temperatures has yet to be determined, but must have more in common with the ‘low’ temperature mechanism, which does not include HgO(g).

Several atmospheric reactions can result in HgO formation, but the most important is the oxidation by ozone. It is expected that the path from gas-phase to solid materials yields an exothermic reaction.

$$Hg_{(g)} + O_{3(g)} \rightarrow HgO_{(g)} + O_{2(g)} \qquad \Delta H_{rxn} \sim +22 \text{ kcal/mol} \qquad \text{Eq. 1-13}$$

$$HgO_{(g)} \rightarrow HgO_{(s,\ olig.)} \qquad \Delta H_{rxn} \sim -70 \text{ kcal/mol} \qquad \text{Eq. 1-14}$$

$$\text{Net: } Hg_{(g)} + O_{3(g)} \rightarrow HgO_{(s,\ olig.)} \qquad \Delta H_{rxn} \sim -48 \text{ kcal/mol} \qquad \text{Eq. 1-15}$$

Despite the importance of the mercury-ozone reaction, solid mercury oxide is rarely found in nature compared with $HgCl_2$, HgS, $HgSO_4$ and organically fixed mercury [53]. It is found that HgO will usually further oxidize to mercury sulfide or an organic-bound mercury.

In 1979, Butler *et al.* found products of mercury and ozone formed both HgO(s) and HgO_2(s) [87] at 10 K in an argon matrix. HgO_2 may either be a stable species or a blend of HgO and Hg [72]. It has been found that HgO(s) will slowly react with SO_2(g) to give a variety of mercury sulfates: i.e. $HgSO_4$, Hg_2SO_4, and $HgSO_4(H_2O)_2$ [88]. This was confirmed much later by Schofield in 2004 [14, 89]. Hall did not observe a reaction between Hg^0 and SO_2 (nor N_2O) [90], implying that HgO as a surface species may be more reactive than gaseous Hg^0. Mercury oxide (red) is known to undergo reduction by carbon monoxide at elevated temperatures (95 ~ 175 °C) [85, 86]:

$$HgO_{(s)} + CO_{(g)} \rightarrow Hg^0_{(g)} + CO_{2(g)} \qquad \text{Eq. 1-16}$$

1.8 *Mercury kinetics in coal power plants*

We have outlined that 2/3 of atmospheric gaseous mercury emissions are anthropogenic in origin. Of these 2000-3000 tonnes emitted annually, about 2/3 of these emissions are from combustion of fossil fuels [28]. Joensuu noted as early as 1971 that coal combustion was a source of atmospheric mercury pollution [91]. Billings and Matson then surveyed coal emissions in the United States and found untreated coal released 90% of the mercury contained therein [19]. In their estimate, a 700 MW plant could expel 2.5 kg of mercury per day. On

average the concentration of mercury in coal is small, about 0.2 ppm [92], however 3.2 billion tons of coal are annually consumed worldwide. Asia accounts for more than half of the coal consumed globally hence more than half of Hg emissions [28]. Clearly anthropogenic emissions are affecting the mercury cycle through combustion activity.

In all coal combustion processes, where temperatures exceed 500°C, gaseous mercury is the only stable species. As emissions cool below 500 °C various mercury oxides may form such as halides ($HgCl_2$) and sulfates (i.e. $HgSO_4$), depending on SO_2 levels [93]. Principally $Hg^0(g)$ dominates in the effluent gas. There is considerable discussion surrounding the chemical composition of the trace oxides emitted from coal.

Because of the higher sulfur content in certain coals (i.e. lignite) and the propensity of mercury to bind with sulfur (cinnabar; HgS), there is an apparent correlation between sulfurous coal and concentration of mercury emissions [14, 93].

It has become clear that in order to mitigate worldwide mercury levels in remote areas, a direct mitigation of mercury coal emissions is required. In March 2005 the U.S. EPA Clean Air Mercury Rule (CAMR) set to cap mercury emissions from coal-fired power plants. In March 2011 the proposed standards were aimed to capture 91% of mercury from coal emissions.

Mercury capture methods designs, if successful, could be profitable for the companies involved. Corporations such as ADA Technologies Inc. have been working with the U.S. EPA for using $Hg^0(g)$-adsorbing chemicals [94-96]. The cost of removing mercury is currently very high; estimates exceed $29,000 USD/lb of mercury [94, 97]. Granite and Presto estimate a cost of $50,000 - $70,000 per pound of mercury removed from emissions [98]. An efficient and cost-effective method for removing a *minimum* 70% of coal fire mercury is sought by the U.S. Department of Energy [99].

Given the high volatility of mercury, especially at elevated temperature, trapping it onto a surface with sufficient binding/adsorbing energy is vital. An early attempt to remove mercury from coal emission was by trapping $Hg^0(g)$ with gold-coated denuders [100]. This technique, which is useful for trace mercury detection, does not scale well given the high cost of gold. Other surfaces include sulfur, activated carbon and proprietary mixtures [94].

One of the main focuses in mercury oxidation in coal flue gases is by some form of surface trapping or heterogeneous oxidation. Norton *et al.* [101] provide a comprehensive survey of fly ash mixtures optimally suited to mercury removal, noting that NO_2, HCl, and SO_2 enhance oxidation when inserted in a flue gas line with catalytic beds.

Instead of trapping elemental mercury on a surface one may instead wish to oxidize mercury to a less volatile form such as HgO(s) or HgS(s). Oxidation to either $HgCl_2$ or $Hg(CH_3)_2$ is undesirable since both are quite volatile (see table 1-4 and 1-5). Oxidation to $HgBr_2$ is potentially viable however injection of bromine or bromine-containing compounds into a hot flue gas may not be ideal. A physical capture technique is by electro-catalytic oxidation: In this instance an electric discharge is emitted downstream, whereby mercury is oxidized to HgO in the resulting plasma [102].

Mercury oxidation can be achieved using inert surfaces that provide a catalytic surface on which to oxidize. These include palladium, vanadia (V_2O_5), titania (TiO_2), fly ash, activated carbon, and aluminum oxide (Al_2O_3) [98]. Schofield observed that almost any surface (of sufficient area) is capable of catalyzing mercury oxidation [14]. In a large-scale field test Blythe *et al.* [103] investigated the used of palladium catalytic converters in series with smokestack emissions. Emission reduction (oxidation) of $Hg^0(g)$ was 93% after 15 days, then dropped to 58% after 62 days. The results showed some difficulties with fly ash contaminating the catalytic bed.

The injection of airborne chemical additives and high-surface species can also promote mercury oxidation. These include NaCl or $CaCl_2$ particles (the chloride ion has an affinity to gaseous mercury oxides), Al_2O_3, TiO_2, or CaO all of which are components of fly ash [104, 105]. The inclusion of chloride may oxidize insoluble mercury to mercuric chloride, a volatile but water-soluble compound then scavenged by wet scrubbers. The inclusion of these species in the flue gas enhances the potential for HCl or other hazardous aerosols into the atmosphere. Concern may be raised whether mercury capture trades one hazardous emission for another. Chelating surfaces may also capture mercury [106], though selectivity and thermal stability can prove challenging.

Surface types affecting adsorption of mercury in fly ash carbon sample by Maroto *et al.* [107]. Carbon surfaces significantly enhance high-temperature reactions between mercury and oxygen [79]. High temperature experiments (T > 100 ºC) show increasing fly ash surface availability enhances $Hg^0(g)$ oxidation [108, 109]. Pavlish *et al*. point to the remaining uncertainties in comparing heterogeneous and homogeneous reactions [110], and stress that more emphasis should be placed on heterogeneous reaction mechanisms in future studies. Galbreath and Zygarlicke [105] propose a pre-adsorption of $Hg^0(g)$ and $O_2(g)$ as a heterogeneous capture mechanism, as well as Fe_2O_3 for its high surface area and ability to catalyze mercury oxidation via NO_x [111].

1.9 *UV Photolysis: titanium dioxide capture of mercury*

The oxidation of mercury by TiO_2 under UV light was first observed by Kaluza and Boehm in 1971 [112] who noted "a dark brown surface layer was formed in which HgO was identified" upon irradiating the TiO_2 surface with 390-420 nm UV light in the presence of liquid mercury. It had been noted that oxygen is necessary for this reaction to occur, and that

hydroxyl radicals formed on the surface from adsorbed water were the oxidant of mercury. As the hydroxyl radical are adsorbed to the surface the oxidation of mercury also occurs entirely on the titania surface.

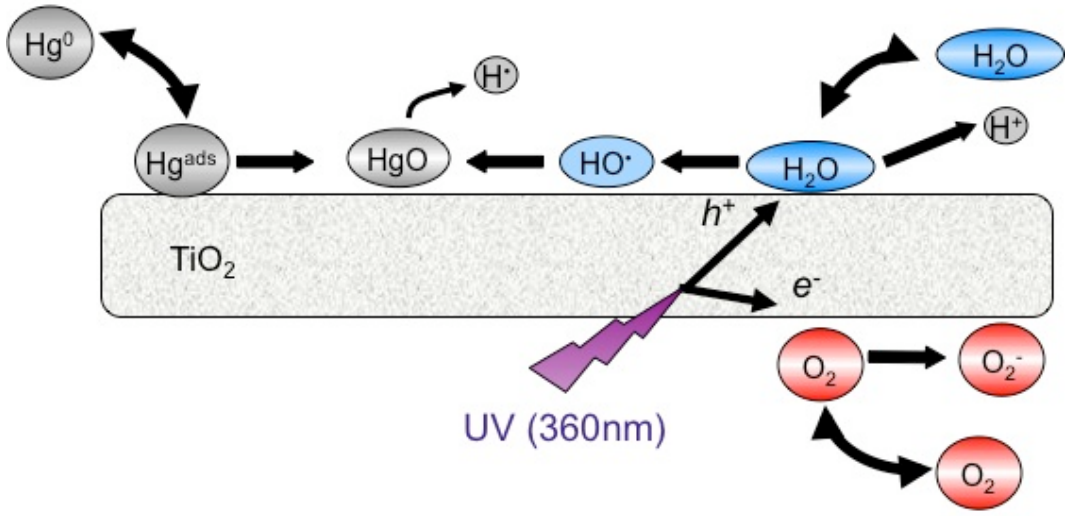

Figure 1-4 Oxidation of mercury through adsorption on a titania (TiO_2) surface. According to Langmuir-Hinshelwood kinetics, a semi-equilibrium exists between the surface ($X_{(ads)}$) and gaseous ($X_{(g)}$) products, where X = H_2O, O_2, Hg. Photons of wavelength < 380 nm (3.2 eV) strike the TiO_2 surface generating an electron-hole pair. The positive 'hole' oxidizes water, which in turn oxidizes Hg^0(ads) oxide. Oxygen traps the free electron creating a superoxide radical.

Oxidation of mercury by TiO_2 gained further interest when mandates were set to reduce coal mercury emissions. Prior to interests in capturing mercury in coal emission, early studies characterized the uptake of aqueous oxidized mercury by TiO_2. Results were generally successful. For a TiO_2 powder suspended in water under 296 nm UV light, greater than 98% of Hg(II) was scavenged [113]. Ruthenium-dyed TiO_2 also oxidized aqueous mercury efficiently [114]. Aqueous oxidation is more complex than atmospheric scavenging since both oxidation

and reduction processes may occur, i.e. the reduction of Hg(II) is possible by the free electron generated in titania [115].

The earliest study to explicitly propose gaseous mercury oxidation in flue gases using TiO_2/UV light was in 1998 [116]. Hg^0 uptake on the titania *in situ* particles was high at 84 – 96% and products were identified as HgO. Their results were difficult to generalize since titania was produced as an aerosol in the gas stream and not on a fixed surface.

The first study to include detailed surface kinetics was performed by Rodriguez *et al.* [117] who also analyzed the influence of water on the uptake of mercury over titania. Hydroxyl radicals are required for mercury oxidation hence water vapor is a reaction prerequisite however the influence of water becomes competitive with mercury at higher concentrations.

More recent studies have looked at the titania surfaces themselves to determine the optimal coating procedure and structure [118, 119]. Lee and Hyun [118] measured the fractal dimension of titania particles. They found larger particles (baked at higher temperatures) enhanced mercury uptake on the surface. This study suffers the same difficulty of comparison since mercury uptake is measured using percent captured. Sol-gel methods, where TiO_2 is blended with SiO_2, were shown to be successful at mercury scavenging as well [120].

Recent work on titania is to shift the band gap into the realm of visible light absorption by n and/or p doping. Zhu *et al.* found that co-doping TiO_2 with chromium and nitrogen doping, may shift the band gap shift from 3.2 eV to below 2.5 eV [121]. Coating manganese oxide on top of titania has also been shown to spontaneously oxidize mercury at elevated temperatures (200 °C) [122]. A considerable body of literature is available on the topic of band gap lowering of titania [123].

1.10 Mercury oxidation, $Hg^0_{(g)} + NO_{2(g)}$

High levels of nitrogen dioxide are predominantly found in the emissions of coal fire power plants ([NO_x] = 300 - 400 ppm [124]). Natural sources of NO_x include lightning storms in the upper troposphere, which accounts for 2 – 20 Mt/yr. Mercury and NO_2 can be closely linked during the post-combustion stages of coal, especially in methods of removal. NO_2 emissions are reduced by selective catalytic reduction (SCR) technology, whereby ammonia gas and a surface of V_2O_5/WO_3 (supported over a bed of TiO_2) reduces NO_x (NO_2 + NO) into nitrogen gas and water:

$$2NO_{2(g)} + 4NH_{3(g)} + O_{2(g)} \rightarrow 6H_2O_{(g)} + 3N_{2(g)} \qquad \text{Eq. 1-17}$$

$$4NO_{(g)} + 4NH_{3(g)} + O_{2(g)} \rightarrow 6H_2O_{(g)} + 4N_{2(g)} \qquad \text{Eq. 1-18}$$

Removal of NO_x from flue gas can be as much as 90% between 360 °C and 450 °C [93]. SCR catalysts have been in use in utility boilers for decades, but only recently have they been found to oxidize mercury as well [98]. A trade-off is necessary: increasing ammonia levels will decrease mercury capture. Products studies are surprisingly scarce but NO_2 and Hg apparently do not directly interact except for a competition of surface sites.

In contrast with SCR reactions, oxidation of gaseous mercury by nitrogen dioxide is not a surface-dependent reaction [125]:

$$Hg^0_{(g)} + NO_{2(g)} \rightarrow \text{products} \qquad \text{Eq. 1-19}$$

The rate law gives third-order overall rate, second order with respect to NO_2:

$$-\frac{d[\mathrm{Hg}]}{dt} = k[\mathrm{NO_2}]^2[\mathrm{Hg}] \qquad \text{Eq. 1-20}$$

where $k = 2.8 \pm 0.5 \times 10^{-35}$ cm^6 $molecule^{-2}$ s^{-1} at 20°C [125]. The rate of this reaction decreases with increased temperatures, suggesting a complex reaction mechanism, possibly involving the

dimer N_2O_4 [125]. Details of the reaction mechanism for Eq. 1-19 are discussed in chapter 4 where it is argued oxidation accomplished by a two-step addition of NO_2. A surface-based analog of the Hg + NO_2 reaction (on a bed of TiO_2) will also be discussed.

1.11 *Kinetic reduction processes of mercury oxides by abiotic means*

In contrast to the gaseous kinetics of mercury oxidation, reduction processes are mechanistically poorly defined and more controversial. Reduction of mercury +1 or +2 species must be caused by an input of energy into the system -be it light, heat, or bacterial in nature- to result in the reduction of mercury from Hg(II) to Hg^0. Once reduced, elemental mercury will return to the global tropospheric cycle. Major gaseous atmospheric inputs include: volcanic eruptions [39], water or snow surfaces energized with sunlight (i.e. 'light reduction') [126], bacterial metabolic processes (i.e. 'dark reduction') [127], forest fires [128], natural emission from soils [129], and anthropogenic coal combustion or incineration [130]. Since bacteria are often more active in daylight, photo-reduction would be coincident with bacterial reduction [131]. Discussion surrounds possible evidence of pure chemical reduction processes occurring independently of photo-assisted pathways. In particular focus after the first few seconds or minutes after a volcanic eruption [76] or coal stack emission [132].

It can be agreed that gaseous oxidized mercury (GOM) must remain stable long enough to deposit onto plants, soil, lakes, or other surface. However these 'intermediate' forms of mercury could be susceptible to reduction. Some forms airborne Hg(II) include $HgSO_3$(aq), $HgBr_2$ or HgO(s), and may appear to convert spontaneously to Hg^0 under certain conditions. This is one way to increase what is interpreted to be the global lifetime of mercury. The reduction of chemically unstable intermediate mercury species such as HgO(g), HgBr(g), or $Hg(OH)_2$(g) is not considered a proper reduction mechanism as these species will quickly form

the more stable species HgO(s), $HgBr_2$(s) and $Hg(OH)_2$(aq), respectively. Hence these latter three species are then the possible sources for chemical reduction. The reduction of HgO by CO can take place at temperatures above 100 °C [86] and possibly at lower temperatures but at atmospherically unrealistic CO concentrations .

Mercury oxides may be reduced by $HO_2\cdot$ [133]. The peroxide radical is found at 5 – 10 ppt concentrations in the troposphere during mid-day or in aerosols, and the reduction is proposed to occur in a two step process:

$$HO_{2(g)} + Hg(II)_{aq} \rightarrow Hg(I)_{aq} + O_{2,aq} + H^{+}_{(aq)} \qquad \text{Eq. 1-21}$$

$$HO_{2(g)} + Hg(I)_{aq} \rightarrow Hg^{0}_{aq} + O_{2,aq} + H^{+}_{(aq)} \qquad \text{Eq. 1-22}$$

However Wang *et al.* point that Hg(II) reduction by $HO_2\cdot$ must be considered together with the plethora of oxidation reactions, such as by OH and bromine [134]. Qualitatively speaking Hg^0 can be oxidized by many routes but Hg(II) is reduced by comparatively few.

A second chemical reduction process, and the most widely proposed for chemical reduction in aerosols, is the reduction of mercury(II) by sulfates. Munthe *et al.* [135] found that $Hg(SO_3)_2$(aq) would decompose and reduce to Hg^0 under 230 nm UV light at a rate inversely proportional to the concentration of HSO_3^- (pH = 3). They have conjectured that when sulfuric acidified aerosols are subjected to intense sunlight mercury(II) could be revolatilized as gaseous Hg^0. This mechanism was cast to doubt by van Loon *et al.* [136] who found Hg^0 would nevertheless bind strongly to dissolved SO_2, effectively preventing loss of gaseous mercury in aerosols. Although SO_2 does not react strongly with Hg this does not entirely preclude a role for sulfur. Such reduction would have to be fast; mercury, once scavenged by aerosols, would precipitate out of the troposphere in a matter of hours or days.

Chemical reduction processes are often discussed in coal emissions. Several studies have noted a decrease between the relative concentration of oxidized mercury to elemental mercury between stack and downwind measurements [132, 137]. Lohman *et al.* show there is more elemental mercury downwind compared with SO_2 levels than what would be expected from dilution [137].

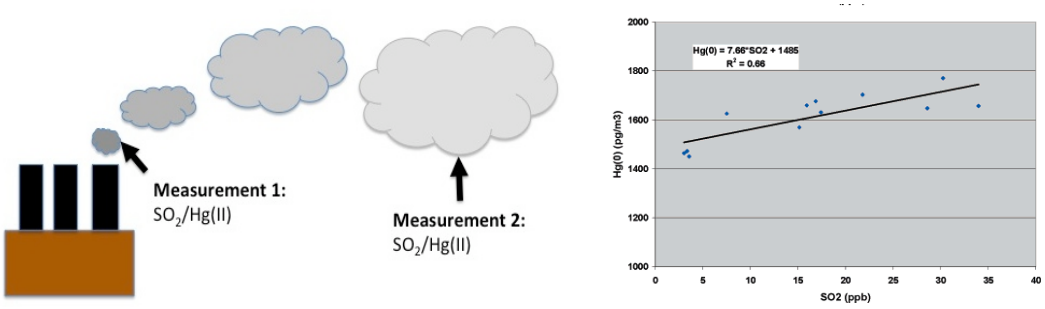

Figure 1-5 Stack emissions measurements from multiple points emitting from a coal fire power plant. It is found that Hg(II) decreases with distance from the plume faster than dilution would seem to account. The graph (right) shows a slight positive correlation between gaseous elemental mercury (GEM) and SO_2 [132].

Prestbo and Gay [138] measured Hg deposition over ten years and did not find SO_2 and total mercury deposition fluxes to be well correlated. Because of these measurement uncertainties, the decrease in relative gaseous oxidized mercury (GOM) between stack and plume measurements is not well understood and a logical mechanism cannot be provided. If reduction processes are in fact real, they do not appear to dependend on aerosol composition or size [139]. GOM uptake by particulates may therefore be more easily explained as dominantly defined by oxidation processes.

The reduction of mercury oxide in the presence of sulfur dioxide was also suspected to occur [140]

$$HgO_{(s)} + SO_{2(g)} \rightarrow Hg^{0}_{(g)} + SO_{3(g)} \qquad \text{Eq. 1-23}$$

The reaction is slightly endothermic at room temperature (ΔH = + 53.3 kJ/mol [65]), so that it is unlikely to proceed. The slow oxidation of HgO by SO_2 does appear to occur [88]. Mercury is likely oxidized into $HgCl_2$ or $HgSO_4$ by HCl(g) and SO_2(g) [98], respectively. Mechanistic studies argue that high capture rates require the presence of both gases [14]. SO_2 alone may in fact *decrease* a sorbent's capture efficiency [141] and conversely sub-bituminous (low-sulfur) coal yields low rates of mercury oxidation [93]. As a possible final product, the low vapor pressure of $HgSO_{4(s)}$ could potentially clog an SCR catalyst over time, whereas $HgCl_{2(s)}$ could revolatilize and, given its high solubility, be captured in a downstream wet scrubber (or escape into the atmosphere).

1.12 Summary of Kinetics

The kinetics of mercury reactions, historically focused on the oxidation of methylmercury (CH_3HgX, X = Cl, OH, CH_3) species, then later expanded to oxidation and transport of inorganic mercury species. It was found that since methylmercury originated from biota near inland locations. But methylmercury species have lifetimes on the order of a few hours, insufficient time to escape to the atmosphere. Reduction of Hg(II) to gaseous mercury is thought to be a significant reduction pathway.

The reaction between $Hg^{0}_{(g)}$ and $O_{3(g)}$ was investigated and it was found accelerated by the presence of liquid water. The lifetime of mercury as defined by ozone oxidation is measured to be under a month even in dry conditions.

Mercury oxidation by $NO_{2(g)}$ is very fast at very high concentrations (> 500 ppm) but negligible at ambient levels due to its second-order dependency on NO_2. The mechanism and product of this reaction are both discussed in chapter 4.

Titanium dioxide, when exposed to ultra-violet light, is a known oxidant of many gaseous organics. It has been recently explored as a novel candidate to removes gaseous mercury from coal fire power plants and studies show such scavenging reactions could be effective in capturing mercury as HgO(s).

Reduction rates are a major component and counterpart to fast mercury cycling via oxidation as there would be little cycling without them. The major non-biological inputs of mercury into the atmosphere are combustion related. Re-emission of oxidized mercury is controlled by photoreduction in lakes and soils and may be assisted by reducing photo-active bacteria [142].

Table 1-6 lists the principal oxidants of mercury in the atmosphere, in particular ozone and bromine and implies mercury has a lifetime of a few months. Since the net mercury lifetime is over one year the discrepancy between these lifetimes implies a complex oxidation and re-emission cycle of mercury. Re-emission and total emission inventories are difficult to measure precisely therefore deposition flux measurements remain an evolving field. Only through laboratory mercury kinetics allow for a better understanding of the life cycle of mercury.

Table 1-6 A summary of atmospheric mercury lifetimes, assuming oxidation by species [X] only. The lifetime of mercury for many species is less than the one-year net lifetime. This discrepancy implies a more complex oxidation cycling route for atmospheric mercury regardless of the precise reduction mechanisms of scavenged mercury.

Atmospheric Oxidants*	Hg lifetime	Reference
[NO_2]		
30 ppt (remote marine/forest)	2.0×10^9 years	[143]
1 ppb (rural)	1.8×10^6 years	
1000 ppb (urban)	1.8 years	
500 ppm (flue gas)	>3.8 minutes	
[Br]		
0.4-4 ppt (remote)	3.3 ~ 0.33 days	[144]
[BrO]		
1-2 ppt (remote)	46 ~ 23 days	[144]
20 ppt (MDEs, Arctic)	2.3 days	[144]
120-170 ppt (MDEs, Dead Sea)	9.2 ~ 6.5 hours	[77, 144]
[OH]		
4-40 ppq	1280-128 days	[145]
[O_3]		
20 ppb (remote)	37 days	
100 ppb (rural)	7.5 days	[146]
400 ppb (urban)	1.9 days	

*$[Hg]_{remote}$ ~ 0.2 ppt.. For $\tau_X = ([X]k_X)^{-1}$, $k_{O3} = 6.2 \times 10^{-19}$ cm^3 $molec^{-1}$ s^{-1} [147], $k_{Br} = 3.6 \times 10^{-13}$ cm^3 $molec^{-1}$ s^{-1} [148], $k_{NO3} < 4\text{-}7 \times 10^{-15}$ cm^3 $molec^{-1}$ s^{-1} [75, 149], $k_{BrO} \sim 10^{-14}$ cm^3 $molec^{-1}$ s^{-1} [150]. Oxidant concentrations were obtained from [146]. MDE = Mercury depletion event

1.13 Instrumentation: Detection of mercury

Detecting mercury at environmental concentrations remains a challenge. Concentrations in the air are typically 1.5 ng m^{-3} (0.2 ppt), requiring a minimum limit of detection (LOD) of 0.15 ng m^{-3} (0.02 ppt), i.e. the limit of quantitation. Particulate and gaseous oxidized mercury concentrations vary, but reach 1-10 pg m^{-3}. Often both change rapidly, and require time resolutions of hours, often minutes, sometimes seconds for accurate kinetics. Concentrations in

water are often less than 1 ng/l and 0.1 ppm in soil. Hair, samples range to 0.1 ppm (by weight) to 100 ppm for highly contaminated individuals. 'Background' blood and urine concentrations are usually < 1 μg/l.

Prior detection of mercury consisted of using cold vapour atomic absorption spectroscopy (CV-AAS) with a detection limit of 20 pg [151]. If sufficient preconcentration is used, detection limits of about 2 ng Hg/m^3 are possible.

Cold-vapour atomic fluorescence detection (CVAFS) has detection limits for Hg^0, $(CH_3)_2Hg$ and CH_3HgCl of 0.3, 0.4 and 2.0 pg, respectively [152]. This requires using a double gold trap, whereby mercury is preconcentrated onto the first gold trap, desorbed (with applied heat of 500°C) then amalgamated to a second trap under an ultra high purity (UHP) mercury-free argon gas. The second trap desorbs the mercury and passes under UHP argon into a fluorescence detector. A typical collection uses 5 minutes of air sampling at 1 l/min. The limit of detection is 0.1 ng/m^3. The commercial version of this instrument is the Tekran Mercury Analyzer 2600 series, which is used in our laboratory.

Mass spectrometry electron ionization (MS-EI) was can be used for very high concentrations of mercury near saturation levels, between 400 – 12,500 μg m^{-3} (50 – 1500 ppb). Air injection volumes of approximately 200 μl are recommended. As electron ionization is a high-energy impact form of ionization, chemical mercury species are typically highly fragmented.

Our lab uses the Hewlett Packard (HP) 5973 Mass Spectrometer preceded by the HP 6890 Gas Chromatogram for the study of gaseous elemental mercury. Mass spectrometry is set to single ion monitoring (SEM) to identify the five major isotopes of mercury; m/z = 198-202.

1.14 Research objectives

The aim of this thesis is to better quantify, understand and distinguish heterogeneous and homogeneous mercury oxidation kinetics. Surfaces are always present both in laboratory and environmental mercury studies and need to be quantified. Surface-enhanced kinetic processes require identification using replicable rate constants. Many studies exist on mercury oxidation but few support detailed mechanistic explanation for mercury oxidation. We establish mechanistic parameters for mercury oxidation by

i) ozone

ii) titania and UV light

iii) nitrogen dioxide

For these kinetics processes listed we manipulate the bath gas (nitrogen and air), surfaces present (TiO_2, halocarbon wax or liquid water), surface-to-volume ratios, and presence of other trace pollutant gases (SO_2 and NO_2). Understanding, quantification and simplification of gaseous mercury reactions are the overreaching goals of this study.

Chapter 2

Effects of Relative Humidity and CO(g) on the O_3-initiated Oxidation Reaction of Hg^0(g): Kinetic & product studies

Contributions by author:

This paper summarizes our work on further studying gaseous mercury oxidation by ozone. The subject is of interest to the studies of atmospheric mercury since mercury-ozone oxidation is known to be deceptively complex, and may involve change drastically due to surface conditions and the nature of the gaseous chemical composition. Pal and Ariya [74] measured the oxidation of mercury by ozone using the relative rate method and conducted preliminary work of surface effects on the rate of reaction. There was evidence for surface enhancement though a change in surface-to-volume ratios.

The present paper measures the absolute oxidation rate constant under variable flask volume and surfaces, as well as variable ozone and mercury concentrations. We varied the levels of humidity up to saturation and included carbon monoxide. My contribution to the paper was in measuring all of these effects on mercury-ozone kinetics and to examine likely kinetics mechanisms. Mercury concentrations were monitored by gas chromatography mass spectrometry; sample mercury signals are shown in the appendix. For the first time we observed the effects of a second gas in the system (CO) and showed gaseous water had no effect on the rate, only liquid water. For further details on the setup of mercury kinetics, the appendix includes a detailed schematic of the reaction system.

This paper is reproduced in full by permission of the Royal Society of Chemistry (**DOI:** 10.1039/B801226A).

Manuscript published in Physical Chemistry Chemical Physics

Effects of Relative Humidity and CO(g) on the O_3-initiated Oxidation Reaction of Hg^0(g): Kinetic & product studies

Graydon Snider, Farhad Raofie, and Parisa A. Ariya*

Departments of Chemistry and Atmospheric and Oceanic Sciences

McGill University, 801 Sherbrooke St. W.

Montreal, PQ, CANADA, H3A 2K6

**Corresponding author's email: parisa.ariya@mcgill.ca*

Abstract

Ozone is assumed to be the predominant tropospheric oxidant of gaseous elemental mercury ($Hg^0(g)$), defining mercury global atmospheric lifetime. In this study we have examined the effects of two atmospherically relevant polar compounds, $H_2O(g)$ and CO(g), on the absolute rate coefficient of the O_3-initiated oxidation of $Hg^0(g)$, at 296 ± 2 K using gas chromatography coupled to mass spectrometry (GC-MS). In CO-added experiments, we observed a significant increase in the reaction rate that could be explained by pure gas-phase chemistry. In contrast, we found the apparent rate constant, k_{net}, varied with the surface-to-volume ratio (0.6 to 5.5 L flasks) in water-added experiments. We have observed small increases in k_{net} for nonzero relative humidity, RH < 100%, but substantial increase at RH ≥ 100%. Product studies were performed using mass spectrometry and high resolution transmission electron microscopy coupled to an electron dispersive spectrometer (HRTEM-EDS). Our results give evidence for enhanced chain growth of HgO(s) on a carbon grid at RH = 50%. A water/surface/ozone independent ozone oxidation rate is estimated to be $(6.2 \pm (1.1; t\sigma/\sqrt{n}) \times 10^{-19}$ cm^3 $molec^{-1}$ s^{-1}. The total uncertainty associated with the ensemble of experiments amount to approximately ≤ 20%. The atmospheric implications of our results and the effect of an added reaction partner in homogeneous and heterogeneous atmospheric chemistry will be discussed.

2.1 Introduction

Elemental mercury is a very toxic heavy metal in the Earth's ecosystem. Estimates of the tropospheric lifetime of gaseous elemental mercury, $Hg^0(g)$, range between 0.7-1.7 years [36, 37, 52, 153, 154] with a ~ 98% [155-157] abundance relative to particulate (Hg_p) and oxidized (Hg(II)) mercury. Recent studies in the marine boundary layer and in the polar-regions indicate that mercury lifetimes can be much shorter, potentially due to the presence of reactive halogen oxidants [59]. Background concentrations in the northern hemisphere have been measured at 1.3 – 1.7 ng m^{-3} (0.16 – 0.21 *parts per trillion*) [158]. Mercury is eventually removed from the atmosphere through wet and dry deposition [52, 159].

In our previous laboratory studies we focused on the oxidation of elemental mercury by halogens, halogen oxides (XO; X= Cl, Br, I), $OH^{\bullet}$, and ozone[74, 160-162]. In those experiments we varied temperature, photochemical sources, different surfaces, chemical probes, scavengers, and reactant concentrations to obtain several mercury oxidation rate constants. Among these oxidants considered, ozone was regarded as the among the most important mercury-depleting compounds in the troposphere outside marine or polar regions.[52]

Previous studies have shown that the apparent rate constant for the oxidation of $Hg^0(g)$ can be increased if water is present; Menke and Wallis[163] found the rate of mercury oxidation by chlorine will triple when increasing RH to 80%. A later study by Lindqvist and Iverfeldt [66] observed that the presence of liquid water and ozone together will enhance deposition of $Hg^0(g)$. The mechanism of this water catalysis, whether through aerosols or the gas-phase, remains imprecise.

We have previously studied ozone-addition with elemental mercury under dry conditions [74]. The net reaction is written:

$$Hg^0_{(g)} + O_{3(g)} \xrightarrow{k_{net}} HgO_{(s)} + O_{2(g)} \qquad \text{Eq. 2-1}$$

Calvert and Lindberg[71] suggest reaction (1) could proceed by an addition of ozone, followed by a re-arrangement into the linear species OHgOO:

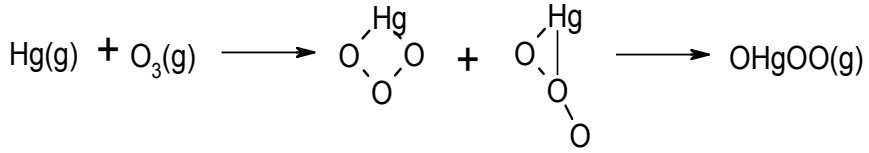

Eq. 2-2

The reaction may be followed by dissociation into O_2 and HgO(g), the latter precipitating immediately to HgO(s).

$$OHgOO_{(g)} \rightarrow HgO_{(g)} \rightarrow HgO_{(s)} \qquad \text{Eq. 2-3}$$

The dissociation and precipitation are essentially irreversible steps.

The apparent rate constant, k_{net}, reaction (1), was previously found by our group [74] to be $(7.5 \pm 0.9) \times 10^{-19}$ cm^3 molecule^{-1} s^{-1}, in good agreement with Sumner *et al.* [75]: $(6.4 \pm 2.3) \times 10^{-19}$ cm^3 molecule^{-1} s^{-1} (performed in a much larger 17 m^3 chamber where heterogeneous reactions were significantly reduced by a decrease in the surface-to-volume ratio). Our rate constant was found to be larger than an earlier study by Hall [73] $(0.3 \pm 0.2) \times 10^{-19}$ cm^3 molecule^{-1} s^{-1}, and smaller than both Schroeder's [156] value, 49×10^{-19} cm^3 molecule^{-1} s^{-1} (no error reported), and Iverfeldt's [66] value, 20×10^{-19} cm^3 molecule^{-1} s^{-1} (no error reported).

Our present experiment evaluates the effect of the third bodies, H_2O and CO, on the apparent rate coefficient, k_{net}. The elementary reaction of interest is the reversible association of Hg^0(g) and O_3:

$$Hg^0_{(g)} + O_{3(g)} \leftrightarrow HgO_{3(g)} \qquad \text{Eq. 2-4}$$

where the intermediate HgO_3 is expected to decompose spontaneously and irreversibly into $HgO_{(s)}$.

$$HgO_{3(g)} \rightarrow \text{Products} \qquad \text{Eq. 2-5}$$

We quantify the dependence of k_{net} on $H_2O(g)$, O_3, CO, and trimethyl benzene (TMB), surface-to-volume ratios, and to the presence of a polymer wax coating. A product study is presented for reactions in both humid and dry conditions, and the best estimate for dry $O_3(g)$ + $Hg^0(g)$ reaction rate is provided. Some discussion on the implications for atmospheric mercury is presented.

2.2 Methods

2.2.1 Kinetic studies:

The apparent rate constant of the $O_3(g)$ + $Hg^0(g)$ reaction was determined by measuring the relative loss of [$Hg^0(g)$] via electron impact (EI) ionization mass spectrometry (HP-5973). The experiments were performed under near-atmospheric conditions (750-770 Torr, T =296 ± 2 K) in ultra high purity N_2. Experiments were carried out in 0.59, 1.1, 2.2, 3.1, and 5.5 l spherical Pyrex flasks supplied with a magnetic stirrer to stimulate mixing. The reaction flask was coated with MTO-Halocarbon Wax (Supelco) as an attempt to reduce surface adsorption of reactants, products, or reaction intermediates to lead undesired side and secondary reactions. Between runs, flasks were washed with concentrated nitric acid, scrubbed with a nylon brush with soap and water, washed with 18.2 MΩ milli-Q water, and then with HPLC-grade acetone.

Halocarbon wax was reapplied through a 10% solution (by weight) of HPLC-grade acetone and dried at 120^{o}C for > 1hour. Samples from then N_2-filled reaction chambers (without reactants) were taken and analyzed using GC-MS to preclude the existence of detectable residual impurities. To prepare reaction mixtures, the reaction chamber was evacuated to a pressure of *ca.* 5×10^{-2} Torr with a two-stage pump (Savant VP 190) and flushed with N_2 gas 3-5 times. Mercury vapour in equilibrium with liquid mercury (under UHP N_2) was transferred via

vacuum line to an evacuated wax-coated reaction flask, and filled to atmospheric pressure with nitrogen gas. The final concentration of mercury vapour in the reaction flask is calculated to be 1-2 ppm (1 ppm ~ 2.46×10^{13} molecule cm^{-3} at 298K and 1 atm). To add humidity in all flasks, milli-Q water (Millipore, 18.2 MΩ) was introduced via a liquid-tight 10 μL syringe (Hamilton series 1700) to the flask. As ozone and trace hydrocarbons may react to form radical by-products, the scavenger 1,3,5-trimethyl benzene (TMB) was included [164]. TMB was injected as a liquid (Hamilton series 700) and allowed to vaporize in the chamber for >30 minutes.

Ozone was produced using an ozone generator (model OL 100/DS, Ozone Services Inc.); the resulting O_3 mixture was then trapped in a *U*-shaped tube containing silica gel cooled to 195 K in a dry ice–acetone bath, and then transferred ozone to an evacuated flask. The ozone flask was brought to atmospheric pressure via UHP nitrogen. A UV-Visible spectrophotometer (Varian Cary-50 Bio) determined the concentration of ozone to be injected. Decay of ozone is negligible within the time-frame of the experiment (< 1% per hour). From Beer's Law, $A_{log10} = \varepsilon[O_3]\ell$ (where $\varepsilon_{\lambda=296.7nm} = (2.64 \pm 0.05) \times 10^{-19}$ cm^2 $molecule^{-1}$ [165], $\ell = 10.28 \pm 0.05$ cm), specific amounts of ozone were transferred to the reaction flask using a gas-tight syringe with relative uncertainties of 2% (1σ). A Teflon-coated hygrometer probe (MC-P, Panametrics) indicated RH < 0.1% for 'water-free' runs, and measured within ± 2% of expected values for RH = 10 to 90%. CO was obtained from a 99.99% pure gas source, filled into an evacuated flask, where the desired aliquots were taken.

We performed the separation of $Hg^0(g)$ from other constituents on a gas chromatograph (HP-6890) equipped with a 30 m × 0.25 mm i.d. × 1.0 μm crossed-linked phenyl–methyl–siloxane column (HP5-MS). The column was operated at a constant flow (1.5 mL min^{-1}) of

Helium. During chromatographic runs, we typically kept the GC oven isothermal at 40 °C for 1 min and increased the temperature at a rate of 25 °C min^{-1} from 40 to 80 °C.

Arbitrary concentrations units of $Hg^{+}(g)$ ions at m/z = 198-202 were monitored via single ion monitoring (SIM) through integrated peak areas. The observed isotopic ratios corresponded with the expected ratios 33:56:78:44:100. From our GC temperature program, the measured retention time of the mercury peak was at *ca.,* 1.3 min. The detection limit of $Hg^{0}(g)$ was 10 ppb. Prior to monitoring mercury blanks were performed by injection of 200 μL of room air into the GC during a SIM standard run; no mercury peak was discernable from background noise.

Initial mixing ratios of the reactants were 1-2 ppm $Hg^{0}(g)$, 10 to 60 ppm O_3, 0.0-31 parts per thousand H_2O (RH = 0-100%), 0.80 to 6.4 parts per thousand CO, and 90 ppm TMB. The volume of the injected gas sample was 200 μL via an 1825 Hamilton gas-tight syringe. TMB was deployed as a radical scavenger to capture undesired radicals, which could form from secondary reactions of ozone with impurities or reaction products and intermediates [74].

The reaction of $Hg^{0}(g)$ with ozone was assumed to behave under pseudo-first-order conditions with respect to $Hg^{0}(g)$ at $T = 296 \pm 1$ K. To obtain the rate coefficient k_{net} for reaction (1), the ozone concentration was assumed to remain constant. The method also assumes that ozone only reacts with elemental mercury. Ozone has a slow thermal loss resulting in O atom production, which might be the cause of additional Hg loss.

The rate-limiting step in reaction (1) is assumed to be the association of $Hg^{0}(g)$ and $O_3(g)$. Hence,

$$-\frac{d[\mathrm{Hg}^0(g)]}{dt} = k_{\mathrm{net}}[\mathrm{O}_3][\mathrm{Hg}^0(g)] \qquad \text{Eq. 2-6}$$

Integration of Eq 3-6 yields slope $k' = [O_3]k_{net}$ when plotting $\ln([Hg^0(g)]_0/[Hg^0(g)]_t)$ versus time. This approximation is valid only if secondary reactions (e.g. with OH or other impurities) are negligible and ozone is in sufficient excess. The latter condition was only approximate; $6 < [O_3]/[Hg^0(g)] < 40$; $[Hg^0(g)] = 1.5$ ppm. Experiments were performed indicating the addition of TMB and the halocarbon wax coating indeed improved linearity of slopes and appeared to affect the reaction rate (figure 1).

2.2.2 Product Study

Transmission Electron Microscopy

Reaction products were collected from the wall of the flask by placing carbon-coated Cu grids on the surface of the reaction flask and collecting the grids upon completion of the reaction. The elemental composition and the morphology of the collected products were analyzed using a high-resolution transmission electron microscope (HRTEM); model JEOL 2000. X-ray spectra were acquired with an electron beam size of 200 nm at 80 kV for 100 seconds (Figures 2a and 3a) and HRTEM images from operating at 200 kV in bright-field mode at Scheerzer defocus conditions (Figures 2b).

Mass Spectrometry studies

A gas sample of the reaction products were passed through a 1.1 mm i.d. ×10 cm length Pyrex tube (Corning) immersed in liquid nitrogen. The chemical structure of the reaction products mixture was identified using mass spectroscopy equipped with a chemical ionization (CI) source (Kratos MS25RFA). The probe temperature was elevated to 430 K. In the chemical ionization source, quasi-molecular ions $[M+H]^+$ are formed by proton transfer with NH_3 as the reagent gas.

2.3 Materials

Mercury (99.9995%) and trimethylbenzene (98%) were supplied by Aldrich. Carbon monoxide UHP (99.99%), Nitrogen UHP (5.0), and oxygen extra dry (2.6) were obtained from MEGS Gases Ltd. Mercury was further purified by transferred it to a gas-tight finger vial cooled at liquid N_2 temperature in a vacuum lines, and pumped for approximately 5 minutes at *ca*. 10^{-2} Torr.

2.4 Results and Discussion

2.4.1 Kinetic results and potential mechanisms: The effect of CO

To further understand potential mechanism for third body dependence ozone oxidation of elemental mercury, we opted to use two polar gases, CO and water, as an additional reactant. In figure 3b, the concentration of CO is approximately proportional to the rate k_{net}. Concentrations of CO were chosen to be ~ 10^{17} molecules cm^{-3}; this concentration was also used in the water vapour experiments in the following section. Like water, CO(g) has a non-zero dipole moment [166, 167]. It is known that CO may act as a radical scavenger [168, 169], though trimethylbenzene was our intended radical scavenger [170]. Given that CO concentrations were ~100 times greater than TMB, CO may have competed for reactive species. As 90 ppm of TMB appeared sufficient to scavenge reactive species, CO was not expected to significantly impact radical removal rates.

Slopes of $\ln([Hg^0_{(g)}])$ versus *time* were linear over a six fold range in $CO_{(g)}$ concentration indicating the reaction was occurring under pseudo-first-order conditions (figure 3a). Data in figure 3b clearly show CO accelerates the oxidation of mercury. We performed two series of experiments (a) adding CO at the beginning of $O_3 + Hg^0(g)$ reactions, and (b) adding after 20-

40% mercury conversion by ozone. Our results of two experiments were similar, suggesting that the O_3-Hg^0(g) reaction was significantly accelerated using CO as the reactant. We did not see under experimental conditions a significant change in mercury concentration when we used only Hg^0(g) and CO(g) in the reaction chamber. We had initially considered the mechanism in the net reaction (1) to be gas-phase, unless CO was to adsorb on the halo wax-coated flask surface that may be unlikely, but it was not determined in this study. We did not observe any reactions under our experimental conditions between gaseous elemental mercury and CO. We hypothesize that CO associates with HgO_3 through reaction (4), which subsequently leads to product formation:

$$HgO_{3(g)} + CO_{(g)} \rightarrow \text{Products} \qquad \text{Eq. 2-7}$$

The rate loss of mercury can then be written using elementary reactions (4) – (6) assuming steady-state concentrations of HgO_3:

$$-\frac{d[Hg^0(g)]}{dt} = k_4\left\{\frac{k_5 + k_6[CO]}{k_{-4} + k_5 + k_6[CO]}\right\}[Hg^0(g)][O_3] \qquad \text{Eq. 2-8}$$

where the apparent rate is given to be

$$k_{net} = k_4\frac{k_5 + k_6[CO]}{k_{-4} + k_5 + k_6[CO]} \qquad \text{Eq. 2-9}$$

Clearly k_{net} is hyperbolically dependent on [CO]. We interpret that much higher levels of CO cause a levelling off effect on k_{net}, but at lower concentrations k_{net} appears linear. It is noteworthy that the suggested above reaction schemes include only one way, and not exclusively, describing the observations in this study.

2.4.2 The effect of water vapour:

We performed a series of experiments with $Hg^0(g)$ and water vapour alone (below saturation), and we did not observe any reactions under experimental conditions used in this study. Figure 4 shows the effect of water (RH = 0 to 95%, T ~ 296 K) on the rate k_{net} in a 1.1 and 3.1 L flask. We have largely found the effect of water on k_{net} is negligible, consistent with Hall [73], specifically for flasks ≥ 3 l. In a 1.1 L flask, the reaction rate increases slightly, between a factor of 1.1 and 1.7, though not with any obvious relationship to water concentration. We obtained a peak value of $k_{net} = (31.3 \pm 5.0) \times 10^{-19}$ cm^3 $molec^{-1}$ s^{-1} at 60% RH, however due to the present magnitude of uncertainties we cannot suggest this to be a clear 'maximum'. Rates in a 1.1 l flask at RH = 20, 60, and 95% were repeated without the wax coating, and k_{net} increased by a factor of 1.2, 1.0 and 1.4, respectively, compared with the dry, untreated Pyrex flask rate constant. Flasks with untreated walls showed rate enhancement of 40-60% over halocarbon-coated flasks. At RH > 100% (i.e. with a visible water mist coating inside the flasks), there is a significant change in the rate law; $\ln[Hg^0(g)]$ versus time is no longer linear. Acceleration of net reaction (1) due to condensed water has been previously noted by Iverfeldt and Lindqvist [66]. Our results show k_{net} is weakly (and nonlinearly) dependent on RH; smaller S/V ratios (larger flasks) lessen statistically significant effects of water vapour. It is unknown what the mechanism between $CO_{(g)}$ and mercury could be and why $H_2O_{(g)}$ does not exhibit similar behaviour. Uncharacterized water-assisted reactions on surfaces clearly take place between mercury and ozone, enhancing the overall rate. Whereas for $CO_{(g)}$, we have not seen under our experimental conditions any evidence for surface enhanced reactions.

2.4.3 Effect of TMB and wax coating

As shown in figure 1, the addition of TMB (~90 ppm) lowered the oxidation rate by a factor of three, as confirmed in previous studies[74]. Specifically, k_{net} decreases by $(35 \pm 11) \times 10^{-19}$ cm^3 $molec^{-1}$ s^{-1}. Mixtures of ozone and TMB alone did not produce a significant decay for either species, nor was decay observed for $Hg^0(g)$ and TMB combined without ozone. Increasing TMB concentrations from 90 ppm to 360 ppm did not lower rates further. The addition of the halocarbon wax coating reduced the oxidation rate by $(7.4 \pm 9.6) \times 10^{-19}$ cm^3 $molec^{-1}$ s^{-1}, which is not statistically significant. Combining halocarbon wax and TMB together lowered the rate to 30% of the original value.

2.4.4 The effect of ozone:

Figure 5 depicts a decrease in our calculated k_{net} value with variable excess ozone concentrations (linearity is observed for individual $\ln[Hg^0(g)]$ versus time plots, i.e. $R^2 > 0.998$). This trend is similar to the $Cl_2(g) + Hg^0(g)$ data of Menke and Wallis [163]. In the previous study of reaction 1 by Hall [73], there was evidence for heterogeneous ozone chemistry. Hall found the rate of $Hg^0(g)$ loss was equal to $k_{net}[Hg^0(g)][O_3]^{\beta}$, where $\beta = 0.81$. Our own analysis did not reveal a consistent β value for different flask volumes, ranging between 0.5 (1.1l flask) and 1.4 (5.5 l flask).

2.4.5 Effects of surface:

We expected the rate to increase with larger surface-to-volume (S/V) ratios (using 5.5, 3.1, 2.2. 1.1, and 0.6 l Pyrex flasks), shown in figure 5. The rate constants for 5.5 and 3.1 l flasks are statistically indistinguishable within 95% confidence level. This provides an indication that we have reached a limit to the S/V effect when halocarbon wax wall deactivation

is performed. Larger flasks are also less affected by the changes in $[O_3]$, indicating some ozone is adsorbed to the flask walls with low surface-to-volume ratio (i.e., 0.6 to 2.2 l flasks).

Empirically we observe k_{net} is proportional to S/V^2, or $1/r^4$, where r is the radius of the spherical flask. If we assume the rate of total mercury loss can be divided into two pathways: i) by spontaneous oxidation within the volume of the flask, proportional to $V \bullet k_{vol}$, and ii) by oxidation on the flask surface, proportional to $S/V \bullet k_{sur}$. Hence the total rate loss is

$$-\frac{d\mathrm{Hg}}{dt} = \left(Vk_{vol} + \frac{S}{V}k_{sur}\right)[\mathrm{Hg}][\mathrm{O_3}] \qquad \text{Eq. 2-10}$$

Dividing Eq 3-10 through by flask volume V,

$$-\frac{d[\mathrm{Hg}]}{dt} = \left(k_{vol} + \frac{S}{V^2}k_{sur}\right)[\mathrm{Hg}][\mathrm{O_3}] = k_{\mathrm{net}}[\mathrm{Hg}][\mathrm{O_3}] \qquad \text{Eq. 2-11}$$

where $k_{net} = (k_{vol} + k_{sur} \times S/V^2)$. The apparent rate constant k_{net} is fixed for a given flask volume and ozone concentration (figure 6). By linear regression, we obtain $k_{vol} = (5.40 \pm 0.56) \times 10^{-19}$ cm^3 $molec^{-1}$ s^{-1} and $k_{sur} = (2.91 \pm 0.12) \times 10^{-15}$ cm^7 $molec^{-1}$ s^{-1} with linearity $R^2 = 0.995$. The surface rate loss k_{sur} has been previously discussed in the literature [149]. We note $Vk_{vol} = k_{sur}S/V$ when $V \sim 2.1$L, hence surface reactions dominate $V < 2.1$L.

2.4.6 Estimating rate constant in equation (2-1)

We compare two methods for obtaining a best estimate k_{net}. The first method uses the k_{net} values for $[O_3]$ = 30, 40 ppm in 3.1 and 5.5 L flasks (see the four points clustered together in figure 5). These k_{net} values are chosen due to their pseudo-first-order behaviour, negligible sensitivity to ozone concentration change, and minimal S/V sensitivity. The slope average of the combined 24 (4 × 6) runs chosen in figure 5 leads to $k_{net} = (6.2 \pm 1.1) \times 10^{-19}$ cm^3 $molec^{-1}$ s^{-1} at a 95% confidence interval. In the second method we extrapolate the y-intercept in figure 6 (S/V

→ 0) and average together the four intercepts of S/V^2 versus time (equation 3) obtaining k_{net} = $(5.8 \pm 3.4) \times 10^{-19}$ cm^3 $molec^{-1}$ s^{-1}. We judge that the first method provides the "best estimate" rate for reaction 1. In method 2 we cannot yet provide a sound mechanistic rationale. Hence, the value of $(6.2 \pm 1.1) \times 10^{-19}$ cm^3 $molec^{-1}$ s^{-1} represents the most reliable value for an ozone-initiated oxidation of elemental mercury. Note that the total uncertainty associated with the ensemble of experiments amount to approximately ≤ 20%.

2.4.7 Product studies on reactions of O_3 + Hg^0(g) at RH = 0 and 50%

Since we observed potential evidence for heterogeneous reactions only in the presence of water vapour in contrast to CO, we performed additional product studies to further comprehend the nature of the products in water rich environment. In the EDS image (Fig 2a), signals for Cu, Ca, Cl, and O are due to carbon-coated Cu grids. Solid HgO exists as a polymerized chain of Hg-O-Hg linkages[171]. The electron dispersive spectrum between RH = 0 and 50% is indistinguishable. We see in figure 2b that water vapour appears to encourage polymerization of HgO clusters, as clusters similar in size to 50% RH were not observed at 0% RH. As previously reported, 90% of HgO(s) is deposited on the flask walls under dry conditions[74]. The oligomerized form of HgO has very low vapour pressures[172] while extremely stable compared with the monomer.[173]

An EDS spectrum of the chemical composition of products in the gas-aerosol mixture revealed the gas-aerosol mixture contains mercury and oxygen. Due to the chemical composition of the reaction products, we expect aerosol should contain HgO(s), confirmed by MS analysis (Figure 2c). Figure 2c shows a signal at m/z = 219 for $HgOH^+$ (NH_3 was used as the reagent gas), the dominant mercury isotope ^{202}Hg. The m/z distribution also appears

identical between 0% and 50% RH, and suggests humidity has little effect on the reaction products.

Exposure of the HgO(s) product (at RH = 50%) to $300 \leq \lambda \leq 400$ nm UV light for ~10 min irradiation did not result in an appreciable change of product morphology determined by HRTEM imaging, nor elemental composition obtained via EDS.

2.4.8 Mechanisms for the formation of HgO(s)

It is clear reaction (1) is spontaneous based on the rapid loss of mercury through the introduction of ozone (precipitated as HgO(s)). A high-level *ab initio* study on the expected intermediate HgO(g), however, was performed by Shepler and Peterson [174], who calculated a relatively weak dissociation energy: D_0 = 4.3 kcal mol^{-1}. A re-arrangement of mercury and ozone into HgO(g) + O_2(g) is calculated by Tossell to be endothermic, ΔE = +18 kcal mol^{-1} [173]. Reaction (1) is exothermic. Following the reaction coordinate between some transition intermediate Hg•O_3 and HgO(s), we expect a significant activation energy in forming HgO(g), followed by its exothermic precipitation. We hypothesize carbon monoxide will act as a catalyst to decrease the formation barrier energy of HgO(g) (see figure 7). Calculations for barrier energies of such a CO + HgO_3 complex may be the basis for further study.

As noted by Sumner *et al.* [175], microscopic layers of water may deposit onto a hydrophobic wax surface below 100% RH. In our study, the maximum rate constant afforded by the presence of water is $k_{net} = (31 \pm 4) \times 10^{-19}$ cm^3 $molecule^{-1}$ s^{-1} (figure 4), far below the oxidation rate found in an aqueous environment, where $k = (800{,}000 \pm 400{,}000) \times 10^{-19}$ cm^3 $molecule^{-1}$ s^{-1} [67]. Once water has condensed, the rate is seen to rapidly accelerate. Likely there are small increases in k_{net} through the presence of a thin water film. Figure 6b provides our only evidence that HgO(s) growth and humidity are related. We must also consider the fact that these

images were obtained over a carbon grid, and not the flask surface. We performed an additional sets of experiments in which HgO(s, yellow) powder were coated over a specific area (*ca.* 1/8 of surface) of the reaction chambers to evaluate the potential importance of HgO effect on the reaction rate enhancement. We noted an increase in the rate of $Hg^0(g)$ removal similar in magnitude to the addition of liquid water. Exploration into the mechanistic understanding of water vapour's effect on the oxidation process is a desired future target.

2.5 *Atmospheric lifetime of $Hg^0(g)$ using the revised apparent rate constant*

We have performed kinetic studies of $Hg^0(g)$ oxidation by ozone over variable %RH, [CO], flask size, and [O_3]. Though product studies show HgO(s) will cluster more readily in the presence of H_2O, the Hg:O ratio, however, remains unchanged. Our kinetics show the rate constant k_{net} is marginally affected by increases in relative humidity below 100%, but proportional to CO concentrations in low parts per thousand. Our measurements of the apparent ozone oxidation rate $k_{net} = (6.2 \pm 1.1) \times 10^{-19}$ cm^3 $molecule^{-1}$ s^{-1} (with +/- 20% additional potential experimental error, e.g., associate with instrumental accuracy) provides an approximate lifetime of gaseous mercury, shown in table 2; about 2-8 days over a polluted city and 19-38 days in more remote areas. However, in presence of likely reduction mechanisms (aqueous or heterogeneous), this calculated lifetime should be significantly prolonged. Reduction mechanisms in aerosols, fogs and clouds, as well as on the interfaces are suggested and we believe that this calculation is merely reflect the importance of oxidation schemes due to ozone initiated reactions of elemental mercury.

Our results indicate that in environmental conditions (such as in aerosols, cloud droplets, in ice flakes, etc), the gas-phase ozone initiated reaction of elemental mercury can be enhanced significantly. The observed gas-phase initiated oxidation rate loss of mercury can be affected by

several environmental conditions. Reactions of mercury and ozone will be catalyzed in cloud, aerosols and fog droplets and air-water-ice-soil interfaces. More detailed mechanistic studies however, particularly involving surfaces, are required.

Acknowledgements:

We would like to thank Andrew Ryzhkov, Kirk Peterson, for helpful comments, Ed Hudson as a perpetual source of advice, Morteza Vahedpour for initiating the project, and a thanks to NSERC, CFI, and Environment Canada for continued financial support. We are grateful to two anonymous reviewers for their constructive comments.

Table 2-1 k_{net} dependency on [H_2O] Each point represents at least 6 experiments.

Relative Humidity (± 2%)	**$k_{net} \times 10^{19}$ cm^3 $molecule^{-1}$ s^{-1} (95% error)**
0	17.8(1.2)
5	19.7(2.8)
10	20.7(8.4)
20	19.2(6.2)
40	26.3(7.0)
60	31.3(5.0)
80	26.0(4.7)
95	24.8(2.7)
≥100	Non-linear

Table 2-2 k_{net} dependency on [CO]. Each point represents a minimum of 6 experiments.

% CO (in N_2)	**$k_{net} \times 10^{19}$ cm^3 $molecule^{-1}$ s^{-1} (95% error)**
0	17.8(1.2)
0.08	19.3(1.7)
0.16	24.7(7.7)
0.32	41.2(6.8)
0.48	50.3(8.0)
0.64	59.7(8.5)

Table 2-3 Mercury life time estimation upon oxidation initiated by ozone in various regions of the globe. The reduction reactions are not included, and they are expected to increase the listed values in this Table significantly. Typical summertime daily maximum ozone concentrations used to estimate Hg^0 lifetimes for RH = 0% and T = 298 K (excluding Hg(II) reduction/re-emission).

Region	**Ozone (ppb*)**	**Hg^0(g) Lifetime (days; $1/k_{net}[O_3]$),**
Urban-suburban	40 - 120	6 – 19
Rural [176]	15 – 40	19 – 51
Marine boundary layer [177]	10 – 20	38 – 76

$k_{net} = (6.2 \pm 1.1) \times 10^{-19}$ cm^3 molec^{-1} s^{-1}

1 ppb = 2.46×10^{10} molecules cm^{-3} (T = 298 K, p = 1 atm)

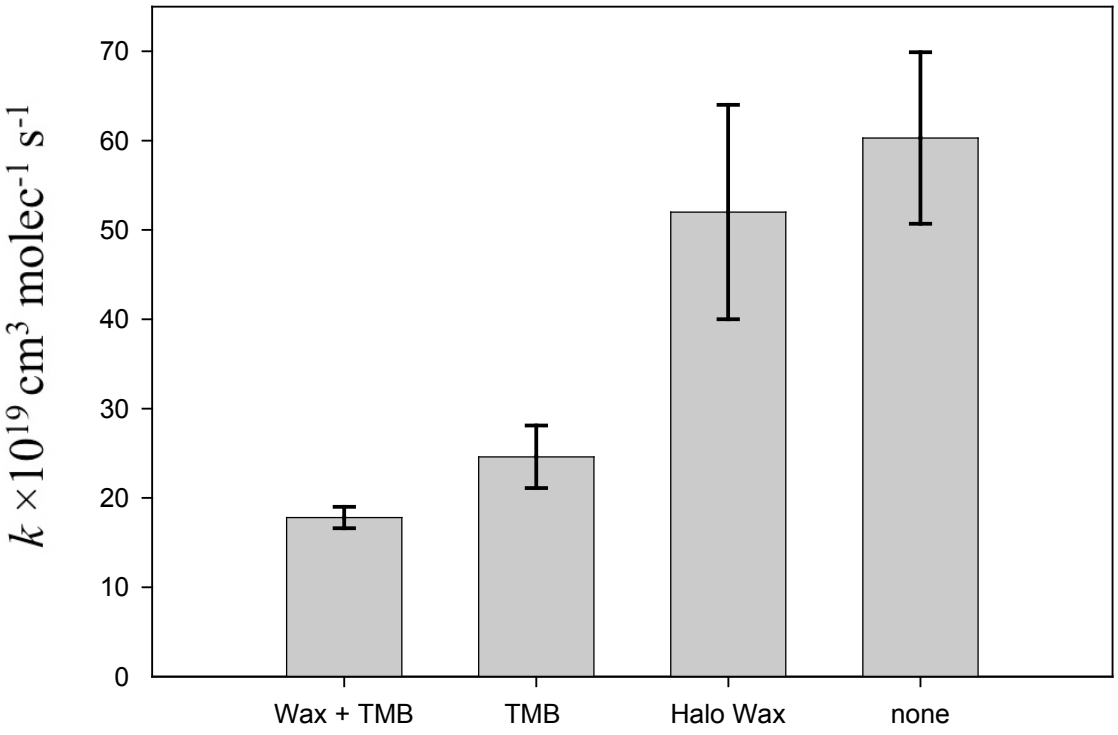

Figure 2-1 Changes to the rate k_{net} via the addition of a halocarbon wax coating and/or the radical scavenger 1,3,5-trimethyl benzene (TMB). Conditions: 1L Pyrex flask, [TMB] = 90 ppm (0.5 μL), [O_3] = 20 ppm. Note: increasing [TMB] to 360 ppm had a negligible effect on k_{net}. Errors of k_{net} are calculated to be $\pm t\sigma/\sqrt{n}$ (95% C.I.), where n = 6, and t is the t-test value for n-1 degrees of freedom.

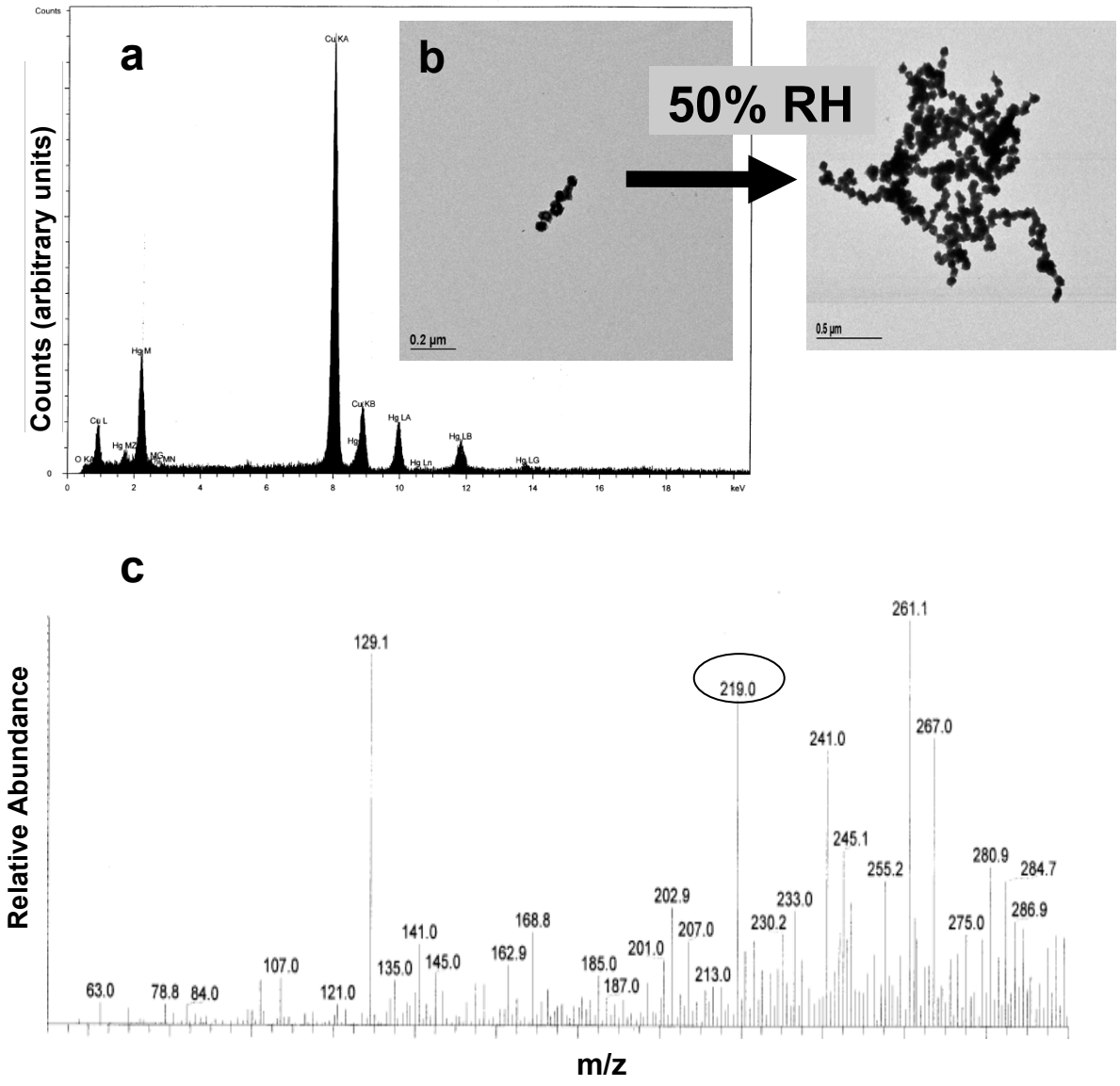

Figure 2-2 **a)** Energy dispersive spectroscopy (EDS) image of HgO **b)** Comparative HRTEM image of HgO deposit at RH = 0% and 50%, and **c)** CI of HgO product at RH = 0% and 50%.

a)

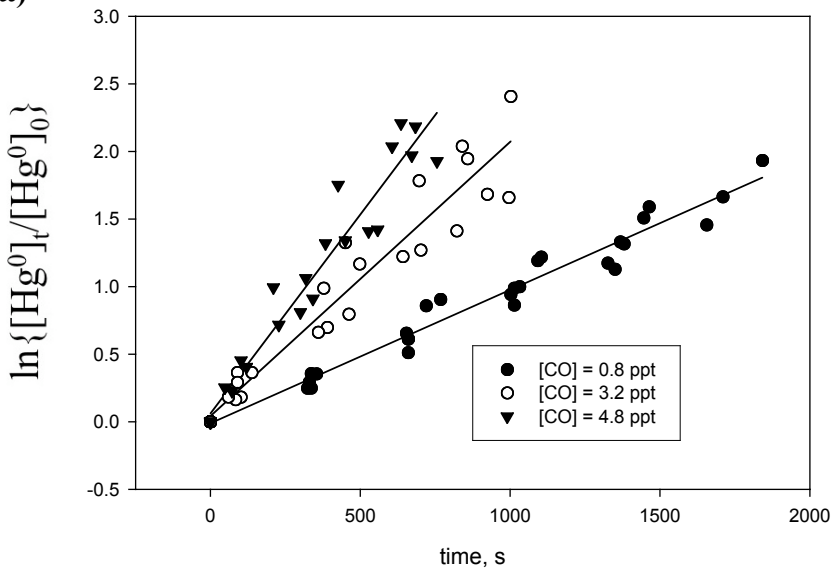

b)

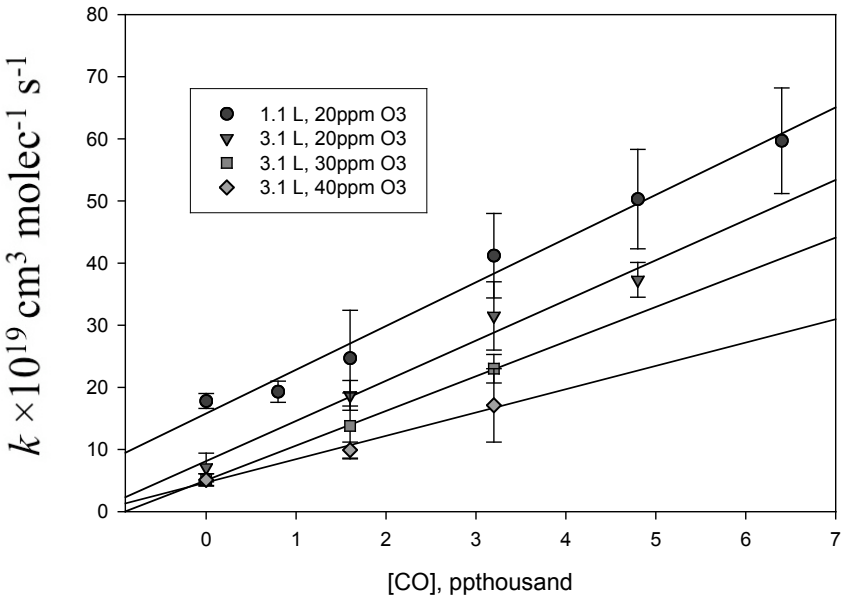

Figure 2-3 **a)** Typical pseudo-first-order slopes of mercury decay using MS SIM peaks area versus time (s) for three [CO] concentrations at 95% C.I. error **b)** Trend of an increasing rate constant with [CO] in a 1L flask. Error bars report slope uncertainty at 95% C.I.

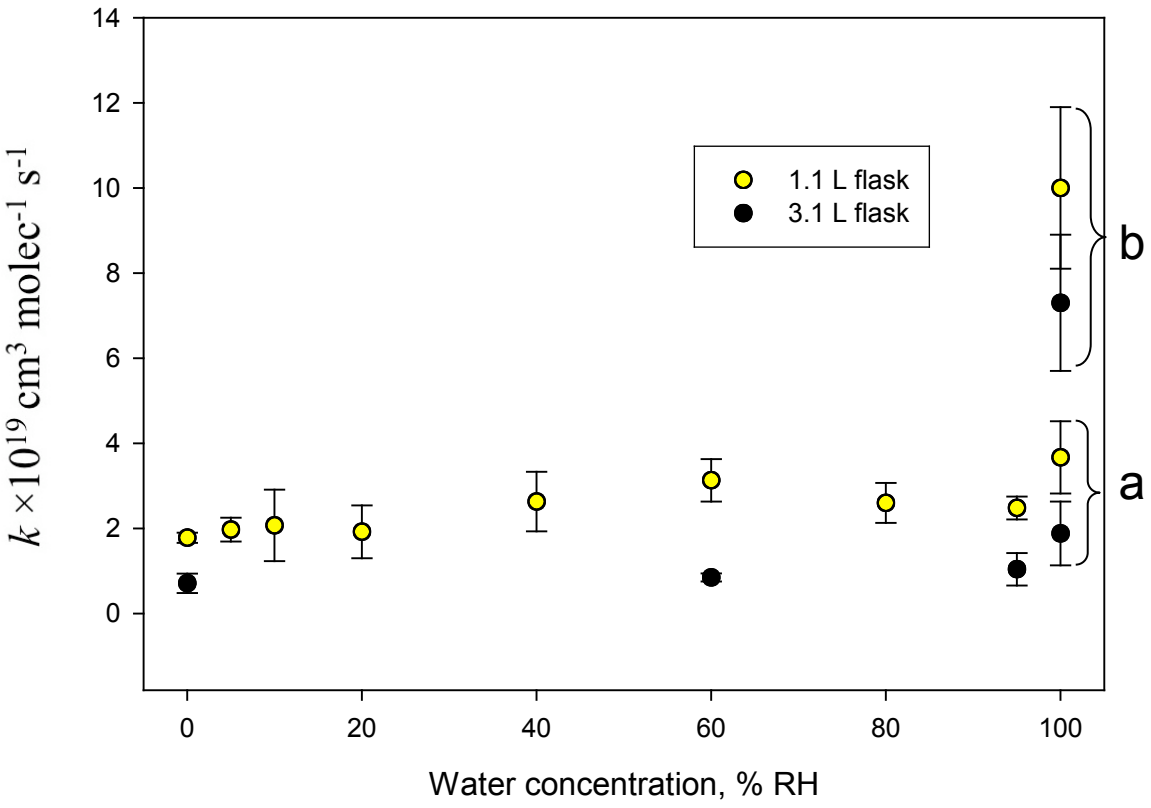

Figure 2-4 Changes in rate constant, k_{net} ($295 \leq T \leq 298$ K), with respect to % RH in a 1.1 and 3.1L flask. Errors of k_{net} are calculated at the 95% C.I. The uncertainty of RH is estimated at ± 2%, omitted for clarity. At 100% RH, rates **a** are taken as the initial tangent to the slope *k*', and **b** is the rate at the latter half of the reaction.

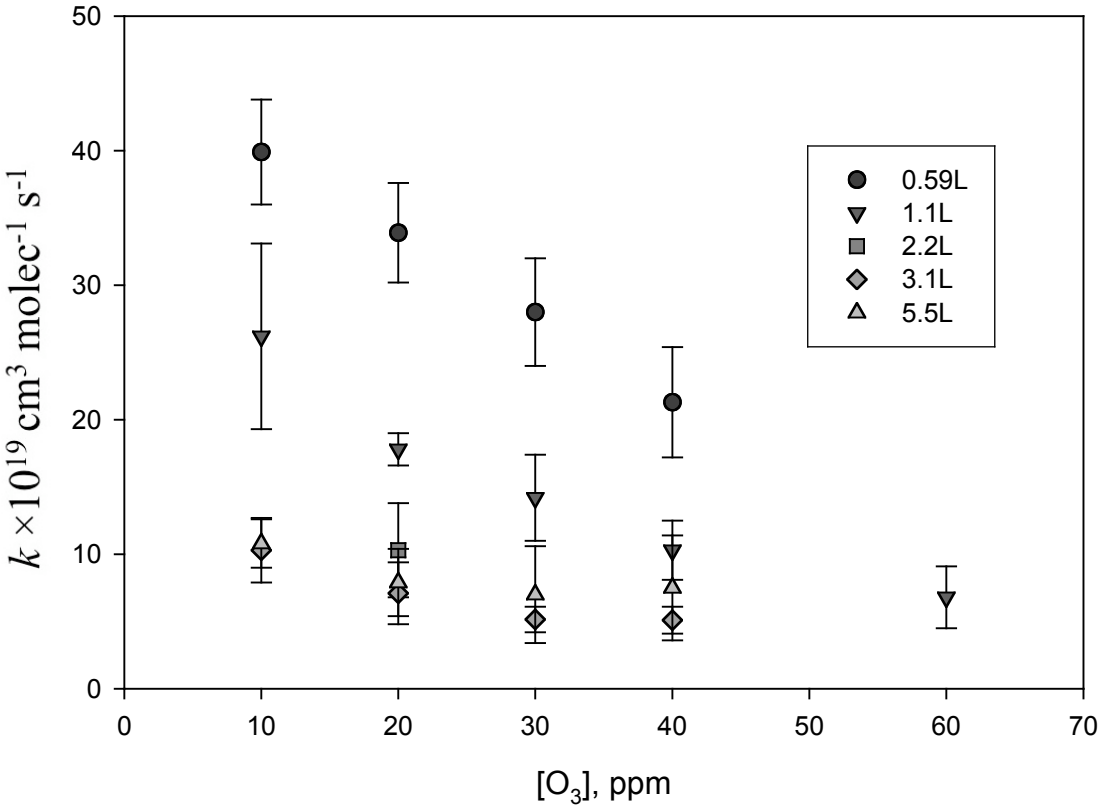

Figure 2-5 Changes observed in the rate constant k_{net} due to various ozone concentrations and flask volumes. Error bars reported at the 95% C.I. The initial concentration of gaseous mercury, $[Hg^0(g)]_0$, is approximately 1-2 ppm. Increase in k_{net} values for decreasing $[O_3]$ indicates reaction order is unlikely first order in ozone.

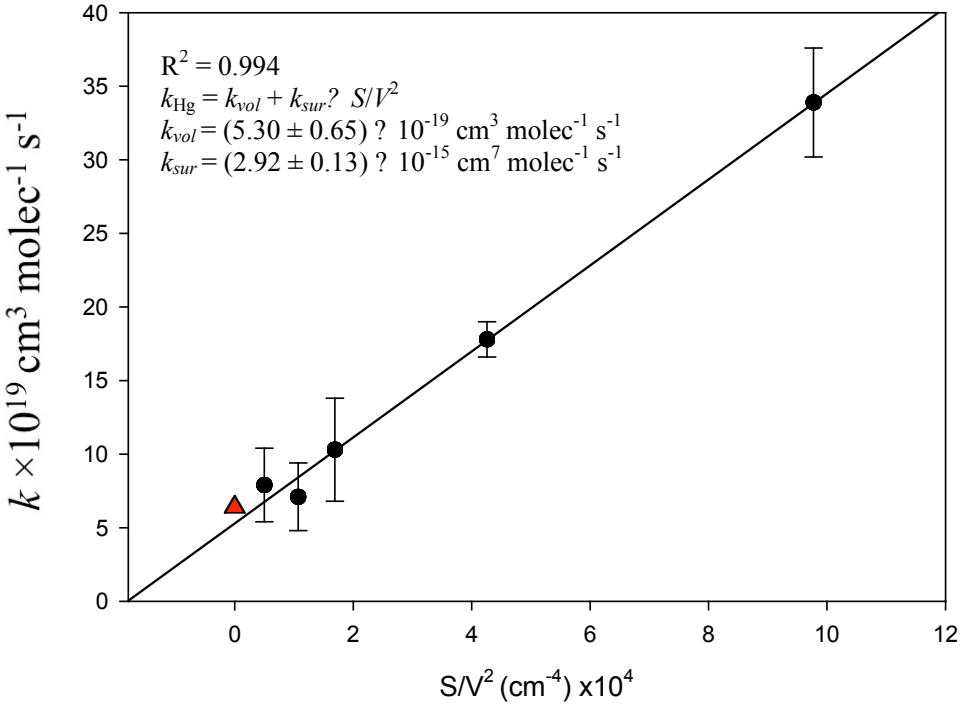

Figure 2-6 Trend in the rate constants k_{net} due to changes in flask volume at constant ozone: $[O_3]$ = 20ppm. Equation of best fit superimposed on graph. Leftmost point( ) from Sumner *et al.*[75] (not included in regression). Error bars reported at 95% C.I.

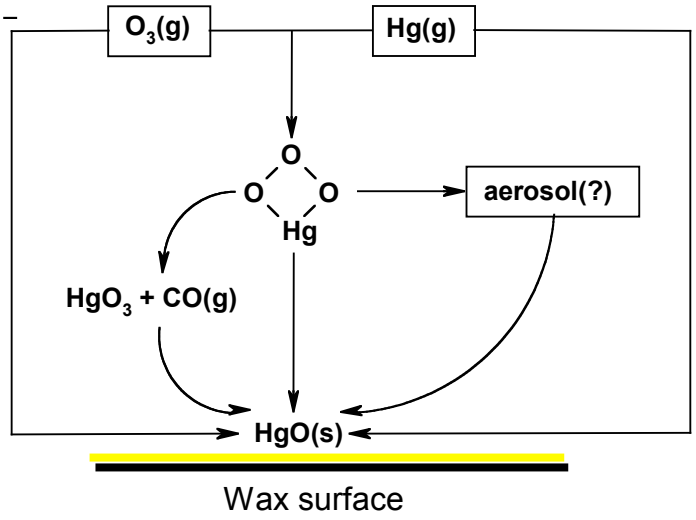

Figure 2-7 Illustration depicting proposed gas-phase and surface reactions beginning with elemental mercury and ozone. Carbon monoxide here plays a side role in assisting the oxidation of the intermediate $Hg•O_3$.

Chapter 3

Photo-Catalytic Oxidation Reaction of Gaseous Mercury over Titanium Dioxide Nanoparticle Surfaces

Contributions by author:

This paper summarizes our work on studying the oxidation of gaseous mercury using a combination of titanium dioxide (TiO_2) and ultra-violet (UV) light from a mercury lamp emitting wavelengths in the 250 – 360 nm range. This subject is of interest to those investigating the removal of mercury from coal fire power plants. Several mercury capture methods have been proposed, and the oxidation by the TiO_2/UV light scheme is a promising method.

I was responsible for the conception of this project, developing the procedure for coating glass disks with TiO_2, the measurement of gaseous species (Hg, SO_2, H_2O), and the calculations that followed to obtain the Langmuir Hinshelwood parameters, i.e. the rate constant *k* and the Langmuir adsorption value K_{Hg}. Mercury concentrations were monitored by gas chromatography mass spectrometry single ion monitoring mode. Experiments were done in a custom-made 950 mL flask, with a quartz window and TiO_2 insert mount.

In addition to measuring the rate and adsorption constant of mercury in air, I added water and sulfur dioxide to the TiO_2-UV-Hg system, allowing time for evaporation in the case of water, in order to observe any effects of competition between gaseous mercury over the TiO_2 surface. The deviations were not statistically strong (within 2σ of error), but there is some indication both SO_2 and H_2O decrease the rate of Hg uptake, though less likely affect the net uptake.

Additional data includes a description of the recirculation flow system experiments, and additional plots of the effects of SO_2 and water. This publication has been reprinted by permission of Elsevier (doi:10.1016/j.cplett.2010.03.062; License No. 2773261422364).

Manuscript published in Chemical Physics Letters

Photo-Catalytic Oxidation Reaction of Gaseous Mercury over Titanium Dioxide Nanoparticle Surfaces

Graydon Snider and Parisa Ariya*

Department of Chemistry, and Department of Atmospheric and Oceanic Sciences

McGill University

801 Sherbrooke St. W., Montreal, PQ, CANADA, H3A 2K6

*Corresponding author;

Emails: parisa.ariya@mcgill.ca and gradyon.snider@mcgill.ca

Abstract

$Hg^0(g)$ is known to undergo photocatalytic oxidation by UVA irradiated TiO_2 surfaces. 1 μm layers of TiO_2 on quartz glass were irradiated within the 240-800 nm range. Gaseous mercury was measured by mass spectrometry single ion monitoring. The surface configuration and elemental characterization of TiO_2 layer was evaluated using scanning electron microcopy with energy dispersive spectroscopy. The LH adsorption constant of was found to be $K_{Hg} = (5.1 \pm 2.4) \times 10^{-14}$ cm^3 and an apparent surface deposition rate of $k = (7.4 \pm 2.5) \times 10^{14}$ min^{-1} cm^{-2} under experimental conditions. Water did not affect the rate constant. We show TiO_2 could be employed to reduce mercury concentrations in gas streams, even at very high Hg^0 concentrations.

3.1 Introduction

Mercury is a neurotoxic heavy metal [178] released anthropogenically not only from coal combustion and trash incineration, but also smelting and cement production [27]. Half of all electrical power in the United States is derived from coal [179]. The only long-term solutions for these problems are drastic reductions on our dependence of non-renewable goods and maximizing recycling. The use of coal as an energy source is likely to grow in the coming decade despite research into alternative energy sources [180]. Interim goals are necessary to reduce heavy metal emissions in the atmosphere. In parallel to the numerous proposals for CO_2 reduction through carbon sequestration, removing toxic heavy metals from combustion is an equally open and active area of research [98]. Here we aim to study the capacity of titanium dioxide for removing gaseous mercury from air with a focus on the physical chemistry of surface adsorption, and the effects of water on uptake efficiency.

Gaseous mercury, $Hg^0(g)$, has a long atmospheric lifetime of 0.5-2 years [30], allowing emissions to disperse globally. Gaseous elemental mercury deposition, both wet and dry, deposits into aquatic ecosystems transformed into methyl mercury by sulfate-reducing bacteria [159]. Methylated mercury can be incorporated and biomagnified through the food chain eventually leading to fish advisories from the increasingly dangerous levels of methyl mercury found in edible fish [159].

Titanium dioxide (TiO_2) is a popular heterogeneous catalyst for hydrocarbon oxidation whose surface properties [123] and photocatalytic potential [181] have been extensively studied. TiO_2 can crystallize into rutile, anatase, or (non-photolytic) brookite structures [182]. A mixture of anatase and rutile TiO_2 are typically found in oxide film coatings [183]. Titanium dioxide is a candidate for scavenging gaseous mercury. It has long been known that TiO_2 powders and films

are photolytically active under UVA ($320 \leq \lambda \leq 400$ nm) light [183]. Hydrocarbons adsorbed to the surface of TiO_2 are oxidized heterogeneously. Such a system has been used to decompose harmful hydrocarbons and bacteria [123]. Elemental mercury can be similarly oxidized under room-temperature conditions in air, to mercury oxide [112, 116], which is a non-volatile solid characterized by nano-scale zigzag chains of Hg-O.

The threshold energy required to generate electron-hole pairs (i.e. excite from the valence to conduction band) in titania is 3.2 eV or about 380 nm (UVA light) [118]. The mechanism of photocatalytic oxidation depends to some extent on the oxidant reaction in question. Here it begins with an adsorbed oxygen molecule that traps the 'free' electron and reducing it to superoxide:

$$O_{2(ads)} + e^- \rightarrow O_2^{\bullet -}{}_{(ads)} \qquad \text{Eq. 3-1}$$

The hole may then oxidize water to the hydroxyl radical:

$$H_2O_{(ads)} + h^+ \rightarrow OH^{\bullet}{}_{(ads)} + H^+{}_{(ads)} \qquad \text{Eq. 3-2}$$

OH was then assumed to oxidize the adsorbed mercury into HgO(s) [117].

It is assumed that HgO(s) will both decompose into $Hg^0(g)$ above 500°C [184] and is soluble in nitric acid, whereas TiO_2 melts at 1560°C and is insoluble in most acids [65]. The proper means for disposing chemisorbed HgO remains to be determined and is a parallel subject of research [185].

A growing body of research is focused on the oxidation of $Hg^0(g)$ by UVA (320-400 nm) irradiated TiO_2 (e.g., Wu *et al.* [116], Lee *et al.* [141], Pitoniak *et al.* [119] and Prairie *et al.* [113]). For instance, Li and Wu [120, 186] oxidized $Hg^0(g)$ using TiO_2-SiO_2 nanocomposites, and Rodriguez *et al.* [117] oxidized mercury over TiO_2 coated on quartz irradiated at $320 \leq \lambda \leq 400$ nm (UVA). The application of TiO_2 films to mercury oxidation is

attractive as it can be performed at room temperature. Several methods require higher temperatures (T > 150°C), such as selective catalytic reduction (SCR), iron oxide coatings (Fe_2O_3), fly ash surfaces, or aluminum oxide (Al_2O_3) [94, 143]. At sufficiently high temperatures (>250°C), TiO_2 also provides a catalytic surface without UV irradiation [105]. TiO_2 can scavenge mercury passively through oxide-coated windows while utilizing solar UV radiation [187]. Such a system may even function under relatively high mercury concentrations.

In this laboratory, we have previously studied various kinetic, thermochemical and mechanisms of mercury in gaseous and aquatic phases [74, 145, 147, 188]. We have also studied heterogeneous oxidative surfaces for instance, oleic acid oxidation by ozone over thin water films via attenuated total reflectance Fourier transform infrared spectroscopy [189]. In the present study, we compared with literature sources the mechanisms and kinetics of mercury capture over irradiated titanium dioxide. Previous studies used significantly lower mercury concentrations (1-10 parts per billion) than our experiments. Consequently we have investigated the exhaustibility of TiO_2 over repeated collections of mercury oxide. We demonstrate that TiO_2 could be employed as an efficient means to reduce mercury concentrations in gas streams, even at very high (1-2 *parts per million*) elemental mercury concentrations. We also attempted to resolve whether high and low levels of water vapour inhibit or promote mercury surface oxidation.

3.2 Method

3.2.1 TiO_2 coating procedure

TiO_2 coating procedure was followed from Fernandez *et al.* [190]. 13 mL of Ti(IV) isopropoxide was added to 87 mL of isopropyl alcohol and stirred together in a small beaker.

Solution depicted slight yellow colour likely due to oxidation with water vapour. A circular disk of quartz (4.8 cm diameter, 0.32 cm thick) was lowered edge-wise into the solution. The disk was slowly removed from solution over 10-15 sec and left to oxidize from moisture in ambient air for *ca.* 3 min. Disk was dipped in solution twice more for a total of three coats. Quartz disk was then heated to 400°C in an oven for 2 hours. Opaque white coating was observed on disk. TiO_2 surface was washed progressively with nitric acid, 18.2 MΩ Milli-Q water, and HPLC-grade acetone.

TiO_2 coating was also removed from one side of disk. Disk was weighed (TiO_2 mass = 1.9 ± 0.1 mg), and density was given as $\rho_{TiO2} = 3.8$ g/cm^3 [65]. Approximate average thickness, h, of TiO_2 coating was estimated as $h = TiO_2\ mass/(disk\ area \times TiO_2\ density) \approx 0.3\ \mu m$. The calculated thickness compares reasonably with Fernandez *et al.* [190], who obtained a thickness of 0.2 μm (no error reported).

The apparent rate constant of the catalytic photo-oxidation of $Hg^0(g)$ over TiO_2 reaction was determined by measuring the relative loss of $[Hg^0(g)]$ via electron impact (EI) ionization mass spectrometry (HP-5973). We performed the separation of $Hg^0(g)$ from other constituents on a gas chromatograph (HP-6890) equipped with a 30 m × 0.25 mm i.d. × 1.0 mm o.d. crossed-linked phenyl-methyl–siloxane column (HP5-MS). The column was operated at a constant flow (1.5 mL min^{-1}) of ultra pure helium. During chromatographic runs, we typically kept the GC oven isothermal at 45 °C (0 °C = 273.15 K) for 1 min and increased the temperature at a rate of 25°C min^{-1} from 45 to 80°C. Prior to monitoring mercury signal loss with time, a blank was performed by injecting 200 μL of room air into the GC during a SIM standard run. Near the expected mercury elution time (1.3 min) no mercury peak was discernable from background noise (about 200 – 300, arbitrary units).

The quartz disk was inserted into the flask, a volume of 950 mL. Except for quartz window, the flask was made of borosilicate glass. Mercury and toluene samples were added to the reaction flask via vacuum line and gas syringe, respectively, and measured for consistency via GC/MS. The reaction flask was coated with MTO-Halocarbon Wax (Supelco) to inactive surface adsorption of reactants, products, or reaction intermediates to lead undesired side and secondary reactions due to non-TiO_2 surfaces. The effect of wax coating has been previously studied by our group [147].

Radiation was produced from a 100 W Hg lamp housed in a casing (Oriel, 6281 and 60076) attached with a rear reflector. The radiation power was measured with a UVA detector (PMA2110, Solar Light Company, Inc. 370 nm peak response). At 15 cm, radiation power was approximately 66 ± 5 mW/cm^2. Temperature of reaction was based on ambient conditions, T = 24 ± 2°C, P = 770 ± 5 torr. Estimation of errors was determined based on daily temperature, pressure, and UV emission fluctuations.

Scanning electron microscopy (SEM) and electron dispersive X-ray spectroscopy (EDS) were performed before and after mercury surface deposition on TiO_2 film. What appeared as mercury deposits were visible in SEM as lightly colored (white) deposits. The HgO deposits appeared concentrated in particular regions. Focusing the X-ray beam on these regions showed the presence of mercury (figure 2). No visible or chemical signs of mercury were found before irradiation and grey areas in figure 2 had a minimum of mercury. Switching to a topographical display (figure 3), the deposits were apparently localized on the summits of TiO_2 growths.

3.3 *Materials*

An initial concentration of 1-2 ppm Hg (1 ppm = 2.46×10^{13} molecules cm^{-3} at T =25°C, P = 760 torr) was used in experiments. Titanium (IV) isopropoxide (97%) was obtained from

Aldrich. HPLC-grade isopropyl alcohol (99.7%), HPLC-grade acetone (99.5%), and 68-70% Nitric acid were all used as delivered from ACP Chemicals. HPLC-grade toluene (99.8%) was obtained from Fisher chemicals.

Standard deviations between repeated experimental trails were performed when available. For individual datum, errors were estimated from equipment uncertainties.

3.4 Results and Discussion

3.4.1 Plotting Langmuir-Hinshelwood rate

It is reported that the heterogeneous rate of reaction is proportional to the available surface area and light intensity [117, 191, 192],

$$r = k\theta I^{\alpha} \qquad \text{Eq. 3-3}$$

where k is the deposition rate constant [units: molecule min^{-1} cm^{-2} $(mW/cm^2)^{-\alpha}$], I is the UV light intensity, and θ the fraction of available surface. We have assumed a constant intensity of UV light, so that I has been incorporated implicitly into k, i.e. $k' \equiv kI^{\alpha}$ (prime is omitted henceforth). Fluctuations in light sources are therefore an experimental source of error. Further assuming mercury adsorption obeyed the Langmuir Hinshelwood mechanism

$$\theta = \frac{K_{Hg}[Hg]}{1 + K_{Hg}[Hg]} \qquad \text{Eq. 3-4}$$

where K_{Hg} was the Langmuir adsorption constant (units: cm^3 $molecule^{-1}$) and [Hg] was the concentration of mercury in the flask, by combining (1) and (2) to form a predictive rate law, we obtained:

$$Rate = -\frac{1}{A_{TiO_2}}\frac{dHg}{dt} = k\frac{K_{Hg}[Hg]}{1 + K_{Hg}[Hg]} \qquad \text{Eq. 3-5}$$

$$-\frac{d[\mathrm{Hg}]}{dt} = \frac{A_{\mathrm{TiO_2}}k}{V_f}\frac{K_{\mathrm{Hg}}[\mathrm{Hg}]}{1+K_{\mathrm{Hg}}[\mathrm{Hg}]} \qquad \text{Eq. 3-6}$$

A_{TiO2} was the area of the TiO_2 disk and V_f was the volume of the flask. The left hand side of the equation, V_f was divided by absolute mercury losses, converting them into mercury losses per unit volume.

Integrating over $[0,t]$ and $[[\mathrm{Hg}]_0,[\mathrm{Hg}]_t]$, we obtained:

$$[\mathrm{Hg}]_0 - [\mathrm{Hg}]_t + \frac{1}{K_{\mathrm{Hg}}}\ln\left(\frac{[\mathrm{Hg}]_0}{[\mathrm{Hg}]_t}\right) = \frac{k}{V_f}A_{\mathrm{TiO_2}}t_{irrad.} \qquad \text{Eq. 3-7}$$

where $t_{irrad.}$ is the irradiation time of the TiO_2 plate. Re-arranging,

$$\frac{\ln\left([\mathrm{Hg}]_0/[\mathrm{Hg}]_t\right)}{[\mathrm{Hg}]_0 - [\mathrm{Hg}]_t} = \frac{A_{\mathrm{TiO_2}}k\mathrm{K_{Hg}}}{V_f} \times \frac{t_{irrad.}}{[\mathrm{Hg}]_0 - [\mathrm{Hg}]_t} - \mathrm{K_{Hg}} \qquad \text{Eq. 3-8}$$

Plotting $y = \dfrac{\ln\left([\mathrm{Hg}]_0/[\mathrm{Hg}]_t\right)}{[\mathrm{Hg}]_0 - [\mathrm{Hg}]_t}$ versus $x = \dfrac{t_{irrad.}}{[\mathrm{Hg}]_0 - [\mathrm{Hg}]_t}$ yielded an intercept $-\mathrm{K_{Hg}}$ and slope $\mathrm{A}k\mathrm{K_{Hg}}/V_{\mathrm{f}}$. The intercept hence must be negative to have physical meaning.

The associated uncertainties are

$$\delta y = \frac{\delta[\mathrm{Hg}]_t}{([\mathrm{Hg}]_0 - [\mathrm{Hg}]_t)^2} \times \left\{\left(\ln([\mathrm{Hg}]_0/[\mathrm{Hg}]_t) - [\mathrm{Hg}]_0/[\mathrm{Hg}]_t + 1\right)^2 + \left(\ln([\mathrm{Hg}]_t/[\mathrm{Hg}]_0) - [\mathrm{Hg}]_t/[\mathrm{Hg}]_0 + 1\right)^2\right\}^{1/2} \qquad \text{Eq. 3-9}$$

$$\delta x = \frac{t_{irrad.}}{[\mathrm{Hg}]_0 - [\mathrm{Hg}]_t}\left\{\left(\frac{\delta t_{irrad.}}{t_{irrad.}}\right)^2 + 2\left(\frac{\delta[\mathrm{Hg}]_t}{[\mathrm{Hg}]_0 - [\mathrm{Hg}]_t}\right)^2\right\}^{1/2} \qquad \text{Eq. 3-10}$$

assuming $\delta[\mathrm{Hg}]_t = \delta[\mathrm{Hg}]_0 \sim 50$ ppb, $\delta t \sim 0.04$ min.

The values k and K_{Hg} can be solved knowing the area of the TiO_2 plate and the flask volume. Typical plot of mercury loss via Hg lamp is shown in Figure 1. The decay was initially

proportional to irradiation time; afterward the decay logarithmically decreased with time. Rate constants are shown in Table 1.

3.4.2 Evaluation of Langmuir-Hinshelwood mechanism

The LH mechanism assumes the reactants (mercury and water) first adsorb onto the surface and then react on the same surface. Mechanistically, mercury appears that it must adsorb onto the surface of the TiO_2 film before reacting; experiments performed without the TiO_2 catalyst in the presence of UV light showed no signs of mercury oxidation. The adsorption of water is quite strong according to previous studies [193]. Finally, the HgO(s) deposit clearly formed onto the surface to such an extent that it became visible after several hours of continuous UV exposure.

The Eley-Rideal mechanism [98] is an alternative explanation to the reaction, whereby water adsorbs to the surface but mercury reacts while remaining in the gas phase. This mechanism would imply gas-phase Hg^0 concentrations would be proportional to reaction rates, i.e. $d[\mathrm{Hg}]/dt = k\theta_{\mathrm{H2O}}[\mathrm{Hg}]$. Experimentally this alternative would be indistinguishable from the L-H rate at low mercury concentrations, i.e. $K_{\mathrm{Hg}}[\mathrm{Hg}] << 1$, whereby Eq. 3-6 would be written $d[\mathrm{Hg}]/dt = k\mathrm{K}_{\mathrm{Hg}}\theta_{\mathrm{H2O}}[\mathrm{Hg}]$.

3.4.3 Comparison of calculated K_{Hg} and k to literature

To our knowledge, no direct measurement of K_{Hg} for photo-activated titanium dioxide surface values has been obtained in the literature, and our current value represents the first estimation. We compared with the model of Rodriguez *et al.* [117] by deriving an interpretive value for K_{Hg}. Rodriguez's rate-loss for mercury predicted for trace water vapour conditions was given as:

$$-\frac{d[\mathrm{Hg}]}{dt} = \frac{1}{2}\frac{ba[\mathrm{Hg}]}{(1+c[\mathrm{Hg}])} \qquad \text{Eq. 3-11}$$

In our experiments where low water vapour concentrations were used (RH ≤ 1%), equation (5) seemed analogous to our own equation (3). Comparatively, adsorption constant K_{Hg} in equation (3) corresponded to constant "c", hence:

$$K_{\mathrm{Hg}} = c \qquad \text{Eq. 3-12}$$

Rate constant "*k"* was also equivalent coefficient in equations (3) and (5):

$$k = \frac{V_f}{A_{\mathrm{TiO_2}}}\frac{ab}{2c} \qquad \text{Eq. 3-13}$$

Converted values were shown in Table 1.

The reported K_{Hg} and *k* values were found to be within the same range of magnitudes as Rodriguez *et al.* [117]. Li and Wu [120], however, clearly show dissimilar values; their calculated K_{Hg} was 30 times larger while k was 10^{-5} times smaller. The agreement between Rodriguez's data is likely explained by both experiments having used a pure TiO_2 surface rather than a SiO_2-TiO_2 composite. It is noteworthy that our operating temperature was lower while UV light intensities were much higher than Rodriguez *et al.* The light intensity effect was studied in the following section.

3.4.4 Sources of uncertainties

The percentage errors for K_{Hg} and *k* were 47% and 34%, respectively. The error ranges are large, likely due to several factors: A) UV intensity varies with distance/ angle of lamp while TiO_2 films also varied in thickness depending on XY-surface position. B) Surface TiO_2 temperatures may vary from the measured bulk temperature of the flask. C) Cleanliness of the TiO_2 plate. D) The presence of any volatile organic compounds (VOCs). TiO_2 is known to

oxidize most VOCs, thus competing with Hg deposition. We did not, however, see any MS signals for VOCs except acetone, whose concentration remained unchanged during experiments.

3.4.5 Light intensity

Light intensity has been shown to affect the Langmuir adsorption constant [194]. We measured a broad range of UVA intensities from the lamp, ranging from 44 to 70 mW cm^{-2} depending on the angle and position of the detector. Hence our Oriel lamp was not a homogenous light source. An "average" intensity near the centre of the beam we report here to be 60 mW cm^{-2}. According to Fujishima *et al.*, given this high intensity range of light our experiments may lie in a mass transport-controlled region of space [191]. Hence UV light at our intensity may have saturated the reaction rate and lamp fluctuations could be of small concern. The verification of this claim remains unchecked, however.

3.4.6 TiO_2 disk characteristics and surface area

The optimal surface density for a TiO_2 coating has been suggested to be 0.23 mg cm^{-2} [195]. Thick films attenuate UV light before reaching the surface while too-thin films do not fully absorb the UV light. Our films were approximately 0.1 – 0.2 mg/cm^2 corresponding well with this "optimal" value. We assumed the surface area of the quartz disk would represent, at least, the perpendicular area exposed to the UV light, about 18 cm^2. Scanning electron microscopy (SEM) analysis of TiO_2 plates (Figure 2) indicated uniform coverage over the surface, with uneven thicknesses throughout the deposition. The surface area in our sample was unknown. Back-scattering images show the areas with HgO accumulation, whereas environmental secondary electron detector (ESED) imaging show a topographical image of

TiO_2 with sharp peaks and valleys. Using energy dispersive X-ray (EDX) spectroscopy, Ti, O, and Hg atomic signals were observed.

3.4.7 Saturated HgO deposits

Experiments in which a mercury-saturated humid air stream passed over the TiO_2 film created a dark deposit of $HgO_{(s)}$. We reached the saturation point of HgO, whereby reactivity of the TiO_2 film, that is to say the uptake of mercury on the film, ceased. The deposit was visible to the naked eye, however the exact thickness is not known.

3.4.8 Mechanism of Hg_{ads} oxidation (with and without presence of water)

In our experiment, hydroxyl radicals was expected to oxidize the adsorbed mercury, Hg_{ads} into HgO (the intermediate HgOH is probably unstable) on the TiO_2 surface [117]. We considered the possibility that ozone was generated in our reaction chamber, however several trails were performed on gaseous mercury without the presence of TiO_2 and no reaction took place.

There has been a dispute as to whether water vapour promotes or inhibits mercury oxidation, depending on its concentration [117, 120, 186]. Mechanistically, water molecules are thought to be required in generating OH radicals that oxidize mercury. The rate-limiting concentration of water needed for mercury oxidation is unclear. In experiments where we heated the TiO_2 plate (to 120°C) prior to chamber assembly and flushing the flask with dry air, the rate-loss of mercury remained constant. Hence we found it unnecessary to add water deliberately to incur reactivity. We estimate between 5 and 20 ppm of water might be present in these 'dry' air experiments. Over a rutile TiO_2 surface, water adsorbs to a significant degree; degassing can be detected above 300^{o}C under vacuum as Hydroxyl groups are chemisorbed to the surface [193].

In more humid conditions (up to 100% relative humidity at 25°C), mercury oxidation again remained the same. Excessive water did not present a strong influence over reactivity, yet is required in only minute concentrations.

Although some studies indicate that the presence of moisture is not necessarily essential to keep up the photocatalytic process [196], further studies under controlled dry conditions and over the larger range of water and other potential co-pollutants concentrations such as NO_x (= NO + NO_2), SO_x (= SO_2 + SO_3), volatile organic compounds are recommended as such species are known to inhibit mercury adsorption [187, 197, 198].

3.5 Conclusions

Titanium dioxide is an attractive method of oxidizing gaseous mercury using potentially safe, low-cost procedures. TiO_2 has a high Hg^0 uptake capacity, is relatively cheap ($1.19 USD/lb [199]), and non-toxic (e.g. used in toothpaste and suntan lotion). The power cost of running continuous UV lights remains a problem [197]. Ultra Violet LEDs will save on energy, hence total cost, provided the LEDs themselves are inexpensive [200]. TiO_2 doped for a shift in visible light conversion may allow for the use of sunlight radiation in mercury capture [187].

We have measured the overall rate constant k and Langmuir adsorption constant K_{Hg} of high concentrations of gaseous mercury in dry and humid air at room temperature and pressure. Our system was inexpensive, requiring no flow apparatus or leak checks beyond verifying stable concentrations of mercury. Measured values were comparable to Rodriguez [117] but clearly distinct from Wu and Li [120, 186]. We have addressed the impact of water vapor on the adsorption-oxidation efficiency of mercury on TiO_2 surfaces and did not observe any major impediments on Hg oxidation process even at higher relative humidities.

As for the utility of TiO_2 nanoparticles for Hg^0 removal in a coal plant, it is known SO_2 will inhibit TiO_2 surface reactions [141] but this is true of other methods as well [98]. Rising temperatures, especially above 100^oC, may inhibit oxidation [141, 192], which in turn emphasizes the potential of TiO_2 nanoparticles for industrial usage, particularly as the downstream and upstream cooling are part of the existing industrial pollution industries. Life-cycle analysis of photo-activated titanium oxides methods for removal of mercury and the secondary reactions in the environment should be studied to assure its benign nature in the environment. Additives such as gold nanoparticles [201-203] to titanium dioxide coatings should be explored for enhanced mercury adsorption properties (creating temporary gold amalgams).

Table 3-1 Langmuir adsorption constant K_{Hg} and rate constant k with comparison of affecting parameters.

Ref.	T (°C)	UV power (mW/cm^2)	[Hg], (ppb)	Air Flow Rate (L/min)	Detection	K_{Hg} (cm^3/molec)	k (molec min^{-1} cm^{-2})
A	**23-26**	**44~70**	**1,000-2,000**	**0**	**MS-EI**	**$5.1 \pm 2.4 \times 10^{-14}$**	**$7.4 \pm 2.5 \times 10^{14}$**
B	75-80	1.85	0.2 –0.3	1	CVAA	13×10^{-14}	3.8×10^{14}
C	43	4	10 – 80	2	ZAAS-HFM	156×10^{-14}	$(2.4 \times 10^{-4}) \times 10^{14}$

A) This work, UV source: Oriel 100W Hg lamp (UVA and B emission), UVA detector: SolarLight PMA2110, MS-EI: HP 5973 Mass Spectrometer Electron Ionization **B**) Rodriguez *et al.* [117], UV source: XX-40 Spectronics 80W (UVA emission), CVAA: cold vapour atomic adsorption (Shimadzu UV-1201S Spectrometer), UV detector unknown. **C**) Li and Wu [120, 186], UV source unknown, UV detector: UVX radiometer with UVX-36 sensor probe (335-380 nm range), ZAAS-HFM: Zeeman atomic absorption spectrometry using high frequency modulated light polarization (OhioLumex Co. RA-915+).

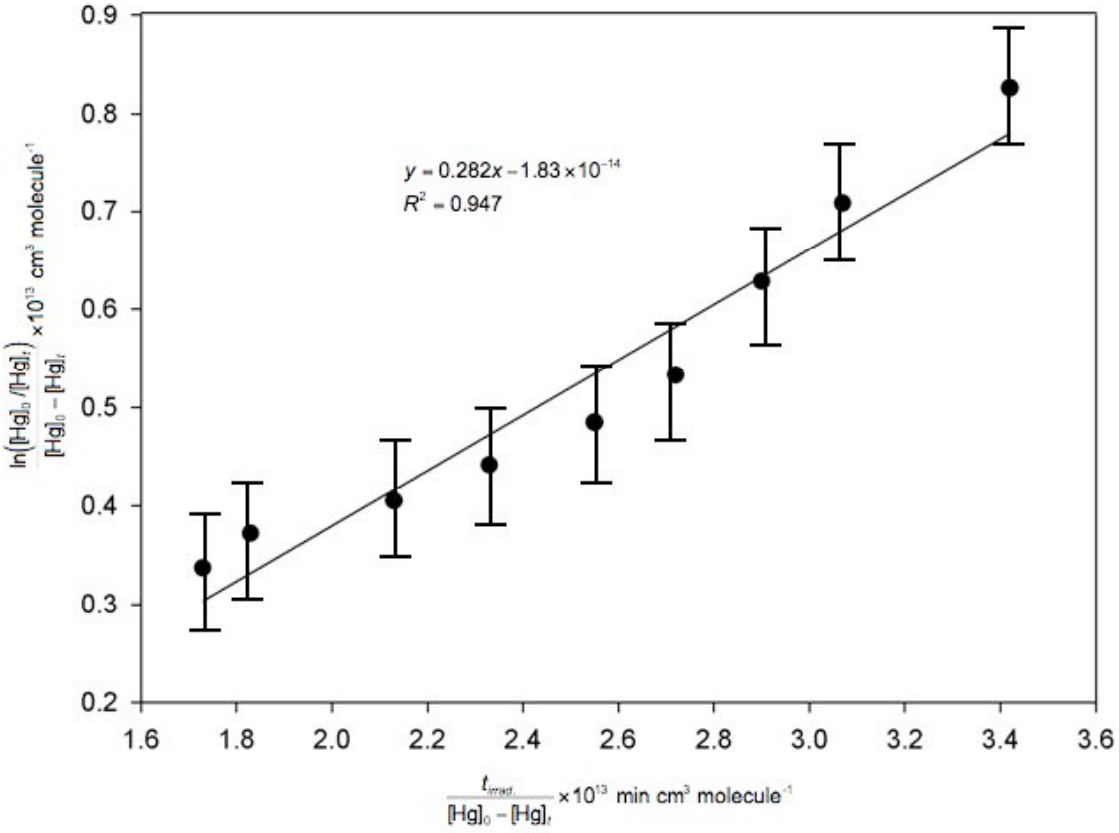

Figure 3-1 Plotting equation (4), monitoring mercury ($Hg^0(g)$) losses from UVA-irradiated TiO_2. While possible concomitant reactions are occurring to explain this graph, the LH mechanism is the best approximation we currently have.

A

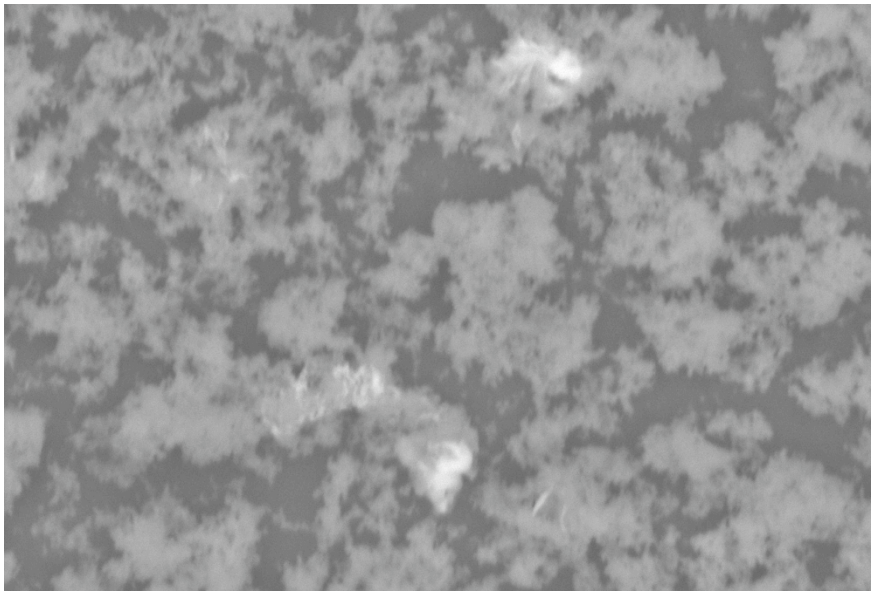

B

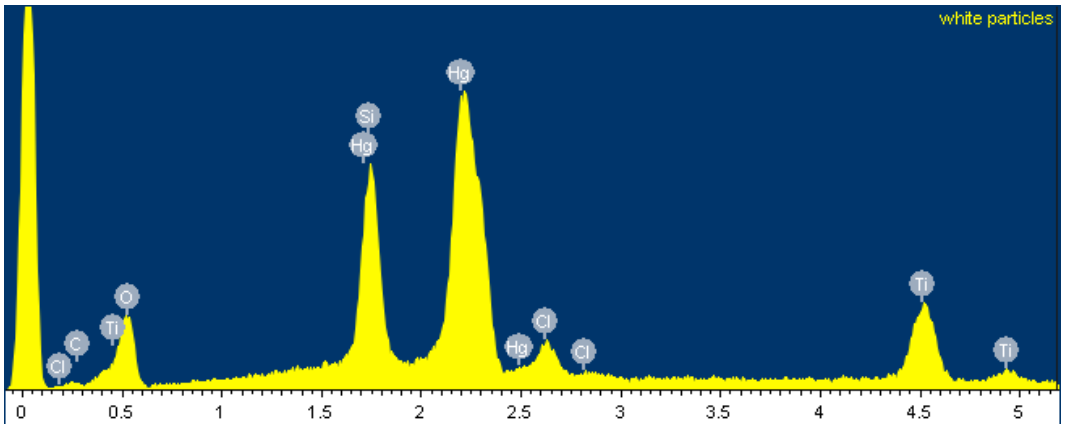

Figure 3-2 (a) SEM image (3000× magnification) of TiO_2 displaying white patches, confirmed to be HgO via EDX. (b) EDX of marked area shows presence of Ti O, and Hg.

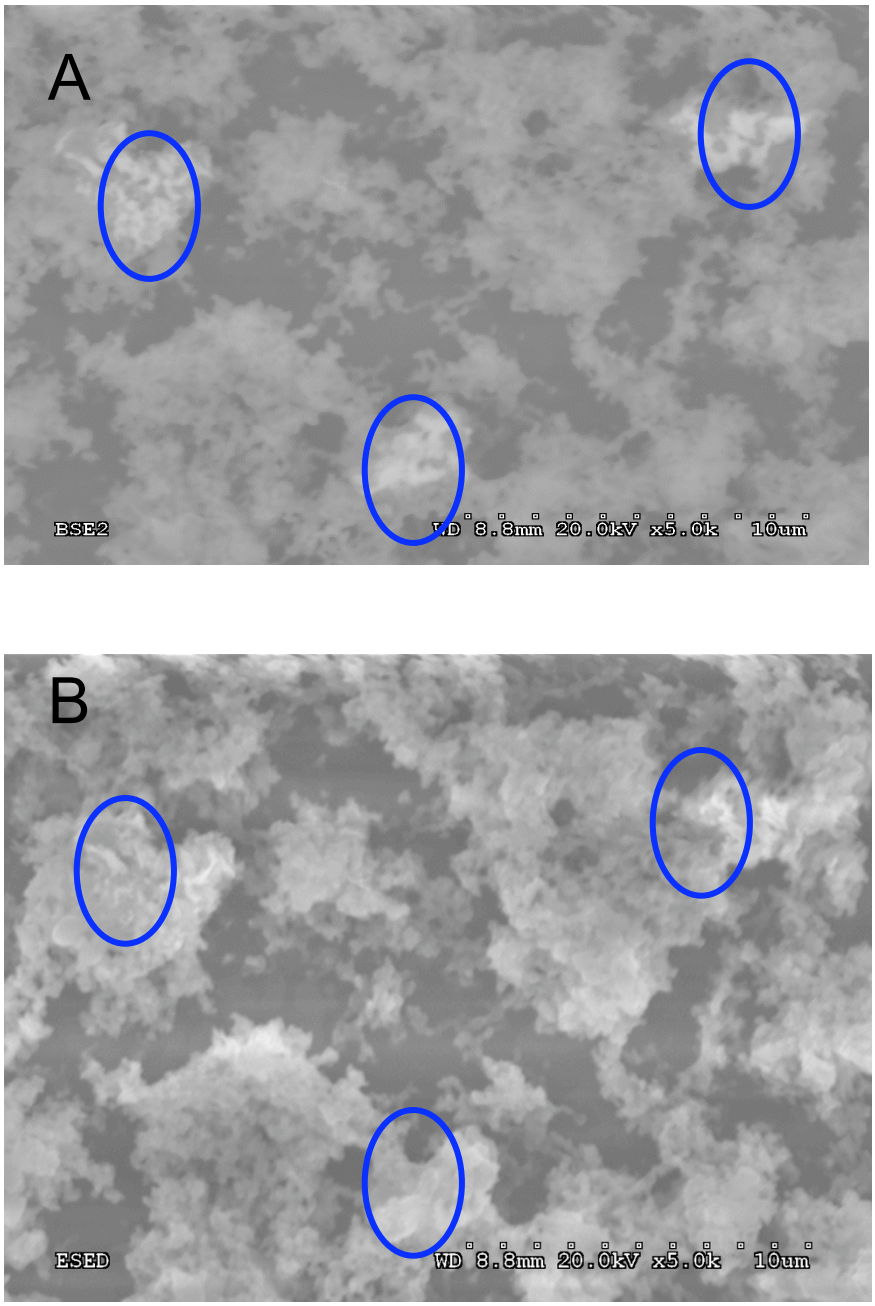

Figure 3-3 (a) TiO_2 image using back-scattered electron (BSE). BSE indicates there are at least two distinct compounds. Deposits are circled. (b) Imaging using environmental secondary electron detector (ESED). ESED topographically shows HgO is located on peaks of TiO_2. It is uncertain what are the thicknesses of HgO coatings, though clearly far less than 1 micron.

Chapter 4

Kinetic and product studies of the reactions of NO_2 with Hg^0 in the gas phase, and in the presence of titania micro-particle surfaces at different relative humidity

Contributions by author:

This paper further expands on the idea from chapter 3 of how mercury can be oxidized in the presence of titanium dioxide and ultra-violet light. In chapter 3 I outlined the method for creating a stationary flask system that could measure the Langmuir adsorption constant and the rate constant following Langmuir-Hinshelwood oxidation. This paper contrasts the oxidation of mercury by homogeneous and heterogeneous processes. In the first part of this paper I was responsible for performing the oxidation reactions of mercury in the presence of nitrogen dioxide. I also determined this was a homogeneous reaction that forms $Hg(NO_3)_{2(s)}$ as a final product. The kinetics mechanism and rate constant, which I was responsible for devising, agreed with previously published material. There was no heterogeneous component to the reaction, as changes in surface-to-volume ratios and addition of TiO_2 had no effect on rate. Addition of liquid water decreased the rate, probably due to losses in NO_2 to form HNO_3(aq).

In the second half of the paper, the focus was on the oxidation of mercury oxide in the presence of nitrogen dioxide. The product was mercury nitrate, which implies in the presence of concentrated NO_2 flue gas there will be significant oxidation of HgO (the capture product of the UV-TiO_2 system described in chapter 4). My work involved coating the glass disks with TiO_2, devising probable mechanisms for the oxidation reactions, and creating thermal desorption GC/MS ramps for mercury, HgO, $Hg(NO_3)_2$, and NO_2.

Submitted to *J. Water Air & Soil Pollut.*

Kinetic and product studies of the reactions of NO_2 with Hg^0 in the gas phase, and in the presence of titania micro-particle surfaces at different relative humidity

Graydon Snider and Parisa Ariya*

Department of Chemistry, and Department of Atmospheric and Oceanic Sciences
801 Sherbrooke St. W., Montreal, PQ, CANADA, H3A 2K6;
Emails: graydon.snider@mail.mcgill.ca; parisa.ariya@mcgill.ca
*The corresponding author

Abstract

As the emission of mercury via coal combustion increases to the atmosphere, a number of techniques and methods using adsorption capture are being developed to prevent the escape of mercury into the atmosphere. Titanium dioxide in the presence of ultra violet light (UV-A; λ_{max} ~ 360 nm) is able to capture mercury as HgO(s), however testing the effects of this oxidation method with other pollutants has so far been limited. We herein performed kinetic and product studies of mercury adsorption in the presence of the major group of mercury co-pollutants NO_x ($NO + NO_2$). The $NO_{2(g)}$ reaction with $Hg^0_{(g)}$ was initiated in the gas phase and in the presence of TiO_2 microparticle surfaces (1 μm thickness) from zero to 100% relative humidity (RH). The reaction, a two-step addition of NO_2, appeared to be predominantly gas-phase under our experimental conditions. The second order rate constant was estimated to be $k = (3.5 \pm 0.5) \times 10^{-35}$ cm^6 $molec^{-2}$ s^{-1}, independent of the presence of titania or total available adsorption surfaces. At RH>100%, non-homogeneous behaviour was observed. The identified reaction product formed was assumed to be solid $Hg(NO_3)_2$. NO_2 exposure to titania surfaces saturated in captured mercury (HgO) increased total mercury uptake onto the surface. This reaction was purely heterogeneous in nature, in contrast with $Hg + NO_2$. We discuss the desorption of reaction products from titania surfaces and the implications to the capture of mercury.

4.1 Introduction

The total atmospheric burden of mercury has remained approximately unchanged in recent decades [4] yet mercury deposition remains several times higher than historic background levels [204]. Anthropogenic atmospheric mercury is also increasingly attributed to coal combustion activities. Coal emissions have been shown to account for 30% of atmospheric mercury deposition and the relative contribution may be rising [28]. Depending on the source, coal combustion can release mercury, CO, NO_x (NO + NO_2), hydrocarbons, HCl and SO_2 into the atmosphere [124]. A combination of catalytic reduction processes and sorbents technologies (chemi- or physi-sorption) seek to reduce these emissions. Suggested sorbents for capture mercury in a coal fire flue gas include fly ash, activated carbon and iron oxides [98]. A frequent issue is the negative effect of the co-pollutants NO_2 and SO_2 on mercury capture efficiencies [14, 198]. An alternative oxidation/adsorption capture method is exposing thin films of titanium dioxide (TiO_2, also known as titania) to ultra violet (UV-A; $\lambda_{max} \sim 360$ nm) light [117, 186, 205, 206]. This technique differs from other sorbent methods as it more selectively captures mercury, whereas hydrocarbons and NO_x are further transformed to gaseous CO_2 [194] and NO [207], respectively. Co-pollutants are less likely to permanently adhere to the titania/UV system but may still decrease oxidation rates due to competition with surface sites [208].

The titania capture method has been successfully applied at a wide range of mercury mixing ratios, ranging from less than one part per billion (ppb) [116, 117, 120] to over 1 parts-per million (ppm) [206] (1 ppmv = 2.45×10^{13} molecule cm^{-3} at standard temperature and pressure). Our previous results identified a film of HgO(s) [206]. The existing experimental works on mercury surface adsorption have been performed under conditions devoid of typical

flue gas NO_2 impurities and to our knowledge there is one previous study that investigated the kinetics of gaseous mercury oxidation by NO_2 [125]:

$$Hg^0_{(g)} + NO_{2\ (g)} \rightarrow \text{products} \qquad \text{Eq. 4-1}$$

To our knowledge no previous study has investigated the competitive adsorbance of elemental mercury and oxides of nitrogen in presence of titania surfaces. Our previous work in mercury capture using titanium dioxide and UV light (200-2000 nm) [206] was characterized by the Langmuir-Hinshelwood equation.

$$-\frac{d[\mathrm{Hg}]}{dt} = k\frac{A_{Geo}}{V_f}\frac{K[\mathrm{Hg}]}{1+K[\mathrm{Hg}]} \qquad \text{Eq. 4-2}$$

$[Hg]_t$ is the mercury concentration at time t, V_f is the flask volume, A_{Geo} is the geometric area of the illuminated titania disk, k is the rate constant and K_{Hg} is the Langmuir adsorption constant. The overall rate constant and the Langmuir surface uptake constants were determined to be $K_{Hg} = (5.1 \pm 2.4) \times 10^{-14}$ cm^3 $molecule^{-1}$ with an apparent surface deposition rate of $k = (7.4 \pm 2.5) \times 10^{14}$ molecule min^{-1} cm^{-2} [206].

As NO_x ($NO + NO_2$) is a prominent co-pollutant in coal combustion we included it in our studies of Hg^0 capture using TiO_2 surfaces. It has been previously shown that mercury is unreactive towards NO [75], so in this study we investigated the kinetics of the reaction of NO_2 with Hg^0 in the gas phase and over titanium oxide surfaces each at a wide range of relative humidity. Desorption studies were also performed on the titania surfaces. We discuss the relevance of our data for atmospheric conditions and for industrial applications at elevated levels of NO_2.

4.2 Experimental Section

4.2.1 Coating surfaces with titania

TiO_2 coating mixture was prepared as directed by Fernandez *et al.* [190] and as described in our previous study [206]. Scanning electron microscope (SEM) images of the surfaces [206] indicated the presence of sub-micron sized TiO_2 particles. Coating of interior of glass tubes with TiO_2 was performed in a similar manner described in detail below.

Ti(IV) isopropoxide (13 mL) was diluted with 87 mL of isopropyl alcohol and mixed thoroughly in a small beaker. Solution had slight yellow color. The Ti(IV) isopropoxide solution smoked while in contact with humid air. The interior of the 0.635 cm glass tubing (0.4 cm interior diameter, 7.8 cm long) was coated with the liquid mixture. A flow of humid air was passed though tube until the coating oxidized into a white solid. The coating procedure was twice more repeated, the tubes were heated in a furnace at 150 ± 5 ^{o}C (1 ^{o}C ~ 273 K) for 30 minutes and 500 ± 5 °C for two hours. Tubes were weighed before and after coating procedure; thickness was estimated to be 1 ± 0.1 μm.

4.2.2 Kinetic experiments

Reactions were performed alternately in two 5.5 L halocarbon wax-coated flasks (Supelco; 1g wax/100 mL acetone) at room temperature, 23 ± 2°C as in previous work [74, 147]. Mercury gas was transferred first to the flask via vacuum line and pressure differential, with a 5.5 L source flask of liquid mercury (99.999% pure) in equilibrium with gaseous mercury. Mercury was allowed to equilibrate for several minutes in flask.

Nitrogen dioxide source was made using an initial source of NO (Matheson Tri gas > 99.0%), at 180 or 360 Torr concentrations, added to a 1 L flask using a digital pressure gauge

(Edwards ASG 2000 mbar). Transferred gas, was clear with a slight brown tinge. An excess of pure oxygen (MEGS extra dry) was added to the flask until a pressure of 760 Torr was reached, whereby the gas immediately turned dark brown. The stoichiometric conversion of NO to NO_2 is 3:2 hence an initial pressure drop was observed:

$$NO_{(g)} + NO_{(g)} + O_{2(g)} \rightarrow 2NO_{2(g)} \qquad \text{Eq. 4-3}$$

Oxygen was further added incrementally to the flask to reach a pressure of ~760 Torr. The third order rate of reaction 4 is $k_{4\text{-}4} = 1.9 \times 10^{-38}$ cm^6 $molec^{-2}$ s^{-1} [209], thereby converting 50% of NO to NO_2 in a half-life time of < 1 sec ($t_{1/2} = (k_{4\text{-}4}[NO][O_2])^{-1}$) assuming an excess of O_2 and an initial NO concentration of 0.5 atmospheres.

Kinetics were following the addition of NO_2 (0.5-10 ml) into the 5.5 l reaction flask. A Hamilton gas-tight syringe was used to sample from the septum port of the flask to the GC-MS instrument. Mercury isotope signals were detected with an electron impact ionization mass spectrometer (HP-5973) using single ion monitoring (SIM) mode for m/z range 198-202. Relative mercury concentrations were determined by peak area integration of SIM signal. Separation of $Hg^0(g)$ from other constituents was performed on a gas chromatograph (HP-6890) equipped with a 30 m × 0.25 mm i.d. × 1.0 mm o.d. crossed-linked phenyl-methyl–siloxane column (HP5-MS). The column was operated at a constant flow (50 mL min^{-1}) of UHP helium. During chromatographic runs GC column was held at 60 °C. Inlet temperatures varied between 100 °C and 250 °C. Retention time for mercury in column was 1.4 minutes. Prior to monitoring MS mercury signal loss with UV exposure time, a blank was performed by injecting 200 μL of room air into the GC during a SIM standard run and no signal peak was discernable from background noise during this interval. Background signal noise was about 200 – 300, arbitrary units.

4.2.3 Measurement of the thermal desorption of mercury

A series of desorption curves of elemental mercury were made using a temperature ramping of the GC inlet. The temperature ramp rate was 16 K/min. Ramps were done with the GC inlet held for 1 minute at 100 °C, then increasing at 16.7 °C/min to 250 °C (for 10 minutes) and held at 250 °C for 10 – 15 minutes. The TiO_2-coated glass tube was placed in the GC inlet while at 100 °C. The GC inlet program was given 5 minutes to flush unabsorbed species, after which time a steady MS signal was observed.

4.2.4 Analysis of uncertainties

Mass spectrometry peak areas (used in SIM mode) were calibrated to gaseous concentrations of mercury. Error of MS signal peaks were estimated to be ± 10% of total signal. Error reported reflects this least squares regression slope error.

For multiple measures of the slope, proportional to *k*' (see Tables 4-1 and 4-3), reported uncertainties represent the standard deviation of the mean of these slopes, i.e. $\sigma_{<k'>} = \sigma_{k'}/\sqrt{n}$. In Table 4-2, errors were obtained from regression analysis of slope data, i.e. $m \pm \sigma_m$, $b \pm \sigma_b$.

Slope of equation 4-8, the order of the reaction, was rounded to the nearest integer. The reported rate constant *k*, related to the intercept b of equation 8, was determined by the averaging measured *k'* values:

$$\langle k \rangle = \frac{1}{n} \sum_i \frac{k'_i}{[NO_2]_i^2} \qquad \text{Eq. 4-4}$$

4.3 *Materials and supplies:*

Usage of Ti(IV) isopropoxide (97% Sigma Aldrich) was done in room air at ambient temperature. A small headspace of argon was placed inside container. Coating of glass disks

was done in room air at ambient temperatures. No additional purification of the isopropoxide solution or of the isopropanol (HPLC grade, Fischer scientific) was performed. Mercury (99.999%, Sigma Aldrich), air (extra dry, Praxair) and nitrogen oxide (> 99.0%, Matheson Tri Gas) gas were all used as received from the manufacturer and no further purification was performed. Distilled water was purified to 18 MΩ (Milli-Q) resistance water before being added to flaks.

4.4 Results and Discussion:

4.4.1 Gas phase NO_2 + $Hg^{(0)}$ kinetics

There is one previously reported rate coefficient for the gas-phase elemental mercury oxidation by NO_2 (equation 4-1) [125]. The rate loss of mercury was determined to be first order in Hg and second order in NO_2:

$$\frac{d[\mathrm{Hg}]}{dt} = -k_{obs}[\mathrm{Hg}][\mathrm{NO_2}]^2 \qquad \text{Eq. 4-5}$$

If one assumes an excess of NO_2 with respect to mercury, a pseudo-first-order rate can is readily made:

$$k' = k_{obs}[\mathrm{NO_2}]^n \qquad \text{Eq. 4-6}$$

Equation 7 can be linearize via

$$\ln k' = \ln k_{\mathrm{obs}} + n \times \ln[\mathrm{NO_2}] \qquad \text{Eq. 4-7}$$

The slope was found to be, within the bounds of error, n = 2 [125]. The overall rate was estimated to be $k_{\mathrm{obs}} = 2.8 \pm 0.5 \times 10^{-35}$ cm^6 molecules^{-2} s^{-1} (at T = 20 °C) showing a negative temperature dependence, where $k_{\mathrm{obs}} = Ae^{-Ea/RT}$ (E_a = -13.2 kJ mol^{-1} and A = 1.25×10^{-37} cm^6 molecules^{-2} s^{-1}). Notably the reacting was invariant to surface-to-volume ratios changes due to

flask size.

As shown in Table 1, our gas-phase kinetic study yielded to similar pseudo-first-order *k'* values. Gaseous NO_2 concentrations were varied between 100 and 550 ppm at ambient temperatures (T = 22 ± 1 °C). Table 4-2 and Fig. 4-1 indicate our (dark) kinetics agree within experimental errors of the reported values where our values were n = 1.92 ± 0.12 and $\ln k_{obs}$ = -76.5 ± 4.3 were obtained. For Hall they were: n = 1.92 ± 0.10 and $\ln k_{obs}$(Hall) = -76.8 ± 3.5. Our study was performed at a smaller S/V ratio (0.27 cm^{-1} versus 1.8) and both sets of kinetic data predict a second order dependence on NO_2. Both predicting similar rates for the overall rate: k_{obs} (Hall) = (2.8 ± 0.6) × 10^{-35} cm^6 $molec^{-2}$ s^{-1} and k_{obs} (This study) = (3.5 ± 0.5) × 10^{-35} cm^6 $molec^{-2}$ s^{-1}).

4.4.2 Factors influencing NO_2-mercury oxidation rate

Compared to reactions done in 760 Torr air and 350 ppm of NO_2, table 4-3 displays the changes on the rate constant *k'* (equation 6) in the presence of titania surfaces, different humidity levels (RH at <1%, 75% and supersaturation), surface to volume ratio. This concentration of NO_2 (350 ppm) was chosen as a realistic concentration that might be found in a coal emission before SCR catalyst scrubbing.

To evaluate the effect of the surface-to-volume ratio on reaction rate coefficients, we performed our experiments in two reaction vessels with volumes of 1.6 L and 5.5 L. Reactions were performed both in dark and light (fluorescent light from lab environment, $\lambda > 400$ nm) Comparing the rate *k'* between each flask volume, presence or absence of light, to within experimental uncertainties, was observed. As illustrated in Table 4-3, to evaluate a potential pressure dependence of the rate coefficient (*k'*), we had modified the total pressure between 75 and 760 Torr. No significant pressure dependency on the rate constant *k'*, within error, was

observed as shown in Table 3. We cannot overrule the pressure effects outside the pressure range deployed in the current study, noting that our experimental design could not guarantee pressures below 30 Torr. The change in oxygen concentration from the reaction chamber did not seemingly affect the reaction rate: $k'(\text{air}) = (2.5 \pm 0.08) \times 10^{-3}\ s^{-1}$ versus $k'(N_2) = (3.1 \pm 0.05) \times 10^{-3}\ s^{-1}$. We note that the experimental setup was not adequate to perform an entirely oxygen-free experiment.

To evaluate the effect of surfaces, we included in the reaction flask a glass disk coated with a titania film (11.4 cm^2). Under our experimental conditions, no statistically significant increase to the observed reaction rate coefficient for the equation (1) was observed. We surmise that this reaction is predominantly a gas-phase under the experimental conditions herein used.

The addition of water vapour below saturation levels did not statistically affect the reaction rate. By contrast when liquid water droplets were included the reaction rate decreased by approximately 50% from $k' = (1.1 \pm 0.26) \times 10^{-3}\ s^{-1}$ to $(2.49 \pm 0.08) \times 10^{-3}\ s^{-1}$. We believe might be attributed to scavenging the NO_2 gas by water droplets [210]. This decrease reaction rate of mercury oxidation over liquid water stands in contrast to the increases found in chlorine or ozone oxidation of mercury over water [66, 67, 147, 211].

4.4.3 Oxidation of HgO by NO_2

Products of reaction (1) have not been identified previously. In a parallel experiment red HgO powder was combined with concentrated NO_2 gas (1% in air), where within one hour it transformed into a white, water-soluble powder. After being dissolved in a small amount of water the red mercury oxide precipitated out within minutes. This precipitation was previously noted by Remy *et al.* for sufficiently high concentrations of dissolved mercury nitrate [64]. The above experiment provides some insight into reaction (1), where the formation of mercury(II)

nitrate as a product (in presence of NO_2) appears possible. Hence the net balanced reaction of equation 1 could be written as

$$Hg^0_{(g)} + 2NO_{2\,(g)} + O_{2(g)} \rightarrow Hg(NO_3)_{2(s)} \qquad \text{Eq. 4-8}$$

Eq. 4-8 predicts that the lack of oxygen would impede the reaction. We did not observe any decrease in reactivity a flask filled with high-purity nitrogen; conversely the rate increased slightly to $k' = 3.12 \times 10^{-3}$ s^{-1} from the original $k' = 2.49 \times 10^{-3}$ s^{-1}. The amount of oxygen needed for Eq. 4-8 to proceed is probably quite small. Due to the possible O_2 leaks in our flask and vacuum line we cannot claim to have excluded oxygen below 1 *Torr*. Oxygen might also form in small concentrations via Eq. 4-9 below, which precludes the complete removal of oxygen from our system.

$$NO_{2(g)} + NO_{2(g)} \rightarrow 2NO_{(g)} + O_{2(g)} \qquad \text{Eq. 4-9}$$

4.4.4 General scheme(s) for oxidation mechanism between Hg and NO_2

It has yet to be established whether mercury reacts with $N_2O_{4(g)}$ or $NO_{2(g)}$ [125]. A previous kinetic study examined whether ethene reacted with $N_2O_{4(g)}$ or $NO_{2(g)}$ [212], and their results pointed to a reaction with $NO_{2(g)}$ as the more plausible. Here we examine both cases by discussing two possible mechanistic schemes.

Scheme I:

$$Hg^0_{(g)} + NO_{2(g)} \Leftrightarrow HgONO^*_{(g)}$$
$$HgONO^*_{(g)} + NO_{2(g)} \rightarrow Hg(ONO)_{2(g)} \qquad \text{Eq. 4-10}$$

The rate loss of mercury thus involves two successive collisions between two NO_2 molecules. Assuming a steady state for HgONO* intermediate, we have

$$r = -\frac{k^0_{Hg,I}}{1+\frac{k^0_{Hg,I}}{k^\infty_{Hg,I}}[NO_2]}[NO_2]^2[Hg] \qquad \text{Eq. 4-11}$$

Where k^0 and k^∞ are the low and high pressure limits of the rate constant, respectively. At (comparatively) low $NO_{2(g)}$ pressures the rate is second order with respect to $NO_{2(g)}$, consistent with our observations

$$r = -k^0_{Hg,I}[NO_2]^2[Hg] \qquad \text{Eq. 4-12}$$

Since at higher NO_2 concentrations the reaction rate is first order with respect to NO_2, this scheme could be verified by exposing mercury to higher concentrations of the nitrate.

Scheme II:

Examples of non-radicals reacting $N_2O_{4(g)}$ are uncommon. Dinitrogen tetroxide apparently reacts as a second order overall reaction with some alcohols (n-C_3H_7OH and C_2H_5OH) [213]. If mercury instead reacts directly with dinitrogen tetroxide, then the two-step reaction would need to be stabilized by a third body:

$$N_2O_{4(g)} + Hg^0_{(g)} \Leftrightarrow HgN_2O_4{}^*_{(g)}$$
$$HgN_2O_4{}^*_{(g)} + M_{(g)} \rightarrow Hg(ONO)_{2(g)} \qquad \text{Eq. 4-13}$$

The reaction rate is then written as

$$r = -K_{NO_2}\frac{k^0_{Hg,II}[M]}{1+\frac{k^0_{Hg,II}}{k^\infty_{Hg,II}}[M]}[NO_2]^2[Hg] \qquad \text{Eq. 4-14}$$

We observed no change in the reaction rate with respect to pressure changes, however the observation of pressure dependence could require a much higher or lower pressure changes than we performed. For pressures close to one atmosphere, Eq. 4-14 would resemble the empirical Eq. 4-5:

$$r = -K_{NO_2} k^{\infty}_{Hg,II} [NO_2]^2 [Hg] \qquad \text{Eq. 4-15}$$

4.4.5 Choosing between Scheme I and II

Assuming scheme I, the rate constant (for reaction 1) is unchanged, where $k_{obs} = k^0_{Hg,I} = (3.5 \pm 0.5) \times 10^{-35}$ cm^6 molec^{-2} s^{-1}, a reasonable collision probability for a third-order reaction. If we use this same net rate for scheme II, then dividing out the equilibrium constant $K_{NO2} = 2.5 \times 10^{-19}$ cm^3 molec^{-1} [214] yields $k^{\infty}_{Hg,II} = k_{obs}/K_{NO2} = 1.4 \times 10^{-16}$ cm^3 molec^{-1} s^{-1}. This value may be fast for a re-arrangement of $N_2O_{4(g)}$ but it is difficult to say with certainty whether one scheme can be more favored over the other. Performing experiments at higher pressures of $NO_{2(g)}$, may confirm our hypothesis, whereby if scheme I is correct we expect the $NO_{2(g)}$ reaction order should approach unity. We speculate the net gas-phase mechanism for reaction 1 is a steady state between the intermediate HgONO and reaction of $Hg(ONO)_2$ with oxygen.

$$Hg^0(g) + NO_{2(g)} \Leftrightarrow HgONO^*_{(g)} \qquad \text{Eq. 4-16}$$

$$HgONO^*_{(g)} + NO_{2(g)} \rightarrow Hg(ONO)_{2(g)} \qquad \text{Eq. 4-17}$$

$$Hg(ONO)_{2(g)} + O_{2(g)} \rightarrow Hg(NO_3)_2(s) \qquad \text{Eq. 4-18}$$

It is recommended that the thermodynamic stability of $Hg(ONO)_2$ be calculated in further studies. Since reaction (1) will proceed above 200°C [125] and given mercury(II) nitrate's decomposition temperature of 160 °C [60, 90], a second mechanism may exist for temperatures above 160°C.

4.4.6 Effects of NO_2 on titania surfaces

The Langmuir-Hinshelwood-Hougen-Watson (LHHW) rate expression for the oxidation of mercury by UV light was described in our previous work [206] and in other studies [116, 117]. The expression also implicitly involves oxygen and water, which are both required to oxidize mercury. We assume water vapor, oxygen, and other species remain nearly constant throughout the experiment. K_{H2O} is not precisely known for our titania surface, however from other studies it can be approximated to be $K_{H2O} \sim 0.00045$ ppmv^{-1} [215] thus much smaller than our measured value for mercury: $K_{Hg} \sim 1.3$ ppmv^{-1} [206]. In this study Eq. 4-2 is simplified using lower concentrations of mercury, i.e. $K_{Hg}[Hg] << 1$, and integrated to a logarithmic relation

$$\ln \frac{[Hg]_t}{[Hg]_0} = -\frac{kK_{Hg}A_{Geo}}{V_f} t \qquad \text{Eq. 4-19}$$

Assuming A_{Geo} and V_f both remain constant, the factor $k K_{Hg}$ can be calculated as a net uptake of mercury on titania.

We exposed mercury oxide to 1% NO_2 for 60 minutes and found uptake of the titania disks for mercury increased significantly. Comparing the rate of uptake before and after exposure the uptake rate increased about 10-fold, where, referring to equation 4-19, $k K_{Hg}$(before NO_2 exposure) = 4.4 ± 0.1 and $k K_{Hg}$(after NO_2 exposure) = 42.5 ± 2.2. The mercury oxide deposits appear transformed on the surface (figure 4-3 a and b). We also observe that mercury(II) deposits heterogeneously on the titantia surface but it is unclear why certain titania regions are favored over others. Possibly this heterogeneity is due to the mix of anatase and rutile crystal structures. After $NO_{2(g)}$ exposure the deposits appear more scattered and smaller than HgO(s) clusters did before. What reaction has precisely occurred on the surface is

unknown. We can hypothesize the formation of $Hg(NO_3)_2$, but without certainty. Powder XRD shows some differences after $NO_{2(g)}$ exposure (figure 4-3), though they are slight. It is clear some reaction is occurring, as the HgO(s) deposits are dark grey in color, and after $NO_{2(g)}$ exposure these areas become bright white. As to the increased reactivity, it is known that titania, when exposed together with UV light, $NO_{2(s)}$ and water, will form surface deposits of $HNO_{3(ads)}$ [207]. In addition the surface re-arrangement of HgO(s) deposits may explain the enhanced oxidation after $NO_{2(g)}$ exposure. These re-arrangements merit further study.

4.4.7 Desorption of mercury compounds on TiO_2 surfaces at elevated temperatures

In a series of MS thermal desorption experiments we exposed 0.635 cm titania-coated glass tubes to elemental mercury gas. We observed that the mercury gas would begin to desorb from these tubes at temperatures above 120°C up to 250 °C. We desorbed mercury oxide from titania mercury and found degassing of mercury would occur above 160°C. We also found NO_2 will desorb from titania above 100°C after exposure of the surface to NO_2 gas. As NO_2, Hg, and $HgO_{(s)}$ each adhere to the TiO_2 surface below 100°C, mercury capture by titania may be feasible at temperatures close to this range.

4.4.8 Role of $NO_{2(g)}$ in atmospheric oxidation of mercury

Because reaction (1) is second order for typical NO_2 concentrations, this reaction is not environmentally significant. Our third order rate constant was measured to be $k_{obs} = (3.5 \pm 0.6) \times 10^{-35}$ cm^6 $molecules^{-2}$ s^{-1} at 22 °C. The lifetime of mercury in 500 ppm of NO_2 is *ca.* 3 min. Only a few seconds of residence time are available in a coal flue gas therefore it is of minor importance for typical combustion systems [125]. Table 5 compares NO_2 to other known

oxidizers of mercury. NO_2 could be of some interest for mercury oxidation in lightning storms [216].

Most surfaces present in coal fire power plants, such as the metal oxides in selective catalytic reduction (SCR) catalysts, will decompose $NO_{2(g)}$ to N_2 and H_2O. Titanium dioxide is among such metal oxides. The deactivation of titania under UV light is due to a saturation of the surface with HgO(s) deposits. The reaction is therefore self-limiting. Saturated titania films can be regenerated by thermal desorption above 250 °C but also by exposure to high levels of $NO_{2(g)}$. Whether this transformation is relevant for coal flue gas systems remains a future point of discussion.

4.5 Conclusions

We oxidized gaseous elemental mercury with nitrogen dioxide at a wide range of NO_2 concentrations. At the concentrations of 350 ppm NO_2 we performed the reaction the presence of TiO_2 surfaces, pressures, and relative humidities. Our gas phase kinetic study of reaction (4-1) was in agreement with previously reported values at room temperature. Both data sets predict a square dependency on NO_2 concentration. Future work should focus on the very fast reaction between high $NO_{2(g)}$ levels (> 1000 ppm) and $Hg^0(g)$. The final product might be $Hg(NO_3)_2$ (reaction 4-17).

By expanding on Hall's investigation of surface dependence of reaction 1, we observed little evidence for surface-dependent kinetics in the presence of titanium dioxide. We also did not observe light, oxygen concentration, pressure, or relative humidity dependence of reaction (1) under experimental conditions used in this study.

It was found that exposure of high $NO_{2(g)}$ concentrations over the titania saturated with HgO(s) will regenerate adsorption activity of the films through conversion of HgO(s) to some

unknown compound, possibly $Hg(NO_3)_{2(s)}$. Assuming a reaction between HgO and gaseous NO_2, it must occur heterogeneously as HgO(s) is not volatile. Future work should investigate the detailed surface mechanisms for this supposed reaction and an explanation for the surface heterogeneity of HgO(s) deposits.

The UV-titania system is functional as a mercury oxidizer in conditions of high NO_2 concentrations and humidity. Mass spectrometry desorption analyses show HgO(s) remains attached on films below 120 °C. The practical implication of this study, combined with our previous study [206], is that high concentrations of mercury (~1 ppm) can be removed in coal fire plant flue gases bearing typical levels of SO_2, H_2O and $NO_{2(g)}$.

Table 4-1 Pseudo-first-order rate constants for equation (3)

$[NO_2]$, ppm	$k' \times 10^3$ s^{-1*}	Number of trials
100	0.176 ± 0.09	4
150	0.45 ± 0.12	4
190	0.96 ± 0.08	4
250	1.63 ± 0.05	4
350	2.49 ± 0.08	6
450	4.29 ± 0.35	4
550	6.49 ± 0.27	4

* k' is defined by d[Hg]/dt = k'[Hg]

Table 4-2 Comparing values in the plot of equation 4-8: $\ln k' = \ln k_{obs} + n \times \ln[NO_2]$

Value	Literature data*	This study
$[NO_2]$ range, ppm	100 - 696	100 – 550
$\ln(k_{obs})$	-76.76 ± 3.51	-76.53 ± 4.30
k_{obs} (cm^6 $molec^{-2}$ s^{-1})	$2.8 \pm 0.6 \times 10^{-35}$	$3.5 \pm 0.5 \times 10^{-35}$
Reaction order for NO_2	1.92 ± 0.10	1.92 ± 0.12
Eqn 1: R^2	0.971	0.985
S/V (cm^{-1})	1.8, 4.0	0.27

* Hall, 1995 [125]

Table 4-3 Rate constant *k'* (equation 4-8) dependence on titania. Bath gas is dry air, unless otherwise indicated. [NO_2] = 350ppm, TiO_2 disk = 3.8 cm diameter × 1μm thick.

Conditions	$k' \times 10^3$ (s^{-1})	Number of trials
5.5 L flask		
NO_2	2.49 ± 0.08	4
NO_2 (76 Torr)	2.77 ± 0.26	3
NO_2 (N_2)	3.12 ± 0.05	2
NO_2 + TiO_2 disk	1.70 ± 0.44	4
NO_2 + TiO_2 disk + H_2O (75% RH)	1.84 ± 0.08	3
NO_2 + TiO_2 disk + H_2O (saturated)	1.10 ± 0.26	4
1.6 L flask		
NO_2	1.41 ± 0.27	4
NO_2 + TiO_2 disk	1.24 ± 0.12	4
NO_2 + TiO_2 disk + H_2O (75% RH)	1.45 ± 0.08	2

Table 4-4 Atmospheric mercury lifetime, assuming oxidation by species [X] only

Atmospheric Oxidants*	Hg lifetime	Ref.
[NO]	No observed reaction	[75]
[NO_2]		
30 ppt (remote marine/forest)	2.0×10^9 years	
1 ppb (rural)	1.8×10^6 years	[146]
1000 ppb (urban)	1.8 years	
500 ppm (flue gas)	>3.8 minutes	[143]
[NO_3]		
8 ~ 20 ppt (remote)	8 ~ 3.3 days	[214]
80 ~ 280 ppt (urban)	20 ~ 5.7 hours	
[Br]		
0.4~4 ppt (remote)	3.3 ~ 0.33 days	[144]
[BrO]		
1-2 ppt (remote)	46 ~ 23 days	[144]
20 ppt (Br explosion, Arctic)	2.3 days	[144]
120-170 ppt (Br explosion, Dead Sea)	9.2 ~ 6.5 hours	[77, 144]
[O_3]		
20 ppb (remote)	37 days	
100 ppb (rural)	7.5 days	[146]
400 ppb (urban)	1.9 days	

*$[Hg]_{remote} \sim 0.2$ ppt.. For $\tau_X = ([X]k_X)^{-1}$, $k_{O3} = 6.2 \times 10^{-19}$ cm^3 molec^{-1} s^{-1} [147], $k_{Br} = 3.6 \times 10^{-13}$ cm^3 molec^{-1} s^{-1} [148], $k_{NO3} < 4\text{-}7 \times 10^{-15}$ cm^3 molec^{-1} s^{-1} [75, 149], $k_{BrO} \sim 10^{-14}$ cm^3 molec^{-1} s^{-1} [150].

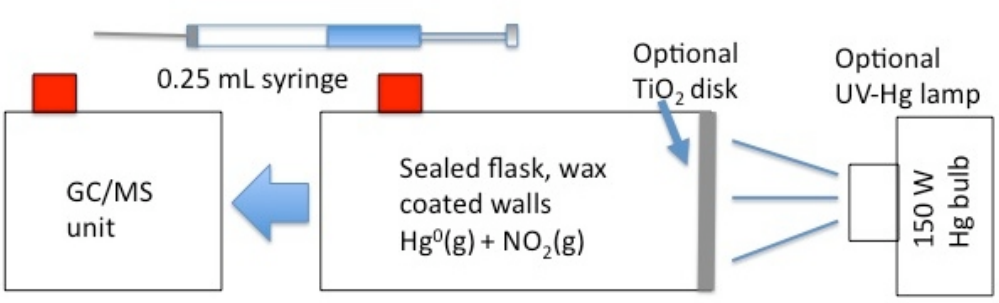

Figure 4-1 Schematic setup for kinetic experiments. Flask is 5.5 or 1.56 litres and sealed with halocarbon wax. Internal pressure was 760 Torr and filled with dry air unless otherwise indicated. A 0.25 mL syringe sampled from flask via septa (colored red) at regular intervals and monitored by GC/MS SIM mode. Optional TiO_2 plate and 150W UV-Hg high-pressure lamp was utilized for specified experiments.

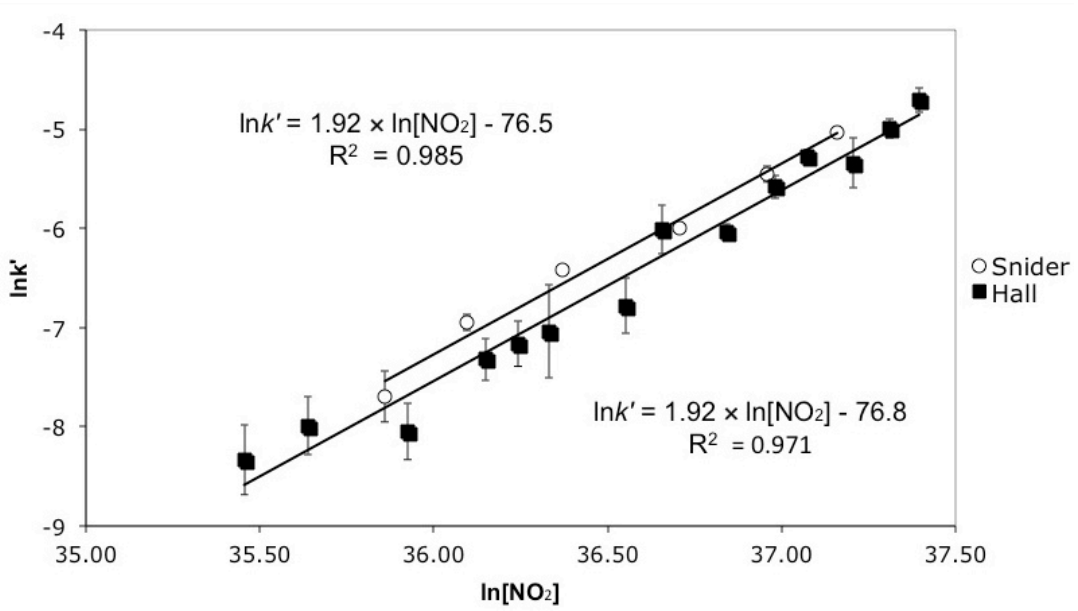

Figure 4-2 ln k' versus ln [NO_2] using equation 4-8. Slopes for both experimental sets agree within limits of error.

A

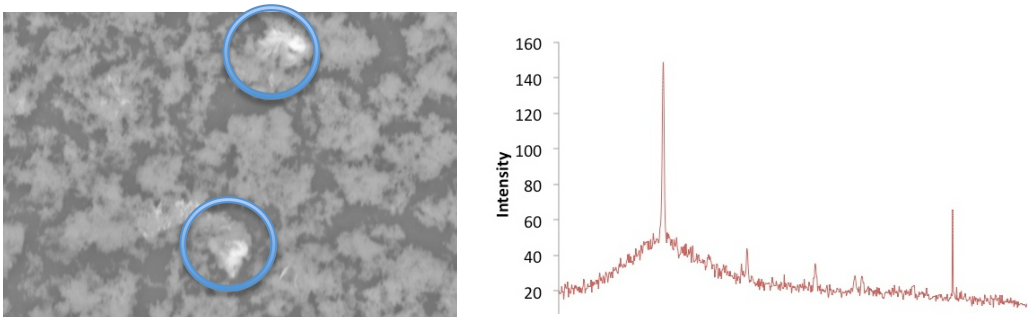

B

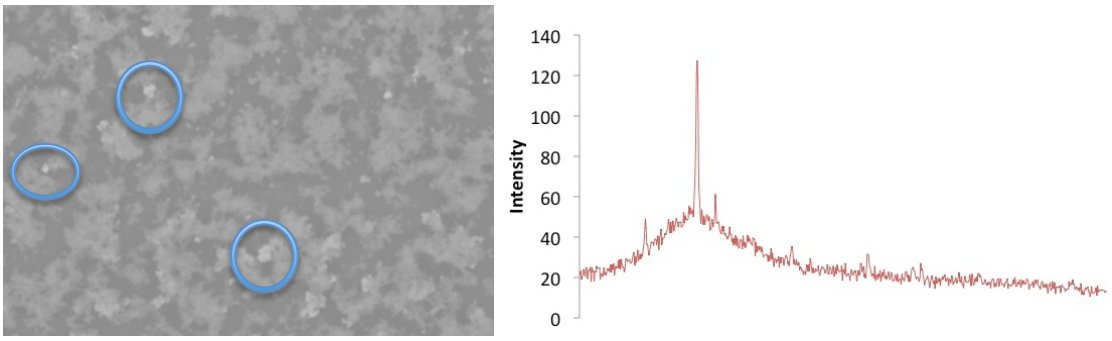

Figure 4-3 a) Possible HgO(s) deposits shown in scanning electron micrograph (SEM) images (2500× magnification) and electron dispersion X-ray (EDX) and powder X-ray diffraction $10° < 2\theta < 80°$ of 0.5 mm × 0.5 mm area. Crystals were created by exposing UV light over TiO_2 coating (borosilicate glass substrate) under humid air and mercury gas. b) HgO(s) deposits from a) were then exposed to approximately 1% Torr of NO_2 gas for 1 hour. Crystals are much smaller, sub-micrometer in size and may have changed in composition.

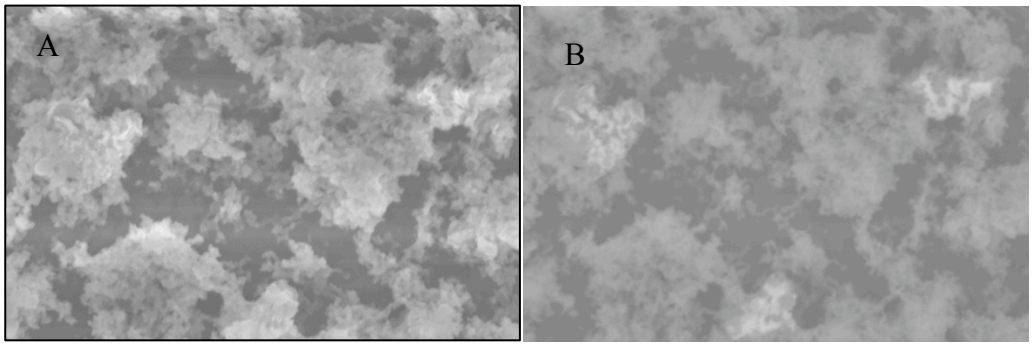

Figure 4-4 Two images of TiO_2 film. A) Backscatter surface enhancement (BSE) of TiO_2, left, versus secondary electron detector (SED), right. Although in an SED image the HgO particles can easily be distinguished from background (HgO = white, TiO_2 = grey), in a topographical BSE image there is little to distinguish one area over another.

Chapter 5

Conclusions and Future work

5.1 Summary and conclusions

We have investigated three types of mercury oxidation reactions: pure gaseous (Hg + NO_2), pure surface (Hg + TiO_2/UV) and heterogeneous (Hg + O_3). Results indicate that gaseous mercury can participate in a wide variety of reaction types. The most important parameter in simulating atmospheric processes is the relative humidity (RH), which was varied between 0 and 100%. None of the reactions appeared to be affected by RH below 100%.

Ozone is one of the most significant scavengers of atmospheric mercury. It can be established that the mercury-ozone reaction is partially gaseous, and partly surface dependent. The reaction can be described by a combined gas-phase and surface equation (with a S/V^2 or $1/r^4$ dependence):

$$-\frac{d[\mathrm{Hg}]}{dt} = \left(k_{vol} + \frac{S}{V^2}k_{sur}\right)[\mathrm{Hg}][\mathrm{O_3}] \qquad \text{Eq. 5-1}$$

Rate constants were reported as k_{gas} = (5.40 ± 0.56) × 10^{-19} cm^3 $molec^{-1}$ s^{-1} and k_{sur} = (2.91 ± 0.12) × 10^{-15} cm^7 $molec^{-1}$ s^{-1}; the former agreed well with literature.

Oxidation of ozone by mercury is affected by the presence of liquid water (not gaseous), the presence of halocarbon wax, and the size of the flask. Additionally the rate is affected by presence of gaseous CO, and the volatilized radical scavenger trimethylbenzene (TMB). Higher concentrations of ozone appeared to increase the rate constant, implying the mercury-ozone mechanism may not precisely follow the straightforward pseudo-first-order mechanism. The rate of mercury loss increased with the presence of liquid droplets (RH >100%) and did not

obey the pseudo-first-order plots. A novel mechanism should be proposed for this separate reaction. Future work on aerosol-loaded chambers, and more detail of oxidation on water, and perhaps on ice surfaces as well, should be performed. Introduction of SO_2 has not been tested, and would be of interest in future work.

In chapter 3 the pure surface-based oxidation reaction of mercury by TiO_2 and UV light is seen with scanning electron microscope (SEM) imaging, where deposits of mercury oxide are clearly seen to cluster in non-uniform regions. It is unknown why mercury deposits cluster in some areas and not others. Possibly this could relate to the distribution of anatase and rutile blends of surface TiO_2. As the TiO_2/UV reaction depends on the presence of both TiO_2 and UV, it is clear that the oxidation occurs on the surface and not in the gas phase. Mechanistically the reaction is well described by the Langmuir-Hinshelwood (LH) equation:

$$-\frac{d[\mathrm{Hg}]}{dt} = \frac{A_{\mathrm{TiO_2}} k}{V_f} \frac{K_{\mathrm{Hg}}[\mathrm{Hg}]}{1 + K_{\mathrm{Hg}}[\mathrm{Hg}]} \qquad \text{Eq. 5-2}$$

The LH equation requires knowledge of the mercury concentration, area of the TiO_2, and flask volume. Results compared well with the available literature, where $K_{Hg} = (5.1 \pm 2.4) \times 10^{-14}$ cm^3 $molec^{-1}$ and $k = (7.4 \pm 2.5) \times 10^{14}$ molec cm^{-2} min^{-1}. Implicitly there is also dependency on UV light intensity (incident photons/s) and oxygen/water concentrations. Although oxidation requires oxygen and water to proceed, drying the flask did not prevent oxidation nor did introducing excess water (RH > 100%). Lack of oxygen prevented mercury oxidation. Therefore in a coal flue gas this reaction would benefit from an O_2 rich environment such as for proposed coal plants designed with CO_2 capture technologies.

Mercury oxidation proceeded at high SO_2 (100 ppm) levels. The precise surface area of the TiO_2 coating is currently unknown; BET measurements were imprecise but suggest it may

be ~100 times greater than the geometric surface area. The TiO_2 surfaces themselves capture mercury (as HgO) in a very uneven/heterogeneous fashion.

The principal difficulty in obtaining accurate rate constants was the unstable UV light source; high-pressure mercury bulbs are prone to flickering and light emissions decrease with bulb lifetime. Mercury bulbs also produce prodigious amounts of IR radiation, therefore we cannot be certain of the surface temperature of the titania. It is likely the disk surface was well above room temperature. Alternate sources of UV light were considered but UV fluorescent bulbs and UV LEDs have insufficient power. However UV LEDs do have a very consistent emission level if combined into a sufficiently large array.

Chapter 4 was an extension of the work in chapters 2 and 3. We found that mercury can be readily oxidized by NO_2 and, unlike ozone, this reaction is unaffected by surfaces. There is no significant change in the rate while changing surface ratios, surface coatings, or humidity levels. The presence of TiO_2 itself did not influence the reaction between gaseous Hg and NO_2. The rate of this reaction is highly sensitive on the concentration of NO_2, proportional to its square:

$$\frac{d[\mathrm{Hg}]}{dt} = -k_{obs}[\mathrm{Hg}][\mathrm{NO_2}]^2 \qquad \text{Eq. 5-3}$$

Where k_{obs} was determined to be $k = (3.5 \pm 0.5) \times 10^{-35}$ cm^6 $molec^{-2}$ s^{-1}. We explain this second-order dependence is due a mechanism in which gaseous NO_2 twice adds to gaseous mercury. This leaves an open the question as to the stability of the intermediates $HgNO_2$ $Hg(NO_2)_2$ and is so far unjustified. Regardless of the mechanism, with NO_2 concentrations above 500 ppm the lifetime of mercury is seconds, but at more ambient NO_2 levels, e.g. 10 ppb, the reaction is not atmospherically significant compared with ozone.

Despite NO_2 having little atmospheric significance the importance of NO_2 in mercury capture is quite relevant. We have found that NO_2 at high concentrations will transform surface-

deposited HgO into $Hg(NO_3)_2$, thus enhancing the scavenging of the TiO_2-UV capture method. SEM images show that NO_2 breaks apart the HgO clumps into smaller fragments, which for undetermined reasons will 'clean' the photoactive TiO_2 regions. Possibly this is accomplished by a re-arrangement of oxide deposits. We have also shown via thermal desorption (monitored by MS) that small quantities of mercury will adsorb strongly to titania surfaces, enough to desorb only above 100 °C. More work is required to predict the mechanism of this surface/gas heterogeneous reaction.

5.2 *Future work (expanding on thesis projects)*

5.2.1 Introducing aerosols and other gasses into ozone-mercury kinetics

The presence of various types of other aerosols in oxidation of mercury by ozone would also be of practical interest. In chapter 2 we stated that mercury losses could be enhanced in the atmosphere in the presence of aerosols. This is due to the enhanced mercury rate loss observed in smaller containers. We suggest atmospheric particles, more rigorously defined in terms of total surface area and composition (e.g soot, salt, sand or acid) would permit better modeling of wet and dry deposition of mercury. Surface equilibrium constants K_{Hg} for mercury would also be useful to quantify the preference of mercury to various surfaces.

The effect of SO_2 on the oxidation of mercury by ozone has not been explored. SO_2 may compete for surface sites, or like CO may accelerate the reaction rate. Changes in flaks pressure may also be of interest, as it could affect the availability of surface sites available and whether "third body" collisions are required to oxidize mercury.

NO_2 is a powerful oxidant of mercury at sufficiently high concentrations. If NO_2 oxidation is considered with ozone there may be an additional surface enhancement due to its

reactivity with HgO(s). Such measurements would have to be precise, since simultaneous mercury oxidation by NO_2 would have to be considered.

5.2.2 Doping TiO_2 surfaces

Research suggests that *p-n* doping TiO_2 surfaces may enhance total mercury uptake by extending the UV bandgap into the visible realm, in principle up to about 440nm [121]. There is considerable interest in solar panels with such an absorption range, though few conclusive results are yet known. Dopants may also include carbon or other metal oxides such as vanadium, aluminum, or iron [217], which can increase strength or total area of surface coating. Gold-doped TiO_2 nanoparticles could enhance the uptake of mercury by amalgamating with single atoms of mercury prior to oxidation [218].

5.2.3 Standardized description of mercury kinetics

There is a lack of reliable or reproducible kinetics regarding the capture of gaseous mercury. Many reports focus on the percentage of mercury captured in a flow experiment, which is subject to the experimental design manipulation and often difficult to reproduce. We recommend that mercury kinetics be consistently described, which allows for some degree of conformity among all experiments. Using Langmuir-Hinshelwood (LH) equation or a related scheme, such as (modified) Elovich or (modified) Ritchie equations [219] could provide more insight into reaction rates and mechanisms than is frequently reported. For a gas (i.e. mercury) adsorbing onto a heterogeneous surface, kinetics based on the LH mechanism are written as

$$-\frac{d[\mathrm{Hg}]}{dt} = k\frac{K[\mathrm{Hg}]}{1+K[\mathrm{Hg}]} \qquad \text{Eq. 5-4}$$

The challenge is that such rates must be well parameterized, i.e. photon flux and wavelengths of light, temperature, and surface area of exposed surface film need to be quantified. A starting

point would be the measure of Langmuir isotherms, which would yield equilibrium constants of mercury K_{Hg} allowing one to define the "stickiness" of mercury.

Quantifying surface kinetics would also be aided by using a Knudsen cell. This is an enclosed cell pumped to low pressures such that particle mean free path ≈ cell width. Within the cell there is a sample of the surface or powder over which to expose the to-be adsorbed (mercury) gas. This apparatus would allow for the determination of net uptake coefficient γ of mercury by a surface. To link the Knudsen cell experiments with those performed in this thesis, the sample holder could be exposed to UV light to observe relative uptake of mercury on a titania coating versus in dark. A version of this has already been performed in our lab using a UV-LED, whereby the inflow of mercury into the CVAFS was compared with UV light on and off.

5.2.4 Mercury oxidation via $HCl_{(g)}$ + $Hg^0_{(g)}$ reaction

$HCl_{(g)}$ is a major constituent of waste incinerators (reaching levels of > 1000 ppm) but the reaction between mercury and HCl has been largely overlooked since it was measured in 1998 [227]. The inclusion of gaseous HCl in simulated mercury capture combustion flow systems is not left wanting, but mechanistic data on the isolated chemical kinetics between Hg and HCl (and how it is affected by humidity and surfaces) remains sparse in the available literature. An interesting future study would include the reactivity of heated HgO(s) with HCl. A surface reaction could occur is postulated by Liu *et al.* [228] to form $HgCl_2$ via

$$HgO_{(g)} + 2HCl_{(g)} \rightarrow HgCl_{2(g)} + H_2O_{(g)} \qquad \text{Eq. 5-5}$$

This was studied in a homogeneous modeling simulation by Xu *et al.* [229], but not yet in a controlled experimental kinetic study.

5.2.5 Varying temperature in UV/TiO_2 flask

As of now there is no data on the dependency of the mercury oxidation by titania and UV light under variable temperature. We have done preliminary experiments to measure desorption of products in the MS at elevated temperatures to show they were stable at 100°C. The temperature of the TiO_2 coating was not well defined because the intense IR bands from the mercury bulb UV source heated the flask walls. Future experiments could use a TiO_2 coating in contact with a water bath to maintain specific temperatures or use a cooler source of UV such as an LED.

5.2.6 Define surface kinetics of HgO(s) deposition and NO_2 oxidation of HgO(s).

We have discovered that the mercury oxidation by TiO_2 via UV light shows complex surface kinetics. Deposits of mercury oxide have been observed to be very heterogeneous, i.e. clustered, over the TiO_2 surface and require some topological explanation to predict why they are located so sparsely. There is also apparently a nucleation phase, where early irradiation of the TiO_2 shows initially no reactivity in the first minute or so of UV exposure, thereafter resumes a normal L-H type depletion. This 'lag' period should be further investigated.

More work is needed to explore the reactivity of mercury oxide with nitrogen dioxide on titania surfaces. Images show there is some re-arrangement of crystals on surface during oxidation of HgO to $Hg(NO_3)_2$. This remodeling on the surface is interesting since the reaction appears to increase the uptake ability of titania. Both HgO and $Hg(NO_3)_2$ are solid and crystalline. The reaction then is between a solid (HgO) and gas (NO_2) to produce another solid ($Hg(NO_3)_2$). More work is needed to quantify the additional uptake of Hg on the surface.

5.2.7 Thermal desorption of mercury oxides

Trace levels of mixed mercury oxides may potentially be separately identified using thermally-ramped surface desorption detected by mass spectrometry [220-222]. Mercury oxides may show complex desorption behaviour that can then be fingerprinted individually. We have produced some preliminary data of our own desorption curves from titania surfaces coated on the insides of ¼" glass tubes in appendix E, and we have observed after heating the species Hg^0(ads) and HgO(s) between 100°C to 250°C that they will desorb over this entire range. Future work should perform a series of temperature dependent ramp rates β (°C/s) monitored by MS at temperatures between 100°C and 600°C. If each ramp yields a characteristic desorption peak $T_M = f(\beta)$, they can used to determine the desorption energy ΔE_a (for X-S → X(g) + S(g)):

$$2\ln T_M - \ln\beta = \frac{\Delta E_a}{RT_M} + \ln\frac{\Delta E_a}{RA} \qquad \text{Eq. 5-6}$$

"A" is the Arrhenius pre-exponential factor and R is the ideal gas constant [223]. To our knowledge no one has yet reported desorption energies for sorbed mercury on titania, nor for any other surface of interest.

5.2.8 UV-LED Irradiation

Mercury capture systems using ultra violet-LEDs are new field still in its infancy. UV-LEDs can supply a narrow wavelength of UV light ($\lambda = 360 \pm 10$ nm), require no warm-up time, are increasingly cheap and have longer lifetimes (50,000 hours) compared with fluorescent (10,000 hours) or high-pressure lamps (1000 hours). Numerous studies have been performed concerning the oxidation of organics using UV-LEDs [224, 225]. Mercury oxidation using LEDs has not been performed. The power output of a single UV-LED is typically < 100 mW, but high power LEDs may be soon available. The stability of LED emission offers the

opportunity for very precise oxidation rates hence may be of considerable use for mercury oxidation studies.

5.3 *Suggested future mercury-related projects*

The following project ideas are not directly connected with the thesis contents, however the author has proposed them for future reference.

5.3.1 Mercury-ozone oxidation using molecular simulations

Referring to the overall reaction between gaseous ozone and mercury

$$Hg(g) + O_3(g) \rightarrow HgO(s) + O_2(g) \qquad \text{Eq. 5-7}$$

there is a missing a link in the mechanistic chain between reactants and products. There appears to be some disagreement over the means by which an intermediate could exist. The reaction

$$Hg(g) + O_3(g) \rightarrow HgO(g) + O_2(g) \qquad \text{Eq. 5-8}$$

creates the intermediate HgO(g) which is quite unstable hence and should be regarded with caution. Calvert and Lindbert address this problem but cannot reach a firm resolution [71]. How HgO(g), a weakly bound complex (D_0 = 4 kcal/mol) [70], survives long enough to deposit to form the stable solid HgO is a open question. It is possible that mercury oxide will accumulate as oligomers before depositing [226]. HgO(g) could require a surface to react, i.e.

$$HgO_{(g)} \rightarrow HgO_{(monomer,\ surface)} \rightarrow HgO_{(s)} \qquad \text{Eq. 5-9}$$

There could also be a mixture of the two processes. It is unknown how mercury deposits, whether as an oligomer or a single particle. A worthwhile study would simulate the aerosol clustering of mercury oxide from the early nucleation stages to oligomer clustering. These

simulations could be compared with surface-based oxidation mechanisms to help resolve intermediates.

5.3.2 SPME mercury traps

Solid-phase microextraction (SPME) is a reliable method for *in situ* sampling of trace substances. Mercury detection by SPME has been investigated by several studies [230]. A coating that traps mercury may later be desorbed in a controlled environment, i.e. placed in a mass spectrometer or CVAFS. New SPME coatings are of interest for specific capture of mercury. Aqueous organo mercury can be trapped using standard polydimethylsiloxane (PDMS) coatings [231] and Guo *et al.* found that mercury ions can be reduced on a gold-coated conducting fibre [232]. But selective capture of gaseous inorganic mercury would require a novel coating, perhaps such as a textured KCl salt or gold surface. SPME trapping could be combined with the thermal desorption ramping methods which desorb various mercury oxides separately from one another at various temperatures [220, 221].

5.3.3 Mercury as an isotope tracer for the atmosphere

There are numerous cases of trace gases being used in atmospheric transportation measurements: SF_6 has been used to determine the interhemispheric exchange times [233], radionuclides (from atomic detonations) have been applied to stratospheric movement times [234], volcanic aerosols emissions (e.g. the 1991 Pinatubo eruption) have been used for testing computer models of aerosol forcing [235], and CFCs are used to date ancient underground water deposits [236].

Lindberg *et al.* noted in their 2007 review of atmospheric mercury that “Hg isotope signatures and tracers of convenience hold promise for source attribution, particularly at the

local scale" [4]. Natural isotopic abundances of mercury can deviate from location to location. Measurements of these deviations can be used to identify chemical reactions. Berquist *et al.* have outlined the multitude of applications now applicable to mercury isotope fractionation, in particular "fingerprinting specific chemical pathways such as photochemical reduction" [237]. Because of mercury's distinct isotopic ratios, a promising area in environmental mercury research is the ability to discern their origins [238-240].

5.3.4 Improving measurements of mercury oxidation by bromine

The rapid loss of gaseous elemental mercury during the arctic springtime is correlated with bromine explosions [6] (a rapid release of atomic bromine from ice and liquid particles into the gas phase) yet we have not determined the precise mechanism for mercury oxidation during these occurrences. Comparing the five species Br_2, Br, HBr, HOBr, and BrO that could be involved with mercury oxidation, the bromine radical Br is often assumed responsible for oxidizing mercury. But rate constants are not available for BrO, HOBr and HBr and the only published data for BrO is highly uncertain, where ($10^{-13} < k < 10^{-15}$) cm^3 $molec^{-1}$ s^{-1} [150]). It is also uncertain to what degree aerosols play a role in mercury oxidation or if humidity affects these rates. More work is needed to determine which of the competing mechanistic hypotheses is correct.

Appendix A

Mercury Transformation at Surfaces: Feedbacks to the Atmosphere

The following material has contributed to the publication of the book chapter "PA Ariya, K Peterson, G Snider, M Amyot, in N. Pirrone, R.P. Mason (Eds.), Mercury Fate and Transport in the Global Atmosphere. Springer US, New York, 2009, p. 459-501. Reprinted with permission from Springer Publishing (License 2773271110497)

Abstract

Mercury is a persistent, toxic and bio-accumulative pollutant of global interest. This element is assumed to exist predominantly in the atmosphere, as elemental mercury, undergoing chemical reactions in the presence of atmospheric oxidants. The oxidized mercury can further deposit on the Earth's surface and may potentially be bioaccumulative in the aquatic food chain, through complex, but not yet well understood, mechanisms. Since the atmosphere plays a significant role as a medium for chemical and physical transformation, it is imperative to understand the fundamentals of the kinetics and thermodynamics of the elementary and complex reactions of $Hg^0(g)$ and oxidized mercury not only in the atmosphere as gas phase, but also the reactions in the aqueous and heterogeneous phases at atmospheric interfaces such as aerosols, fogs, clouds, and snow-water-air interfaces. In this chapter, we compile a comprehensive set of theoretical, laboratory and field observations involving mercury species in the course of homogeneous and heterogeneous reactions. We herein describe the state-of-the-knowledge in this domain and put forward the open questions and future direction of research.

A.1 Introduction:

The importance of environmental surfaces has been increasingly gathering attention over a large span of scientific issues ranging from heterogeneous reactions on aerosols and clouds (e.g., ozone destruction on polar clouds) to release of active halogens in the marine boundary layer. Surfaces can act as reactive sites for chemical reactions, active sites for catalysis, and as a platform for exchange between different planetary ecosystem compartments such as air-snow, air-water (lake/ocean), vegetation-air, water-soil and air-soil. However, due to the complexity of the nature of surfaces, its variability, its sensitivity towards environmental variables, its temporal and spatial heterogeneity, environmental surfaces studies are one of the major scientific domain of uncertainty that will face environmental scientists in this new century. Mercury, as a fluid metal with high vapor pressure at ambient conditions, can exist at different oxidation states with complex organic, inorganic and organometallic chemical compositions and at different physical characteristic, as gases, aerosols, particulate matter in water and snow, within biological organisms at various degrees of evolution in the food web (Figure A-1). As there are excellent reviews for gas and liquid phase mercury transformations, and various mercury compounds physical and chemical characteristics (e.g., [56, 249, 250]), we herein only focus to gather all known on surface physics, chemistry and biological interactions at environmental interfaces. Shown in Table is the collection of such vast data set on surface reactions of mercury at environmentally relevant or potentially relevant conditions.

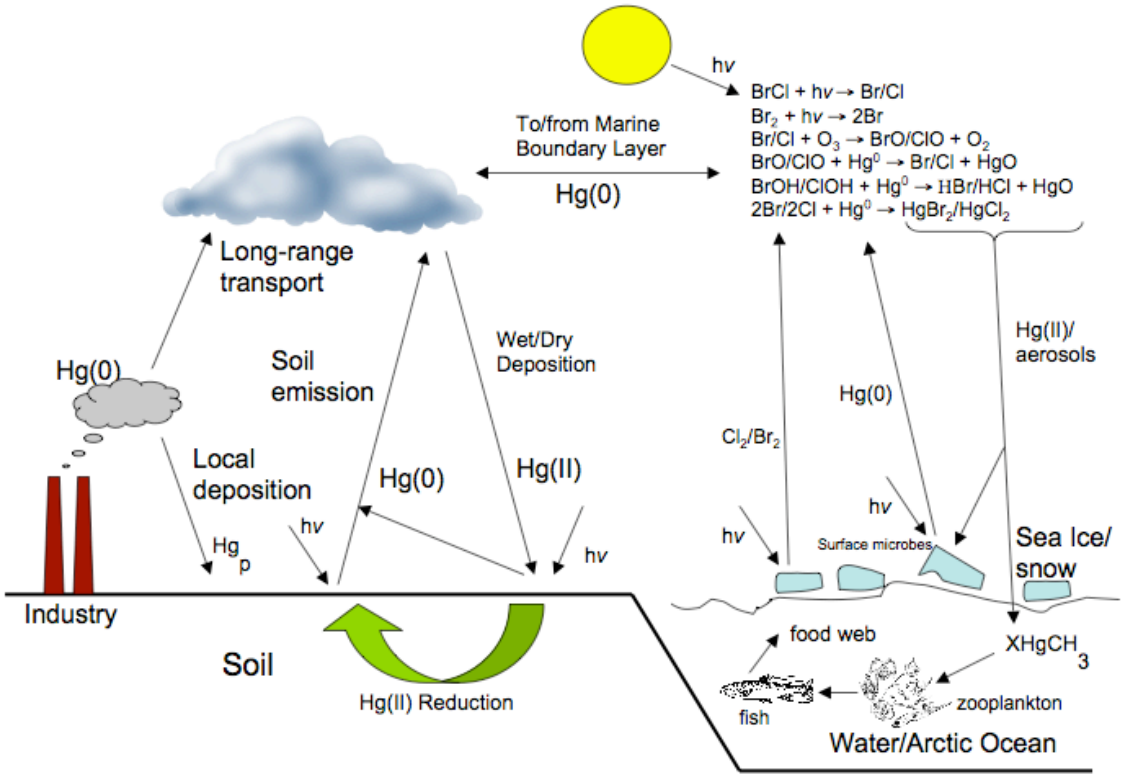

Figure A-1 Simplified schematic of mercury transformation in the Earth's environment (inspired by [4, 59, 251]).

The volatilization of gaseous elemental mercury from surfaces, chemical transformation in gas and condensed phases (liquid/solid/heterogeneous), and deposition mechanisms are not well-defined processes. For instance, not much is known about chemical reactions occurring in the snow, especially catalytic and heterogeneous reactions occurring at the surface of snow grains and removal of $Hg^0(g)$ over fly ash, but field observations support the importance of such surfaces in mercury cycling [252],[110]. Pure gaseous oxidation of mercury is mechanistically difficult to explain as well, and in some cases can be explained via heterogeneous phase chemistry ([74, 150, 253]. Inconsistencies between kinetic and thermodynamic data describing the homogeneous gas phase oxidation of mercury such as in case of one of the most

predominant atmospheric oxidant, ozone or its well reactions. [71, 125]. Attempts to more clearly understand reduction of Hg(II)(s,aq) to Hg^0(g) (or the reverse oxidation) are motivated by uncertainties in the Hg chemistry of the Arctic and in finding suitable surface catalysts for Hg^0(g) emission reduction in coal fire combustion. Noting the lack of detailed *mechanistic* understanding of mercury redox reactions, we herein strive to examine what changes alter surface reactivity, including the presence of water, various trace surface impurities, photochemistry, temperature, or other competing reactions. We will discuss the importance of environmental interfaces and environmentally relevant (or potentially relevant) carbon surfaces (such as fly ash, charcoal).

A.2 Chemical and Physical adsorption

One of the first steps for mercury to undergo in a surface reaction is adsorption. There are two principal modes of adsorption of mercury molecules on any surface. The basis of distinction is the nature of the bonding between the molecule and the surface. In physical adsorption (physi-sorption), the bonding is by weak Van der Waals - type forces. There is no significant redistribution of electron density in either the molecule or at the substrate surface. In a chemisorption process a chemical bond, involving substantial rearrangement of electron density, is formed between the adsorbate and substrate. The nature of this bond may lie anywhere between the extremes of virtually complete ionic or complete covalent character, and hence it is significantly stronger than physical adsorption (40-800 kJ/mol in comparison to 5-40 kJ/mol) [254]. There are a few ways to distinguish physisorption and chemisorption. The temperature over which chemisorption occurs can be only over a small surface, but is almost unlimited. However, for physisorption the temperature range is around condensation point of a gas such as Hg(0). Physisorption is generally reversible, non-dissociative, potentially multilayer and fast,

whereas chemisorption however is dissociative and often include an activated process with wide range kinetic desorption and limited to monolayers. To distinguish the type of adsorption, one can evaluate the vibrational frequency of substrate-adsorbate bond, or shift in energy or intensity of the valence orbitals in the substrate and adsorbate surface. For most mercury environmental surface studies, the fundamental difference between chemi- and physi-sorption are not yet evaluated, and should be studied in future.

A.3 Mercury at air/land interfaces

Air/land interfaces are very dynamic with respect to Hg cycling. The main surfaces interacting with the air compartment are soil, vegetation, snow, ocean and lake surfaces. These interfaces are sites of redox reactions and Hg exchange with the atmosphere. We here present an overview of Hg behavior at these interfaces, with respect to its reactivity and evasional flux.

A.3.1 Lake surface

Lake surfaces represent about 1% of landmass surfaces, and are therefore not major players in controlling global fluxes [29]. However, evasion of Hg(0) from surfaces can significantly alter the Hg budget in these systems, with a potential impact on the contamination of fish. Results from a whole-ecosystem loading experiment (METAALICUS, Mercury Experiment to Assess Atmospheric Loading in Canada and the United States) have established that 45% of newly deposited Hg could be transformed near the water/air interface of a small boreal lake and returned to the atmosphere [126, 255]. For one of the greatest freshwater systems, Lake Superior, [256] estimated that Hg evasion from the lake surface completely counterbalanced atmospheric Hg deposition.

Mercury transformations at the air/lake interface are usually dominated by the photoreduction of Hg(II) to Hg(0) [257]. This production of Hg(0) typically displays both diel and seasonal patterns with maxima under sunlit and warm conditions [258]. Photoreduction of Hg(II) can be induced by UV and, to a lesser extent, by visible radiation. The fact that visible radiation can induce this reduction suggests that DOC chromophores may be involved [259]. Filtration experiments have shown that this photoreduction can be homogeneous. It can be mediated by iron(III) [260] and humic acids [261]. However, it can also be biologically-mediated [49]. The relative importance of these mechanisms will differ with pH, light attenuation and DOC levels at the surface. An in-depth review on this topic is presented in [262].

Of lesser importance in lakes, (photo)oxidation of Hg(0) to Hg(II) has been observed and also follows a diel cycle [263]. This oxidation is mainly promoted by the UV-A waveband and can be driven by the formation of strong Hg oxidizing agents (e.g. OH radicals) or be indirectly caused by the photoproduction of hydrogen peroxide which, in turn, regulates microbial oxidation processes [49].

Current models do not predict well the formation of Hg(0) and its evasion from lake surfaces. Processes occurring in the surface microlayer need to be better assessed in order to establish the actual Hg(0) gradient at all water/air interfaces (for lakes, oceans and estuaries).

A.3.2 Surface of Oceans

Oceanic surfaces are a major site of Hg exchange at the global scale, with evasional fluxes accounting for about 39% of global Hg emissions [29]. Hg at this interface undergoes similar transformations to those described for lakes. Rolfhus and Fitzgerald [127] estimated that about

70% of volatile Hg formed in coastal seawaters was of photochemical origin, 20% came from bacterial processes, and 10% from uncharacterized dark reduction.

In addition, two major differences can be highlighted between freshwater and saltwater interfaces. First, in addition to Hg(0), ocean waters also contain significant concentrations of another highly volatile species, dimethylHg. This species formed at depth can be brought up to the air/seawater interface by upwelling currents in coastal areas. Second, oxidation of Hg(0) to Hg(II) is far more prevalent in saltwaters and will hamper the evasional fluxes of Hg(0). This oxidation is photo-induced and promoted by halogen chemistry both above and below the water/air interface [264, 265].

Accidental Hg reduction by marine microorganisms has been proposed as a significant source of Hg(0) in the mixing layer for a long time [142]. Recent evidence indicates that, at least at polar latitudes, this biological reduction may be partly mediated by mercury-resistant bacteria [131], even at remote locations.

As mentioned for lakes, very few studies have focus on the sea surface microlayer, even though microscale processes in this layer may have an important impact on evasional fluxes.

In a study by Sheu and Mason [264], aqueous NaCl/NaBr salts were photolyzed in the presence of $Hg^0(g)$. It was discovered that $Hg^0(g)$, in the presence of water, salt, and under a Xe-lamp, the oxidation rate constant increased 100-fold compared with irradiated salt-free water. Work was done at ambient temperatures in a quartz container. Mechanisms proposed involved volatilization of halogen species, which then react with mercury. Many secondary reactions of mercury were also considered (i.e. those with OH, BrO, ClO, and O_3), generally initiated by the presence of salt and light energy. Sheu and Mason also note reactions of Hg + Br were 25 faster than with Cl radicals.

Using *ab-initio* chemistry, Shepler *et al.* [266] noted water microsolvation (using 1-3 water molecules) favored the oxidation of mercury in the presence of bromine.

$$Hg_{(g)} + Br_{(g)} \rightarrow HgBr_{(g)} \qquad \text{Eq. A-1}$$

$$HgBr_{(g)} + Br_{(g)} \rightarrow HgBr_{2(g)} \qquad \text{Eq. A-2}$$

$$HgBr_{(g)} + Br_{(g)} \rightarrow Hg + Br_{2(g)} \qquad \text{Eq. A-3}$$

Reactions (1) and (2) were found more favorable in the presence of water, whereas reaction (3) was less favorable when solvated. They conclude it is probable the effects of ice, snow, and water surfaces enhance the scavenging of mercury by halogens.

A.3.3 Snow surface

The role of the snow surface on the reactivity of Hg and its release to the atmosphere has been discussed for polar regions in Chapter 9 of Steffen *et al.* [78]. Here we focused on temperate snowpacks. It has been demonstrated that in suburban and remote temperate areas, about 50% of newly deposited Hg is returned back to the atmosphere within 24 to 48 hours [43]. This release results from the photoreduction of Hg(II) to Hg(0) in the snowpack, mostly induced by UV-B radiation [267]. The processes leading to this reduction have not been elucidated.

In forested areas, the canopy has a significant impact on the behavior of Hg in the underlying snowpack [268]. Snow under canopy has typically higher Hg levels than snow from open areas (e.g. frozen lake surfaces); photoreduction of Hg(II) followed by evasion is less efficient in forested areas because of light attenuation by the canopy. Poulain *et al.* (2007c) calculated net winter gain of Hg in snow under canopies dominated by conifers whereas, under a deciduous canopy, the pool of Hg stored at the end of the winter was comparable to that of wet deposition. Coniferous trees were both a source of Hg to the forest floor (via throughfall) and an

obstacle to Hg photoreduction in underlying snow. Snow over lakes acted as a winter source of Hg to the atmosphere. Whereas most Hg deposited by snow on lakes is lost before snowmelt, Hg deposited on the forested watershed is largely retained in snowpacks.

Snow can house a number of different Hg(II) species, i.e. HgC_2O_4, $Hg(OH)_2$, HgOHCl, HgO [269], and possibly others. It is clear from experiments that Hg(II) on snowpacks is photo-reduced by natural sunlight [252]. Mercury over snow originates from atmospheric $Hg^0(g)$ through dry deposition [6] and oxidation mainly via O_3, BrO, and Br [59]. Concentrations of arctic mercury on snowpacks are guided by incoming and outgoing fluxes, which depend on light intensity and oxidant concentration, respectively. Oxidation of mercury over snowpacks is part of a dynamic system of ice, snow, ozone, UV-Vis light, Cl, and Br radicals (see Lindberg *et al.* [270]). It is believed that aerosol ice surfaces catalyze oxidation of $Hg^0(g)$ to HgO or $HgBr_2/Cl_2$ during the Arctic spring [270]. Oxidation is aided by the destruction ozone by Br over ice and formation of Hg(0) oxidants [59, 271].

Methylmercury ($MeHg^+$) has been observed in Arctic snowpacks [272]. The origins of $MeHg^+$ are aqueous (oceans, lakes), however its volatility is low: $K_p = [HgMe(g)]/[HgMe(aq)] = 2 \times 10^{-5}$, at 298 K [273]. By contrast, volatility of dimethylmercury (Me_2Hg) is much higher: $K_p = 0.31$ [273]. St Louis *et al.* [272] hypothesize MeHg originates from nearby ocean sources as $MeHg_2$, then converts to MeHgCl in the salty snow. They note there is a positive correlation between total mercury and Cl concentrations over snowpacks. The salinity of Arctic snow can range anywhere between 20 – 2000 mg l^{-1} [59].

Snow spiked with hydrogen peroxide was observed to enhance Hg(II) deposition five-fold under natural Arctic springtime sunlight [274]. The mechanism of oxidation is not known, though it is suggested equilibrium can be formed with chlorine in acidic conditions:

$$H_2O_2 + 2H^+ + Hg^0 + 2Cl^- \Leftrightarrow 2H_2O + HgCl_2 \qquad \text{Eq. A-4}$$

Samples were spiked with 50 μM H_2O_2, similar to natural concentrations (30 μM). Hence H_2O_2 was suggested to play a significant role in Hg^0 oxidation under UV light hat should be further confirmed. Bromine, as well as Cl, can oxidize Hg^0 in snow. Fain *et al.* [275] calculated from field samples a mercury + bromine oxidation rate constant very similar to lab studies; 2×10^{-11} cm^3 $molec^{-1}$ s^{-1} at -10°C.

Poulain *et al.* [276] observe 100-fold higher concentrations of total mercury in snow found near Arctic sea/ice boundaries than inland. They note melting of the snow/ice during springtime further enhances mercury deposition (until enhanced light intensity of the spring re-volatilizes condensed mercury). Douglas *et al.* [277] observe various crystalline morphologies of snow will exhibit varying degrees of $Hg^0(g)$ scavenging, with up to an order of magnitude difference in deposited concentrations. Heterogeneous mercury reactions evidently depend on surface morphology in addition to surface species present. Aspmo *et al.* [278] observed $Hg^0(g)$ concentrations over sea ice, noting some increase in concentration (1.82 ng/m^3) compared with background north Atlantic ocean levels (1.53 ng/m^3). Analyses were done in the summer and spring, leading to the possibility of re-emission of Hg(II) over ice and snow. Depth profiles of mercury concentration over snow show generally higher levels than atmospheric background levels. Despite observed rapid mercury depletion events in the polar regions [6, 247], but the over all fate is an subject of debate [279]. The total volume of mercury entering the Arctic circle is calculated to be about 300 tons per year, via global model simulation [59]. This influx is largely scavenged over ice, snow, and water via bromine explosions [280]. However, this deposition in part is rapidly reduced to $Hg^0(g)$ later during Arctic springtime [279].

There is evidence the bacterial mercuric reductase enzyme (MerA) will reduce MeHg and inorganic Hg(II) species to Hg^0(g) in Arctic coastal and marine environments [131]. It is noted this reduction is an apparently deliberate self-preservation of certain biota against methylmercury contamination in water. In addition to photoreduction recycling mercury, bacteria are capable of re-volatilizing the metal at comparable levels even with only 1% of cells active.

Frost flowers have been a known source of halogen from sea ice for several years [281]. Now it is possible these ice crystals provide via high surface areas a scavenging of mercury [277]. It was found crystals formed in the vapour phase have higher mercury concentrations (2-10 times as much) than snow deposits. The only difference between frost flowers and snow deposits would appear to be their morphology; hence the surface design (diamond dust, surface hoar, blowing snow, glass trays) may also affect kinetics of Hg(II/I). A previous study already supposed Br radicals are released from the sea ice crystals [282], implying heterogeneous reactions are responsible in part for mercury oxidation. However, we point out that the Br/BrO + Hg^0 oxidation itself is gaseous. Trace species affecting Hg reduction/oxidation in snow include, but are not limited to, Br^-, Cl^-, microbes, and ice/snow morphology.

A.3.4 Soil surface

Mercury air–soil exchange is an important component of the Hg cycle at regional and global scales [283]. Hg(0) volatilization from soils has been correlated to soil Hg concentration [284], soil moisture [285], atmospheric oxidants [286], and meteorological conditions (barometric pressure, temperature, wind speed and turbulence, and solar radiation).

Under low atmospheric Hg concentrations, barren soils can act as Hg sources to the atmosphere during the day or sinks of Hg at night [287]. Photochemical processes are likely the

main driver of Hg(0) formation and evasion when the substrate is moist or after rain events [288], whereas solar-induced thermodesorption of Hg(0) is probably more important under dry conditions [289]. The sorption properties of soils will be dictated by the mineralogical composition. For instance, the presence of kaolinite, montmorillonite, and goethite in soils has been shown to enhance the sorptive capacity of soils [287].

Since soils can significantly differ in their sorption capacity and their reactivity, and current evasional estimates are site-specific, the overall global fluxes associated with soils are still poorly constrained and need further assessment.

A.3.5 Vegetation surface

Vegetated areas are key players in global Hg cycling. According to Mason and Sheu [29], net Hg evasion from land is 8 Mmol y^{-1}; emissions from vegetated areas (forest, prairies and farmland) are estimated at 9 Mmol y^{-1} and uptake of Hg(0) by plant drives a depositional flux of -7 Mmol y^{-1}. Because of the magnitude of these vegetation fluxes, a far better understanding of these surfaces is needed to constrain flux estimates.

The plant/air interface is a site of both passive and active exchange of Hg(II) and Hg(0). For example, atmospheric particulate Hg and reactive gaseous Hg can be absorbed on leaf surfaces after dry deposition [290]. Stomata can actively take up atmospheric Hg(0) [291]. This assimilated Hg can come either from passing air masses or from soil Hg emissions below the canopy; in the latter case, this uptake results in a fast cycling of Hg within the forest. In contaminated sites, plants can translocate Hg from soils to leaves, with some Hg being released through stomata or through litterfall. The leaf surface has also been shown to be a site of photochemical transformations of deposited

Hg(II) to Hg(0), followed by its evasion to the atmosphere. The UV band was shown to be the most efficient radiation in this reduction.

Table A-1 Inter-phase (heterogeneous/surface) kinetics and emission rates of mercury, both natural and artificial

Surfaces	Type of experiment	Interface	Temp. (K)	Rates/rate constants/results; No general units	Ref.
$Hg^0(g) \rightarrow Hg^0(ads)$	Abs	N_2, 1 atm,	293	4.5×10^{-6} s^{-1}	[73]
		N_2/Teflon wall	323	1.7×10^{-5} s^{-1}	
		(s/v = 0.58 cm^{-1})	348	3.0×10^{-5} s^{-1}	
$Hg^0(g) \rightarrow Hg^0(ads)$	Abs	air, 1 atm,	293	$90\text{-}120 \times 10^{-4}$ s^{-1}	
		air/carbon	423-523	$1.3\text{-}5.0 \times 10^{-4}$ s^{-1}	
			573	~ 0 s^{-1}	[79]
	Abs	air, 1 atm,	293	81×10^{-4} s^{-1}	
		air/fly ash	423-523	$11.2\text{-}27.2 \times 10^{-4}$ s^{-1}	
			573	$6.8\text{-}7.7 \times 10^{-4}$ s^{-1}	
$HgO/HgF_2/HgNO_3$ (aq) + hν $\rightarrow$ Hg(l)	Lab Expt, Hg lamp	Water/TiO_2 surface	293	90% conversion after 40 min irradiation. Lower pH = less reduction.	[292]
$Hg(l) + \Delta \rightarrow Hg^0(g)$		TiO_2 surface/N_2 flow	423	Removes Hg(l) in ~1 hour	
$Hg^0(g) \rightarrow Hg^0(ads)$	Model/field data	Air/Forest floor	Ambient	0.12 cm s^{-1}	[293]
				0.006 cm s^{-1}	
$Hg^0(g) \rightarrow Hg^0(ads)$	Field study	Air/ground dry deposition	Ambient	0.5 cm s^{-1} (particulate; Hg_p)	[6]
				0.1 cm s^{-1} ($Hg^0(g)$)	
		Air/(snow/ barren ground)	Ambient	12.5 ± 2.5 pmol m^{-2} h^{-1}	
Hg(II)/humic acid + hν $\rightarrow$ Hg(g)	Lab study, xenon radiation	Water/air,	ambient	2×10^{-2} s^{-1}	
$Hg(OH)_2 + h\nu \rightarrow Hg(g)$				1.2×10^{-4} s^{-1}	[294]
$Hg^0(g) + H_2O_2(ads) + h\nu \rightarrow Hg(II)$	Field study	Air/snow pack		5-fold increase in $Hg^0(g)$ deposition with H_2O_2-spiked snow	[274]
$Hg^0(I/II)_g \rightarrow Hg^0(I/II)_{ads}$	Field study	Air/snow; dry dep.	Ambient	1 cm s^{-1}	[270]
$Hg^{2+}(ads) \rightarrow Hg^{2+}(snowpack)$	Field study	Snow/Snow vertical diffusion	273	5.8 – 7.0 pg m^{-2} h^{-1}	[295]
$Hg^0(ads, II) + h\nu \rightarrow Hg^0(g)$	Field study	Snow/air	273	> 20% reduction loss in 3h	[59]
	Field study	Snow/air	273	> 40% reduction in 24h	[267]
	Field study	Snow/air,	269	0.24 h^{-1}, 45 pmol m^{-2} h^{-1}. Reduc enhanced by $H_2O(l)$	[296]
$Hg^0(g) + h\nu \rightarrow Hg^0(ads,II)$	Lab study, Xe-lamp	Air/snow	258 – 313	0.25 h^{-1}, 0.18 h^{-1}	[252]
$HgS^{2-} + h\nu \rightarrow Hg^0(aq)$	Field	Water/air	ambient	Not significant	[258]
$Hg^0/Hg(CH_3)_2 \rightarrow Hg^0(g)/Hg(CH_3)_2(g)$	Field study	Soil/air	ambient	< 1 nmol m^{-2} h^{-1}	[273]
		Temperate, boreal	ambient	55 pmol m^{-2} h^{-1}	
$Hg^0(ads, II) \rightarrow Hg^0(g)$	Field study	Contaminated	ambient	~6500 pmol m^{-2} h^{-1}	
		Open, temperate			
		Air/soil	ambient	12 pmol m^{-2} h^{-1}	[283]
		Temperate Forest	ambient	47 pmol m^{-2} h^{-1}	
$Hg^0(g) \rightarrow Hg^0(ads, II)$	Field study	Air/soil Throughfall/ litterfall	ambient	190 nmol m^{-2} a^{-1}	
$Hg^0(ads, II) \rightarrow Hg^0(ads, II)$	Field study	Soil sequestration	ambient	25 nmol m^{-2} a^{-1}	
$Hg^0(aq) \rightarrow Hg^0(g)$		Water/air	ambient	25 pmol m^{-2} h^{-1}	[258]
	Model/Field study	Forest soild/air	ambient	250 pmol m^{-2} h^{-1}	[293]
$Hg(II)[Cl^-/NO_3^-]$ + surface sediment $\rightarrow$ $Hg^0(aq)$	Field expt	Lake water/ sediment	~298	$\sim 10^{-5} - 10^{-6}$ min^{-1}	[297]
$Hg^0(aq) \rightarrow Hg^0(g)$	Model fit, empirical data	Water/air	298	5.7 pmol m^{-2} h^{-1} loss	[298]

	Field study	Lake water/air	298?	16 pmol m^{-2} h^{-1} loss (0.6% h^{-1})	[126]
$Hg^0(aq) + h\nu \rightarrow Hg(g)$	Lab study	River water/air	?	0.2×10^{-4} s^{-1}	[299]
		Sea water/air		0.3×10^{-4} s^{-1}	
$Hg^0(ads) + Br \rightarrow HgBr$	Field study	In snow (20-60 cm deep)	~263	2×10^{-11} cm^3 $molec^{-1}$ s^{-1}	[275]
$Hg(g) + Cl_2(g) \rightarrow (HgCl)_n(s)$	Lab	Air/surface	525	50 second reaction	[300]
	Lab	Air/water	-	Some enhancement	[211]
	Lab	Air/water +sulfite	298	6.1×10^{9} M^{-1} s^{-1}	[301]
$Hg^0(g) + Cl_2(aq) \rightarrow Hg^{2+} + 2Cl^-$	Lab	Water + NaOCl	298	1.7×10^{15} M^{-1} s^{-1}	
	Lab	Water + NaOCl	328	1.4×10^{17} M^{-1} s^{-1}	[302]
$Hg^0(g) + H_2O(g) + O_2(g) + h\nu \rightarrow HgO(s)$	Lab	Air/TiO_2 surface	297-408	$k = Ae^{-(Es-\lambda)/RT}$ $d[Hg]/dt = k[Hg]^{(1.4\pm0.1)}[J_{UV}]^{(0.35\pm0.05)}$	[192]
$Hg^0(g,ads) + O_2(g,ads) \rightarrow$ Product	Experiment Langmuir-Hinshelwood mech.	Air/Fly ash surface	373-573	$1.5 - 6.5 \times10^{-12}$ $(cm^{-3}$ $molec^{-1})^{0.5}$ s^{-1}	[79]
$Hg^0(g) + SO_2 + O_2 \rightarrow HgSO_4(s)$	Lab	Air/Pt	348-673	3.5 mg Hg/hr (348-600K)	[89]
	Field test	Air/Pd		93% oxidation	
		Air/SCR catalyst	450	62% oxidation	[303]
$Hg^0(g) \rightarrow$ Product		Air/TMT-15 catalyst*		Inconclusive; intended to prevent re-emission of Hg	[103]
$Hg^0(g) + SO_2 + NO_2 + HCl \rightarrow Hg(s)^{2+}$	Lab	Air/Fly Ash	453	~30 % Hg(g) oxidation	[101]
$Hg^0(g) \rightarrow Hg(ads)$	Lab	Air/Fly Ash + carbon	293, 313	More mercury adsorption at 20°C than 40°C	[304]
$Hg^0(g) + h\nu \rightarrow$ prod.				1.2×10^{-5} s^{-1}	
$Hg^0(g) + h\nu + H_2O(l) \rightarrow$ prod		Air/quartz surface		4.0×10^{-5} s^{-1}	
$Hg^0(g) + h\nu + NaCl \rightarrow$ prod	Lab, Xenon lamp		293	1.6×10^{-3} s^{-1}	[264]
$Hg^0(g) + h\nu + NaCl + H_2O(l) \rightarrow$ prod				1.7×10^{-3} s^{-1}	
$HgCl_2(g) + H_2 \rightarrow Hg_2Cl_2(s) + 2HCl$	Lab, laser study	N_2/Stainless steel surface	473	Unknown mechanism	[305]
$Hg^0(g) + (HCl) \rightarrow Hg(ads)$	Lab	N_2/Stainless steel surface or PTFE teflon	423	HCl enhances Hg^0 removal SS: (0 → 44 ng) SS: (66 → 128 ng)	
$Hg(g) \rightarrow Hg(ads)$	Lab work	N_2 and trace gas/Gold	411	25 nm thick Au sheet absorbs for 33 min vs. 5 min for 2.5 nm sheet. Hg penetrates Au.	[94]
$HgCl_2(g) \rightarrow HgCl_2(ads)$	Simulated flue gas	N_2/gold Trace gas	422	Acid gases (HCl or NO_2) + SO_2 reduce ads. cap. $HgCl_2$ adsorbs; no rxn. Similar to carbon surf. ads.	
$HgCl_2$ + dodecyl sulfate(DS) + $h\nu \rightarrow Hg(I)$	Lab		Ambient	97% reduction in 6 min	
$HgCl_2 + h\nu +$ cetyltrimethyl ammonium (CTA^+) → Hg(I)	Lab	Water/TiO_2 surface	Ambient	99% reduction in 25 min	[258, 306]
$HgCl_2 + h\nu$ + arginine → Hg(I)	Lab	Water/TiO_2 surface	Ambient	arginine binds Hg(II) to TiO_2, facilitates charge transfer	[307]
$Hg^{2+}(aq)$ + N719-TiO_2 →	Lab	Water/N719-TiO2	~298	Hg^{2+} binding constant: 3×10^5 M^{-1} 65% scavenging eff.	[114]
$Hg(NO_3)_2(aq) \rightarrow Hg_{ads}(II)$	Lab	Water/Fly ash	303	Freundlich parameters: k = 1.230, 1/n = 0.361 @ pH = 4.2, > 90% adsorption	[308]
$Hg^0(II)_{aq} \rightarrow Hg(II)_{ads}$	Lab	Water/ Activated carbon	300	Freundlich parameters: k = 0.1427, 1/n =0.71	[309]
			318	k = 0.0663, 1/n =0.75	
			338	k = 0.01073, 1/n =1.38	
$Hg^0(g) + Cl_2 \rightarrow HgCl_2$	Lab	Air/Au surface	448-498	40-60 % oxidation $k \sim 10^{-8}$ cm^3/(molec/s) (473 K) ? Langmuir-Hinshelwood mechanism proposed	[310]

$Hg(NO_3)_2(aq) + 2e^- \rightarrow HgAu(s)$	Lab expt	Au-coated microparticle surface	298	0.35 V causes AuHg amalgam formation	[311]
$Hg^0(g) + (H_2S) \rightarrow HgS(s) + S(s)$	Simulated flue gas	Flue gas/Fe_2O_3(N)	353	H_2S initiates Hg removal rxn up to 65% Hg loss in stream. -no effect from H_2 or CO. H_2O *reduces* Hg adsorbance.	[312]
$Hg^0(g) + (HCl) \rightarrow HgO(s)$	Lab, simulated flue combustion	Fe_2O_3, Fe_2O_3-$Ca(OH)_2$, FeS_2, Fe_2O_3(1% wt)/TiO_2 surfaces	353	Fe_2O_3: 50% removal Fe_2O_3/TiO_2: 80% Fe_2O_3-$Ca(OH)_2$: 70% FeS_2: 60% HCl(g) suppressed Fe_2O_3 activity only	[313]
$Hg^0(g) + UV \rightarrow HgO(s)$	Lab, simulated flue combustion	SiO_2-TiO_2 surface	408	99% removal	[314]
$Hg^0(g) + \Delta \rightarrow HgO(s)$	Lab, simulated flue combustion	Extensive list of metal oxide surface mixtures, Mars-Maessen mech.	410	Cr_2O_3/Al_2O_3, MnO_2/Al_2O_3, and MoS_2 show high Hg adsorption capacities.	[315]
$Hg^0(g) + \Delta \rightarrow HgO(s)$	Lab, simulated flue combustion	Various metal surface catalysts. Het. rate constants measured.	411	Rank: Ir > Ir/HCl > Darco > Thief/HCl (in terms of oxidation efficiency)	[124]
$HgBr_2(s) + Ag_2WO_4(s) \rightarrow HgWO_4(s) + AgBr(s)$	Lab, glass tube diffusion	Solid-state reaction	413 – 463	$K = 1.10 \times 10^{-4}$ cm h^{-1} @ 120°C $(\text{thickness})^2 = Kt$	
$HgCl_2(s) + Ag_2WO_4(s) \rightarrow HgWO_4(s) + AgCl(s)$			438 - 481	$K = 2.25 \times 10^{-4}$ cm h^{-1} @ 145°C	[316]
$Hg^0(g) \rightarrow Hg^0(ads)$	Lab, over activated C	Ptolemais lignite + S	323	300 – 900 ng Hg/mgAC addn of S incrss. ads	[317]
$HgCl_2(g) \rightarrow Hg^0(ads)$	Lab	Air/Cysteine over silica	298 - 398	Capture eff CE: 12mg/g < CE < 33 mgHg/g	[318]

A.4 *Carbon (fly ash, charcoal):*

Knowledge that coal combustion is a source for mercury dates back over 35 years [91]. Residues of coal combustion in industrial power plants generate fly ash, composing mostly of SiO_2 and Al_2O_3. Fly ash composition and morphology make it suitable for zeolite synthesis [319]. Flue gas may be comprised of CO_2, O_2, CO, NO, NO_2, SO_2, H_2S, HCl, NH_3, N_2O, and Hg [90]. Incomplete combustion ($T < 400^oC$) leads to carbon in fly ash, usually enhancing mercury adsorption [110]. Presence of carbon also leads to high "Loss on ignition" (LOI), which is defined in the context of coal combustion as the fly ash weight loss at a given (elevated) temperature. Thus the carbon content may be expelled when sufficiently heated, possibly taking absorbed mercury with it. Presence of carbon was found to increase the BET surface area of fly ash, enhancing adsorption [320]. Surface area per unit mass, and per unit area in the flue, is significant in describing adsorption. Carbon content ranges from 6 to 850 m^2/g, with ~70 m^2/g in charcoal [321]. The BET surface area of iron oxide is 62 m^2/g [312]. Soot/fly ash may disperse globally; fly ash has been shown to be a component of Arctic aerosols [322]. It is possible carbon in aerosols will affect mercury oxidation rates under environmental conditions.

Presto and Granite [98] have efficiently summarized the significant contributions carbon, metal, metal oxide, and other surfaces in simulated and experimental coal-combustion conditions. We attempt to avoid duplication of their review material by further updating this subject, though some reference material of theirs is necessarily highlighted. We also refer the reader to Pavlish *et al.* [110] for an earlier review of mercury capture in power plants.

Activated carbon can absorb mercury in aqueous solutions as well gaseous systems [323-325]. Sen and De [308] found that aqueous $Hg(NO_3)_2$ was readily adsorbed by fly ash at a pH = 3.5 – 4.5. At a pH of 5, Hg(II) was hypothesized to transform into $Hg(OH)_2$ over the carbon

[323]. Chen [321] noted that $H_2O(g)$ did not affect mercury oxidation. Some experiments have noted humidity negatively affecting oxidation [326, 327].

It is clear that many factors affect the adsorption - hence redox - reactions of mercury over fly ash. The most important trace elements affecting the oxidation rate are HCl, ClO, and Cl_2. Mechanistically, we suspect that the majority of oxidation in the presence of fly ash or carbon is heterogeneous based on the evidence of Presto and Granite [98]. Temperature is a significant factor in oxidation rate; optimal values must be achieved to balance reaction efficiency and total adsorption. Hall *et al.* [73] discovered a mixture of oxygen and mercury at 100-300 ^oC would react in the presence of fly ash or carbon. There was a measurable oxidation rate constant of $\sim 10^{-4}$ s^{-1} [79]. Surface kinetics have been postulated to obey a Langmuir-Hinshelwood mechanism, where both mercury and oxygen adsorb onto the carbon surface before reacting. A temperature of about 200^oC was found optimal. Xu *et al.* [328] (see also [329]) compared mercury oxidation by different pathways using a combination of kinetic modeling and *ab initio* chemistry over a carbon surface. They conclude that Hg^0 + ClO reactions may be more significant at T > 130^oC than mercury reactions with either Cl_2 or HCl.

We conclude this section by stating the use of fly ash or charcoal in removing mercury is not cost-effective [330], varying between 14,000 – 38,000 USD/lb Hg. The useful temperature range is not wide for carbon; the peak efficiency temperature is ~200^oC [79]. Carbon is not effective at high temperatures (> 400^oC) due to its LOI. Some studies find temperature to be inversely proportional to Hg^0 removal [108]; it is found that carbon at 20^oC absorbs Hg^0 better than at 40^oC [304]. Fly ash is stable at high temperatures, however efficiency also decreases with increasing temperature. Fly ash also does not efficiently oxidize mercury unless other additives (HCl,H_2S) are present. Although carbon/fly ash injection is a very natural method to

removing $Hg^0(g)$, it remains the engineers' and physical chemists' goal to achieve improved mercury absorbency by more robust and cheaper adsorbents.

A.5 Open questions and future directions

The knowledge of mercury chemical, physical and biological interactions at environmental surfaces is scarce at best. It is now evident that the existence of the surfaces, different type of the surfaces, different environmental conditions, can alter the transformation of mercury in pure gas phase or aqueous phase. However, the quantification of the impact of surfaces are yet to be understood. The challenges facing the surface chemistry includes:

- Lack of knowledge of detailed mercury chemical speciation. Currently, the existing techniques are quite poor in providing detailed chemical structure of mercury compounds at the environmental interfaces as at the matter of fact even in atmosphere, water and snow. The operational definitions are used to discern amongst different functional groups, however, as they are not based on fundamental understanding of physical and chemical structures of molecules, it is very difficult to use them adequately for proper understanding of surface chemistry and physics of mercury. Further development of targeted techniques for detailed mercury analysis is essential.
- Fundamental surface sciences during the last several decades have achieved break through understanding of interfaces at molecular and cluster levels. It is wise for mercury scientists to take advantage of this existing body of knowledge including techniques such as various types of electron microscopy (e.g. transmission to electron force) to further understand the physical property of the surfaces, and the nature of the bonds between substrate and surface, as well as substrate-substrate configuration changes upon interactions with surfaces. This case is particularly valid for surfaces such

as snow, as well as aerosols and cloud droplets. It is of outmost interest to understand the mechanism(s) for these surface reactions.

- The nature of diffusion of mercury species in surfaces and interfaces (e.g., snow/ice) should be characterized.
- The importance of so-called "micro-layer" within the interface in relation to the entire surface should be studied.
- There is an amazing range of biological surfaces available for mercury transformation. Reactions are shown to occur on the surface or be altered within the biological bodies. The detailed chemical transformation of such reactions implicating biological transformation of mercury and its impact on physical and chemical characteristics of mercury compounds in environment is a fascinating field of studies that should be attempted from nano to macro scales.
- We know presently full well that to grasp the mercury transformation on this planet, the knowledge of pure gas, or condensed-phase physics and chemistry will not suffice. The feedbacks of gas phase on surfaces or liquid/solid/heterogeneous phase on environmental surfaces are ought to be characterized. The impact of heterogeneity on surfaces in local, regional and global scales is ought to be understood.
- Anthropogenic activities in the domains of new materials and nanotechnology, has produces novel surfaces as product of by-product of such activities. These molecules are in addition to oxidized transition metals (Fe, Mn, V, Cu, Ti), noble metals (Au, Pd, Ag, Cu) and metal oxides, glass type structures that are known to be involved in mercury transformations or its removal. There is not much known on the interactions of human-made novel surfaces with mercury compounds. As anthropogenic activities currently

represent the major mercury emission in the atmosphere, the importance of these surfaces on Hg transformation should be understood.

Acknowledgement:

We acknowledge Natural Science Foundation of Canada (NSERC) and Canadian Foundation for innovation (CFI) and McGill University for financial support.

Appendix B

Historical and background information on mercury

B.1 *List of terms*

Amalgam: An amalgam, by definition, is an alloy formed between mercury and another metal. Amalgams form between mercury and gold, silver, tin, zinc, indium, and sodium metal. Mercury does not amalgamate with iron. Amalgams are often resin-like, initially soft, and harden within minutes. Amalgams separate at elevated temperatures or pressures (e.g. > 500-600°C), but stable at room temperature (and with negligible mercury vapor pressure). Unusual for other mercury compounds, amalgams are often non-toxic and have been used in such application as artisanal gold mining capture (HgAu), dental fillings (HgAg) and sodium metal capture in the chlor-alkali process.

Atmospheric lifetime or half-life ($t_{1/2}$): The approximate time that a species X resides in the atmosphere. For rate removal k from the atmosphere, $d[X]/dt = -k[X]$, the half-life is $t_{1/2} = \ln 2/k$. The 'lifetime' is $\tau = 1/k$, where $\ln 2 \approx 0.693$ is omitted for simplicity of calculation. For a rate proportional to the n^{th} power of [X] (n > 2), $d[X]/dt = -k[X]^n$, the half-life is $t_{1/2} = [X]_0^{1-n}(1/2^{1-n} - 1)/[k(n-1)]$. A lifetime can appear much longer than k would suggest if rapid recycling exists between products and reactants. The atmospheric lifetime for gaseous mercury is about 1 year.

Cold vapor atomic fluorescent spectroscopy (CVAFS): Mercury detection through measurement of the stimulated $Hg^0(6^1S_0 \leftarrow 6^3P_1)$ emission at 253.7 nm. CVAFS has a very low limit of detection, about 0.2 pg, which is currently the best available.

Dissolved gaseous mercury (DGM), dissolved elemental mercury (DEM)**,** or $Hg^0(aq)$. Elemental mercury dissolved in large bodies of water, liquid droplets, or in liquid aerosols. Mercury has a low solubility in water (5.6×10^{-6} g/100 g water at 25°C) so does not accumulate, rather it is expelled back into atmosphere.

Elemental mercury (Hg): Depending on the context, mercury in its elemental form could be denoted Hg, Hg^0, or Hg^0(*ads, aq, s, l,* or *g*), where *ads* = adsorbed (to a surface such as water, ice, or solid/liquid aerosols), *aq* = aqueous, *s* = solid, *l* = liquid, *g*=gas. In the pure gas phase it is known as gaseous elemental mercury (GEM). The author intends to use the notation Hg^0 for most of the thesis, as mercury referred here is typically in the gas phase. If electronic energy

levels need specifying, then the ground state and first excited state are $Hg^0(6^1S_0)$ and $Hg^0(6^3P_1)$, respectively.

KCl denuder: An annular tube about 25 cm long coated in a layer of potassium chloride used to catch RGM or GOM. Oxidized mercury, in particular $HgCl_2$, is known to 'stick' to KCl surfaces [331]. Other oxidized mercury species are expected to stick as well but not well characterized on the denuder. KCl denuders cannot distinguish between the various oxides of mercury, i.e. whether $HgBr_2$ or $HgCl_2$ has been deposited. The effect of ozone or other competing adsorbates on the denuder surface is not well understood.

Marine Boundary Layer (MBL): The atmospheric interface between land and ocean-influenced chemical processes. There is no strictly defined cutoff in altitude or distance from actual interface; it is where marine/land mixing chemistry is dominant.

Particulate mercury (PM or Hg_p), includes all forms of mercury associated with particles, sometimes operationally defined as larger than 2.5 μm in diameter $PM_{>2.5}$, or as would be caught in a particle filter. Atmospheric lifetime of PM is usually days or weeks [332].

Reactive gaseous mercury (RGM/RGHg), alternatively known as gaseous oxidized mercury (GOM) or reactive mercury (RM) or gaseous ionic mercury (Hg^{II}), consisting of any/all oxidized mercury species (Hg^{2+} and Hg^{+}) found in the atmosphere. These include $HgCl_2$, $HgBr_2$, HgO(s) and $Hg^{+/2+}$(aq).

Total atmospheric mercury (TAM) or total gaseous mercury (TGM): The combined concentrations of RGM and Hg^0. Typically measured by pyrolizing the incoming airflow to ~500°C before measuring, e.g. attaching a furnace tube before entering CVAFS.

Wet and dry mercury deposition. Wet deposition: mercury scavenged by precipitation events. Dry deposition: mercury particles diffusing to land or water surfaces at rates between 1 – 4 cm/s [333]. It has not yet been feasible to distinguish between wet and dry mechanism. Mercury scavenged through wet and dry deposition together draw out 10 – 15 Mmol per year.

B.2 *Units*

Temperature:

Degrees Celsius = °C

Kelvin = K; 0 °C = 273.15 K

Volume:

1 m^3 = one cubic meter

1 cm^3 = one cubic centimeter = 10^{-6} m^3

Weights:

1 kg = one kilogram = 10^3 grams

1 tonne = 10^3 kilograms

1 ng = one nanogram = 10^{-9} grams

Pressure:

1 atmosphere = 760 *Torr* (or mmHg) = 101,300 Pa

Concentration:

1 part per million (1 ppm) = 2.5×10^{13} molecules cm^{-3} at 298 K and 1 atm.

1 part per billion (1 ppb) = 2.5×10^{10} molecules cm^{-3} at 298 K and 1 atm.

1 part per trillion (1 ppt) = 2.5×10^7 molecules cm^{-3} at 298 K and 1 atm.

Brackets [X] signify the concentration of species X at given, or implied, units

Percent Relative Humidity = %RH. The percentage of water in the air compared with a saturated atmosphere at a given temperature T.

B.3 An extended history of mercury metal (from ancient times to ca. 1975)

B.3.1 18th – mid 19th century use

Until the mid 19th century few chemical uses for mercury had been explored. Prior to this time mercury's low compressibility and thermal expansivity were used for barometers and thermometers, respectively. Parallel to the discovery of electromagnetism, applications rapidly exploited mercury's high electrical conductivity.

Mercury has been known for millennia to be able to blend with silver and gold, forming solid, shiny silver-colored amalgams. This knowledge led to widespread use in gold and silver mining extraction. Latin America, coastal Africa and Asia are particularly well known for this practice. In Central America the practice has been prevalent since the arrival of the Spanish. Artisanal small-scale mining (ASM) continues to this day in impoverished countries. Globally ASM contributes to the release of perhaps 800-1000 tonnes of mercury per year [334].

One of the first chemical applications of mercury emerged in the 17th century though the carrotting of fur hats, whereby hatters rub mercury nitrate [$Hg(NO_3)_2$] on pelts to eliminate fur. The process was known since the mid 1800s to cause severe speech slurring and other ailments among those workers exposed. Studies then emerged that such practices were causally linked with mercury [335]. It was not until 1941 that carrotting was voluntarily banned in the United States and coinciding with the increased demand for mercury detonators during the second World War [336].

Other chemically oriented roles for mercury emerged between the late 19th and early 20th century. These include early development of photographic plates in 1839 (known as daguerreotypes) and the zinc-mercury galvanic batter cell [337] in 1884, which became popular due to its steady voltage.

The shock-sensitive explosive, mercury fulminate $Hg(ONC)_2$, was discovered in 1800 by Edward Charles Howard. The Castner-Kellner process was used in the 1890s for enhancing the isolation of chlorine gas from NaCl(aq). The amalgam process increased the reduction potential of sodium metal and its isolation purity from the surrounding salt solution:

$$\text{Anode: } 2Cl^- \rightarrow Cl_2 + 2e^- \qquad \text{Eq. B-1}$$

$$\text{Cathode: } 2Na^+ + 2e^- \rightarrow 2Na(Hg) \qquad \text{Eq. B-2}$$

$$\text{Net: } 2Na(Hg) + 2H_2O \rightarrow 2NaOH + H_2\uparrow + 2Hg(l) \qquad \text{Eq. B-3}$$

Mercury gas was known to emit discreet spectral lines under an electric current, which was investigated in detail in 1835 by Charles Wheatstone. By 1860 the 253.7 nm mercury emission line was discovered [338] and lighting applications were further investigated. The lack of an aesthetically appealing fluorescent coating (and to mitigate UV emission) meant mercury lamps were restricted to industrial applications. High-pressure mercury lamps (150 - 1000 W) were common by the 1930s, and emitted intense UV spectral lines with the exception of the re-absorption of the 253.7 nm UV-B line [339]. The predecessor for modern fluorescent light bulbs became commercially available in the 1940s.

B.3.2 20th-century use

In the early 20th century the electrical conductivity of mercury was further exploited to produce 'mercury switches', found to create less abrupt contacts with an active circuit or touch-sensitive explosive (e.g. land mines). By 1925 the Lilly Research laboratories recognized mercury (in particular merthiolates in the form R_1-Hg-S-R_2) could be effective germicides [340]. Hence mercury was often used as a medicinal preservative (e.g. thiomersal) and as an anti-fungal agent in grains (e.g. ethylmercurychloride, phenylmercury, or alkylmercury) intended for planting.

In 1881 it was discovered that the presence of mercury sulfate enhanced the hydration of alkenes and alkynes [341]. This was most significantly used in the catalytic conversion of ethylene to acetaldehyde and/or vinyl chloride. These processes quickly reached an industrial scale in Germany in 1914, Canada in 1914, and Japan in 1932 [24, 341].

From the 1920s to 1950s, mercury metal served in many applications on an industrial scale, from pesticides, mining, catalysis, electrical connections and preservatives. As most applications required only trace quantities of mercury, demand for the metal remained steady but low; globally several thousand tonnes of cinnabar were mined each year. Relatively speaking mercury's highest demands were in chlor-alkali industries, catalysis, and artisanal gold mining [333]. Ironically the largest modern source of atmospheric mercury is not directly related to mercury mining or its use in industry, rather due to the combustion of coal [39]. Not coincidental was that in the 1950s the potential for a global scale distribution of mercury pollution was recognized.

B.3.3 Organomercury poisonings in Japan

The pivotal year towards recognizing the environmental dangers of industrial mercury waste came in 1956 with the discovery of the widespread and unexplained poisoning of people of Minamata, Japan. Mercury had been used in the Chisso Corporation's acetaldehyde production plant between 1932 and 1968, but only in 1951 did the process become severely toxic to local residents, whereby ferric sulfide was substituted for manganese dioxide in the acetaldehyde production (an attempt to improve mercury's catalytic longevity). Mercury waste, previously expelled as $HgSO_4$ (with low bioavailability), leeched out as the highly bio-available methylmercury [342].

For five years, between 1951 – 1956, evidence accumulated that there was something causing widespread illness in city of Minamata. Methylmercury attacks the central nervous system, kidneys, brain, and other organs leading to cerebral palsy-like symptoms [343]. For these five years local doctors were aware of an increased incidence of birth defects, patients with numbness in their limbs, and anecdotal evidence of cats and other animals showing signs of 'insanity'. Officials outside city limits soon knew of these effects, including researchers at Kumamoto University (located 100 km North-East from Minamata). Once it was clear there was something local causing illness, the Chisso plant, the only major industrial center upstream, was soon implicated. Direct accusations towards the Chisso plant were hindered by its employment of the majority of the city's workforce. Disruption of manufacturing was not in immediate self-interest of Minamata's citizens.

Between the years 1956 and 1959 Kumamoto University investigated the claims that something in the water was causing a widespread 'disease' in the city. In 1958 the British neurologist Dr. Douglas McAlpine visited the city originally in search of Multiple Sclerosis incidence in Japan. He then recognized the afflicted patients had symptoms matching methylmercry poisoning. A research team from the university, led by Takeuchi, performed autopsies on several deceased patients. The preliminary results published in 1957 noted a 'sporadic outbreak of encephalopathia from unknown causes' [344]. A full documentation of the outbreak was published in 1962 by Takeuchi *et al.* [345], whereby they had established that "an unusual neurological disorder resulted from eating a large amount of fish and shellfish of Minamata bay in Japan". By this time well over 2200 victims were officially recognized to be affected in the bay area [346]. In 1968 the Chisso plant ceased acetaldehyde production and had

been ordered to commence monetary compensation for victims. The initial confusion over the origin of the Minamata 'disease' and a lack of official environmental regulations resulted in a long wait of several years, sometimes decades, before compensation was fully awarded to families. By 1969 when a cleanup of the bay was well under way, concentrations of methylmercury in the bay area fish again reached 'pre-industrial' levels of 0.5 ppm, down from an all-time high of 9 ppm [346]. The imprint of the outbreak had left its mark, and the city of Minamata became symbolic of industrial arrogance. Eugene and Aileen Smith's photographic tour of Minamata between 1971 and 1974 later emphasized the visual impact of mercury poisoning [347].

After Minamata there was new environmental awareness of mercury pollution, though this did not prevent a second methylmercury poisoning incidence in 1964 in Niigata, Japan under similar circumstances [348], though compensations were awarded by the company much sooner [346].

B.3.4 Organomercury poisonings in Iraq

Between 1971-72, a mass outbreak of mercury poison occurred in Iraq when several villages consumed imported grain treated with ethylmercury [349]. The grain was imported from Mexico and the warning signs were illegible to the Iraqi villagers. Despite the early recognition of the poisoning, there was little to be done outside of further studying the detrimental effects, so instead researchers set out to measure the impact on villagers. The cause and symptoms of "Minamata Disease" were now well established, but meaningful threshold limits on mercury consumption had not yet been determined.

Analytical techniques had improved from the 1950s, in part due to studies done after Minamata, and mercury could now be detected at the parts per million level by cold-vapor atomic absorption (CVAA) in blood, urine, and hair [350]. Bakir *et al.* [178] systematically collected blood and hair samples from the affected villages in Iraq, comparing their symptoms to unaffected villages. Symptoms were correlated with mercury hair and blood concentrations. From this data meaningful threshold limits of exposure were estimated, i.e. patients above ~10 ppm Hg in hair were found to show an onset mild symptoms. Bakir's study spawned decades of new research in low-level, long-term mercury consumption in various populations, e.g. Seychelles, Faroe Islands, and Amazon communities [10, 12, 351-353]. The study became the

foundation of the current United States Environmental Protection Agency (US-EPA) organic mercury consumption guideline of 0.1 microgram per kilogram of body weight per day [13].

Studies of mercury pollution were now expanding in both number and scope. Stricter laws requiring better accountability of wastewater were increasing; Sweden introduced the world's first environmental protection agency in 1967 and banned organo-mercury pesticides the same year [354]. The United States Environmental Protection Agency was established in 1970 under Nixon to enforce stricter controls on pollution; by 1971 the USEPA had listed mercury (along with asbestos and beryllium) as a "Hazardous Air Pollutant". Environment Canada (under Pierre Trudeau) and accompanying provincial ministries were established in 1971 to enforce environmental regulations of dangerous substances. An early test came in 1970 where discharge from a local chlor-alkali plant was found contaminating commercial fish in Lake St Clair (Sarnia, ON); the plant was then required to install new treatment facilities.

The increased pressure from environmental organizations led many companies to find alternatives to mercury metal. A gradual substitution of mercury for other materials such as in batteries and paints have contributed to the global downturn in demand and environmental risk. Mercury was no longer needed as a catalyst in acetaldehyde production, being replaced instead by the Wacker process after 1960 [355]. Chlor-alkali plants continued to use mercury, but with stricter accountability for mercury waste. Improved disposal techniques, such as sulfur dust in scavenging mercury vapor, were implemented. Evidence of the dwindling need for mercury came from the closing of the largest mercury mine in Almaden, Spain [333] in the 1980s. In the United States, a tax on imported mercury was introduced in 1986, further discouraging trade. Data suggest the peak modern demand for mercury metal reached 6000-7000 tonnes in the 1980s, and has steadily decreased to the current 3500 tonnes per year [333].

As most mercury waste spilled directly into rivers and lakes, the initial environmental concern was devoted to measuring levels of mercury found in aquatic ecosystems [356]. Mercury poisonings were understood to result from eating fish, as in Minamata. Sources of the pollutant were thought to be regional in scale, usually downstream from a shared body of water. In the 1960s an important link was confirmed: that inorganic mercury could be methylated by aquatic microorganisms [22]. This implied that inorganic waste, considered less dangerous, would be slowly converted to the far more hazardous organo-mercury. Lakes were perhaps more

polluted than originally assumed. More worrisome still was the growing evidence that pristine lakes were somehow being contaminated by methylmercury.

B.4 *Physical properties of mercury metal*

B.4.5 Bulk properties of Hg^0

Here we present summary of mercury's physical properties including bulk properties, comparative reactivity, ionization and reduction potentials, and amalgamation properties. We then summarize the reactivity of mercury and important mercury oxides involved in atmospheric oxidation processes.

Mercury is a shiny, silver-colored transition metal and the only metal liquid at STP (25°C and 1 atm), and historically provided the standard for several measures. Its liquid density is 13.53 g/mL at 25°C, among the heavier metals, less than gold (19.32 g/cm^3) but heavier than lead (11.35 g/cm^3). Surface tension for mercury is exceptionally high, with γ = 485.48 mN/m at 25 °C (in comparison, the surface tension for water is 71.99 mN/m at 25 °C) [65]. The high surface tension of mercury is exhibited in the highly rounded, convex meniscus when stored in glassware. Electrical resistivity for mercury is also very high for a metal, at 95.8 μohm cm^{-1} [60] and provides reference substance for the measure of the *international ohm*.

Mercury has a freezing point of -38.8°C and boiling point of 356.7°C; thus mercury is liquid over a 395.6K temperature span. The liquid thermal expansion coefficient of mercury, α, is 1.8×10^{-4} K^{-1} at 20°C [65], which is similar to water's value of 2.1×10^{-4} K^{-1}. Liquid mercury is very resistant to compression, where $\kappa_T = 4.0 \times 10^{-6}$ $bar^{-1,}$ making it a useful hydraulic fluid in certain applications (water's compressibility is 4.6×10^{-5} bar^{-1}). Mercury's vapour pressure at 20°C is 0.17 Pa or 1.3 mTorr, giving the metal a concentration of 1.7 *parts per million* (ppm) in an enclosed atmosphere [357]. This is a high vapour pressure for a metal but low for a liquid. As a dense, low-compressibility liquid with comparatively low vapour pressure, it has been historically suitable for both thermometers and barometric instruments, hence the common pressure units mmHg or *Torr*.

Despite existing in a liquid state at low temperatures it has one of the smallest liquid ranges of any metal (gold's range is 1876K; m.p. 1064°C b.p. 2940°C). Skewing its own

cultural portrayal, the truly exceptional feature of this metal is its propensity to become a stable monatomic gas.

Isotopes

There are seven stable isotopes of mercury (% relative abundance): 196 (0.15%), 198 (9.97%), 199 (16.87%), 200 (23.1%), 201 (13.18%), 202 (29.86%), and 204 (6.87%). Hence it has an average molecular weight of 200.59 g/mol. The large array of stable isotopes allows for a fortuitous and unambiguous identification in a mass spectrum signal. Mercury is the third-heaviest element with a stable isotope, behind thallium and lead. The longest living radioisotope is ^{194}Hg at 444 years, but does not occur in nature hence cannot be used in dating typical of ^{14}C.

Since the natural isotopic abundance of mercury is well known, measurements of deviations of these isotope fractions can be used to identify chemical reactions that may, or may not, be affected by a certain isotopic mass. Deviations of one isotope M compared to another (referenced by an accepted standard, i.e. ratios given above) are labeled as δ^{M}Hg, in units of *parts per thousand, ‰*. For instance, if referencing mass deviations of M compared to the mass M=198 isotope, then

$$\delta^{M}\mathrm{Hg} \equiv 1000 \times \left(\frac{{}^{M/198}R_{sample}}{{}^{M/198}R_{reference}} - 1 \right) \qquad \text{Eq. B-4}$$

where *R* denotes the ratio of the heavy to light isotope (M and 198). Typical deviations may rage from -3 to +3‰ [238], but may vary. Depending on the

chemical reaction, atypical mass deviations may be observed in natural mercury systems, possibly due to a magnetic isotope effect unique to odd isotopes and their spin coupling with the valence electrons [241]. The [typically biological] mercury kinetics which exhibit such isotopic mass deviations are beyond the scope of this thesis, but remain an active area of field and theoretical research.

B.4.6 Excited states of Hg^0(g)

The lowest electronic spin-allowed ground to first excited state excitation is $6^1S_0 \rightarrow 6^3P_1$, which is its 253.7 nm line of UVB light. In a dilute atmosphere of mercury gas ($[Hg^0] \sim 1$ ppm), the application of a potential current will emit at the 253.7nm UVB line. High-pressure Hg lamps (where bulb pressures reach 200 atm) will also emit lines of 365, 405, 436, 546, and

578nm. Power in high pressure lamps can range from 100-800W. The 253.7 nm mercury line however is re-absorbed. A quartz bulb will also emit a 185nm line, producing some ozone outside of the bulb.

Table B-1 First few electronic states of $Hg^0(g)$. g_i is the degeneracy of the state, ε_i is the transition energy/wavelength [358]:

Electronic state	ε_i		g_i
	cm^{-1}/ (λ, nm)	kJ/mol (kcal/mol)	
$^1S_0$	0	0	1
$^3P_0$	37,645.080 (265.6 nm)	450.647 (107.71)	1
$^3P_1$	39,412.300 (253.7 nm)	471.802 (112.76)	3
$^3P_2$	44,042.977 (227.1 nm)	527.236 (126.01)	5

B.4.7 Amalgams

An amalgam, by definition, is an alloy formed between mercury and another metal [65]. Amalgams include gold, silver, tin, zinc, indium, and sodium metal (mercury does not form an amalgam with iron). The property of these mixtures is typically that of a resin, initially soft, that hardens within minutes. The solid resins decompose at elevated temperatures or pressures, but remain quite stable at room temperature (with negligible vapor pressure). Notably, among all mercury compounds, only amalgams are considered non-toxic. Amalgams have been used in such application as artisanal gold mining capture (HgAu) and dental fillings (HgAg). If we combine mercury's conductivity and its amalgamation with alkali metals; the reduction of certain metal ions into a mercury amalgam can be more favorable (and more stable) than direct reduction of the metal [359].

$$K^+ + e^- \rightarrow K(s) \quad E^\circ = -2.94 \text{ V} \qquad \text{Eq. B-5}$$

$$K^+ + e^- + Hg \rightarrow K(Hg) \quad E^\circ = -1.98 \text{ V} \qquad \text{Eq. B-6}$$

Mercury's ability to serve simultaneously as an alloy and electrode has been utilized both on the industrial (e.g. chlor-alkali plants) and analytical (e.g. polarography) scale.

B.4.8 Electronic and reactive properties of Hg^0

Mercury's ground electron configuration is [Xe] $4f^{14}$ $5d^{10}$ $6s^2$, breaking the conventional electron orbital filling rules that would have placed the $6s^2$ orbital behind the $4f^{14}$ $5d^{10}$ blocks. Since the 6s orbital is the highest occupied molecular orbital (HOMO), this leads to a limited comparatively limited choice in oxidations states for a d-block element, at either +1 or +2. The 6s valence orbital also has a high density near the nuclear core. The high 6s electron density near the core contracts the orbital as the electron approaches a significant fraction of light speed. Because of significant relativistic contraction of inner shell electrons, there is a shrinking orbital cascade effect whereby 6s electrons are then closer to the core making mercury far less reactive than adjacent species [360]. Due to its filled electron valences, elemental mercury does not readily oxidize compared with cadmium or zinc, and conversely oxidized mercury can be more easily reduced than either of these element.

The +1 and +2 valence mercury oxides both may yield stable compounds, as noted below. Reacting 2 moles of gaseous mercury with 2 moles chlorine gas can either lead to mercury(II) or mercury (I) chloride also known as calomel. Both species are air-stable and decompose only at elevated temperatures.

Table B-2 Henry's law partitioning coefficient [gas]/[aq]; v/v at 20-25 °C

Mercury species	Partitioning coefficient [gas]/[aq]; v/v	Reference
Hg^0	0.29	[361]
$(CH_3)_2Hg$	0.31	[362]
CH_3HgCl	1.9×10^{-5}	[363]
$HgCl_2$	2.9×10^{-8}	[52]

B.5 *Bimolecular and pseudo-first-order reactions*

For an elementary bimolecular reaction between molecules A and B,

$$A_{(g)} + B_{(g)} \rightarrow \text{products} \qquad \text{Eq. B-7}$$

The differential law rate loss for A is

$$-\frac{\mathrm{d[A]}}{\mathrm{d}t} = k[\mathrm{A}][\mathrm{B}] \qquad \text{Eq. B-8}$$

If [B] is much higher in concentration than [A], then we may assume steady state concentrations for [B], roughly constant, so that

$$\ln\left(\frac{[\mathrm{A}]_t}{[\mathrm{A}]_0}\right) = -k[\mathrm{B}]_0 t \qquad \text{Eq. B-9}$$

This gives a pseudo-first-order rate constant $k' = k[\mathrm{B}]_0$. A plot of $\ln([\mathrm{A}]_t)$ versus t yields slope $m = k[\mathrm{B}]_0$.

B.6 *Temperature dependence on k*

The empirical Arrhenius equation is

$$k(T) = A\exp\left(-\frac{E_a}{RT}\right) \qquad \text{Eq. B-10}$$

where A is the Arrhenius constant, E_a is the activation energy per mole, R is the gas constant (8.314 J/Kmol) and T is temperature (K). The temperature dependence is found plotting ln(k) versus 1/T, giving slope $-E_a/R$ and intercept lnA. Semi-empirical gas phase collision theory gives the similar result

$$k(T) = \rho\pi b_{\max}^2 v_r \exp\left(-\frac{\varepsilon^*}{k_B T}\right) \qquad \text{Eq. B-11}$$

where ρ is the empirical steric factor ($0 < \rho < 1$), $b_{\max} = r_1 + r_2$, the sum of hard sphere or Van der Waals molecular radii r_1 and r_2. ε* is the threshold barrier energy (approximately the same as the activation energy, E_a). v_r is the average relative velocity, where

$$v_r = \sqrt{\frac{8k_B T}{\pi\mu}} \qquad \text{Eq. B-12}$$

and k_B is Boltzmann's constant, μ is the reduced mass [$\mu = m_A m_B/(m_A + m_B)$].

The rate is more fully expressed by integrating over all possible relative velocities

$$k(T) = \frac{1}{k_B T}\left(\frac{8}{\pi\mu k_B T}\right)^{1/2}\int_0^\infty \varepsilon\sigma(\varepsilon)\exp\left(-\frac{\varepsilon}{k_B T}\right)d\varepsilon \qquad \text{Eq. B-13}$$

For a barrier-less collision, the activation energy is near zero ε* ~ 0, so that

$$k(T) = \rho \pi b_{\max}^2 \sqrt{\frac{8k_B T}{\pi \mu}} \qquad \text{Eq. B-14}$$

Depending on the mechanism, barrier-free reactions show different dependencies on temperature, so that we often write

$$k(T) = AT^n \qquad \text{Eq. B-15}$$

where *n* may vary widely, and be positive or negative. Such reactions include radical or atomic combinations, such as the reaction between mercury and chlorine radicals

$$Hg_{(g)} + Cl_{(g)} \rightarrow HgCl_{(g)} \qquad \text{Eq. B-16}$$

Suppose we observe a reaction between a mercury and chlorine atom. We estimate the hard sphere radii to be related to the van der Waals radii [364], so that $r_{Hg} \sim 155\text{pm}$ $r_{Cl} \sim 175\text{pm}$ and $\mu = 30.13\ \text{g/mol} = 5.0 \times 10^{-26}\,\text{kg}$. If we assume the temperature is ambient and that ρ is unity (Hg and Cl are isotropic), then

$$\begin{aligned} A &= \pi b_{\max}^2 v_r \\ &= \pi (3.30 \times 10^{-10}\,\text{m})^2 \sqrt{\frac{8(1.38 \times 10^{-23}\,\text{JK}^{-1})(300\text{K})}{\pi (5.0 \times 10^{-26}\,\text{kg})}} \\ &= (3.42 \times 10^{-19}\,\text{m}^2)(459.2\text{ms}^{-1}) \\ &= 1.57 \times 10^{-10}\,\text{cm}^3\text{s}^{-1} \end{aligned} \qquad \text{Eq. B-17}$$

Hence we may estimate the rate as $k_{Hg+Cl} = 1.57 \times 10^{-10}\ \text{cm}^3\ \text{s}^{-1}$

The pre-factor is roughly 10× larger than literature values $1.5 \times 10^{-11}\ \text{cm}^3\ \text{s}^{-1}$ [365] and $1.0 \times 10^{-11}\ \text{cm}^3\ \text{s}^{-1}$ [162]. This calculation therefore implies there is an activation barrier.

B.7 Relative rates

If two parallel reactions are occurring, both reacting with B (assumed to be in excess),

$$\begin{aligned} A_{(g)} + B_{(g)} &\rightarrow \text{products} \\ \text{ref}_{(g)} + B_{(g)} &\rightarrow \text{products} \end{aligned} \qquad \text{Eq. B-18}$$

then a ratio of the two rates can be determined

$$\ln\left(\frac{[A]_t}{[A]_0}\right) = \frac{k_A}{k_{ref}} \ln\left(\frac{[ref]_t}{[ref]_0}\right) \qquad \text{Eq. B-19}$$

This eliminates the need to measure the initial concentration of the oxidant B (see Eq B-3). Relative rates may be useful if B is, say, a free radical, which cannot easily be measured and whose absolute concentration is difficult to assess. We are assuming that B reacts simultaneously, and independently with A and Ref. Reaction products must be carefully. Also the rate of interest k_A should be close (same order of magnitude) as k_{ref}. One must also be aware of whether the rate k_{ref} is itself derived from a relative rate, as the propagation of errors can rapidly increase.

B.8 *Surface kinetics*

B.8.1 Diffusion to a surface:

The root mean square distance traveled by a gaseous molecule is

$$z_{rms} = (2Dt)^{1/2}$$

$$D = \frac{1}{3} < v > \lambda \qquad \text{Eq. B-20}$$

$$< v >= \left(\frac{8kT}{\mu\pi}\right)^{1/2}, \quad \lambda = \frac{N_A kT}{\sqrt{2}\pi d^2 p} \qquad \text{Eq. B-21, Eq. B-22}$$

The time it take to travel to a surface from a point to the wall on which a reaction will take place is related to z_{rms}.

For a particle A in equilibrium with a surface site S,

$$A_{(g)} + S \Leftrightarrow A_{(ads)}\text{-}S \qquad \text{Eq. B-23}$$

the coverage depends on the availability of surface sites and the equilibrium constant *K,* which is a temperature *T* and surface site binding energy ΔG_{SS} dependent value.

$$K = \exp\left(-\frac{\Delta G_{SS}}{RT}\right) \qquad \text{Eq. B-24}$$

Using the Langmuir model we have equilibrium between gaseous species A and the adsorbed surface site S.

$$\theta_A = \frac{K[\mathrm{A}]}{1 + K[\mathrm{A}]} \qquad \text{Eq. B-25}$$

where K is the Langmuir equilibrium constant, equal to the rate of sorption and desorption from the surface ($K = k_{ads}/k_{des}$), and "[A]" denotes the concentration of species A. The unimolecular surface reaction of A on surface site S is an equilibrium of A with surface site S followed by formation of product P formed on the surface,

$$\begin{aligned} \mathrm{A_{(g)}} + \mathrm{S} &\Leftrightarrow \mathrm{A\text{-}S} \\ \mathrm{A\text{-}S} &\rightarrow \mathrm{P\text{-}S} \\ \mathrm{P\text{-}S} &\rightarrow \mathrm{P_{(g)}} + \mathrm{S} \end{aligned} \qquad \text{Eq. B-26}$$

If the rate-limiting step is surface reaction, then the reaction rate is then proportional to the amount of A sorbed (chemisorbed or physisorbed) to a surface site S in pseudo-equilibrium:

$$-\frac{d[\mathrm{A}]}{dt} = k\theta_A = k\frac{K[\mathrm{A}]}{1 + K[\mathrm{A}]} \qquad \text{Eq. B-27}$$

This pseudo-equilibrium assumes that the product will desorb and not compete for surface sites. The rate is only affected by the concentration of A. This equation can be integrated:

$$\ln\left(\frac{[\mathrm{A}]_0}{[\mathrm{A}]}\right) + K([\mathrm{A}]_0 - [\mathrm{A}]) = kKt \qquad \text{Eq. B-28}$$

Although the equation is not itself linear, it can be linearized when plotting $\ln([\mathrm{A}]_0/[\mathrm{A}])/([\mathrm{A}]_0 - [\mathrm{A}])$ versus $t/([\mathrm{A}]_0 - [\mathrm{A}])$. Alternatively one may plot the upper and lower bounds of the equation, for K[A] >> 1 and K[A] << 1.

The previous example assumed the product formed also desorbs. If the product P does *not* desorb, then it must accumulate and compete with A for surface sites:

$$\begin{aligned} -\frac{d[\mathrm{A}]}{dt} &= k\frac{K[\mathrm{A}](1 - \theta_\mathrm{p})}{1 + K[\mathrm{A}]} \\ \frac{d[P]}{dt} &= k\theta_A \end{aligned} \qquad \text{Eq. B-29}$$

where θ_p is the fraction of surface covered by the product. This equation is not readily solvable, but can be estimated by assuming the product coverage rises exponentially towards unity,

$$1-\theta_p = \exp(-kKt)$$

Eq. B-30

$$-\frac{d[\mathrm{A}]}{dt} = k\frac{K[\mathrm{A}]\mathrm{e}^{-kKt}}{1+K[\mathrm{A}]}$$

Eq. B-31

Integrating we get a similar equation but with an exponential term in time. If k or K is sufficiently small, this reduces back to the previous equation:

$$\ln\left(\frac{[\mathrm{A}]_0}{[\mathrm{A}]}\right) + K([\mathrm{A}]_0 - [\mathrm{A}]) = 1-e^{-kKt}$$

Eq. B-32

If there are two species that react together on the surface (e.g. species A and B), then both species must be present on the surface to react. The surface coverage then represents a competition between species A and B:

$$\mathrm{A}_{(g)} + \mathrm{S} \Leftrightarrow \mathrm{A\text{-}S}$$
$$\mathrm{B}_{(g)} + \mathrm{S} \Leftrightarrow \mathrm{A\text{-}S}$$
$$\mathrm{A\text{-}S} + \mathrm{B\text{-}S} \rightarrow \mathrm{P\text{-}S}$$

Eq. B-33

$$\theta_A = \frac{K_A[\mathrm{A}]}{1+K_A[\mathrm{A}]+K_B[\mathrm{B}]}$$

Eq. B-34

The rate-loss of A is then proportional to the fraction of adjacent species A and B available for reaction on the surface

$$-\frac{d[\mathrm{A}]}{dt} = k\theta_B\theta_A = k\frac{K_A[\mathrm{A}]K_B[\mathrm{B}]}{\left(1+K_A[\mathrm{A}]+K_B[\mathrm{B}]\right)^2}$$

Eq. B-35

This equation assumes that the species migrate quickly compared to the rate of reaction. If species B is in excess of A (i.e. [B] >> [A]), then the fraction of B remains relatively constant. If we apply a steady state assumption on B:

$$-\frac{d[\mathrm{B}]}{dt} = 0$$
$$\theta_B \sim \text{constant}$$

Eq. B-36

the rate loss of A is approximately the fraction of A on the surface sites S, while species B is implicitly accounted for in the now simplified equation, i.e.

$$-\frac{d[\mathrm{A}]}{dt} = k\theta_{B,SS}\theta_A = k'\frac{K'_A[\mathrm{A}]}{1+K'_A[\mathrm{A}]} \qquad \text{Eq. B-37}$$

where $k' = k\theta_B$ and $K'_A = K_A/(1+K_B[\mathrm{B}])$

The condensed equation is now kinetically identical to a unimolecular surface reaction. The rate K_A can be obtained if K_B is known. We note that the Langmuir constant K_A could be larger than K_B so that even in the steady state approximation the factor $K_A[A]$ is not necessarily negligible with respect to $K_B[B]$.

B.9 *Other gaseous oxidation reactions of mercury*

B.9.1 $Hg_{(g)} + H_2O_{2(g)}$, *and* $OH_{(g)}$

The oxidation of mercury by OH led early experiments to predict the existence of $Hg(OH)_2(g)$. For instance it was 'known' that mercury would react with hydrogen peroxide to give gaseous $Hg(OH)_2$:

$$Hg_{(g)} + H_2O_{2(g)} \rightarrow Hg(OH)_{2(g)} \qquad \text{Eq. B-38}$$

Considering the apparently simplicity of the reaction, it was an attractive mechanism to propose [55]. It was known that $Hg(OH)_2$ existed in the aqueous phase at low pH . Apparent stability of gaseous $Hg(OH)_2$ was also shown by early density functional theory work [366]. It was not until 1998 that a rate constant was obtained, $k = 6 \times 10^{-19}$ cm^3 $molecule^{-1}$ s^{-1} [367]. Wang and Andrews found $Hg(OH)_2$ to stable only in a solid matrix of argon [368]. The oxidation of mercury by the hydroxyl radical was measured by Pal and Ariya [145]:

$$Hg_{(g)} + OH_{(g)} \rightarrow HgO_{(g/s?)} \qquad \text{Eq. B-39}$$

There are clearly several steps to the reaction. Despite the uncertainty of the mechanism, Pal and Ariya established the rate to be $(9.0 \pm 1.3) \times 10^{-14}$ cm^3 $molecule^{-1}$ s^{-1} using the photolysis of isopropyl nitrite ($\lambda = 300$ nm) [145]. Their identification of
the product as HgO(s), found on the flask walls and in aerosols, supported that $Hg(OH)_2$ is not possible in the gas phase, although it did not dismiss the possibility of HgO(g).

B.9.2 $Hg_{(g)} + SO_{2(g)}$

No reaction is thought to occur between SO_2 and Hg. In principle such a reaction is quite exothermic, with an enthalpy of $\Delta H = -468.8$ kJ/mol.

$$Hg^0_{(g)} + SO_{2(g)} + O_{2(g)} \rightarrow HgSO_{4(s)} \qquad \text{Eq. B-40}$$

Therefore there must be a high activation energy barrier as no activity is seen at room temperature [90]. The reaction may occur on a suitable surface at sufficiently high temperature but there is no evidence of a low-temperature reaction. Surprisingly there is thought to be a reaction between HgO and SO_2 producing Hg_2SO_4, $HgSO_4$ and $HgSO_4 \cdot 2H_2O$ [88].

B.9.3 $CH_3HgCH_{3(g)}$ + $Cl_{(g)}$, $OH_{(g)}$

Dimethylmercury was one of the earliest species to be investigated kinetically. Due to methylating bacteria found in lakes and the high volatility of the resultant compound, early schematics of mercury transportation had shown dimethylmercury as a potential component to the global transport cycling of mercury. In particular because the marine boundary layer contains higher levels of Cl and OH radicals, the oxidation rate with dimethylmercury has a lifetime of only a few hours (also yielding very water-soluble products):

$$OH_{(g)} + CH_3HgCH_{3(g)} \rightarrow CH_3HgOH_{(g)} + CH_{3(g)} \qquad \text{Eq. B-41}$$

$$Cl_{(g)} + CH_3HgCH_{3(g)} \rightarrow CH_3HgCl_{(g)} + CH_{3(g)} \qquad \text{Eq. B-42}$$

Where $k_{OH} = (1.97 \pm 0.23) \times 10^{-11}$ cm^3 $molec^{-1}$ s^{-1} [369] and $k_{Cl} = (2.75 \pm 0.30) \times 10^{-10}$ cm^3 $molec^{-1}$ s^{-1} [370]. With such short atmospheric lifetimes methylmercury species do not participate in the transportation cycle.

B.9.4 $Hg^0_{(g)}$ + $Cl_{2(g)}$, $Cl_{(g)}$ and $HCl_{(g)}$

The reaction between mercury and chlorine gas had been conducted as early as 1979 by Madhekar *et al.*, who found it to be a heterogeneous reaction with the product $(HgCl_2)_n$ [300]. The next year Menke and Wallis returned to this reaction to find there is also gas-phase component:

$$Hg_{(g)} + Cl_{2(g)} \rightarrow HgCl_{2(s)} \qquad \text{Eq. B-43}$$

They also found the gaseous oxidation of mercury by chlorine gas was enhanced in higher humidity (80% versus 13%), suggesting the heterogeneous component is affected by water (where $HgCl_2$ is highly soluble) [326]. The gas-phase reaction between mercury and

chlorine gas had also been conducted in 1992 [211]. Though no homogeneous reactions were detected, again there was evidence of heterogeneous chemistry. This is in contrast to Hall's 1991 study that found mercury reacts with Cl_2 at room temperature [90, 371] and again Ariya *et al.*'s confirmation that it is a gas-phase reaction [162] (here surfaces were pacified with halocarbon wax). Hall also noted that mercury reacts with HCl [90]:

$$Hg_{(g)} + HCl_{(g)} \rightarrow HgCl_{(g)} + H_{(g)} \qquad \text{Eq. B-44}$$

A laser-induced oxidation of mercury with atomic chlorine yields a pressure-dependent reaction rate of $k_{Hg+Cl} = 5.5 \times 10^{-13}$ cm^3 molecule^{-1} s^{-1} at 298 K and 1 atm [372], which implies mercury is quite capable of reacting with chlorine if photolysis of the chlorine species is possible. More recently it was found that mercury sulfate ($HgSO_4$) can be oxidized to $HgCl_2$ by HCl, but not by Cl_2. Hence certain mercury oxides can be transformed from one species to another. The direct oxidation of Hg^0 by HCl has not been measured since Hall's work in 1991, however there has been some kinetic work done using ab initio theoretical calculations by Wilcox *et al.* [373, 374]. These rates vary considerably with the basis set and method used, and gaseous computational chemistry often neglects more complex reaction schemes that yield stabler products, i.e.

$$Hg_{(g)} + 2HCl_{(g)} + \tfrac{1}{2}O_{2(g)} \rightarrow HgCl_{2(g)} + H_2O_{(g)} \qquad \text{Eq. B-45}$$

The relative degree of heterogeneous versus gaseous chlorine chemistry in the oxidation of mercury has not yet been explicitly measured. Indirect methods continue to be applied designed to measure the affinity of $HgCl_2$ to surfaces. It has been found that sea salt aerosols have show a high uptake efficiency for $HgCl_2$ [375]. Conversely coal combustion simulations at higher temperatures (100 – 250 °C) find higher losses of mercury with increase chlorine levels [105, 376, 377]. Typically such studies rely on capture by fly ash or other surfaces available in combustion systems; at high temperatures mercury chloride is quite volatile hence lost in flow systems. Frequently reports on heterogeneous uptake do not employ detailed kinetics, instead reporting percentage Hg^0 uptake in the presence/absence of chlorine species. Chlorine reactions have received a disproportionate level of attention in part due to the formation of the product $HgCl_2$(s). Mercury chloride is the most easily detectable form of oxidized mercury because of its volatility, as well its affinity to KCl denuders has been well characterized compared with $HgBr_2$ or HgO(s) [331, 378].

B.9.5 $Hg^0_{(g)}$ + $Br_{2(g)}$, $Br_{(g)}$, $BrO_{(g)}$ and $HBr_{(g)}$

Reactions with bromine species were scarce until the last 10 years, when it was discovered that bromine is responsible for atmospheric mercury depletion events (AMDEs) [6]. Mercury is thought to react quickly with atomic bromine:

$$Hg_{(g)} + Br_{(g)} + M_{(g)} \rightarrow HgBr_{(g)} + M_{(g)} \qquad \text{Eq. B-46}$$

where $k = (4.31 \pm 0.21) \times 10^{-33}\ (T/298)^{-1.86\pm1.49}$ [M] cm^3 $molecule^{-1}$ s^{-1} or $k = 1.1 \times 10^{-13}$ cm^3 $molecule^{-1}$ s^{-1} at 298 K and 1 atm [148]. The rate is weakly dependent on temperature and requires a third body to stabilize the collision. The reaction between atomic bromine and mercury is fast, but the surface dependence of the reaction is not well known. Despite the uncertainties, Holmes *et al.* have conjectured bromine is the most important oxidizer of mercury in the troposphere [379]. It is already known to be the single fastest oxidizer at the marine boundary layer [59, 77].

The reaction of gaseous mercury with BrO has not been measured with any precision.

$$Hg_{(g)} + BrO_{(g)} \rightarrow \text{products?} \qquad \text{Eq. B-47}$$

Raofie *et al.* estimated the reaction to be $10^{-13} < k < 10^{-15}$ cm^3 $molec^{-1}$ s^{-1} [150], but no certainty of the rate value, the oxidation mechanism or the dependency of k on surfaces has been established by any study.

In 1936 Ogg et remarked on the lack of study of gaseous mercury with halogens [380]. Ogg *et al.* were considering the mechanisms of the mercury-molecular bromine reaction,

$$Hg_{(g)} + Br_{2(g)} \rightarrow HgBr_{2(g)} \qquad \text{Eq. B-48}$$

The rate constant was estimated to be between 2×10^{-17} to 2×10^{-19} cm^3 $molec^{-1}$ s^{-1}. The degree to which the reaction is pure homogeneous, or comprises some heterogeneous aspect, is still controversial. In large chamber studies no reaction was found [75] Reactions with Br_2 have been measured by Ariya *et al.* [162], where $k = (9 \pm 2) \times 10^{-15}$ cm^3 $molec^{-1}$ s^{-1}. Field product studies of $HgBr_2$ are ambiguous [77]. Since all mercury oxides are classified as gaseous oxidized mercury (GOM), we cannot resolve one oxide over another. There is no direct proof that one pathway is preferred over another.

Appendix C

Chapter 2 supplementary data

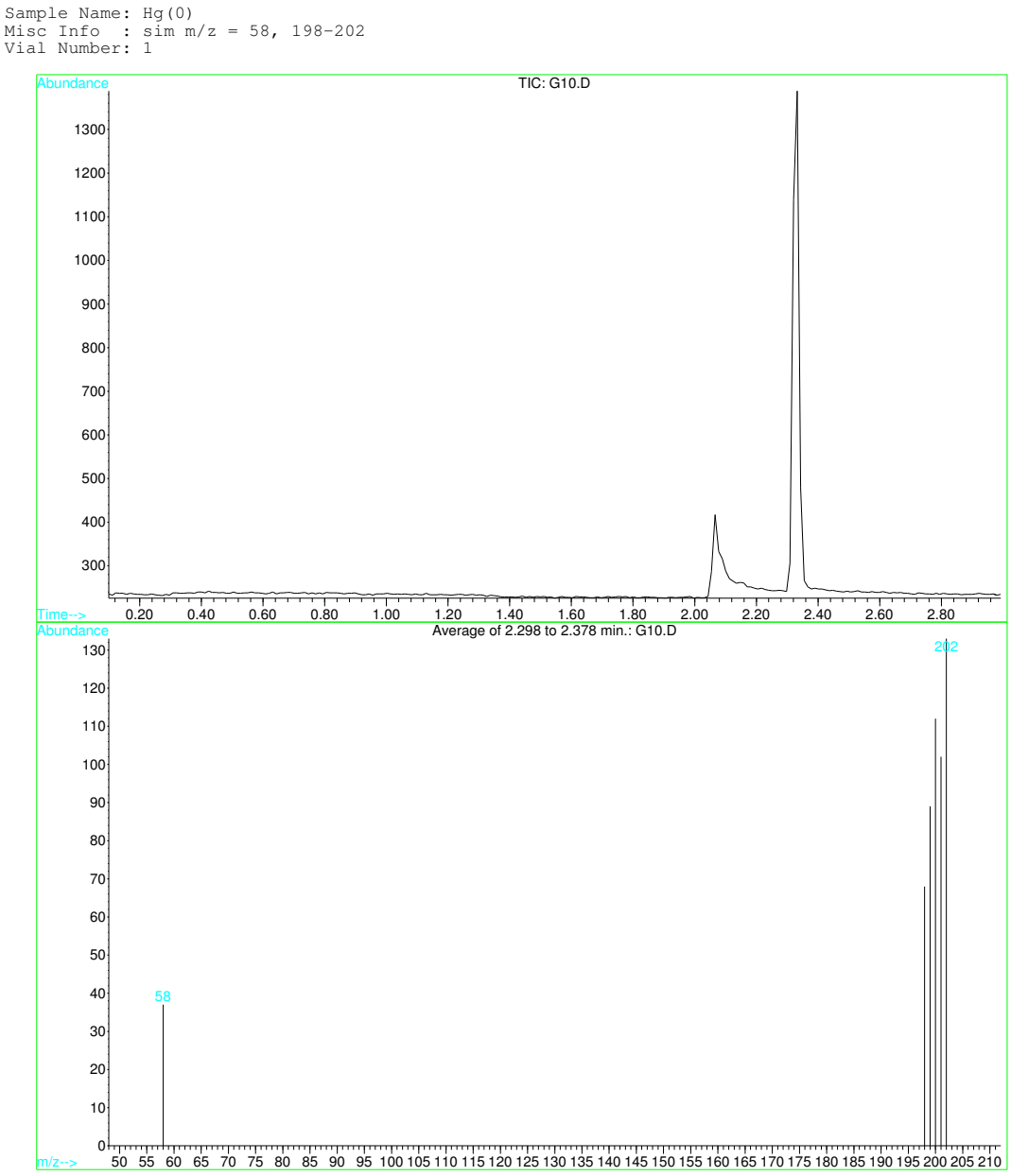

Figure C-1 Sample of a single ion monitoring (SIM) run. Mercury is identified using the isotopes m/z = 198-202. The peak at m/z = 58 is a reference SIM point, a baseline to distinguish mercury signal from background.

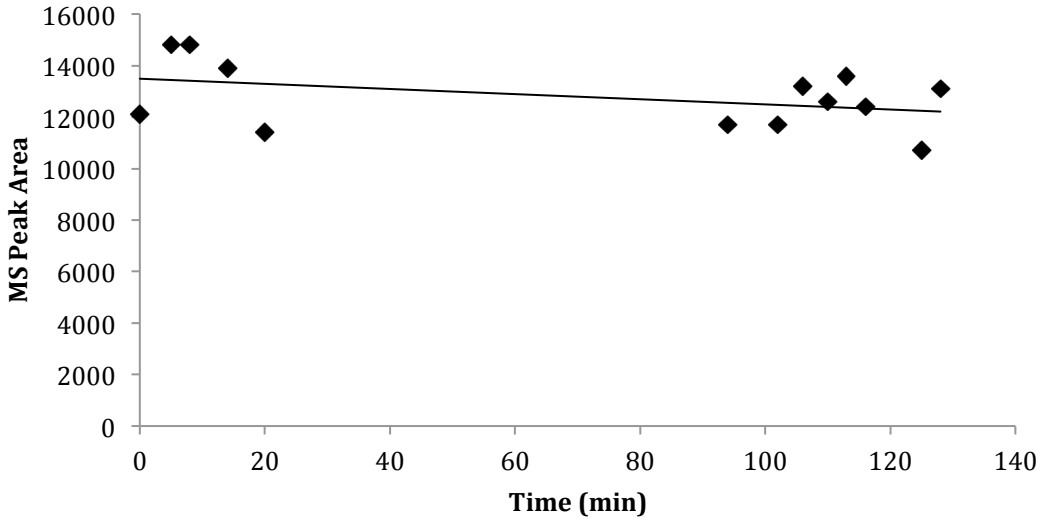

Figure C-2 Sample of a gaseous elemental mercury loss with time for a 5 L flask coated in halocarbon wax. Timescale reflects a typical run length. Losses are small compared with 90+ % $Hg^0_{(g)}$ removal due to addition of ozone.

Table C-1 Variation of mercury concentration (MS signal area) with time

Trial #	Area (Hg)	Area (Hg)	Area (Hg)	Area (Hg)
1	25500	26200	26800	27200
2	25000	22000	27200	26700
3	25200	23600	25200	25800
4	26200	27300	29700	26400
5		24900	26600	
6		25500	27800	
7		24600		
average	25475	24871	27217	26525
SD/√n	263	655	609	293

SD = Standard deviation

Table C-2 Variation of mercury reaction rates due to variable ozone concentrations

$[O_3]$	1L flask		3L flask		5L flask	
	$k([O_3]) \times 10^{18}$ $cm^3\ molec^{-1}\ s^{-1}$	$t^*\sigma/\sqrt{n}$	$k([O_3]) \times 10^{18}$ $cm^3\ molec^{-1}\ s^{-1}$	$t^*\sigma/\sqrt{n}$	$k([O_3]) \times 10^{18}$ $cm^3\ molec^{-1}\ s^{-1}$	$t^*\sigma/\sqrt{n}$
10	2.62	0.69	1.03	0.24	1.08	0.18
20	1.78	0.12	0.71	0.23	1.06	0.34
30	1.42	0.32	0.515	0.095	0.70	0.36
40	1.03	0.22	0.51	0.10	0.75	0.39
60	0.68	0.23				

$n = 6 \rightarrow t(95\%\ \text{C.I.}) = 2.57$

Note for Table C-2: The impression obtained from the above information is that for $[O_3] \geq 30$ ppm and $V_{flask} \geq 3L$, the concentration and S/V effects are minimal. Hence using a 3L flask with 30 ppm O_3 is acceptable; however using a 1L flask at (apparently) *any* concentration will not represent realistic rate constants. It is also apparent that much larger flasks will not be particularly beneficial. As seen above, increasing flask size to 5L only increases the magnitude of the error bars, yet the magnitude of k_{net} seems relatively unchanged from 3L flasks (error bars 3L and 5L values overlap considerably).

Table C-3 Decay of mercury concentration with time upon addition of ozone. 1 L flask, 20% RH, Halo Waxed

time (s)	area	ln(area)
60	44200	0.00
444	37300	0.17
804	28300	0.45
1188	19500	0.82
1554	13500	1.19
1950	8400	1.66
2292	5700	2.05

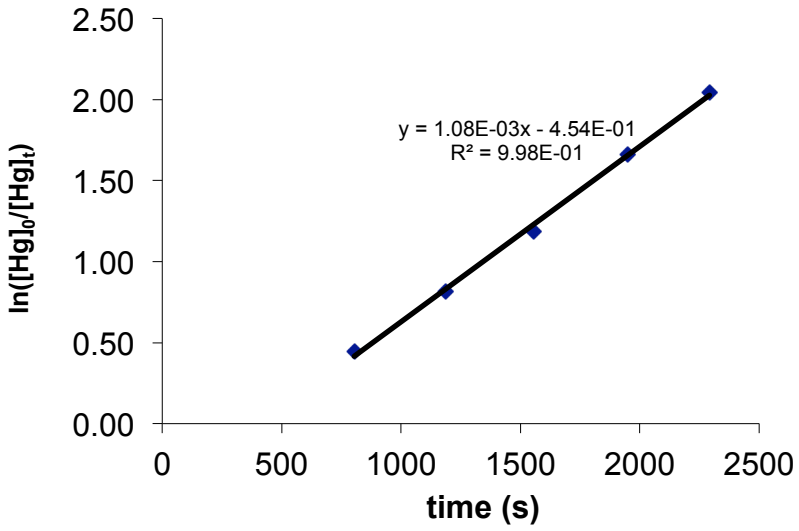

Figure C-3 Log-scale plot of mercury concentration with time: decay with time upon addition of ozone.

Table C-4 Mercury decay with time upon addition of ozone in a 5L flask, with mid-addition of CO (20 parts per thousand)

time (s)	area	ln(area)
120	27900	0.00
744	23700	0.16
1434	19500	0.36
added 30 mL CO at t = 43.0 min		
2094	16100	0.55
2754	13400	0.73
3414	9200	1.11
4092	5500	1.62
4794	3300	2.13

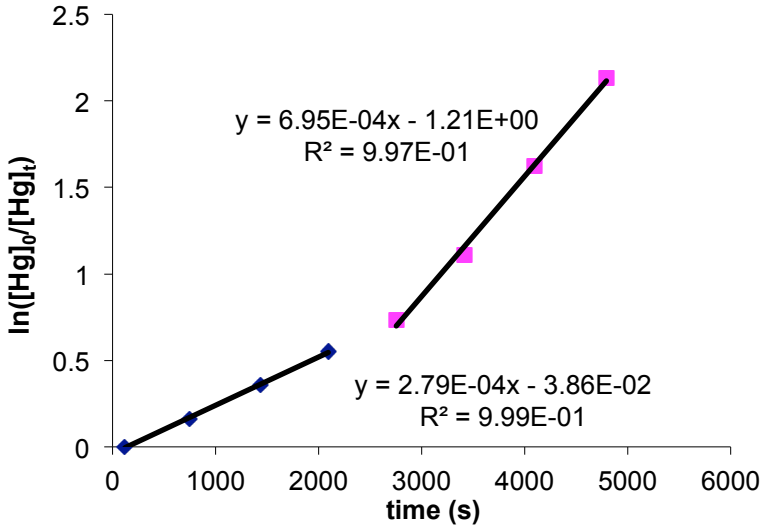

Figure C-4 Mercury decay with time upon addition of ozone, with mid-addition of CO (at 20 parts per thousand).

Table C-5 The effect of increasing [CO] on $Hg + O_3$ decay rate constant in a) a 1L flask and b) a 3L flask.

a)

1l, [CO], ppT	***k* × 10^{18} cm^3 $molec^{-1}$ s^{-1}**	**95% C.I.***
0	1.78	0.12
0.8	1.93	0.17
1.6	2.47	0.77
3.2	4.12	0.68
4.8	5.03	0.80
6.4	5.97	0.85

95% CI = Confidence interval within two standard deviations from mean

1 ppT = 2.48×10^{16} molecules cm^{-3}

b)

3l, [CO], ppT	***k* × 10^{18} cm^3 $molec^{-1}$ s^{-1}**	**95% C.I.***
0	0.71	0.23
3.2	3.15	0.55

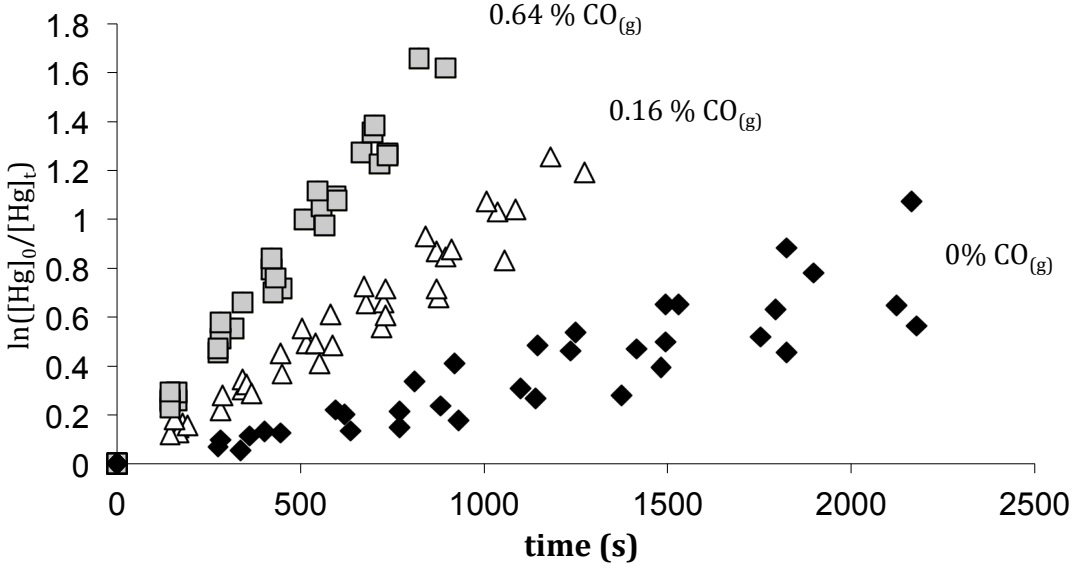

Figure C-5 Semi log plots of mercury losses with time. Rate is equal to slope on plot. Addition of CO(g) (via syringe injection into the 3l flask) increases rate. Seen here are three $CO_{(g)}$ concentrations: 0 parts per thousand (ppT), 1.6 ppT and 6.4 ppT. Additional aliquots of $CO_{(g)}$ are proportional to rate.

Appendix D

Chapter 3 supplementary data including uptake of $Hg^0(g)$ in a flow-type system

The following data did not appear in the original publication "Snider, G. and P. Ariya, *Photo-catalytic oxidation reaction of gaseous mercury over titanium dioxide nanoparticle surfaces.* Chemical Physics Letters, 2010. **491**(1-3): p. 23-28" and is supplementary to it.

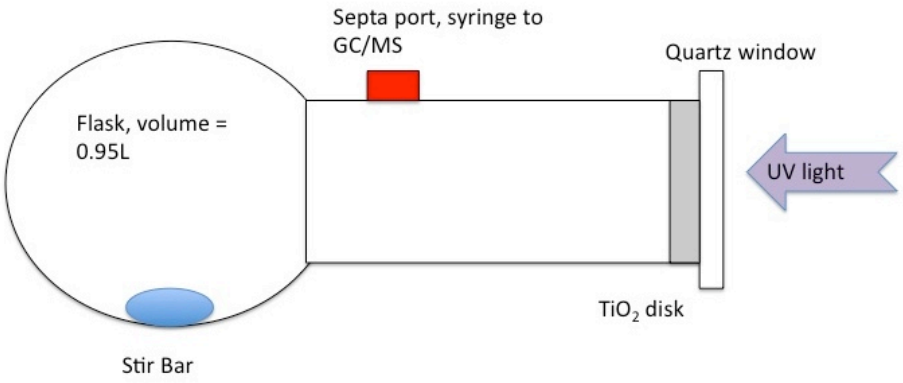

Figure D-1 Illustrated representation of flask used in this chapter 4. Flask is 950 mL in volume, has room for a round insert for a TiO_2 disk, and stir bar in the main chamber.

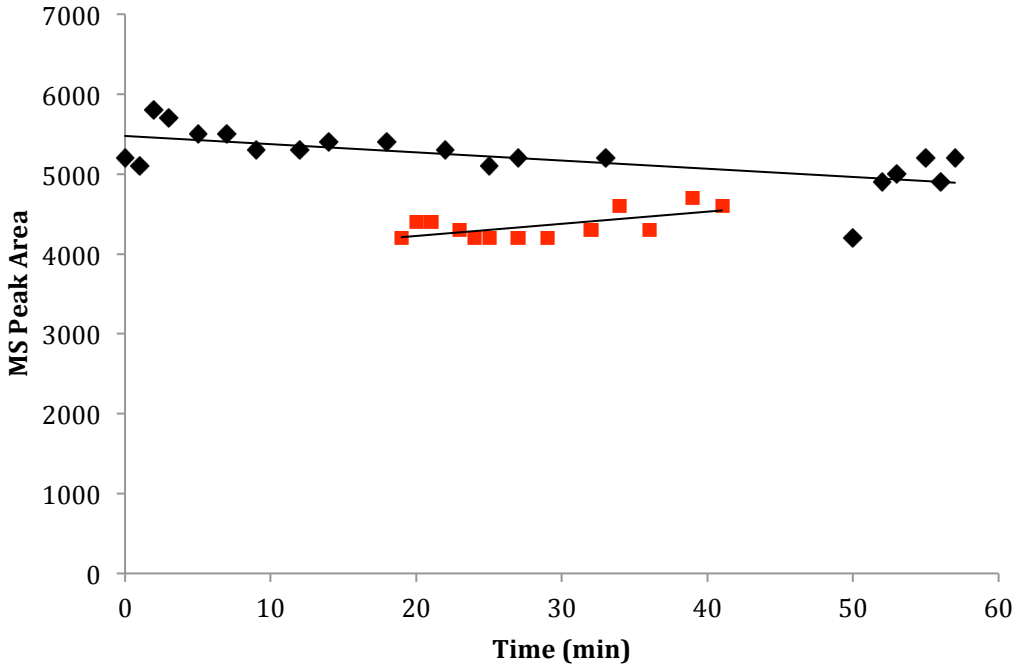

Figure D-2 Stability of mercury losses in two runs for flask shown in figure D-1. There is some observable loss of mercury with time in one run, but the second there is a positive slope. Changes in area may also refelct the variance in gas syringe injections. Losses on timescale shown are small compared with UV-realted loses shown in figure D-6.

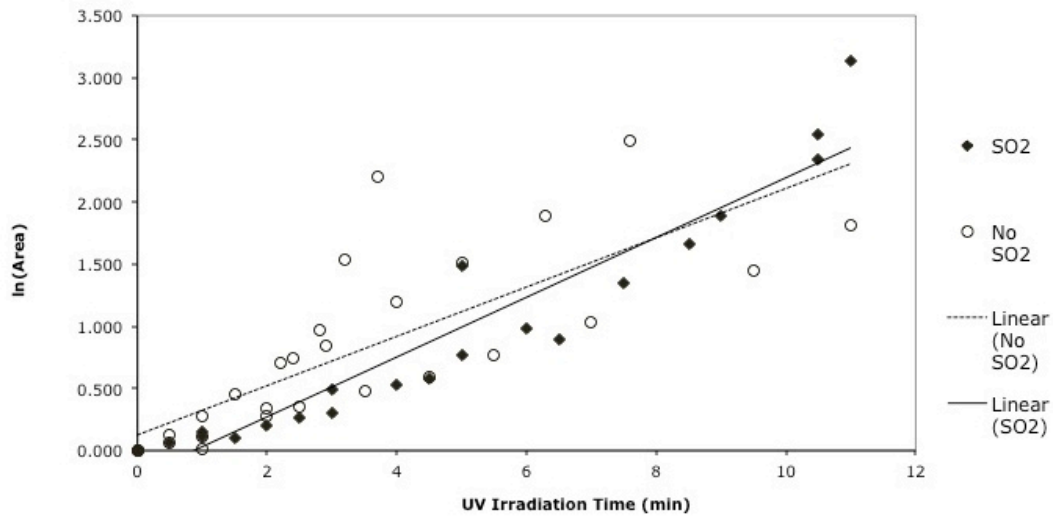

Figure D-3 Comparison of mercury losses from SO_2 (105 ppm) and without SO_2. There is no statistically significant change of rate in the presence of SO_2.

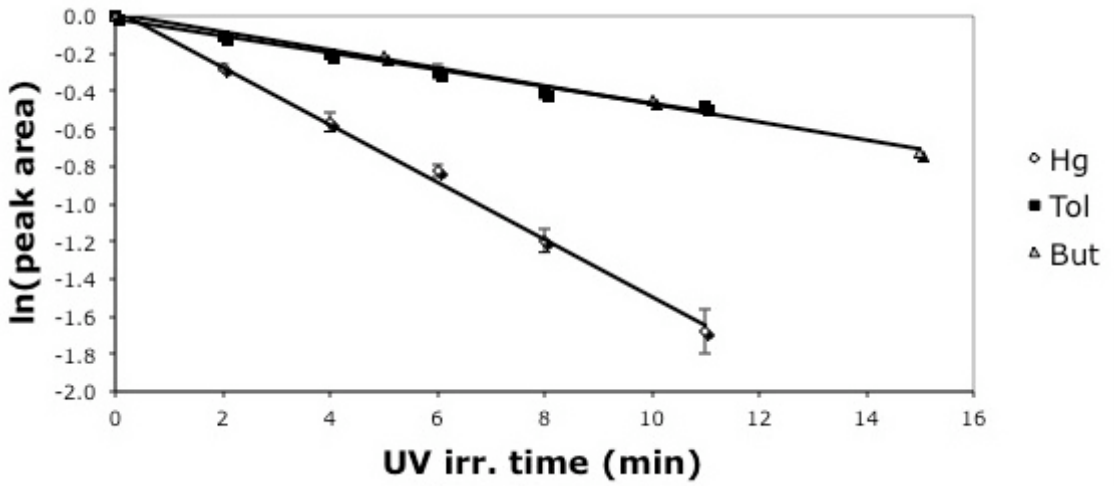

Figure D-4 Loss of mercury (1 ppm) versus toluene (~10 ppm) and butene (~10 ppm). The loss of toluene and butene are relatively quite similar, whereas mercury is notable considerably faster. Mercury loss was monitored in same flask as toluene oxidation. Hence values can be compared relative to one another. Photo-oxidation was performed using the same mercury UV lamp as in principal experiments.

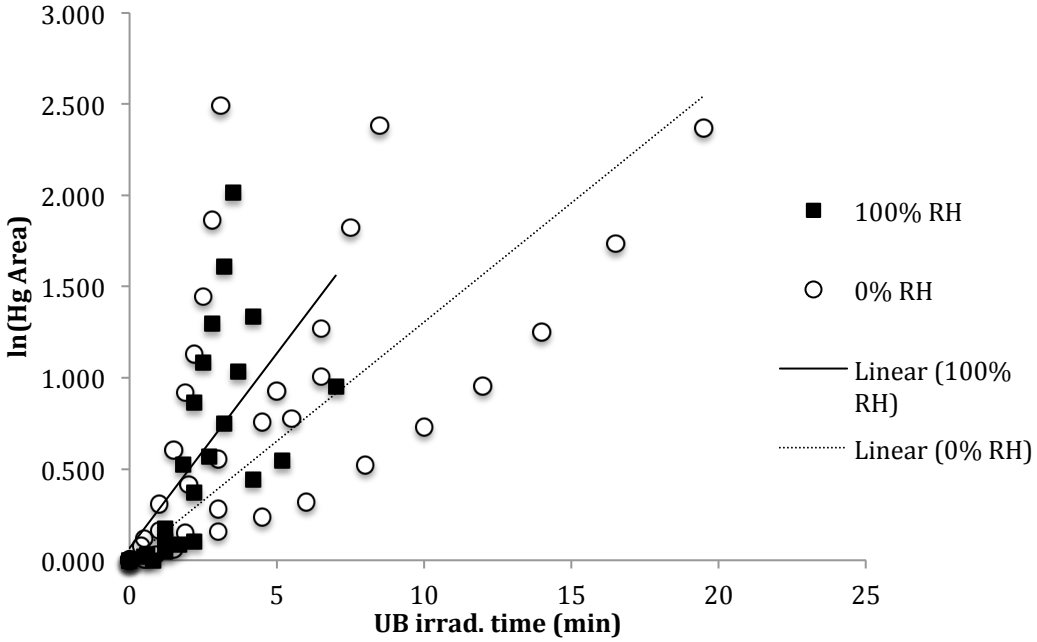

Figure D-5 Combined runs at 100% relative humidity (RH) and 0% RH. Runs for 100% RH used a fresh TiO_2-coated plate and 20 μL of water in 0.95 L flask at room temperature (~100% RH). There is no statistically significant difference in mercury loss between either level of humidity.

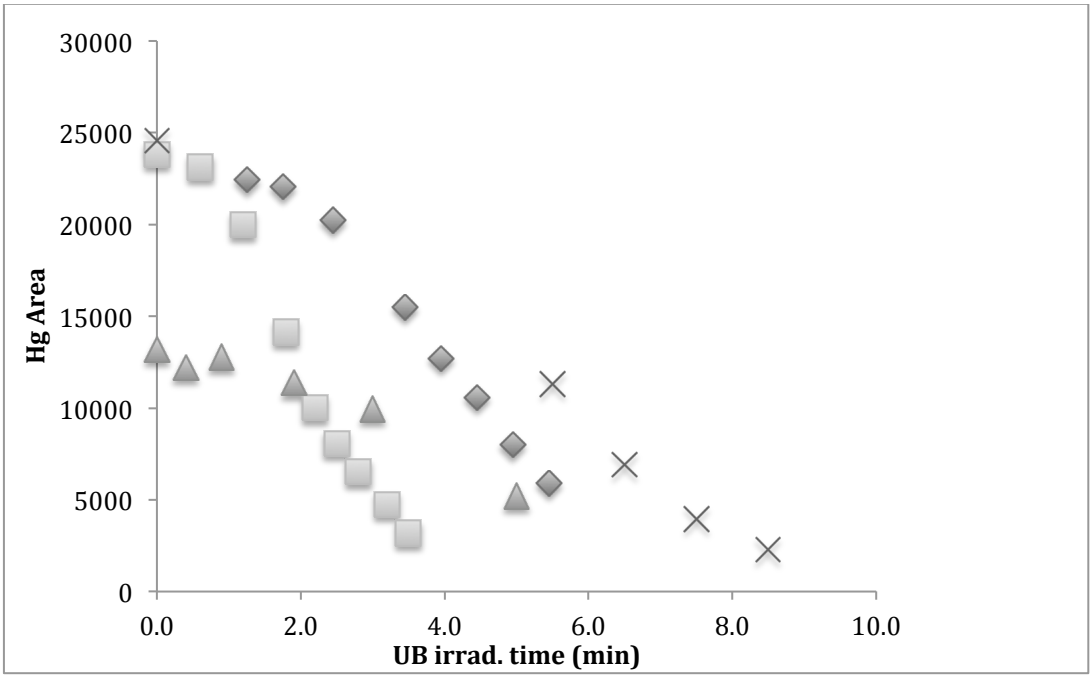

Figure D-6 Oxidation of mercury at room temperature on clean TiO_2 plate. Note there no mercury loss during the first few runs. This is the case for any initial run used on a fresh TiO_2 plate. There may be some nucleation phase that precedes the subsequent oxidation phase.

Table D-1 Derivation of the rate constant, *k*, and the Langmuir adsorption constant K_{Hg}

Trial #	Linear, min^{-1}	Log, no units
1	1847	0.220
2	2705	0.538
3	13646	1.625
4	7521	0.767
5	14127	1.462
6	12095	0.676
7	10220	0.819
8	9200	1.083
9	8367	0.852
Avg = $\Sigma x_i/n$ StDev = $2\sigma/\sqrt{n}$ (95% conf)	**Avg = 7037 ± 2409 min^{-1}**	**Avg = 0.716 ± 0.242**

Equation used to obtain data in table D-1:

$$-\frac{d[Hg]}{dt} = \frac{A_{TiO_2} k}{V_f} \frac{K_{Hg}[Hg]}{1 + K_{Hg}[Hg]} \qquad \text{Eq. D-1}$$

Conversion constant, Hg concentration $\alpha = 2.0 \times 10^9$ molecule cm^{-3}

Flask volume V = 950 cm^3

TiO_2 Area, A = 18 cm^2

k_{avg} = linear*α*V/A

= 7.4 ± 2.5 × 10^{14} molec min^{-1} cm^{-2}

$K_{Hg,avg}$ = linear/(α*log)

= 5.1 ± 2.4 × 10^{-14} cm^3 $molec^{-1}$

Derivation of the capture efficiency, "Q", for gaseous elemental mercury for a re circulating flow system. Here we derive an expression for a closed circuit, re-circulating flow system. The steps are illustrated below.

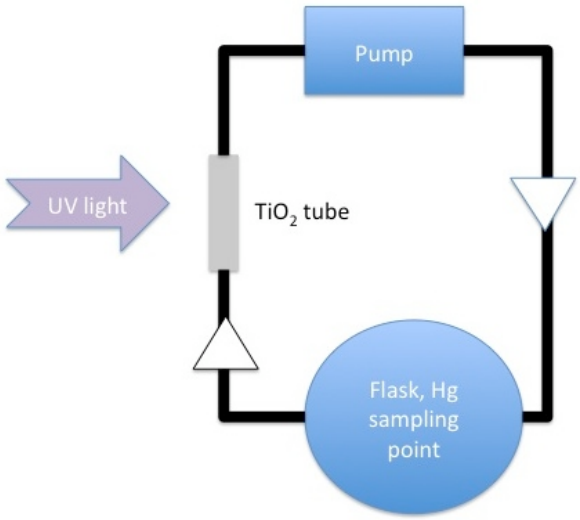

Figure D-7 Trap recirculation diagram.

Referring to Figure D-7, the pump recirculates the gas at flow rate F, the flask has volume V and the trap captures the pollutant of initial concentration $[A]_0$ with efficiency Q yielding the equation $[A] = [A]_0 e^{-FQt/V}$. White arrows show flow direction. Sampling of mercury is done at flask, monitored by single ion monitoring mass spectrometry (SIM-MS). Flask volume is 3.3 liters; the volume Teflon connections linking flask and pump are considered negligible. Pumping rate is 1 L/min. Leak check shows only small loss of mercury with time (<5%/hour) compared with experiment time (~15-30 minutes). UV source is a 100W Hg lamp approximately 10 cm distance from flow tube. Illuminated section of tube is approximately 5 cm on one side.

The Reynolds number Re is above 4000 for a turbulent flow in a tube.

$$\mathrm{Re} = \frac{FL\rho}{A\mu} \qquad \text{Eq. D-2}$$

L is the tube length, ρ is the gas density, A is the tube area, F is the flow rate and μ is the dynamic gas viscosity. Assuming F = 1.0 l/min, A = 0.126 cm^2 (2 mm radius), L_{tube} = 10 cm, ρ_{air} = 1.18 kg m^{-3} (25 °C) [65], and $\mu_{air} = 1.98 \times 10^{-5}$ kg m^{-1} s^{-1} (25 °C) [65], then

$$\begin{aligned} \mathrm{Re} &= \frac{FL\rho}{A\mu} \\ &= \frac{(1.7\times10^{-5}\ \mathrm{m^3\ s^{-1}})(0.1\ \mathrm{m})(1.18\ \mathrm{kg\ m^{-3}})}{(1.26\times10^{-5}\ \mathrm{m^2})(1.98\times10^{-5}\ \mathrm{kg\ m^{-1}\ s^{-1}})} \\ &= 7900 \end{aligned} \qquad \text{Eq. D-3}$$

Under these conditions the flow is turbulent.

The effectiveness of the trap is measured by comparing the concentration of the pollutant before and after entering the trap, i.e. C_{in} vs C_{out}. The uptake efficiency Q of a trap that captures a gaseous substance in a flow tube is defined as the relative amount of substance A entering and leaving the apparatus:

$$\text{Efficiency } "Q" = \frac{C_{in} - C_{out}}{C_{in}} \qquad \text{Eq. D-4}$$

For an ideal trap Q is unity, meaning the trap absorbs all of the substance onto the surface. A 'good' value might be 0.8 to 0.99 [98]. Q is to some extent arbitrary. For any sufficiently large trap Q approaches unity and conversely for any sufficiently dirty trap Q will approach zero.

Each time a parcel of mercury-saturated air passes through the TiO_2 tubing some of the mercury is lost to oxidation. Hence a change in mercury concentration, ΔC_{Hg}, is measured:

$$\Delta C_{Hg} \equiv \frac{m_{in} - m_{out}}{v_{TiO_2}} \qquad \text{Eq. D-5}$$

v is TiO_2-tube volume and m is the mass of mercury within volume *v*.
The efficiency of the mercury capture is defined as fraction of mercury lost between incoming and outgoing air packet entering and leaving the flow tube.

$$Q \equiv \frac{C_{Hg}^{in} - C_{Hg}^{out}}{C_{Hg}^{in}} = \frac{\Delta C_{Hg}}{C_{Hg}^{in}} \qquad \text{Eq. D-6}$$

The time it takes for the reaction to pass through the TiO_2 tube is

$$\delta t = v / F \qquad \text{Eq. A-7}$$

where F is the flow rate to/from flask of volume V.

The change in the total flask concentration (during time δt) is also small, even if Q is unity. Taking into account the equal flow rates coming into and from flask (i.e. 'flow in' = 'flow out'), then the small change in overall mercury concentration in flask in time δt is

$$\frac{dC_{Hg}}{dt} = \frac{F}{V} C_{Hg}(1-Q) \qquad \text{Eq. D-8}$$

Integrating we have

$$\ln \frac{C_{Hg}(t)}{C_{Hg}(0)} = -t \frac{F}{V}(1-Q) \qquad \text{Eq. D-9}$$

so that a plot of the left side versus time yields slope *m*:

$$Q = 1 - \frac{mV}{F} \qquad \text{Eq. D-10}$$

Table D-3 shows the efficiency Q obtained from experiments using a flow system (data in Table D-2 and using equation D-10).

The above derivation did not consider the type of surface involved. We can also relate Q to the LH rate loss kinetic parameters *k* and K_{Hg}.

$$-\frac{dm}{dt} = Ak\theta \qquad \text{Eq. D-11}$$

Where $\theta = K_{Hg}[Hg]/(1+K_{Hg}[Hg])$ and the loss in mercury *dm* describes the mercury lost in a single pass through the TiO_2 tube in time *dt*.

$$\delta m \approx Ak\theta\delta t = Ak\theta \frac{v}{F} \qquad \text{Eq. D-12}$$

Where A is the TiO_2 area and v is the TiO_2 tube volume. Dividing by tube volume v,

$$-\frac{dm}{dt}\frac{1}{v} = Ak\theta\frac{1}{v}$$
$$-\frac{dC_{Hg}}{dt} = \frac{Ak}{v}\theta \qquad \text{Eq. D-13}$$

Integrating,

$$\int_{C_{Hg}^{in}}^{C_{Hg}^{out}} \frac{dC_{Hg}}{\theta} = -\int_0^{\delta t} \frac{Ak}{v} dt$$

$$C_{Hg}^{in} - C_{Hg}^{out} + \frac{1}{K_{Hg}} \ln\left(C_{Hg}^{in} / C_{Hg}^{out}\right) = \frac{AkK_{Hg}}{v} \delta t \qquad \text{Eq. D-14}$$

$$= \frac{AkK_{Hg}}{F}$$

Substituting the definition of Q into equation D-14,

$$QC_{Hg}^{in} - \frac{1}{K_{Hg}} \ln(1-Q) = \frac{AkK_{Hg}}{vF} \qquad \text{Eq. D-15}$$

Simplifying, the upper limit and lower limits of Q ($Q_{big} \rightarrow 1$, $Q_{small} \rightarrow 0$) are

$$Q_{big} \approx 1 - e^{-Ak/vF} \qquad \text{Eq. D-16}$$

$$Q_{small} \approx \frac{AkK_{Hg}}{vF} \frac{1}{C_{Hg}^{in} + K_{Hg}^{-1}} \qquad \text{Eq. D-17}$$

Table D-2 Irradiation time and mercury concentration with time in a flow system

UV time	Area(Hg)	ln(area)
0.0	14050	0.00
4.6	9140	0.43
7.0	7200	0.67
9.5	5250	0.98
12.0	3730	1.33
14.5	2950	1.56
17.2	2210	1.85
19.8	1860	2.02
22.6	1500	2.24
25.0	1140	2.51

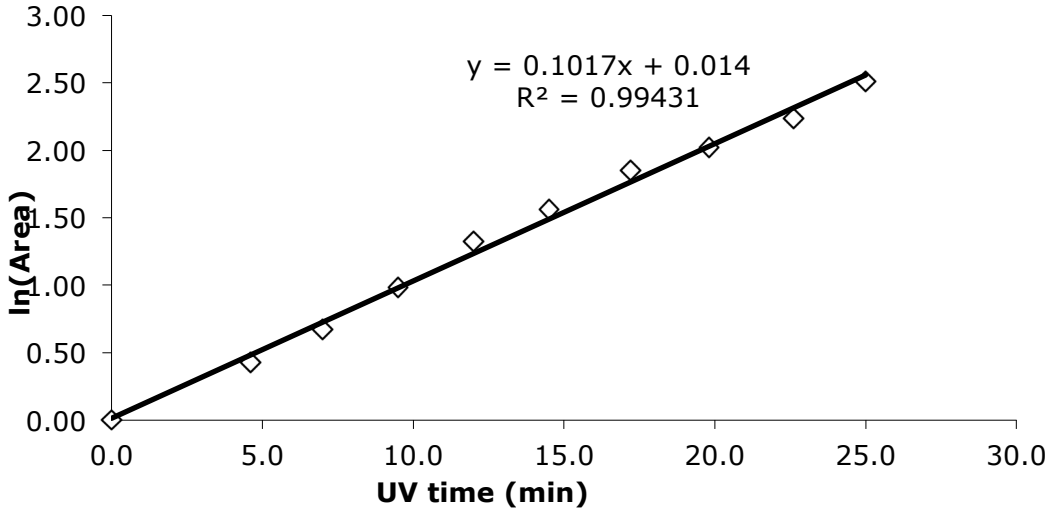

Figure D-8 Plot of gaseous mercury losses with time. Mercury is captured by the TiO_2/UV recirculating flow system, and the concentrations at a time t is measured by GC/MS SIM peak area. In this instance capture efficiency Q was determined to be 62% (table D-4).

Table D-3 Calculation of capture efficiency Q from figure D-7 and table D-2

UV source dist	18.5	cm
Flow rate	0.52	L/min
Flask volume	3.16	L
line slope	0.102	L/min
Q	**0.62**	No units

Appendix E

Chapter 4 Supplementary data

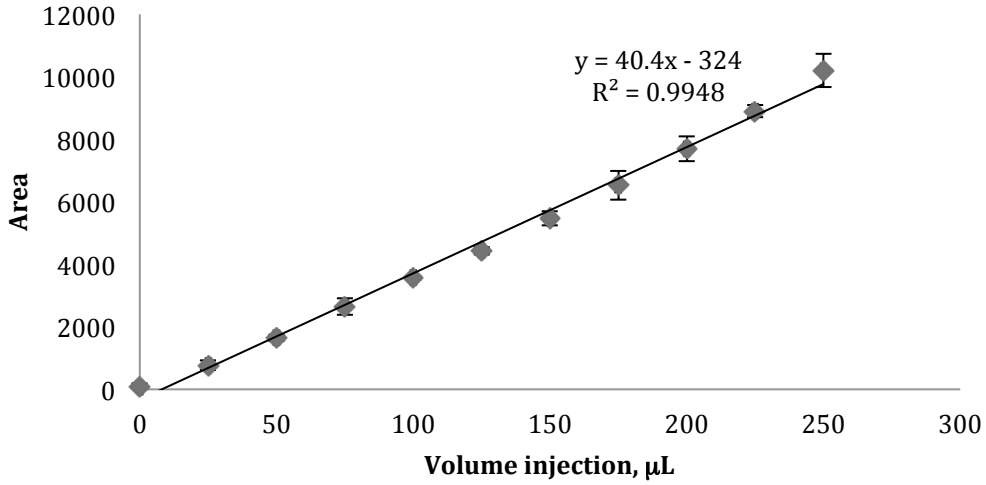

Figure E-1 Sample Calibration line of a 250 µL syringe injection of gaseous mercury (SIM mode, m/z = 198-202). Flask size was 5.5 L, error bards are from triplicate sampling at each concentration and transferred by vacuum line from a 5L flask in equilibrium with liquid mercury at 295 K.

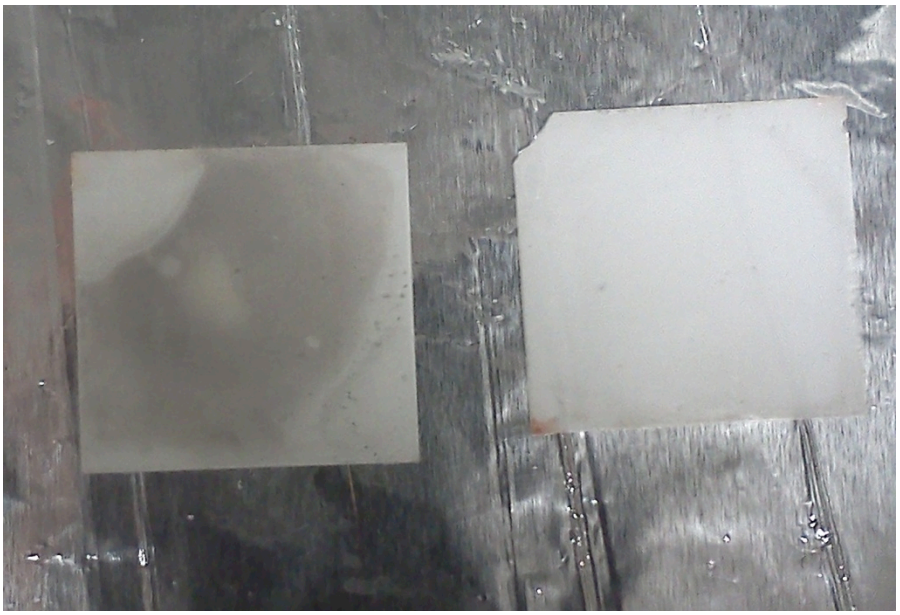

Figure E-2 TiO_2 film saturated in HgO(s) (left). On right is film saturated in HgO(s), as on left, then exposed to 1% gaseous concentration of NO_2.

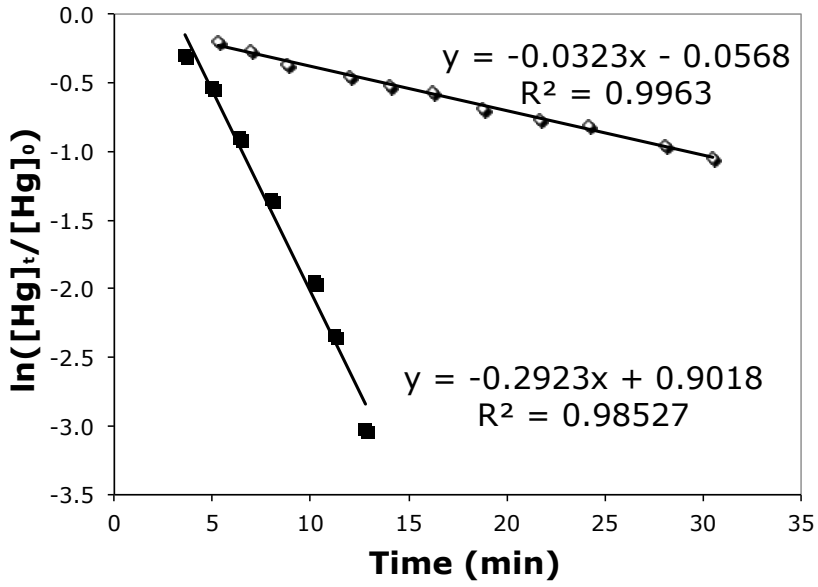

Figure E-3 Change in rate of mercury uptake onto TiO_2 (proportional to slope) after near saturation of surface with HgO(s) deposits (white squares), then same film after exposure to a 1% gaseous concentration of $NO_{2(g)}$ (dark squares).

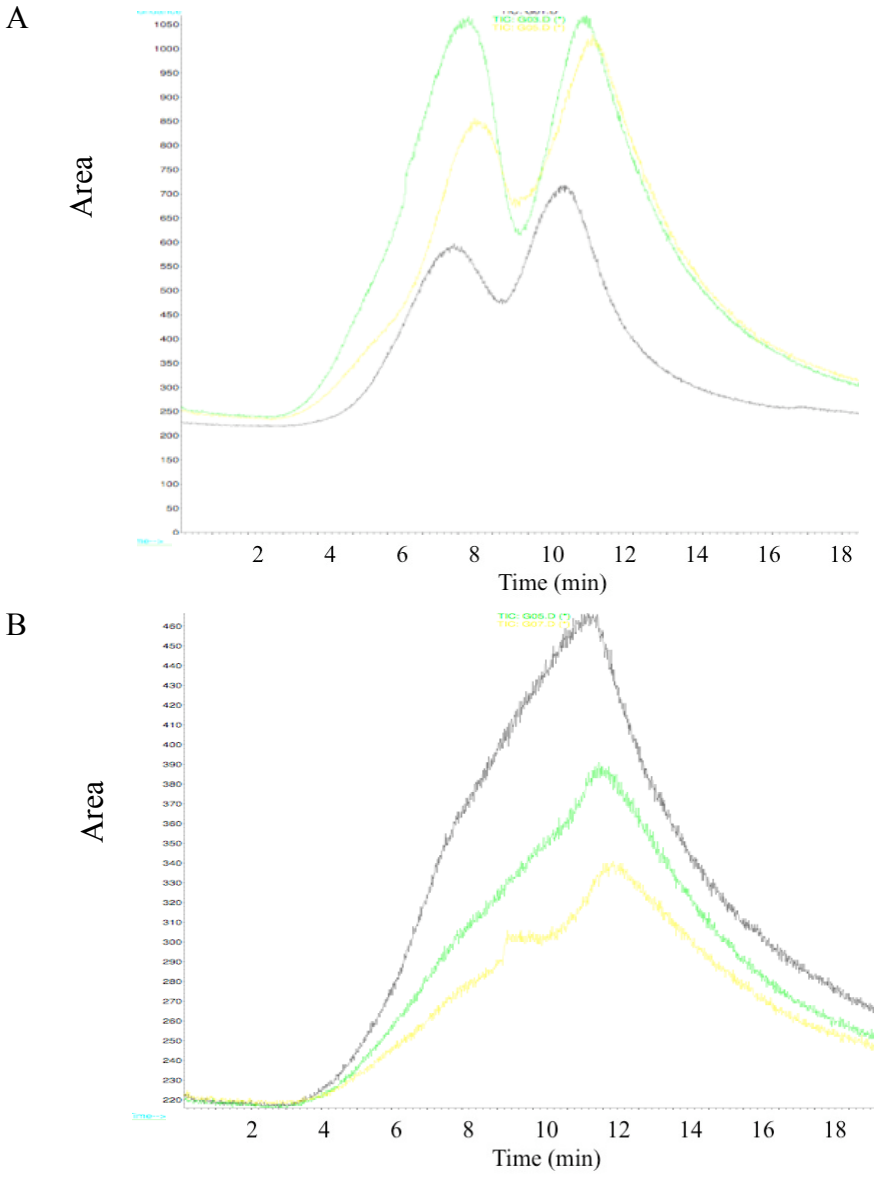

Figure E-4 A) Thermal desorption of Hg^0 desorbed from titania. B) Thermal desorption curves of HgO (after UV exposure of Hg over titania).

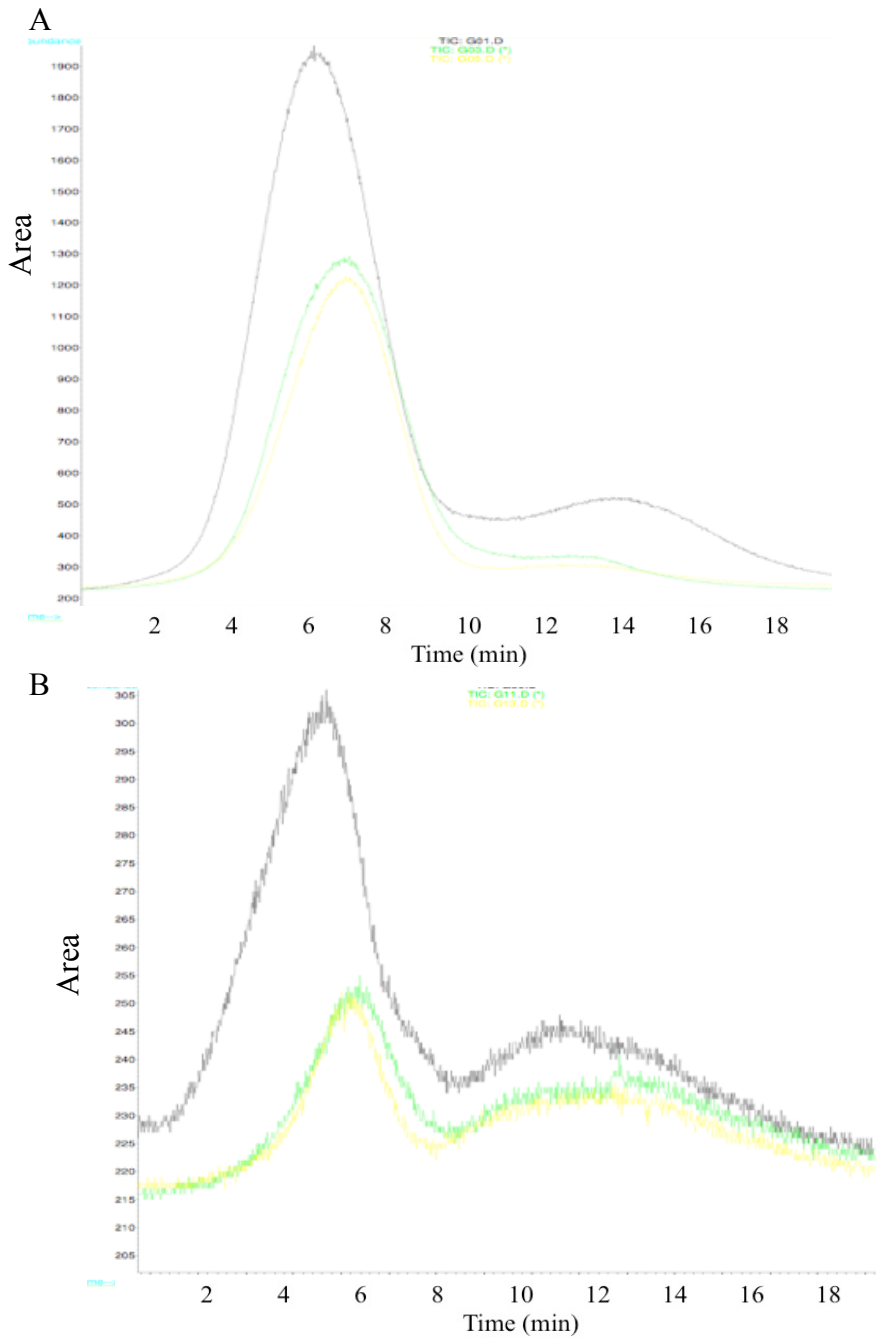

Figure E-5 A) Thermal desorption curves after successive exposure of mercury gas (1 ppm), vacuum, then NO_2 (10 torr) over titania. B) Thermal desorption curves after successive exposure of NO_2 (10 torr), vacuum, then mercury gas (1 ppm) over titania.

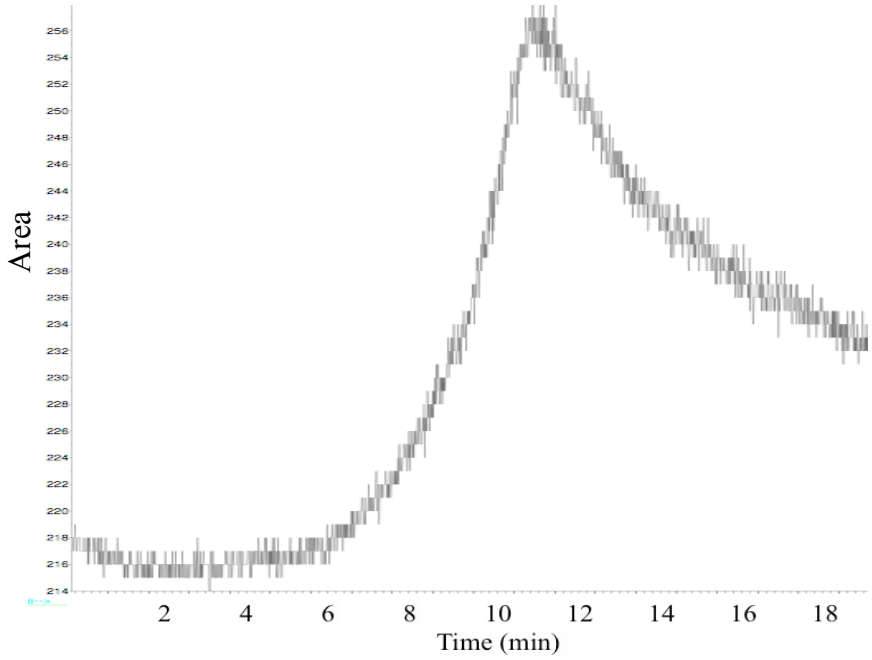

Figure E-6 Desorption of pure HgO over pure silica gel, 1mg at 90µg/g gel.

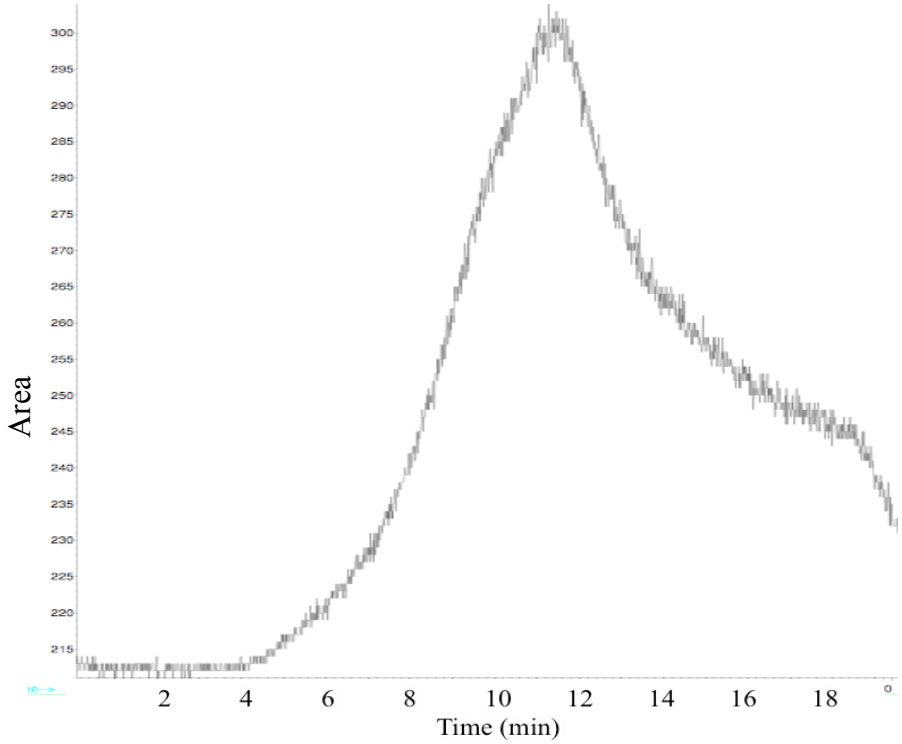

Figure E-7 Desorption of pure $Hg(NO_3)_2 \bullet 2H_2O$ over silica gel 1 mg at 13mg/g gel.

REFERENCES

1. Goldwater, L.J. and W. Stopford, *Mercury*, in *The Chemical Environment*, J. Lenihan and W.W. Fletcher, Editors. 1977, Academic Press: New York & San Francisco.
2. Mozaffarian, D. and E.B. Rimm, *Fish intake, contaminants, and human health - Evaluating the risks and the benefits.* Jama-Journal of the American Medical Association, 2006. **296**(15): p. 1885-1899.
3. Egeland, G.M. and J.P. Middaugh, *Balancing fish consumption benefits with mercury exposure.* Science, 1997. **278**(5345): p. 1904-1905.
4. Lindberg, S., et al., *A Synthesis of Progress and Uncertainties in Attributing the Sources of Mercury in Deposition.* AMBIO: A Journal of the Human Environment, 2007. **36**(1): p. 19-33.
5. Hedgecock, I.M. and N. Pirrone, *Chasing Quicksilver: Modeling the Atmospheric Lifetime of Hg0(g) in the Marine Boundary Layer at Various Latitudes.* Environmental Science & Technology, 2003. **38**(1): p. 69-76.
6. Schroeder, W.H., et al., *Arctic springtime depletion of mercury.* Nature, 1998. **394**(6691): p. 331-332.
7. Slemr, F., et al., *Worldwide trend of atmospheric mercury since 1977.* Geophysical Research Letters, 2003. **30**(10): p. -.
8. Slemr, F., et al., *Worldwide trend of atmospheric mercury since 1995.* Atmos. Chem. Phys., 2011. **11**(10): p. 4779-4787.
9. Wyn, B., et al., *Increasing Mercury in Yellow Perch at a Hotspot in Atlantic Canada, Kejimkujik National Park.* Environmental Science & Technology, 2010. **44**(23): p. 9176-9181.
10. Lebel, J., et al., *Neurotoxic Effects of Low-Level Methylmercury Contamination in the Amazonian Basin.* Environmental Research, 1998. **79**(1): p. 20-32.
11. Crompton, P., et al., *Assessment of Mercury Exposure and Malaria in a Brazilian Amazon Riverine Community.* Environmental Research, 2002. **90**(2): p. 69-75.
12. Grandjean, P., et al., *Cognitive Deficit in 7-Year-Old Children with Prenatal Exposure to Methylmercury.* Neurotoxicology and Teratology, 1997. **19**(6): p. 417-428.
13. *Mercury Study Report to Congress: Overview*. 2010 [cited 2011 June 16]; Available from: http://www.epa.gov/mercury/reportover.htm.
14. Schofield, K., *Fuel-Mercury Combustion Emissions: An Important Heterogeneous Mechanism and an Overall Review of its Implications.* Environmental Science & Technology, 2008. **42**(24): p. 9014-9030.
15. Swiderski, R.M., *Quicksilver: A History of the Use, Lore and Effects of Mercury*2008, Jefferson, North Carolina: McFarland & Company, Inc.
16. Brosset, C., *Total airborne mercury and its possible origin.* Water, Air, & Soil Pollution, 1982. **17**(1): p. 37-50.
17. Sallsten, G., L. Barregard, and B. Jarvholm, *Mercury in the Swedish Chlor-Alkili Industry- an Evaluation of the Exopsure and Preventative Measures over 40 Years.* Annals of Occupational Hygiene, 1990. **34**(2): p. 205-214.
18. Lindqvist, O., et al., *Mercury in the Swedish Environment - Recent Research on Causes, Consequences and Corrective Methods.* Water Air and Soil Pollution, 1991. **55**(1-2): p. R11-&.
19. Billings, C.E. and W.R. Matson, *Mercury Emissions from Coal Combustion.* Science, 1972. **176**(4040): p. 1232-1233.
20. Seiler, W., C. Eberling, and F. Slemr, *Global Distribution of Gaseous Mercury in the Troposphere.* Pure and Applied Geophysics, 1980. **118**(4): p. 964-974.
21. Johnels, A., G. Tyler, and T.r. Westermark, *A History of Mercury Levels in Swedish Fauna.* Ambio, 1979. **8**(4): p. 160-168.
22. Jernelov, A., L. Landner, and T. Larsson, *Swedish Perspectives on Mercury Pollution.* Journal (Water Pollution Control Federation), 1975. **47**(4): p. 810-822.
23. Tonomura, K., et al., *Stimulative Vaporization of Phenyl-mercuric Acetate by Mercury-resistant Bacteria.* Nature, 1968. **217**(5129): p. 644-646.
24. Matsumura, F., G.M. Boush, and T. Misato, *Environmental toxicology of pesticides: proceedings of a United States-Japan seminar, held in ≈åiso, Japan, October, 1971*1972: Academic Press.
25. Nriagu, J.O. and J.M. Pacyna, *Quantitative assessment of worldwide contamination of air, water and soils by trace metals.* Nature, 1988. **333**(6169): p. 134-139.
26. Pirrone, N., G.J. Keeler, and J.O. Nriagu, *Regional differences in worldwide emissions of mercury to the atmosphere.* Atmospheric Environment, 1996. **30**(17): p. 2981-2987.

27. Pacyna, E.G. and J.M. Pacyna, *Global Emission of Mercury from Anthropogenic Sources in 1995.* Water, Air, & Soil Pollution, 2002. **137**(1): p. 149-165.
28. Pacyna, E.G., et al., *Global anthropogenic mercury emission inventory for 2000.* Atmospheric Environment, 2006. **40**(22): p. 4048-4063.
29. Mason, R.P. and G.R. Sheu, *Role of the ocean in the global mercury cycle.* Global Biogeochemical Cycles, 2002. **16**(4): p. -.
30. Lamborg, C.H., et al., *A non-steady-state compartmental model of global-scale mercury biogeochemistry with interhemispheric atmospheric gradients.* Geochimica et Cosmochimica Acta, 2002. **66**(7): p. 1105-1118.
31. Pirrone, N., et al., *Global mercury emissions to the atmosphere from anthropogenic and natural sources.* Atmos. Chem. Phys., 2010. **10**(13): p. 5951-5964.
32. Pirrone, N., et al., *Global Mercury Emissions to the Atmosphere from Natural and Anthropogenic Sources*, in *Mercury Fate and Transport in the Global Atmosphere*, R. Mason and N. Pirrone, Editors. 2009, Springer US. p. 1-47-47.
33. Streets, D.G., Q. Zhang, and Y. Wu, *Projections of Global Mercury Emissions in 2050.* Environmental Science & Technology, 2009. **43**(8): p. 2983-2988.
34. Hylander, L.D. and M. Meili, *500 years of mercury production: global annual inventory by region until 2000 and associated emissions.* The Science of The Total Environment, 2003. **304**(1-3): p. 13-27.
35. Nriagu, J.O., *A global assessment of natural sources of atmospheric trace metals.* Nature, 1989. **338**(6210): p. 47-49.
36. Mason, R.P., F.M.M. Morel, and W.F. Fitzgerald, *The biogeochemical cycling of elemental mercury: Anthropogenic influences.* Geochimica et Cosmochimica Acta, 1994. **58**(15): p. 3191-3198.
37. Seigneur, C., et al., *Global source attribution for mercury deposition in the United States.* Environmental Science & Technology, 2004. **38**(2): p. 555-569.
38. Slemr, F., G. Schuster, and W. Seiler, *Distribution, speciation, and budget of atmospheric mercury.* Journal of Atmospheric Chemistry, 1985. **3**(4): p. 407-434.
39. Schuster, P.F., et al., *Atmospheric Mercury Deposition during the Last 270 Years: A Glacial Ice Core Record of Natural and Anthropogenic Sources.* Environmental Science & Technology, 2002. **36**(11): p. 2303-2310.
40. Boutron, C.F., et al., *A forty year record of Mercury in central Greenland snow.* Geophys. Res. Lett., 1998. **25**(17): p. 3315-3318.
41. Roos-Barraclough, F., et al., *A 14 500 year record of the accumulation of atmospheric mercury in peat: volcanic signals, anthropogenic influences and a correlation to bromine accumulation.* Earth and Planetary Science Letters, 2002. **202**(2): p. 435-451.
42. Shotyk, W., et al., *Accumulation rates and predominant atmospheric sources of natural and anthropogenic Hg and Pb on the Faroe Islands.* Geochimica et Cosmochimica Acta, 2005. **69**(1): p. 1-17.
43. Lalonde, J.D., A.J. Poulain, and M. Amyot, *The role of mercury redox reactions in snow on snow-to-air mercury transfer.* Environmental Science & Technology, 2002. **36**(2): p. 174-178.
44. Dommergue, A., et al., *The fate of mercury species in a sub-arctic snowpack during snowmelt.* Geophys. Res. Lett., 2003. **30**(12): p. 1621.
45. Steffen, A., et al., *A synthesis of atmospheric mercury depletion event chemistry in the atmosphere and snow*, 2008, Copernicus GmbH.
46. Kraepiel, A.M.L., et al., *Sources and Variations of Mercury in Tuna.* Environmental Science & Technology, 2003. **37**(24): p. 5551-5558.
47. Banic, C.M., et al., *Vertical distribution of gaseous elemental mercury in Canada.* Journal of Geophysical Research-Atmospheres, 2003. **108**(D9): p. -.
48. Swartzendruber, P.C., et al., *Observations of reactive gaseous mercury in the free troposphere at the Mount Bachelor Observatory.* J. Geophys. Res., 2006. **111**(D24): p. D24301.
49. Siciliano, S.D., N.J. O'Driscoll, and D.R.S. Lean, *Microbial reduction and oxidation of mercury in freshwater lakes.* Environmental Science & Technology, 2002. **36**(14): p. 3064-3068.
50. Slemr, F., W. Seiler, and G. Schuster, *Latitudinal Distribution of Mercury Over the Atlantic Ocean.* J. Geophys. Res., 1981. **86**(C2): p. 1159-1166.
51. Sprovieri, F., et al., *A review of worldwide atmospheric mercury measurements.* Atmos. Chem. Phys., 2010. **10**(17): p. 8245-8265.
52. Lindqvist, O. and H. Rodhe, *Atmospheric Mercury - a Review.* Tellus Series B-Chemical and Physical Meteorology, 1985. **37**(3): p. 136-159.

53. Kromer, E., G. Friedrich, and P. Wallner, *Mercury and mercury compounds in surface air, soil gas, soils and rocks.* Journal of Geochemical Exploration, 1981. **15**(1-3): p. 51-62.
54. P'yankov, V.A., *Kinetics of the Reaction of Mercury Vapors with Ozone.* Journal of General Chemistry of USSR. , 1949. **19**: p. 187-192.
55. Schroeder, W., G. Yarwood, and H. Niki, *Transformation processes involving mercury species in the atmosphere — results from a literature survey.* Water, Air, & Soil Pollution, 1991. **56**(1): p. 653-666.
56. Schroeder, W.H. and J. Munthe, *Atmospheric mercury--An overview.* Atmospheric Environment, 1998. **32**(5): p. 809-822.
57. Strode, S.A., et al., *Air-sea exchange in the global mercury cycle.* Global Biogeochemical Cycles, 2007. **21**(1): p. -.
58. Seigneur, C., et al., *On the effect of spatial resolution on atmospheric mercury modeling.* Science of the Total Environment, 2003. **304**(1-3): p. 73-81.
59. Ariya, P.A., et al., *The Arctic: a sink for mercury.* Tellus Series B-Chemical and Physical Meteorology, 2004. **56**(5): p. 397-403.
60. Greenwood, N.N. and A. Earnshaw, *Chemistry of the Elements (2nd Edition)*, 1998, Elsevier. p. 1201-1226.
61. Filatov, M. and D. Cremer, *Revision of the Dissociation Energies of Mercury Chalcogenides—Unusual Types of Mercury Bonding.* ChemPhysChem, 2004. **5**(10): p. 1547-1557.
62. Burger, L., et al., *Chapter 3 Growth of Mercuric Iodide*, in *Semiconductors and Semimetals*1995, Elsevier. p. 85-110.
63. Zhang, J. and P.L. Bishop, *Stabilization/solidification (S/S) of mercury-containing wastes using reactivated carbon and Portland cement.* Journal of Hazardous materials, 2002. **92**(2): p. 199-212.
64. Remy, H., *Treatise on inorganic chemistry: Sub-groups of the periodic table and general topics*1959: Elsevier.
65. Weast, R.C., *CRC Handbook of Chemistry and Physics*. 87th ed, ed. D.R. Lide2007, Boca Raton, FL: CRC Press.
66. Iverfeldt, A. and O. Lindqvist, *Atmospheric Oxidation of Elemental Mercury by Ozone in the Aqueous Phase.* Atmospheric Environment, 1986. **20**(8): p. 1567-1573.
67. Munthe, J., *The Aqueous Oxidation of Elemental Mercury by Ozone.* Atmospheric Environment Part a-General Topics, 1992. **26**(8): p. 1461-1468.
68. Grade, M. and W. Hirschwald, *Energetics and Stabilities of the IIB/VIA-Compounds at High-Temperature Equilibrium Conditions.* Berichte der Bunsengesellschaft für physikalische Chemie, 1982. **86**(10): p. 899-907.
69. Chase Jr., M.W., *NIST-JANAF Thermochemical Tables, Fourth Edition, Monograph No. 9.* Journal of Physical and Chemical Reference Data, 1998.
70. Shepler, B.C. and K.A. Peterson, *Mercury Monoxide: A Systematic Investigation of Its Ground Electronic State.* J. Phys. Chem. A, 2003. **107**(11): p. 1783-1787.
71. Calvert, J.G. and S.E. Lindberg, *Mechanisms of mercury removal by O-3 and OH in the atmosphere.* Atmospheric Environment, 2005. **39**(18): p. 3355-3367.
72. L'Vov, B.V., *Kinetics and mechanism of thermal decomposition of mercuric oxide.* Thermochimica Acta, 1999. **333**(1): p. 21-26.
73. Hall, B., *The gas phase oxidation of elemental mercury by ozone.* Water, Air, & Soil Pollution, 1995. **80**(1): p. 301-315.
74. Pal, B. and P.A. Ariya, *Studies of ozone initiated reactions of gaseous mercury: kinetics, product studies, and atmospheric implications.* Physical Chemistry Chemical Physics, 2004. **6**(3): p. 572-579.
75. Sumner, A., et al., *Environmental Chamber Studies of Mercury Reactions in the Atmosphere*, in *Dynamics of Mercury Pollution on Regional and Global Scales:*2005. p. 193-212.
76. von Glasow, R., *Atmospheric chemistry in volcanic plumes.* Proceedings of the National Academy of Sciences, 2010. **107**(15): p. 6594-6599.
77. Obrist, D., et al., *Bromine-induced oxidation of mercury in the mid-latitude atmosphere.* Nature Geoscience, 2011. **4**(1): p. 22-26.
78. Steffen, A., et al., *A synthesis of atmospheric mercury depletion event chemistry linking atmosphere, snow and water.* Atmos. Chem. Phys. Discuss., 2007. **7**(4): p. 10837-10931.
79. Hall, B., P. Schager, and J. Weesmaa, *The homogeneous gas phase reaction of mercury with oxygen, and the corresponding heterogeneous reactions in the presence of activated carbon and fly ash.* Chemosphere, 1995. **30**(4): p. 611-627.

80. Hynes, A.J., et al., *Our current understanding of major chemical and physical processes affecting mercury dynamics in the atmosphere and at the air-water/terrestrial interfaces*
Mercury Fate and Transport in the Global Atmosphere, R. Mason and N. Pirrone, Editors. 2009, Springer US. p. 427-457.
81. Aurivilius, K., *Structural Chemistry of Inorganic Mercury(II) Compounds - Some Aspects of Determination of Positions of Light Atoms in Presence of Heavy Atoms in Crystal Structures.* Arkiv for Kemi, 1965. **24**(2): p. 151-&.
82. Batsanov, S., et al., *Colored forms of mercuric oxide.* Journal of Structural Chemistry, 1970. **10**(5): p. 730-733-733.
83. Garrett, A.B. and A.E. Hirschler, *The Solubilities of Red and Yellow Mercuric Oxides in Water, in Alkali, and in Alkaline Salt Solutions. The Acid and Basic Dissociation Constants of Mercuric Hydroxide.* Journal of the American Chemical Society, 1938. **60**(2): p. 299-306.
84. Cooney, R. and J. Hall, *An analysis of the vibrational spectra of orthorhombic mercury(II) oxide and hexagonal mercury(II) sulphide.* Australian Journal of Chemistry, 1969. **22**(2): p. 331-336.
85. McCullough, J.D., R.A. Crane, and A.O. Beckman, *Determination of Carbon Monoxide in Air by Use of Red Mercuric Oxide.* Analytical Chemistry, 1947. **19**(12): p. 999-1002.
86. Fay, I.W. and A.F. Seeker, *REDUCIBILITY OF SOME METALLIC OXIDES BY HYDROGEN AND CARBON MONOXIDE.* Journal of the American Chemical Society, 1903. **25**(6): p. 641-647.
87. Butler, R., et al., *Identification of mercury oxide (HgOx) species by matrix isolation spectroscopy.* The Journal of Physical Chemistry, 1979. **83**(20): p. 2578-2580.
88. Zacharewski, T.R., E.A. Cherniak, and W.H. Schroeder, *FTIR investigation of the heterogeneous reaction of HgO(s) with SO2(g) at ambient temperature.* Atmospheric Environment 1987. **21**(11): p. 2327-2332.
89. Schofield, K., *Let them eat fish: hold the mercury.* Chemical Physics Letters, 2004. **386**(1-3): p. 65-69.
90. Hall, B., P. Schager, and O. Lindqvist, *Chemical-Reactions of Mercury in Combustion Flue-Gases.* Water Air and Soil Pollution, 1991. **56**: p. 3-14.
91. Joensuu, O.I., *Fossil Fuels as a Source of Mercury Pollution.* Science, 1971. **172**(3987): p. 1027-1028.
92. Yudovich, Y.E. and M.P. Ketris, *Mercury in coal: a review: Part 1. Geochemistry.* International Journal of Coal Geology, 2005. **62**(3): p. 107-134.
93. Yudovich, Y.E. and M.P. Ketris, *Mercury in coal: a review Part 2. Coal use and environmental problems.* International Journal of Coal Geology, 2005. **62**(3): p. 135-165.
94. Turchi, C.S., *Novel Process for Removal and Recovery of Vapor-Phase Mercury*, 2000, ADA Technologies, Inc. : Littleton, CO. p. 57.
95. Berry-Helmlinger, L. *ADA Technologies lends Mother Nature a hand with cleanup*. 2004 Feb 14, 2008]; Available from: http://www.bizjournals.com/denver/stories/2004/05/03/focus2.html.
96. Butz, J.R., et al., *Evaluation of Amended Silicates™ Sorbents for Mercury Control* 2003, ADA Technologies, Inc. and CH2M HILL: Littleton, CO and Englewood, CO. p. 16.
97. Brown, T.D., et al., *Mercury measurement and its control: what we know, have learned, and need to further investigate.* Journal of the Air and Waste Management Association, 1999. **49**(8): p. pp. 628-640.
98. Presto, A.A. and E.J. Granite, *Survey of Catalysts for Oxidation of Mercury in Flue Gas.* Environ. Sci. Technol., 2006. **40**(18): p. 5601-5609.
99. *Pollution Control Innovations for Power Plants*. 2006 Jan 18, 2006 Feb 13, 2008]; Available from: http://www.fossil.energy.gov/programs/powersystems/pollutioncontrols/.
100. Munthe, J., et al., *Removal of gaseous mercury from air using a gold coated denuder.* Atmospheric Environment. Part A. General Topics, 1990. **24**(8): p. 2271-2274.
101. Norton, G.A., et al., *Heterogeneous oxidation of mercury in simulated post combustion conditions.* Fuel, 2003. **82**(2): p. 107-116.
102. Wang, M., et al., *Oxidation of gaseous elemental mercury in a high voltage discharge reactor.* Journal of Environmental Sciences, 2009. **21**(12): p. 1652-1657.
103. Blythe, G.M., *Field Testing of a Wet FGD Additive for Enhanced Mercury Control – Pilot-scale Test Results*, 2006, URS Corporation: Austin, Texas.
104. Skodras, G., et al., *Postcombustion measures for cleaner solid fuels combustion: Activated carbons for toxic pollutants removal from flue gases.* Energy & Fuels, 2005. **19**(6): p. 2317-2327.
105. Galbreath, K.C. and C.J. Zygarlicke, *Mercury transformations in coal combustion flue gas.* Fuel Processing Technology, 2000. **65-66**: p. 289-310.

106. Ali Abu-Daabes, M., *Synthesis and Characterization of Nano-Structured Chelating Adsorbents for the Direct Removal of Mercury Vapour from Flue-Gases*, in *Chemical Engineering*2004, University of Cincinnati: Cincinnati. p. 215.
107. Maroto-Valer, M.M., et al., *Effect of porous structure and surface functionality on the mercury capacity of a fly ash carbon and its activated sample.* Fuel, 2005. **84**(1): p. 105-108.
108. Dunham, G.E., R.A. DeWall, and C.L. Senior, *Fixed-bed studies of the interactions between mercury and coal combustion fly ash.* Fuel Processing Technology, 2003. **82**(2-3): p. 197-213.
109. Choi, H.K., et al., *Gaseous mercury removal in a hybrid particulate collector.* Korean Journal of Chemical Engineering, 2007. **24**(2): p. 361-367.
110. Pavlish, J.H., et al., *Status review of mercury control options for coal-fired power plants.* Fuel Processing Technology, 2003. **82**(2-3): p. 89-165.
111. Galbreath, K.C., et al., *Effects of NOx, [alpha]-Fe2O3, [gamma]-Fe2O3, and HCl on mercury transformations in a 7-kW coal combustion system.* Fuel Processing Technology, 2005. **86**(4): p. 429-448.
112. Kaluza, U. and H.P. Boehm, *Titanium dioxide catalyzed photooxidation of mercury.* Journal of Catalysis, 1971. **22**(3): p. 347-358.
113. Prairie, M.R., et al., *An Investigation of Tio2 Photocatalysis for the Treatment of Water Contaminated with Metals and Organic-Chemicals.* Environmental Science & Technology, 1993. **27**(9): p. 1776-1782.
114. Li, X., et al., *Functionalized titania nanoparticles for mercury scavenging.* Journal of Materials Chemistry, 2007. **17**(19): p. 2028-2032.
115. Wang, X., S.O. Pehkonen, and A.K. Ray, *Photocatalytic reduction of Hg(II) on two commercial TiO2 catalysts.* Electrochimica Acta, 2004. **49**(9-10): p. 1435-1444.
116. Wu, C.Y., et al., *Capture of mercury in combustion systems by in situ-generated titania particles with UV irradiation.* Environmental Engineering Science, 1998. **15**(2): p. 137-148.
117. Rodríguez, S., et al., *A mechanistic model for mercury capture with in situ-generated titania particles: role of water vapor.* J Air Waste Manag Assoc. , 2004. **54**(2): p. 149-156.
118. Lee, T.G. and J.E. Hyun, *Structural effect of the in situ generated titania on its ability to oxidize and capture the gas-phase elemental mercury.* Chemosphere, 2006. **62**(1): p. 26-33.
119. Pitoniak, E., et al., *Adsorption Enhancement Mechanisms of Silica-Titania Nanocomposites for Elemental Mercury Vapor Removal.* Environmental Science & Technology, 2005. **39**(5): p. 1269-1274.
120. Li, Y., P. Murphy, and C.-Y. Wu, *Removal of elemental mercury from simulated coal-combustion flue gas using a SiO2-TiO2 nanocomposite.* Fuel Processing Technology, 2008. **89**(6): p. 567-573.
121. Zhu, W., et al., *Band Gap Narrowing of Titanium Oxide Semiconductors by Noncompensated Anion-Cation Codoping for Enhanced Visible-Light Photoactivity.* Physical Review Letters, 2009. **103**(22): p. 226401.
122. Ji, L., et al., *Manganese Oxide/Titania Materials for Removal of NO x and Elemental Mercury from Flue Gas.* Energy & Fuels, 2008. **22**(4): p. 2299-2306.
123. Diebold, U., *The surface science of titanium dioxide.* Surface Science Reports, 2003. **48**(5-8): p. 53-229.
124. Presto, A.A., et al., *A kinetic approach to the catalytic oxidation of mercury in flue gas.* Energy & Fuels, 2006. **20**(5): p. 1941-1945.
125. Hall, B., P. Schager, and E. Ljungström, *An experimental study on the rate of reaction between mercury vapour and gaseous nitrogen dioxide.* Water, Air, & Soil Pollution, 1995. **81**(1): p. 121-134.
126. Amyot, M., et al., *Formation and evasion of dissolved gaseous mercury in large enclosures amended with (HgCl2)-Hg-200.* Atmospheric Environment, 2004. **38**(26): p. 4279-4289.
127. Rolfhus, K.R. and W.F. Fitzgerald, *Mechanisms and temporal variability of dissolved gaseous mercury production in coastal seawater.* Marine Chemistry, 2004. **90**(1-4): p. 125-136.
128. Sigler, J.M., X. Lee, and W. Munger, *Emission and Long-Range Transport of Gaseous Mercury from a Large-Scale Canadian Boreal Forest Fire.* Environmental Science & Technology, 2003. **37**(19): p. 4343-4347.
129. Gustin, M.S., H. Biester, and C.S. Kim, *Investigation of the light-enhanced emission of mercury from naturally enriched substrates.* Atmospheric Environment, 2002. **36**(20): p. 3241-3254.
130. Carpi, A., *Mercury from Combustion Sources: A Review of the Chemical Species Emitted and Their Transport in the Atmosphere.* Water, Air, & Soil Pollution, 1997. **98**(3): p. 241-254.
131. Poulain, A.J., et al., *Potential for mercury reduction by microbes in the high arctic.* Applied and Environmental Microbiology, 2007. **73**(7): p. 2230-2238.

132. Edgerton, E.S., B.E. Hartsell, and J.J. Jansen, *Mercury Speciation in Coal-fired Power Plant Plumes Observed at Three Surface Sites in the Southeastern U.S.* Environmental Science & Technology, 2006. **40**(15): p. 4563-4570.
133. Pehkonen, S.O. and C.J. Lin, *Aqueous photochemistry of mercury with organic acids.* Journal of the Air & Waste Management Association, 1998. **48**(2): p. 144-150.
134. Wang, Z. and S.O. Pehkonen, *Oxidation of elemental mercury by aqueous bromine: atmospheric implications.* Atmospheric Environment, 2004. **38**(22): p. 3675-3688.
135. Munthe, J., Z. Xiao, and O. Lindqvist, *The aqueous reduction of divalent mercury by sulfite.* Water, Air, & Soil Pollution, 1991. **56**(1): p. 621-630-630.
136. Van Loon, L.L., E.A. Mader, and S.L. Scott, *Sulfite Stabilization and Reduction of the Aqueous Mercuric Ion: Kinetic Determination of Sequential Formation Constants.* The Journal of Physical Chemistry A, 2001. **105**(13): p. 3190-3195.
137. Lohman, K., et al., *Modeling Mercury in Power Plant Plumes.* Environmental Science & Technology, 2006. **40**(12): p. 3848-3854.
138. Prestbo, E.M. and D.A. Gay, *Wet deposition of mercury in the U.S. and Canada, 1996-2005: Results and analysis of the NADP mercury deposition network (MDN).* Atmospheric Environment, 2009. **43**(27): p. 4223-4233.
139. Allen, A.G., et al., *Size distributions of trace metals in atmospheric aerosols in the United Kingdom.* Atmospheric Environment, 2001. **35**(27): p. 4581-4591.
140. Scott, S.L., et al., *Homogeneous and heterogeneous reactions of atmospheric mercury(II) with sulfur(IV).* Journal De Physique Iv, 2003. **107**: p. 1201-1204.
141. Lee, T.G., P. Biswas, and E. Hedrick, *Comparison of Hg(0) capture efficiencies of three in situ generated sorbents.* American Institute of Chemical Engineers, 2001. **47**(4): p. 954-961.
142. Mason, R.P., F.M.M. Morel, and H.F. Hemond, *The Role of Microorganisms in Elemental Mercury Formation in Natural-Waters.* Water Air and Soil Pollution, 1995. **80**(1-4): p. 775-787.
143. Granite, E.J. and H.W. Pennline, *Photochemical Removal of Mercury from Flue Gas.* Industrial & Engineering Chemistry Research, 2002. **41**(22): p. 5470-5476.
144. Platt, U. and G. Hˆnninger, *The role of halogen species in the troposphere.* Chemosphere, 2003. **52**(2): p. 325-338.
145. Pal, B. and P.A. Ariya, *Gas-phase OH-Initiated reactions of elemental mercury: Kinetics, product studies, and atmospheric implications.* Environmental Science and Technology, 2004. **38**(21): p. 5555-5566.
146. Seinfeld, J.H. and S.N. Pandis, *Atmospheric Chemistry and Physics - From Air Pollution to Climate Change*. 2nd ed1998, Toronto: John Wiley & Sons.
147. Snider, G., F. Raofie, and P.A. Ariya, *Effects of relative humidity and CO(g) on the O-3-initiated oxidation reaction of Hg-0(g): kinetic & product studies.* Physical Chemistry Chemical Physics, 2008. **10**(36): p. 5616-5623.
148. Donohoue, D.L., et al., *Temperature and pressure dependent rate coefficients for the reaction of Hg with Br and the reaction of Br with Br: A pulsed laser photolysis-pulsed laser induced fluorescence study.* Journal of Physical Chemistry A, 2006. **110**(21): p. 6623-6632.
149. Sommar, J., et al., *On the Gas Phase Reactions Between Volatile Biogenic Mercury Species and the Nitrate Radical.* Journal of Atmospheric Chemistry, 1997. **27**(3): p. 233-247.
150. Raofie, F. and P.A. Ariya, *Kinetics and product study of the reaction of BrO radicals with gaseous mercury.* Journal De Physique Iv, 2003. **107**: p. 1119-1121.
151. Slemr, F., et al., *The determination of total gaseous mercury in air at background levels.* Analytica Chimica Acta, 1979. **110**(1): p. 35-47.
152. Bloom, N. and W.F. Fitzgerald, *Determination of volatile mercury species at the picogram level by low-temperature gas chromatography with cold-vapour atomic fluorescence detection.* Analytica Chimica Acta, 1988. **208**: p. 151-161.
153. Bergan, T., L. Gallardo, and H. Rodhe, *Mercury in the global troposphere: a three-dimensional model study.* Atmospheric Environment, 1999. **33**(10): p. 1575-1585.
154. Shia, R.L., et al., *Global simulation of atmospheric mercury concentrations and deposition fluxes.* Journal of Geophysical Research-Atmospheres, 1999. **104**(D19): p. 23747-23760.
155. Lindberg, S.E. and W.J. Stratton, *Atmospheric mercury speciation: Concentrations and behavior of reactive gaseous mercury in ambient air.* Environmental Science & Technology, 1998. **32**(1): p. 49-57.
156. Schroeder, W.H., G. Yarwood, and H. Niki, *Transformation Processes Involving Mercury Species in the Atmosphere - Results from a Literature Survey.* Water Air and Soil Pollution, 1991. **56**: p. 653-666.

157. Poissant, L., et al., *A year of continuous measurements of three atmospheric mercury species (GEM, RGM and Hgp) in southern Quebec, Canada.* Atmospheric Environment, 2005. **39**(7): p. 1275-1287.
158. Ebinghaus, R., et al., *Long-term measurements of atmospheric mercury at Mace Head, Irish west coast, between 1995 and 2001.* Atmospheric Environment, 2002. **36**(34): p. 5267-5276.
159. Morel, F.M.M., A.M.L. Kraepiel, and M. Amyot, *The chemical cycle and bioaccumulation of mercury.* Annual Review of Ecology and Systematics, 1998. **29**: p. 543-566.
160. Pal, B. and P.A. Ariya, *Gas-phase HO center dot-Initiated reactions of elemental mercury: Kinetics, product studies, and atmospheric implications.* Environmental Science & Technology, 2004. **38**(21): p. 5555-5566.
161. Raofie, F. and P.A. Ariya, *Product study of the gas-phase BrO-initiated oxidation of Hg-0: evidence for stable Hg1+ compounds.* Environmental Science & Technology, 2004. **38**(16): p. 4319-4326.
162. Ariya, P.A., A. Khalizov, and A. Gidas, *Reactions of gaseous mercury with atomic and molecular halogens: Kinetics, product studies, and atmospheric implications.* Journal of Physical Chemistry A, 2002. **106**(32): p. 7310-7320.
163. Menke, R. and G. Wallis, *Detection of Mercury in Air in the Presence of Chlorine and Water-Vapor.* American Industrial Hygiene Association Journal, 1980. **41**(2): p. 120-124.
164. Coquet, S. and P.A. Ariya, *Kinetics of the gas-phase reactions of Cl atom with selected C-2-C-5 unsaturated hydrocarbons at 283 < T < 323 K.* International Journal of Chemical Kinetics, 2000. **32**(8): p. 478-484.
165. Daumont, D., et al., *Ozone Uv Spectroscopy .1. Absorption Cross-Sections at Room-Temperature.* Journal of Atmospheric Chemistry, 1992. **15**(2): p. 145-155.
166. Arin, L.M. and P. Warneck, *Reaction of Ozone with Carbon-Monoxide.* Journal of Physical Chemistry, 1972. **76**(11): p. 1514-&.
167. Stedman, D.H. and H. Niki, *Ozonolysis Rates of Some Atmospheric Gases.* Environmental Letters, 1973. **4**(4): p. 303-310.
168. Gutbrod, R., et al., *On the use of CO as scavenger for OH radicals in the ozonolysis of simple alkenes and isoprene.* International Journal of Chemical Kinetics, 1997. **29**(9): p. 717-723.
169. Horie, O. and G.K. Moortgat, *The effect of the addition of CO on the reaction of ozone with ethene.* Chemical Physics Letters, 1998. **288**(2-4): p. 464-472.
170. Kramp, F. and S.E. Paulson, *On the Uncertainties in the Rate Coefficients for OH Reactions with Hydrocarbons, and the Rate Coefficients of the 1,3,5-Trimethylbenzene and m-Xylene Reactions with OH Radicals in the Gas Phase.* J. Phys. Chem. A, 1998. **102**(16): p. 2685-2690.
171. Aurivillius, K., *The Crystal Structure of Mercury(II)Oxide.* Acta Crystallographica, 1956. **9**(8): p. 685-686.
172. Taylor, G.B. and G.A. Hulett, *The dissociation of mercuric oxide.* Journal of Physical Chemistry, 1913. **17**(7): p. 565-591.
173. Tossell, J.A., *Calculation of the energetics for the oligomerization of gas phase HgO and HgS and for the solvolysis of crystalline HgO and HgS.* Journal Of Physical Chemistry A, 2006. **110**(7): p. 2571-2578.
174. Shepler, B.C. and K.A. Peterson, *Mercury monoxide: A systematic investigation of its ground electronic state.* Journal of Physical Chemistry A, 2003. **107**(11): p. 1783-1787.
175. Sumner, A.L., et al., *The nature of water on surfaces of laboratory systems and implications for heterogeneous chemistry in the troposphere.* Physical Chemistry Chemical Physics, 2004. **6**(3): p. 604-613.
176. Meagher, J.F., et al., *Rural ozone in the southeastern United States.* Atmospheric Environment (1967), 1987. **21**(3): p. 605-615.
177. Thompson, A.M., et al., *Ozone observations and a model of marine boundary layer photochemistry during SAGA 3.* Journal of Geophysical Research, 1993. **98**(D9): p. 16955-16968 ; PL:.
178. Bakir, F., et al., *Methylmercury Poisoning in Iraq.* Science, 1973. **181**(4096): p. 230-241.
179. Luna-Camara, J., *Electric Power Monthly* D.o. Energy, Editor 2009, Energy Information Administration.
180. Yi, H., J. Hao, and X. Tang, *Atmospheric environmental protection in China: Current status, developmental trend and research emphasis.* Energy Policy, 2007. **35**(2): p. 907-915.
181. Linsebigler, A.L., G. Lu, and J.T. Yates, *Photocatalysis on TiO2 Surfaces: Principles, Mechanisms, and Selected Results.* Chemical Reviews, 1995. **95**(3): p. 735-758.
182. Rajeshwar, K. and J. Ibanez, *Environmental electrochemistry: Fundamentals and applications in pollution abatement*1996, San Diego: Academic Press Inc. 776.

183. Bickley, R.I., et al., *A structural investigation of titanium dioxide photocatalysts.* Journal of Solid State Chemistry, 1991. **92**(1): p. 178-190.
184. Feng, X., et al., *Analysis of inorganic mercury species associated with airborne particulate matter/aerosols: method development.* Analytical and Bioanalytical Chemistry, 2004. **380**(4): p. 683-689.
185. Noel, J.D., P. Biswas, and D.E. Giammar, *Evaluation of a Sequential Extraction Process Used for Determining Mercury Binding Mechanisms to Coal Combustion Byproducts.* Journal of the Air & Waste Management Association, 2007. **57**(7): p. 856-867.
186. Li, Y. and C.-Y. Wu, *Kinetic Study for Photocatalytic Oxidation of Elemental Mercury on a SiO2–TiO2 Nanocomposite.* Environmental Engineering Science, 2007. **24**(1): p. 3-12.
187. Granite, E.J., et al., *Implications of mercury interactions with band-gap semiconductor oxides.* Main Group Chemistry, 2008. **7**(3): p. 227 - 237.
188. Ariya, P.A., et al., *Mercury chemical transformations in the gas, aqueous and heterogeneous phases: state-of-the-art science and uncertainties*, in *Mercury Fate and Transport in the Global Atmosphere*, N. Pirrone and R.P. Mason, Editors. 2009, Springer US: New York. p. 459-501.
189. Hung, H.-M. and P. Ariya, *Oxidation of Oleic Acid and Oleic Acid/NaCl(aq) Mixture Droplets with Ozone: Changes of Hygroscopicity and Role of Secondary Reactions.* Journal of Physical Chemistry A, 2007. **111**(4): p. 620-632.
190. Fernandez, A., et al., *Preparation and characterization of TiO2 photocatalysts supported on various rigid supports (glass, quartz and stainless steel). Comparative studies of photocatalytic activity in water purification.* Applied Catalysis B: Environmental, 1995. **7**(1-2): p. 49-63.
191. Fujishima, A., T.N. Rao, and D.A. Tryk, *Titanium dioxide photocatalysis.* Journal of Photochemistry and Photobiology C: Photochemistry Reviews, 2000. **1**(1): p. 1-21.
192. Lee, T.G., P. Biswas, and E. Hedrick, *Overall Kinetics of Heterogeneous Elemental Mercury Reactions on TiO2 Sorbent Particles with UV Irradiation.* Ind. Eng. Chem. Res., 2004. **43**(6): p. 1411-1417.
193. Rouquerol, F., J. Rouquerol, and K. Sing, *Adsorption by Metal Oxides*, in *Adsorption by Powders and Porous Solids*1999, Academic Press: London. p. 287-354.
194. Xu, Y. and C.H. Langford, *Variation of Langmuir adsorption constant determined for TiO2-photocatalyzed degradation of acetophenone under different light intensity.* Journal of Photochemistry and Photobiology A: Chemistry, 2000. **133**(1-2): p. 67-71.
195. Keller, V., P. Bernhardt, and F. Garin, *Photocatalytic oxidation of butyl acetate in vapor phase on TiO2, Pt/TiO2 and WO3/TiO2 catalysts.* Journal of Catalysis, 2003. **215**(1): p. 129-138.
196. Hager, S., R. Bauer, and G. Kudielka, *Photocatalytic oxidation of gaseous chlorinated organics over titanium dioxide.* Chemosphere, 2000. **41**(8): p. 1219-1225.
197. McLarnon, C.R., E.J. Granite, and H.W. Pennline, *The PCO process for photochemical removal of mercury from flue gas.* Fuel Processing Technology, 2005. **87**(1): p. 85-89.
198. Presto, A.A. and E.J. Granite, *Impact of Sulfur Oxides on Mercury Capture by Activated Carbon.* Environmental Science & Technology, 2007. **41**(18): p. 6579-6584.
199. Terry, L. *Titanium Dioxide (TiO2) Prices and Pricing Information*. 2009 January 19, 2010]; Available from: http://www.icis.com/V2/Chemicals/9076545/titanium-dioxide/pricing.html.
200. Fujishima, A. and X. Zhang, *Titanium dioxide photocatalysis: present situation and future approaches.* Comptes Rendus Chimie, 2006. **9**(5-6): p. 750-760.
201. Daté, M., et al., *Performance of Au/TiO2 catalyst under ambient conditions.* Catalysis Today, 2002. **72**(1-2): p. 89-94.
202. Arabatzis, I.M., et al., *Characterization and photocatalytic activity of Au/TiO2 thin films for azo-dye degradation.* Journal of Catalysis, 2003. **220**(1): p. 127-135.
203. Presto, A.A. and E.J. Granite, *Noble Metal Catalysts for Mercury Oxidation in Utility Flue Gas.* Platinum Metals Review, 2008. **52**: p. 144-154.
204. Biester, H., et al., *Modeling the Past Atmospheric Deposition of Mercury Using Natural Archives.* Environmental Science & Technology, 2007. **41**(14): p. 4851-4860.
205. Granite, E.J., H.W. Pennline, and J.S. Hoffman, *Effects of Photochemical Formation of Mercuric Oxide.* Ind. Eng. Chem. Res., 1999. **38**(12): p. 5034-5037.
206. Snider, G. and P. Ariya, *Photo-catalytic oxidation reaction of gaseous mercury over titanium dioxide nanoparticle surfaces.* Chemical Physics Letters, 2010. **491**(1-3): p. 23-28.
207. Ohko, Y., et al., *Photocatalytic Oxidation of Nitrogen Dioxide with TiO2 Thin Films under Continuous UV-Light Illumination.* The Journal of Physical Chemistry C, 2008. **112**(28): p. 10502-10508.

208. Ao, C.H., et al., *Photodegradation of formaldehyde by photocatalyst TiO2: effects on the presences of NO, SO2 and VOCs.* Applied Catalysis B: Environmental, 2004. **54**(1): p. 41-50.
209. Atkinson, R., et al., *Evaluated kinetic and photochemical data for atmospheric chemistry: Volume I - gas phase reactions of Ox, HOx, NOx and SOx species.* Atmos. Chem. Phys., 2004. **4**(6): p. 1461-1738.
210. Goodman, A.L., G.M. Underwood, and V.H. Grassian, *Heterogeneous Reaction of NO2: Characterization of Gas-Phase and Adsorbed Products from the Reaction, 2NO2(g) + H2O(a) => HONO(g) + HNO3(a) on Hydrated Silica Particles.* The Journal of Physical Chemistry A, 1999. **103**(36): p. 7217-7223.
211. Skare, I. and R. Johansson, *Reactions between mercury vapor and chlorine gas at occupational exposure levels.* Chemosphere, 1992. **24**(11): p. 1633-1644.
212. Cottrell, T.L. and T.E. Graham, *The kinetics of the oxidation of ethylene by nitrogen dioxide.* Journal of the Chemical Society (Resumed), 1953(112): p. 556-563.
213. Wojcik-Pastuszka, D., A. Gola, and E. Ratajczak, *Gas phase kinetics of the reaction system of 2NO <=> N2O4 and simple alcohols between 293-358 K.* Polish J. Chem., 2005. **79**: p. 1301 - 1313.
214. Finlayson-Pitts, B.J. and J.N. Pitts, *Chemistry of the Upper and Lower Atmosphere: Theory, Experiments, and Applications*1999: Elselvier. 969.
215. Obee, T.N. and S.O. Hay, *Effects of Moisture and Temperature on the Photooxidation of Ethylene on Titania.* Environmental Science & Technology, 1997. **31**(7): p. 2034-2038.
216. Fraser, A., et al., *Lightning-produced NO2 observed by two ground-based UV-visible spectrometers at Vanscoy, Saskatchewan in August 2004.* Atmos. Chem. Phys., 2007. **7**(6): p. 1683-1692.
217. Litter, M.I. and J.A. Nav√≠o, *Comparison of the photocatalytic efficiency of TiO2, iron oxides and mixed Ti(IV)ÓóÏFe(III) oxides: photodegradation of oligocarboxylic acids.* Journal of Photochemistry and Photobiology A: Chemistry, 1994. **84**(2): p. 183-193.
218. Matsuoka, J., et al., *Preparation of gold microcrystal-doped TiO2, ZrO2 and Al2O3 films through sol-gel process.* Journal of Sol-Gel Science and Technology, 1997. **9**(2): p. 145-155.
219. Cheung, C.W., J.F. Porter, and G. McKay, *Elovich equation and modified second-order equation for sorption of cadmium ions onto bone char.* Journal of Chemical Technology & Biotechnology, 2000. **75**(11): p. 963-970.
220. Wu, S., et al., *Fundamental Study on Decomposition Characteristics of Mercury Compounds over Solid Powder by Temperature-Programmed Decomposition Desorption Mass Spectrometry.* Energy & Fuels, 2011. **25**(1): p. 144-153.
221. Lopez-Anton, M.A., et al., *Analysis of mercury species present during coal combustion by thermal desorption.* Fuel, 2010. **89**(3): p. 629-634.
222. Murakami, A., et al., *Study of the Mercury Sorption Mechanism on Activated Carbon in Coal Combustion Flue Gas by the Temperature-Programmed Decomposition Desorption Technique.* Energy & Fuels, 2010. **24**(8): p. 4241-4249.
223. Houston, P.L., *Chemical kinetics and reaction dynamics*2006: Dover Publications.
224. Daniel, D. and I.G.R. Gutz, *Microfluidic cell with a TiO2-modified gold electrode irradiated by an UV-LED for in situ photocatalytic decomposition of organic matter and its potentiality for voltammetric analysis of metal ions.* Electrochemistry Communications, 2007. **9**(3): p. 522-528.
225. Chen, H.-W., Y. Ku, and A. Irawan, *Photodecomposition of o-cresol by UV-LED/TiO2 process with controlled periodic illumination.* Chemosphere, 2007. **69**(2): p. 184-190.
226. Tossell, J.A., *Calculation of the Energetics for the Oligomerization of Gas Phase HgO and HgS and for the Solvolysis of Crystalline HgO and HgS.* J. Phys. Chem. A, 2006. **110**(7): p. 2571-2578.
227. Widmer, N.C., et al., *Practical Limitation of Mercury Speciation in Simulated Municipal Waste Incinerator Flue Gas.* Combustion Science and Technology, 1998. **134**(1): p. 315 - 326.
228. Liu, Y., et al., *Catalytic oxidation of gas-phase mercury over Co/TiO2 catalysts prepared by sol,Äìgel method.* Catalysis Communications, 2011. **12**(14): p. 1291-1294.
229. Xu, M., et al., *Modeling of homogeneous mercury speciation using detailed chemical kinetics.* Combustion and Flame, 2003. **132**(1-2): p. 208-218.
230. DÌez, S. and J.M. Bayona, *Determination of Hg and organomercury species following SPME: A review.* Talanta, 2008. **77**(1): p. 21-27.
231. Guidotti, M. and M. Vitali, *Determination of Urinary Mercury and Methylmercury by Solid Phase Microextraction and GC/MS.* Journal of High Resolution Chromatography, 1998. **21**(12): p. 665-666.
232. Guo, F., et al., *Solid-phase microextraction combined with electrochemistry.* Analytical Communications, 1996. **33**(10): p. 361-364.

233. Maiss, M., et al., *Sulfur hexafluoride--A powerful new atmospheric tracer.* Atmospheric Environment, 1996. **30**(10-11): p. 1621-1629.
234. Feely, H.W. and J. Spar, *Tungsten-185 fron Nuclear Bomb Tests as a Tracer for Stratospheric Meteorology.* Nature, 1960. **188**: p. 1062-4.
235. Brasseur, G. and C. Granier, *Mount Pinatubo Aerosols, Chlorofluorocarbons, and Ozone Depletion.* Science, 1992. **257**(5074): p. 1239-1242.
236. Szabo, Z., et al., *Age Dating of Shallow Groundwater with Chlorofluorocarbons, Tritium/Helium: 3, and Flow Path Analysis, Southern New Jersey Coastal Plain.* Water Resources Research, 1996. **32**(4): p. 1023-1038.
237. Bergquist, B.A. and J.D. Blum, *The Odds and Evens of Mercury Isotopes: Applications of Mass-Dependent and Mass-Independent Isotope Fractionation.* ELEMENTS, 2009. **5**(6): p. 353-357.
238. Bergquist, B.A. and J.D. Blum, *Mass-Dependent and -Independent Fractionation of Hg Isotopes by Photoreduction in Aquatic Systems.* Science, 2007. **318**(5849): p. 417-420.
239. Foucher, D. and H. Hintelmann, *High-precision measurement of mercury isotope ratios in sediments using cold-vapor generation multi-collector inductively coupled plasma mass spectrometry.* Analytical and Bioanalytical Chemistry, 2006. **384**(7): p. 1470-1478-1478.
240. Feng, X., et al., *Tracing Mercury Contamination Sources in Sediments Using Mercury Isotope Compositions.* Environmental Science & Technology, 2010. **44**(9): p. 3363-3368.
241. Ghosh, S., et al., *Mass-independent fractionation of mercury isotopes in the environment.* Geochemistry, Geophysics, Geosystems, 2008. **9**(3): p. Q03004.
242. Malinovsky, D. and F. Vanhaecke, *Mass-independent isotope fractionation of heavy elements measured by MC-ICPMS: a unique probe in environmental sciences.* Analytical and Bioanalytical Chemistry, 2011. **400**(6): p. 1619-1624-1624.
243. Estrade, N., J. Carignan, and O.F.X. Donard, *Tracing and Quantifying Anthropogenic Mercury Sources in Soils of Northern France Using Isotopic Signatures.* Environmental Science & Technology, 2011. **45**(4): p. 1235-1242.
244. Sonke, J.E., et al., *Sedimentary mercury stable isotope records of atmospheric and riverine pollution from two major European heavy metal refineries.* Chemical Geology, 2010. **279**(3-4): p. 90-100.
245. Biswas, A., et al., *Natural Mercury Isotope Variation in Coal Deposits and Organic Soils.* Environmental Science & Technology, 2008. **42**(22): p. 8303-8309.
246. Gehrke, G.E., et al., *Mercury Isotopes Link Mercury in San Francisco Bay Forage Fish to Surface Sediments.* Environmental Science & Technology, 2011. **45**(4): p. 1264-1270.
247. Ebinghaus, R., et al., *Antarctic Springtime Depletion of Atmospheric Mercury.* Environ. Sci. Technol., 2002. **36**(6): p. 1238-1244.
248. Balabanov, N.B. and K.A. Peterson, *Mercury and Reactive Halogens: The Thermochemistry of Hg + {Cl2, Br2, BrCl, ClO, and BrO}.* J. Phys. Chem. A, 2003. **107**(38): p. 7465-7470.
249. Ariya, P. and K. Peterson, *Chemical Transformation of Gaseous Elemental Hg in the Atmosphere*, in *Dynamics of Mercury Pollution on Regional and Global Scales:*2005. p. 261-294.
250. Ariya, P.A. and M.E. Goodsite, *Applications of Theoretical Methods and Experimental Studies to Evaluate the Oxidation of Hg(0) in the Atmosphere.* Adv. in Quantum Chemistry, 2008. ***in pres.***
251. Macdonald, R.W., T. Harner, and J. Fyfe, *Recent climate change in the Arctic and its impact on contaminant pathways and interpretation of temporal trend data.* Science of The Total Environment, 2005. **342**(1-3): p. 5-86.
252. Dommergue, A., et al., *Laboratory simulation of Hg-0 emissions from a snowpack.* Analytical and Bioanalytical Chemistry, 2007. **388**(2): p. 319-327.
253. Raofie, F. and P.A. Ariya, *Product study of the gas-phase BrO-initiated oxidation of Hg-0: evidence for stable Hg1+ compounds.* Environmental Science and Technology, 2004. **38**(16): p. 4319-4326.
254. Atkins, P. and J. de Paula, *Atkins' Physical Chemistry*. 7th Edition ed2002, New York: Oxford University Press.
255. Southworth, G., et al., *Evasion of Added Isotopic Mercury from a Northern Temparate Lake.* Environmental Toxicology and Chemistry, 2007. **26**(1): p. 53-60.
256. Rolfhus, K.R., et al., *Distribution and Fluxes of Total and Methylmercury in Lake Superior.* Environ. Sci. Technol., 2003. **37**(5): p. 865-872.
257. Amyot, M., et al., *Sunlight-Induced Formation of Dissolved Gaseous Mercury in Lake Waters.* Environmental Science & Technology, 1994. **28**(13): p. 2366-2371.

258. Zhang, H., *Photochemical Redox Reactions of Mercury*, in *Recent Developments in Mercury Science*2006. p. 37-79.
259. Fitzgerald, W.F., C.H. Lamborg, and C.R. Hammerschmidt, *Marine biogeochemical cycling of mercury.* Chemical Reviews, 2007. **107**(2): p. 641-662.
260. Zhang, H. and S.E. Lindberg, *Sunlight and iron(III)-induced photochemical production of dissolved gaseous mercury in freshwater.* Environmental Science & Technology, 2001. **35**(5): p. 928-935.
261. Allard, B. and I. Arsenie, *Abiotic Reduction of Mercury by Humic Substances in Aquatic System - an Important Process for the Mercury Cycle.* Water Air and Soil Pollution, 1991. **56**: p. 457-464.
262. Zhang, L. and M.H. Wong, *Environmental mercury contamination in China: Sources and impacts.* Environment International, 2007. **33**(1): p. 108-121.
263. Garcia, E., M. Amyot, and P.A. Ariya, *Relationship between DOC photochemistry and mercury redox transformations in temperate lakes and wetlands.* Geochimica Et Cosmochimica Acta, 2005. **69**(8): p. 1917-1924.
264. Sheu, G.-R. and R.P. Mason, *An Examination of the Oxidation of Elemental Mercury in the Presence of Halide Surfaces.* Journal of Atmospheric Chemistry, 2004. **48**(2): p. 107-130.
265. Lalonde, J.D., et al., *Photooxidation of Hg(0) in artificial and natural waters.* Environmental Science & Technology, 2001. **35**(7): p. 1367-1372.
266. Shepler, B.C., et al., *Aqueous Microsolvation of Mercury Halide Species.* J. Phys. Chem. A, 2007. **111**(44): p. 11342-11349.
267. Lalonde, J.D., et al., *Photo-induced Hg(II) reduction in snow from the remote and temperate Experimental Lakes Area (Ontario, Canada).* Journal of Geophysical Research-Atmospheres, 2003. **108**(D6): p. -.
268. Poulain, A.J., V. Roy, and M. Amyot, *Influence of temperate mixed and deciduous tree covers on Hg concentrations and photoredox transformations in snow.* Geochimica Et Cosmochimica Acta, 2007. **71**(10): p. 2448-2462.
269. Ferrari, C.P., et al., *Mercury speciation in the French seasonal snow cover.* Science of the Total Environment, 2002. **287**(1-2): p. 61-69.
270. Lindberg, S.E., et al., *Dynamic Oxidation of Gaseous Mercury in the Arctic Troposphere at Polar Sunrise.* Environ. Sci. Technol., 2002. **36**(6): p. 1245-1256.
271. Oltmans, S.J., et al., *Seasonal Surface Ozone and Filterable Bromine Relationship in the High Arctic.* Atmospheric Environment, 1989. **23**(11): p. 2431-2441.
272. St.Louis, V.L., et al., *Methylated Mercury Species in Canadian High Arctic Marine Surface Waters and Snowpacks.* Environ. Sci. Technol., 2007. **41**(18): p. 6433-6441.
273. Schlüter, K., *Review: evaporation of mercury from soils. An integration and synthesis of current knowledge.* Environmental Geology, 2000. **39**(3): p. 249-271.
274. Lahoutifard, N., L. Poissant, and S.L. Scott, *Scavenging of gaseous mercury by acidic snow at Kuujjuarapik, Northern Quebec.* Science of The Total Environment, 2006. **355**(1-3): p. 118-126.
275. Fain, X., et al., *Fast depletion of gaseous elemental mercury in the Kongsvegen Glacier snowpack in Svalbard.* Geophysical Research Letters, 2006. **33**(6): p. -.
276. Poulain, A.J., et al., *Mercury distribution, partitioning and speciation in coastal vs. inland High Arctic snow.* Geochimica Et Cosmochimica Acta, 2007. **71**(14): p. 3419-3431.
277. Douglas, T.A., et al., *Influence of Snow and Ice Crystal Formation and Accumulation on Mercury Deposition to the Arctic.* Environ. Sci. Technol., 2008.
278. Aspmo, K., et al., *Mercury in the atmosphere, snow and melt water ponds in the North Atlantic Ocean during Arctic summer.* Environmental Science & Technology, 2006. **40**(13): p. 4083-4089.
279. Steffen, A., et al., *Atmospheric mercury concentrations: measurements and profiles near snow and ice surfaces in the Canadian Arctic during Alert 2000.* Atmospheric Environment, 2002. **36**(15-16): p. 2653-2661.
280. Tackett, P.J., et al., *A study of the vertical scale of halogen chemistry in the Arctic troposphere during Polar Sunrise at Barrow, Alaska.* Journal of Geophysical Research-Atmospheres, 2007. **112**(D7): p. -.
281. Kaleschke, L., et al., *Frost flowers on sea ice as a source of sea salt and their influence on tropospheric halogen chemistry.* Geophysical Research Letters, 2004. **31**(16): p. -.
282. Gauchard, P.-A., et al., *Study of the origin of atmospheric mercury depletion events recorded in Ny-Alesund, Svalbard, spring 2003.* Atmospheric Environment, 2005. **39**(39): p. 7620-7632.
283. Grigal, D.F., *Inputs and outputs of mercury from terrestrial watersheds: a review.* Environmental Reviews, 2002. **10**(1): p. 1.

284. Gustin, M.S., S.E. Lindberg, and M.A. Allan, *Special Section: Constraining mercury emissions from naturally enriched surfaces: Assessment of methods and controlling parameters (Mercury Flux) - Preface.* Journal of Geophysical Research-Atmospheres, 1999. **104**(D17): p. 21829-21830.
285. Gustin, M. and S. Lindberg, *Terrestial Hg Fluxes: Is the Next Exchange Up, Down, or Neither?*, in *Dynamics of Mercury Pollution on Regional and Global Scales:*, N. Pirrone and K.R. Mahaffey, Editors. 2005. p. 241-259.
286. Gustin, M.S., et al., *New insights into mercury exchange between air and substrate.* Geochimica Et Cosmochimica Acta, 2005. **69**(10): p. A700-A700.
287. Xin, M. and M.S. Gustin, *Gaseous elemental mercury exchange with low mercury containing soils: Investigation of controlling factors.* Applied Geochemistry, 2007. **22**(7): p. 1451-1466.
288. Edwards, J.R., R.K. Srivastava, and J.D. Kilgroe, *A study of gas-phase mercury speciation using detailed chemical kinetics.* Journal of the Air and Waste Management Association, 2001. **6**(51): p. 869-877.
289. Poissant, L., et al., *Atmospheric mercury speciation and deposition in the Bay St. Francois wetlands.* Journal of Geophysical Research-Atmospheres, 2004. **109**(D11): p. -.
290. Hanson, P.J., et al., *Foliar exchange of mercury vapor: Evidence for a compensation point.* Water, Air, & Soil Pollution, 1995. **80**(1): p. 373-382.
291. Lee, X., G. Benoit, and X.Z. Hu, *Total gaseous mercury concentration and flux over a coastal saltmarsh vegetation in Connecticut, USA.* Atmospheric Environment, 2000. **34**(24): p. 4205-4213.
292. Habibi, M.H., G. Habibian, and M.A. Haghighipor, *Photocatalytic reduction and recovery of inorganic mercury compounds as environmental pollutants in aquatic system using TiO2 suspension.* Fresenius Environmental Bulletin, 2003. **12**(7): p. 808-812.
293. Lindberg, S.E., et al., *Atmosphere-Surface Exchange of Mercury in a Forest - Results of Modeling and Gradient Approaches.* Journal of Geophysical Research-Atmospheres, 1992. **97**(D2): p. 2519-2528.
294. Xiao, Z.F., D. Stromberg, and O. Lindqvist, *Influence of Humic Substances on Photolysis of Divalent Mercury in Aqueous-Solution.* Water Air and Soil Pollution, 1995. **80**(1-4): p. 789-798.
295. Ferrari, C.P., et al., *Profiles of Mercury in the snow pack at Station Nord, Greenland shortly after polar sunrise.* Geophysical Research Letters, 2004. **31**(3): p. -.
296. Fain, X., et al., *Diurnal production of gaseous mercury in the alpine snowpack before snowmelt.* Journal of Geophysical Research-Atmospheres, 2007. **112**(D21): p. 311.
297. Peretyazhko, T., et al., *Formation of dissolved gaseous mercury in a tropical lake (Petit-Saut reservoir, French Guiana).* Science of The Total Environment, 2006. **364**(1-3): p. 260-271.
298. Hines, N.A. and P.L. Brezonik, *Mercury dynamics in a small Northern Minnesota lake: water to air exchange and photoreactions of mercury.* Marine Chemistry, 2004. **90**(1-4): p. 137-149.
299. Amyot, M., G.A. Gill, and F.M.M. Morel, *Production and loss of dissolved gaseous mercury in coastal seawater.* Environmental Science & Technology, 1997. **31**(12): p. 3606-3611.
300. Medhekar, A.K., et al., *Surface catalyzed reaction of Hg + Cl2.* Chemical Physics Letters, 1979. **65**(3): p. 600-604.
301. Roy, S. and G.T. Rochelle, *Simultaneous absorption of mercury and chlorine in sulfite solutions.* Chemical Engineering Science, 2004. **59**(6): p. 1309-1323.
302. Zhao, L.L. and G.T. Rochelle, *Mercury absorption in aqueous hypochlorite.* Chemical Engineering Science, 1999. **54**(5): p. 655-662.
303. *Pilot Testing of Mercury Oxidation Catalysts for Upstream of Wet FGD Systems, Final Report*, 2005, EPRI, Palo Alto, CA, and the U.S. Department of Energy National Energy Technology Laboratory, Pittsburgh, PA.
304. Hwang, J.Y., X. Sun, and Z. Li, *Unburned Carbon from Fly Ash for Mercury Adsorption: Separation and Characterization of Unburned Carbon.* The Journal of Minerals and Materials Characterization and Engineering, 2002. **1**(1): p. 39-60.
305. Wang, R.G., M.A. Dillon, and D. Spence, *A phenomenological study of heterogeneous chemical reactions of mercuric chloride on heated stainless steel surfaces.* The Journal of Chemical Physics, 1983. **79**(2): p. 1100-1101.
306. Horvath, O., E. Bodnar, and J. Hegyi, *Photoassisted oxidative degradation of surfactants and simultaneous reduction of metals in titanium dioxide dispersions.* Colloids and Surfaces a-Physicochemical and Engineering Aspects, 2005. **265**(1-3): p. 135-140.
307. Skubal, L.R. and N.K. Meshkov, *Reduction and removal of mercury from water using arginine-modified TiO2.* Journal of Photochemistry and Photobiology a-Chemistry, 2002. **148**(1-3): p. 211-214.

308. Sen, A.K. and A.K. De, *Adsorption of mercury(II) by coal fly ash.* Water Research, 1987. **21**(8): p. 885-888.
309. Mohan, D., et al., *Kinetics of mercury adsorption from wastewater using activated carbon derived from fertilizer waste.* Colloids and Surfaces A: Physicochemical and Engineering Aspects, 2000. **177**(2-3): p. 169-181.
310. Zhao, Y., et al., *Application of Gold Catalyst for Mercury Oxidation by Chlorine.* Environ. Sci. Technol., 2006. **40**(5): p. 1603-1608.
311. Barrosse-Antle, L.E., et al., *The expansion/contraction of gold microparticles during voltammetrically induced amalgamation leads to mechanical instability.* New Journal of Chemistry, 2007. **31**(12): p. 2071-2075.
312. Wu, S., M. Azhar Uddin, and E. Sasaoka, *Characteristics of the removal of mercury vapor in coal derived fuel gas over iron oxide sorbents.* Fuel, 2006. **85**(2): p. 213-218.
313. Wu, S., et al., *Development of iron-based sorbents for Hg0 removal from coal derived fuel gas: Effect of hydrogen chloride.* Fuel, 2008. **87**(4-5): p. 467-474.
314. Li, Y., P. Murphy, and C.-Y. Wu, *Removal of elemental mercury from simulated coal-combustion flue gas using a SiO2-TiO2 nanocomposite.* Fuel Processing Technology. **In Press, Corrected Proof**.
315. Granite, E.J., H.W. Pennline, and R.A. Hargis, *Novel sorbents for mercury removal from flue gas.* Industrial & Engineering Chemistry Research, 2000. **39**(4): p. 1020-1029.
316. Jain, A. and M.A. Beg, *Kinetics and mechanism of solid state reactions of silver tungstate with mercuric bromide and mercuric chloride.* Polyhedron, 1995. **14**(15-16): p. 2293-2299.
317. Skodras, G., I. Diamantopoujou, and G.P. Sakellaropoujos, *Role of activated carbon structural properties and surface chemistry in mercury adsorption.* Desalination, 2007. **210**(1-3): p. 281-286.
318. Abu-Daabes, M.A. and N.G. Pinto, *Synthesis and characterization of a nano-structured sorbent for the direct removal of mercury vapor from flue gases by chelation.* Chemical Engineering Science, 2005. **60**(7): p. 1901-1910.
319. Querol, X., et al., *Synthesis of Na-zeolites from fly ash.* Fuel, 1997. **76**(8): p. 793-799.
320. Hower, J.C., et al., *Mercury Capture by Distinct Fly Ash Carbon Forms.* Energy Fuels, 2000. **14**(1): p. 224-226.
321. Chen, X., *Impacts of Fly Ash Composition and Flue Gas Components on Mercury Speciation* in *Civil and Environmental Engineering*2007, University of Pittsburgh: Pittsburgh. p. 87.
322. Daisey, J.M., R.J. Mccaffrey, and R.A. Gallagher, *Polycyclic Aromatic-Hydrocarbons and Total Extractable Particulate Organic-Matter in the Arctic Aerosol.* Atmospheric Environment, 1981. **15**(8): p. 1353-1363.
323. Namasivayam, C. and K. Kadirvelu, *Uptake of mercury (II) from wastewater by activated carbon from an unwanted agricultural solid by-product: coirpith.* Carbon, 1999. **37**(1): p. 79-84.
324. Ranganathan, K., *Adsorption of Hg(II) ions from aqueous chloride solutions using powdered activated carbons.* Carbon, 2003. **41**(5): p. 1087-1092.
325. Yardim, M.F., et al., *Removal of mercury (II) from aqueous solution by activated carbon obtained from furfural.* Chemosphere, 2003. **52**(5): p. 835-841.
326. Menke, R. and G. Wallis, *Detection of mercury in air in the presence of chlorine and water vapor.* American Industrial Hygiene Association Journal, 1980. **41**(2): p. 120 - 124.
327. Seigneur, C., W. Jacek, and C. Elpida, *A Chemical Kinetic Mechanism for Atmospheric Inorganic Mercury.* Environ. Sci. Technol, 1994. **28**(9): p. 1589-1597.
328. Xu, M., et al., *Kinetic calculation and modeling of trace element reactions during combustion.* Powder Technology, 2008. **180**(1-2): p. 157-163.
329. Zheng, C., et al., *Kinetic mechanism studies on reactions of mercury and oxidizing species in coal combustion.* Fuel, 2005. **84**(10): p. 1215-1220.
330. Change, R. and G.R. Offen, *Mercury emission control technologies: An EPRI synopsis.* Journal: Power Engineering (Barrington); Journal Volume: 99; Journal Issue: 11; Other Information: PBD: Nov 1995, 1995: p. Size: pp. 51-56; Other: PL:.
331. Xiao, Z., et al., *Sampling and determination of gas phase divalent mercury in the air using a KCl coated denuder.* Journal of Analytical Chemistry, 1997. **358**(3): p. 386-391.
332. Russell Bullock, J.O., *Modeling assessment of transport and deposition patterns of anthropogenic mercury air emissions in the United States and Canada.* The Science of The Total Environment, 2000. **259**(1-3): p. 145-157.

333. Pirrone, N. and K. Mahaffey, *Dynamic of mercury pollution on regional and global scales: Atmospheric Atmospheric Processes and Human Exposures Around the World*, in *Dynamics of Mercury Pollution on Regional and Global Scales:*2005, Springer.
334. Veiga, M.M., et al., *Protocols for environmental and health assessment of mercury released by artisanal and small-scale gold miners*2004: Global Mercury Project, UNIDO.
335. Neal, P.A., et al., *A Study of Chronic Mereurialism in the Hatter's Fur-Cutting Industry.* Public Health Bulletin. Vol. 234. 1937: Washington. 70.
336. Wedeen, R.P., *Were the hatters of new jersey "mad"?* American Journal of Industrial Medicine, 1989. **16**(2): p. 225-233.
337. Clarke, C.L., *Galvanic Battery*, U.S.P. Office, Editor 1884: United States.
338. Hewitt, P.C., *Method of manufacuting electric lamps*, U.S.P. Office, Editor 1901: United States.
339. *The Effects of Mercury Vapour Pressure*. 2003 [cited 2011 June 16]; Available from: http://www.lamptech.co.uk/Documents/M3 Spectra.htm.
340. Powell, H.M. and W.A. Jamieson, *Merthiolate as a Germicide.* American Journal of Epidemiology, 1931. **13**(1): p. 296-310.
341. Ponomarev, D.A. and S.M. Shevchenko, *Hydration of Acetylene: A 125th Anniversary.* Journal of Chemical Education, 2007. **84**(10): p. 1725-null.
342. *Minamata, Japan* 2011 June 15, 2011]; Available from: http://www.hgtech.com/Information/Minamata_Japan.html.
343. Mergler, D., et al., *Methylmercury Exposure and Health Effects in Humans: A Worldwide Concern.* AMBIO: A Journal of the Human Environment, 2007. **36**(1): p. 3-11.
344. Takeuchi, T., et al., *Pathological Studies On Encephalopathia From Unknown Cause in Minamata District Of Kumamoto Prefecture (The So-called Minamata-disease) in Japan.* Pathology International, 1957. **7**: p. 607-611.
345. Takeuchi, T., et al., *A pathological study of Minamata disease in Japan.* Acta Neuropathologica, 1962. **2**(1): p. 40-57.
346. *Minamata Disease The History and Measures*. 2002 [cited 2011 June 15th]; Available from: http://www.env.go.jp/en/chemi/hs/minamata2002/ch2.html.
347. Smith, W.E. and A.M. Smith, *Minamata*1975: Holt, Rinehart, and Winston.
348. Mizukoshi, K., et al., *Neurotological Studies upon Intoxication by Organic Mercury Compounds.* ORL, 1975. **37**(2): p. 74-87.
349. Michael, R.G., *Methylmercury poisoning in Iraq. An epidemiological study of the 1971-1972 outbreak.* Journal of Applied Toxicology, 1985. **5**(3): p. 148-159.
350. Magos, L., *Selective atomic-absorption determination of inorganic mercury and methylmercury in undigested biological samples.* Analyst, 1971. **96**(1149): p. 847-853.
351. Grandjean, P., et al., *Neurobehavioral deficits associated with PCB in 7-year-old children prenatally exposed to seafood neurotoxicants.* Neurotoxicology and Teratology, 2001. **23**(4): p. 305-317.
352. Lodenius, M. and O. Malm, *Mercury in the Amazon.* Reviews of Environmental Contamination & Toxicology, 1998. **157**: p. 25-52.
353. Davidson, P.W., et al., *Effects of Prenatal and Postnatal Methylmercury Exposure From Fish Consumption on Neurodevelopment: Outcomes at 66 Months of Age in the Seychelles Child Development Study.* JAMA, 1998. **280**(8): p. 701-707.
354. Lundgren, L.J., *Sweden's Environment Problems and Protection, 1960-2010*, 2010, the Swedish environmental Protection agency: Stockholm.
355. Jira, R., *Acetaldehyde from Ethylene—A Retrospective on the Discovery of the Wacker Process.* Angewandte Chemie International Edition, 2009. **48**(48): p. 9034-9037.
356. Peakall, D.B. and R.J. Lovett, *Mercury: its occurrence and effects in the ecosystem.* BioScience, 1972. **22**(1): p. 20-25.
357. Huber, M.L., A. Laesecke, and D.G. Friend, *The Vapor Pressure of Mercury*, T.A. U.S. Dept. of Commerce, Editor 2006, NIST, Physical and Chemical Properties Division, Boulder, CO 80303-3328 p. 1-56.
358. Burns, K., K.B. Adams, and J. Longwell, *Interference Measurements in the Spectra of Neon and Natural Mercury.* J. Opt. Soc. Am., 1950. **40**(6): p. 339-344.
359. Harris, D.C., *Quantitative chemical analysis*2003: W.H. Freeman and Co.
360. Pyykko, P., *Relativistic effects in structural chemistry.* Chemical Reviews, 1988. **88**(3): p. 563-594.

361. Sanemasa, I., *Solubility of Elemental Mercury-Vapor in Water.* Bulletin of the Chemical Society of Japan, 1975. **48**(6): p. 1795-1798.
362. Talmi, Y. and R.E. Mesmer, *Studies on vaporization and halogen decomposition of methyl mercury compounds using gc with a microwave detector.* Water Research, 1975. **9**(5-6): p. 547-552.
363. Iverfeldt, A. and O. Lindqvist, *Distribution Equilibrium of Methyl Mercury-Chloride between Water and Air.* Atmospheric Environment, 1982. **16**(12): p. 2917-2925.
364. Khalizov, A.F., et al., *A theoretical study on the reactions of Hg with halogens: Atmospheric implications.* Journal of Physical Chemistry A, 2003. **107**(33): p. 6360-6365.
365. Horne, D.G., R. Gosavi, and O.P. Strausz, *Reactions of Metal Atoms .I. Combination of Mercury and Chlorine Atoms and Dimerization of Hgcl.* Journal of Chemical Physics, 1968. **48**(10): p. 4758-&.
366. Strömberg, D., *Some mercury compounds studied by relativistic quantum chemical methods*, in *Oorganisk kemi*1990, University of Gothenburg: Gothenburg.
367. Tokos, J.J.S., et al., *Homogeneous gas-phase reaction of Hg with H2O2, O3, CH3I, and (CH3)2S: Implications for atmospheric Hg cycling.* Atmospheric Environment, 1998. **32**(5): p. 823-827.
368. Wang, X. and L. Andrews, *Infrared Spectrum of Hg(OH)2 in Solid Neon and Argon.* Inorganic Chemistry, 2004. **44**(1): p. 108-113.
369. Niki, H., et al., *A Long-Path Fourier-Transform Infrared Study of the Kinetics and Mechanism for the HO-Radical Initiated Oxidation of Dimethylmercury.* Journal of Physical Chemistry, 1983. **87**(24): p. 4978-4981.
370. Niki, H., et al., *A Fourier-transform infrared study of the kinetics and mechanism of the reaction of atomic chlorine with dimethylmercury.* The Journal of Physical Chemistry, 1983. **87**(19): p. 3722-3724.
371. Hall, B., O. Lindqvist, and E. Ljungstrom, *Mercury Chemistry in Simulated Flue-Gases Related to Waste Incineration Conditions.* Environmental Science & Technology, 1990. **24**(1): p. 108-111.
372. Donohoue, D.L., D. Bauer, and A.J. Hynes, *Temperature and pressure dependent rate coefficients for the reaction of Hg with Cl and the reaction of Cl with Cl: A pulsed laser photolysis-pulsed laser induced fluorescence study.* Journal of Physical Chemistry A, 2005. **109**(34): p. 7732-7741.
373. Wilcox, J., et al., *Theoretically Predicted Rate Constants for Mercury Oxidation by Hydrogen Chloride in Coal Combustion Flue Gases.* Environ. Sci. Technol., 2003. **37**(18): p. 4199-4204.
374. Wilcox, J., *A Kinetic Investigation of High-Temperature Mercury Oxidation by Chlorine.* The Journal of Physical Chemistry A, 2009. **113**(24): p. 6633-6639.
375. Malcolm, E., et al., *Experimental investigation of the scavenging of gaseous mercury by sea salt aerosol.* Journal of Atmospheric Chemistry, 2009. **63**(3): p. 221-234-234.
376. Ko, K.B., et al., *Influence of HCl on oxidation of gaseous elemental mercury by dielectric barrier discharge process.* Chemosphere, 2008. **71**(9): p. 1674-1682.
377. Galbreath, K.C. and C.J. Zygarlicke, *Mercury Speciation in Coal Combustion and Gasification Flue Gases.* Environmental Science & Technology, 1996. **30**(8): p. 2421-2426.
378. Lu, J.Y. and W.H. Schroeder, *Sampling and Determination of Particulate Mercury in Ambient Air: A Review.* Water, Air, & Soil Pollution, 1999. **112**(3): p. 279-295.
379. Holmes, C.D., D.J. Jacob, and X. Yang, *Global lifetime of elemental mercury against oxidation by atomic bromine in the free troposphere.* Geophysical Research Letters, 2006. **33**(20): p. -.
380. Ogg Jr, R.A., H.C. Martin, and P.A. Leighton, *Kinetics of the Vapor Phase Reaction of Mercury and Halogens.* 1936. **58**: p. 1922-.

0